PHD

Membranes for Gas Separation

Pengilley, Christine

Award date:
2016

Awarding institution:
University of Bath

Membranes for Gas Separation

Christine Njoki Pengilley

A thesis submitted for the degree of Doctor of Philosophy

University of Bath
Department of Chemical Engineering

November 2015

ABSTRACT

The effective separation of ammonia from the synthesis loop in ammonia synthesis plants is an important step in its manufacture. This work presents the use of nanocomposite MFI zeolite membranes prepared by a pore-plugging method for this separation process. Performance of a zeolite membrane is highly dependent on the operating conditions. Therefore, the influences of differential pressure, temperature, sweep gas flow, feed gas flow and gas composition are studied experimentally.

Transport of NH_3 in this membrane is by surface diffusion in the intracrystalline (zeolite) pores in parallel with capillary condensation in the intercrystalline (non-zeolite) pores. The separation of NH_3 from a mixture with H_2 and N_2 is by preferential adsorption of NH_3, which hinders the permeation of weakly adsorbed H_2 and N_2. Differential pressure has only relatively small effects in the pressure range 300kPa – 1550kPa. Increase in sweep flow rate has little effect on NH_3 gas permeance, but H_2 and N_2 permeances increase thereby decreasing the selectivities. Increase in feed flowrate also has little effect on NH_3 permeance. However, the N_2 and H_2 permeances increase and there is a subsequent decrease in selectivities. Membrane performance was found to be highly dependent on temperature. NH_3 permeance in the mixture increases linearly with temperature. NH_3 selectivity was found to increase with temperature up to 353K after which it starts to decrease due to N_2 and H_2 permeances increasing with temperatures beyond 353K ($\alpha NH_3/N_2 = 46$ and $\alpha NH_3/H_2 = 15$) and is therefore the optimum temperature for separation.

A potential barrier model is developed to describe the hindering effect of NH_3 on H_2 and N_2 permeance. The model fails to predict correctly H_2 and N_2 permeances in the ternary mixture using pure gas (H_2 and N_2) permeances. Binary mixture permeation H_2/N_2 studies showed that there are diffusion effects (single file diffusion) that have not been taken into account in the potential barrier model. When permeances of the individual components in the binary mixture are used in the model instead of the pure gas permeances, there is an improved agreement between experimental and predicted results.

ACKNOWLEDGMENTS

Firstly, I would like to acknowledge and thank Professor Barry Crittenden and Dr Semali Perera for their supervision and guidance throughout this PhD.

Special thanks are due to Dr Olivier Camus for his scholarly chats and advice and to Mervin Newnes for both technical and emotional support. Gratitude is also extended to Mr John Bishop, Mr Robert Brain, Mr Fernando Acosta and Mr Richard Bull for their active support and technical assistance. Thanks are also due to all the friends I have made at Bath for their constant encouragement.

Extreme gratitude to Mum, I would not be where I am without your extreme kindness, support and consistent encouragement, Russell, for your patience and for being there throughout, Mr and Mrs Pengilley for their encouragement and support. Finally I would like to thank my extended family for your love and support.

CONTENTS

INDEX OF FIGURES

INDEX OF TABLES

NOMENCLATURE

A	total membrane surface area	m^2
A_n	membrane surface area of a volume element n	m^2
b	adsorption affinity constant	Pa^{-1}
b_0	affinity constant at reference temperature	Pa^{-1}
dp	pore diameter	m
E	potential energy barrier	J mol^{-1}
E_H	activation energy for Arrhenius dependency of permeance on temperature	J mol^{-1}
$E_{o,i}$	potential energy barrier introduced by pure component "i" at its saturation condition	J mol^{-1}
F_n	total flowrate on the feed/retentate side entering volume element n	ml s^{-1}
F_0	total feed flow rate	ml s^{-1}
F_{50}	total retentate flow rate	ml s^{-1}
$F_{n,i}$	flow rate of component "i" on the feed/retentate side entering a volume element n	ml s^{-1}
F_n^I	total flow rate on the sweep/permeate side entering a volume element n	ml s^{-1}
F_0^I	total permeate flow rate	ml s^{-1}
F_{50}^I	total sweep flow rate	ml s^{-1}
$F_{n.i}^I$	flow rate of component "i" on the sweep/permeate side entering a volume element n	ml s^{-1}
G_{mol}	molecular flow of gas	mol s^{-1}
ΔH	heat of adsorption	kJ mol^{-1}
J	molar flux	mol m^{-2} s^{-1}
J_i	flux of component "i" across the membrane	mol m^{-2} s^{-1}
J_n	total flux across the membrane at the volume element n	mol m^{-2} s^{-1}
$J_{n,i}$	flux of component "i" across the membrane for a volume element n	mol m^{-2} s^{-1}
J_o	constant defined in equation 5.19	mol m^{-2} s^{-1}
Jv, Jk	molar fluxes defined in equations 5.14 and 5.16 respectively	mol m^{-2} s^{-1}
k	proportionality constant defined in equation 6.3	m^{-1}

K	Freundlich model constant	m
l	thickness of the membrane	m
L	pore length	m
M	molar mass	kg mol^{-1}
M_i	molar mass of component “i”	kg mol^{-1}
M_j	molar mass of component “j”	kg mol^{-1}
n	Freundlich model heterogeneity parameter	-
N_a	Avogadro’s number	mol^{-1}
N_d	number of data points	-
N_p	number of parameters	-
P	pressure	Pa
P_H	pre-exponential factor in Arrhenius dependency of hydrogen permeance on temperature	mol m^{-2} s^{-1} Pa^{-1}
$\prod_i$	permeance of component “i”	mol m^{-2} s^{-1} Pa^{-1}
P_i^{reten}	partial pressure of component “i” in the retentate	Pa
P_i^{feed}	partial pressure of component “i” in the feed	Pa
P_i^{perm}	partial pressure of component “i” in the permeate	Pa
P_i^{sweep}	partial pressure of component “i” in the sweep	Pa
$P_{n,i}$	partial pressure of component “i” on the feed/retentate side in a volume element n	Pa
$\prod_o$	permeance of pure non-adsorbing gas	mol m^{-2} s^{-1} Pa^{-1}
ΔP	differential pressure across the membrane	kPa
P_m	mean pressure	Pa
q^*	total amount adsorbed	mmol g^{-1}
q_s	maximum adsorption capacity of Adsorbent	mmol g^{-1}
Q	steady state effluent gas flow rate of permeate	
Q_{st}	Isosteric heat of adsorption	kJ mol^{-1}
r	pore radius	m
R	universal gas constant	J mol^{-1} K^{-1}
$S_{i/j}$	selectivity estimated from molar fraction	$S_{i/j}$
t	Toth model Heterogeneity parameter	-
T	absolute temperature	K
x	thickness in membrane	m

x_i	molar fraction of component “i”	-
x_0	thickness of membrane	m
y	experimental observation	-
y_i	model prediction	-
Z	compressibility constant	-

Greek

$\alpha_{i/j}$	selectivity estimated from permeances	-
α_{kn}	Knudsen selectivity	-
$\beta_{i/j}$	selectivity estimated from molar fraction	-
θ	adsorption fractional coverage	-
θ_i	adsorption fractional coverage of component i	-
θ_0	adsorption fractional coverage at feed side of membrane	-
$\theta_{I,0}$	adsorption fractional coverage at permeate side of membrane	-
ε	porosity	-
λ	mean free path	m
μ	gas viscosity	Pa s
τ	tortuosity factor	-

CHAPTER 1

INTRODUCTION

1.0 Ammonia Separation

Ammonia synthesis is one of the largest and oldest petrochemical processes with a global production capacity of over 195 million metric tonnes (Varotto, 2014). Ammonia has many uses including production of plastics, fibres, fertilizers, explosives, and intermediates for dyes and pharmaceuticals which makes it one of the most highly produced inorganic chemicals. Worldwide production in 2014 was estimated at 170,500,000 metric tonnes (MC group, 2014) and approximately 80% or more of the ammonia produced is used in the manufacture of fertilizer. The manufacturing of ammonia and fertilizers has made it possible to grow abundant quantities of reasonably-priced food. Nevertheless, over 800 million people or 13% of the world's population still do not have enough food (FAO report, 2014). With the rapid growth in population which is forecast to reach 8.5 billion people by 2030, governments worldwide are looking to provide food security to their nations. There is therefore a rising demand for nitrogen fertilizers so as to increase food supplies (Heffer and Prud'homme, 2014). With this projected growth in world population and the ongoing requirement for more nitrogen based products it is anticipated that global ammonia capacity will rise from 205 million metric tonnes in 2010 to 239 million

metric tonnes by 2020 (Anantharaman et al, 2012) which will result in the construction of new ammonia plants.

Ammonia is still largely produced by the Haber Bosch process via the catalytic reaction of hydrogen and nitrogen at high temperatures (300–550ºC) and pressures (150-250 Bar). The reactor effluent is typically 12-18% ammonia with the remainder consisting of unreacted nitrogen and hydrogen and inerts such as methane and argon (Choe at al, 1995). This gas mixture is cooled to a relatively low temperature effecting the condensation of ammonia from the remaining lighter gases. The liquefied ammonia is separated from the other components of the mixture, and the remaining nitrogen and hydrogen are subsequently re-heated to the operating temperature for ammonia conversion and are recycled to the reactor. There are two major disadvantages to this technique for ammonia separation:

1. As the separation of ammonia by condensation does not go to completion, the gas recycled to the reactor can contain a significant amount of ammonia which may decrease ammonia production efficiency.
2. Cooling the gas mixture to separate ammonia requires large amounts of refrigeration which makes the whole process considerably energy intensive. (Whitlock, 1999).

In addition, this method of separation is economical only on a very large scale, since both investment and operating costs are high. On small and intermediate scales, ammonia can be separated by gas absorbers. This technique has some drawbacks, including high investment costs, complex operation and the loss of absorbing solutions due to degradation (Helminen et al, 2000). Adsorption has also been suggested as a method to separate ammonia (Lavie, 1985, Helminen et al, 2000). Although this process may be advantageous to some systems, the process would be uneconomical in ammonia production due to the large volumes of synthesis gas recycled in ammonia production (Whitlock, 1999). The process also requires high amounts of energy for regeneration of sorbents.

Membrane separation processes have become one of the emerging technologies that have undergone a rapid growth in the past few decades (Camus et al, 2006, Caro, 2011). This advancement has been triggered by the need to search for alternatives to traditional energy intensive separation methods such as absorption, cryogenic distillation, and pressure swing adsorption (PSA). These techniques require large, complex chemical plants and can be expensive to operate and maintain. In comparison, membrane-based separations can be energy efficient and cost effective as they offer potentially cheaper capital and utility costs (Tsai et al, 2000). It is generally accepted that membrane processes not only offer significant energy savings compared to more conventional processes (Molinari et al, 1995, Stephan et al, 1995) but are also environmentally better since no additive materials such as extractors and adsorbents which may be potential pollutants are needed for the separation (Wenten, 2002). In addition, gas separation membrane units are smaller than other types of plants (e.g. amine stripping plants) and therefore can have relatively small foot prints. Membrane systems are also easy to operate as they do not have a great deal of associated hardware and no moving parts (Stephan et al, 1995). Membrane use in separation processes has seen a dramatic increase in the last two decades, indicating that its industrial potential is clearly being identified (Caro et al, 2000).

It is desirable to provide a method and apparatus for ammonia separation that provides improved efficiency and reduced cost. Considering the advantages a membrane process has to offer, it is believed that this could be a suitable replacement for the current refrigeration system. In addition, an ammonia-selective membrane could avoid the refrigeration of unreacted hydrogen and nitrogen, and hence reduce the overall cost of ammonia manufacture (Tricoli and Cussler, 1995). For a membrane to be successful, it would have to have both a high permeance and be highly selective towards ammonia. Most importantly it should be able to withstand the extreme operational conditions of the process.

The basic refrigerated ammonia recovery flow sheet is shown in Figure 1.1. A flow sheet with a membrane recovery base case is shown in Figure 1.2. Comparison of the two demonstrates the greater simplicity of the membrane flow sheet in terms of equipment.

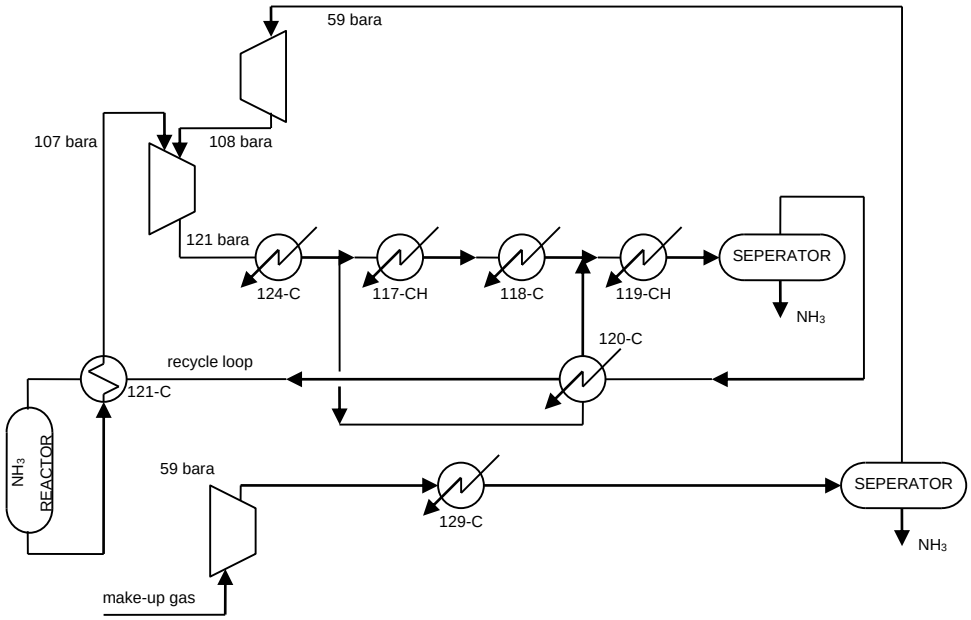

Figure 1.1: Basic refrigeration ammonia recovery process

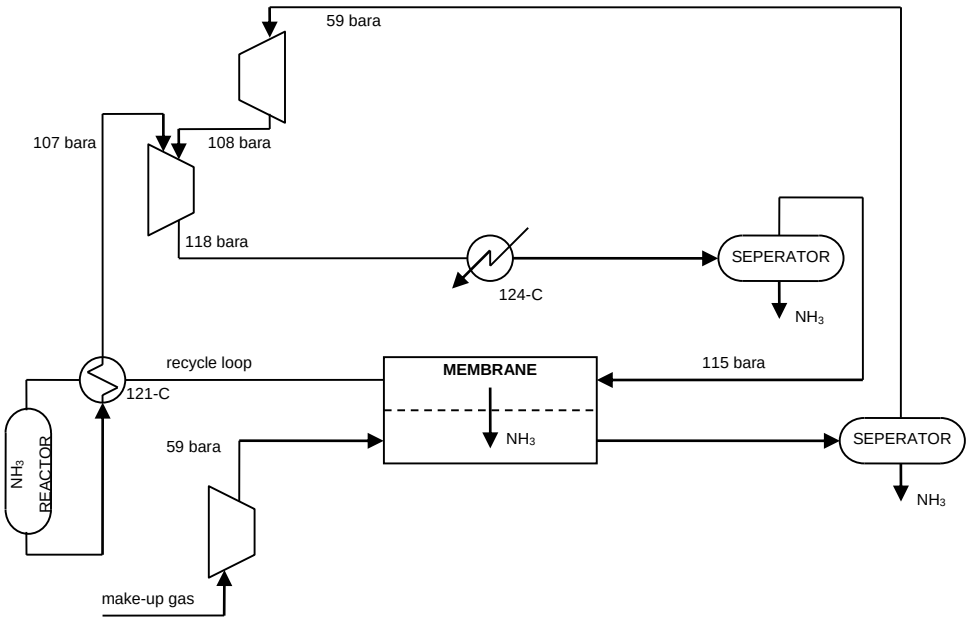

Figure 1.2: Proposed membrane ammonia recovery (adapted from IMPRESS project Report, 2004)

The use of membranes for the separation of ammonia has been suggested by various authors. Most of these studies are based on polymeric membranes with particular interest in polyvinylammonium thiocyanate (Laciak and Pez, 1988, Bhown and

Cussler, 1991) and perfluorosulfonic acid (Timashev et al, 1991, He and Cussler, 1992, Tricoli and Cussler 1995). These membranes have been shown to be highly selective for ammonia and present promising performance characteristics. However, they are unable to withstand the extreme operating conditions of the ammonia production process. A key requirement for the application of membranes for ammonia separation in the synthesis loop is for the process to be performed without substantial reductions to operating temperature and pressure. Considering the high pressure/high temperature system of ammonia manufacture, polymeric membranes would be destroyed without some cooling of the gas and are therefore unsuitable in practice.

On the other hand inorganic membranes have the ability to overcome this problem since they are potentially highly resistant to high temperatures and pressures**.** Other advantages of inorganic membranes include resistance to corrosive liquids and gases and a reasonable mechanical stability (Caro, 2011, Caro et al, 2000, Lin et al, 2002). Microporous ceramic membranes also exhibit much higher gas permeabilities than polymeric membranes, although they tend to exhibit much lower selectivities. The situation is changing however with improved membrane synthesis techniques for ceramic membranes as reported by various authors (Au and Yeung, 2001, Algieri et al, 2003, Coronas et al, 1997, Lai and Gavalas, 2000, Miachon et al, 2006). Another advantage microporous ceramic membranes have over organic polymeric membranes is the elimination of multiple gas-cooling and heating steps.

Zeolite membranes in particular have received great interest due to their excellent thermal and mechanical capabilities (Camus et al, 2006). They also have well defined sub-nanometre pores that can be tuned for size exclusion separations. Zeolite membranes have been envisioned as replacements for the costly and energy-intensive cryogenic distillation technologies used in many industrial processes today. Furthermore, the membranes could be easily and cheaply retrofitted into existing production plant designs (Freemantle, 2005). Zeolite membranes are capable of separating compounds through molecular sieving, selective adsorption and differences in diffusion rates (Vroon et al, 1996, Coronas et al, 1997 & 1998, Keizer et al, 1998) and therefore can separate different types of mixtures. Indeed, these qualities of zeolite membranes have led to the development of Na-A zeolite membranes being used

industrially for the dehydration of bioethanol fuel in a pilot plant in Japan (Caro, 2011, Iwamoto and Kawamoto, 2009). This progress in the development of zeolite membranes is promising and it is envisioned that there will be more industrial applications in the future.

MFI (Silica and ZSM-5) zeolite membranes have been popular as they have small pores of about 0.55nm that make them suitable for many industrial gas separations. These membranes have been widely studied and show a lot of promising results that have been presented in gas separation publications (Noack et al, 2002, Miachon et al, 2006). Zeolite membrane structures typically consist of zeolite films laid on a porous support that ensures mechanical strength and resistance. The membranes can be prepared on various porous supports by in situ crystallization (Davis et al, 1990), seeding and secondary growth (Xu et al, 1990), and vapour phase transport methods (Hedlund et al, 1999). In this work, zeolite membranes are used, whereby the zeolite crystals are grown within the pores of a ceramic alumina substrate until blocking of the pore by the zeolite (pore plugging) occurs. These nanocomposite membranes have better structural properties when compared to conventional zeolite film layers and have fewer defects which give the prospect of higher selectivities (Miachon et al, 2006).

For zeolite membranes to find applications in ammonia gas separations, an understanding of the synthesis procedure, mass transport properties including factors governing separation behaviour, and the ability to predict the permeation properties through these membranes have to be prioritised (McCleary et al, 2006). Concerning the description of the transport and the separation properties of zeolite membranes, a proper understanding of the diffusion as well as of the equilibrium adsorption is needed (van den Broeke et al, 1999a). Precise modelling of the permeation and separation performance of the membrane is also required as this reduces development costs since membrane performance can be predicted, thereby reducing the amount of experimentation required.

Demonstration of the viability of a zeolite membrane in the ammonia recovery application, where the operating conditions are extremely demanding, may provide a catalyst for their much wider use in other gas separation applications. The target

performance set by the IMPRESS project is an ammonia permeance of 2.4 x 10^{-7}mol m^{-2} s^{-1} Pa^{-1} and an NH_3/H_2 selectivity >10 at 30^{o}C.

1.1 Scope of Thesis

The overall objective of the project is the development of a ceramic membrane based process for the effective separation of ammonia from the synthesis loop of ammonia synthesis plants. The driving force behind this is to reduce the energy consumption of the ammonia process by replacing the refrigeration system.

This research is concerned with the assessment of the potential of zeolite membranes as suitable materials for ammonia gas separation. The separation performance of a zeolite membrane is highly dependent on operating conditions such as temperature, total pressure and composition (van de Graaf et al, 1998). A series of experiments have been performed to evaluate the performance of a multi-channel tubular membrane for ammonia gas separation made by Pall Exekia. These studies include single and multi-component gas permeation experiments.

Adsorption characteristics of zeolite MFI membranes have the potential to determine membrane performance. Adsorbed molecules may significantly hinder the transport of non-adsorbed components across a membrane. The effects of this phenomenon on the multi-component permeation of the $NH_3/H_2/N_2$ system are investigated and a mathematical model that describes this hindering effect, the potential barrier model, is applied.

These results will not only provide essential data for the application of zeolite membranes in the ammonia separation process, but also an improved fundamental understanding of multi-component transport in nanocomposite multi-channel tubular membranes.

1.2 Thesis Structure

The thesis has been divided into seven chapters, including this one. Chapter 2 discusses the different separation methods in relation to ammonia separation and provides background information on related and published research on membranes for gas separation. A discussion of membrane transport mechanisms as well as membrane applications is given. A critical review of past work in ammonia separation using membranes is also presented in relation to the current status of ammonia production. This chapter closes with a clear statement of the aims and objectives of the current research. Chapter 3 concentrates on MFI zeolite membranes and their structure. Membrane synthesis and quality criteria are also discussed. Chapter 4 contains a detailed description of the experimental methods used to analyse the membrane performance. Chapter 5 presents the permeation results obtained by the methods described in Chapter 4. Mathematical methods used to analyse these results are also presented here. In Chapter 6, the effect of adsorption on the ammonia separation system is investigated using a potential barrier model and the applicability of this model to describe the hindering effect of strongly adsorbed ammonia on the permeation of weakly adsorbed hydrogen and nitrogen is discussed. The thesis summary, conclusions and suggestions of future work are finally presented in Chapter 7.

CHAPTER 2

LITERATURE REVIEW

2.0 Introduction

This chapter introduces ammonia gas separation and the importance of replacing the energy intensive method currently in use in commercial processes. Relevant literature on gas separation methods, the issues surrounding them and hence the benefits of replacing these methods with a membrane separation system are discussed. Different types of membranes that can be used in this process are also reviewed. MFI zeolite membranes are presented as being a suitable membrane for ammonia gas separation. Finally, the chapter concludes with a statement of the aims and objectives of the current research described in this thesis.

2.1 Ammonia Gas Separation

A number of industrial processes require the separation of ammonia from its mixture with other gases. These include the separation of ammonia from gas streams in the manufacture of acrylonitrile, from methane, carbon monoxide, air and from HCN in the Andrusow process for the manufacture of HCN (Laciak and Pez 1988). This thesis however is concerned with the largest scale separation which is the separation of

ammonia from hydrogen and nitrogen in ammonia synthesis plants. Currently, this separation is accomplished by refrigeration, with ammonia being removed in the liquid state. In other operations such as in petroleum refineries and other related industries, ammonia is removed by steam stripping.

In a typical ammonia plant, an approximately 3:1 mixture of hydrogen and nitrogen (with some Ar and CH_4) is compressed to about 206 bar and passed through a catalytic converter resulting in about 13% conversion to ammonia. The product stream is subsequently cooled, ultimately by refrigeration, to condense most of the ammonia and the remaining mixture of NH_3, N_2 and H_2, Ar and CH_4 is reheated and recycled through the reactor. This process however, is not energy efficient and significant savings in power and capital could be achieved by avoiding or reducing the extent of the refrigeration step.

Various attempts have been made to develop a more efficient and practical system for the selective removal and recovery of ammonia. The replacement of the refrigeration system with an energy efficient system has been proposed by several groups and include both adsorption and absorption processes. These are described in the next sub-section.

2.1.1 Ammonia Separation using Absorbents and Adsorbents

The separation of ammonia using sorption processes has been studied widely. A number of organic polymer systems have been shown to sorb ammonia from gaseous mixtures. Cation exchange resins in hydrogen or other forms have been shown to exchange ammonia reversibly. The use of cation exchange resins in the ammonium form (NH_4^+) for ammonia absorption has been suggested by Prokop and Setinek, (1974). Another example is given by Lochmuller et al (1985) who have reported the use of Co^{2+} ion exchanged Nafion (available in the Na^+ form from DuPont) as a reversible sorbent for ammonia. In their pursuit to find an ammonia absorbent other than water, Foote and Hunter (1920) showed that ammonia could be sorbed by ammonium thiocyanate and suggested the possibility of its use in the removal of

ammonia fom the recycle loop in an ammonia synthesis plant. Additionally, Rice and Busa (1974) disclosed the use of solutions of ammonuim diacid phosphate as selective, reversible sorbents for ammonia (Pez and Laciak, 1984).

Aluminosilicate zeolites and high surface area carbons have also been widely studied as ammonia sorbents. It should be noted that most of these are processes described in patents, rather than scientific papers or industrial applications. Doshi (1978), for example, described a process for ammonia adsorption from an ammonia synthesis loop using activated carbon. A pressure swing adsorption (PSA) process with four adsorbers was disclosed and the adsorbers were regenerated using some of the cleaned purge gas. Lavie (1985) disclosed a process that utilises granular activated carbon for the separation of ammonia from the mixture of gases present in the recycle loop of an ammonia plant.

Talu (1992) combined adsorption and absorption to increase sorption capacity for ammonia. In this patent, the use of an activated adsorbent bed of porous carbon particles with steam to form a moisture film accompanied by liquid adorption is suggested. This is followed by the absorption of a portion of the ammonia in the liquid medium, while adsorbing a further portion of the ammonia in the adsorbent particles to provide increased sorption capacity. Desorption of the adsorbed and absorbed ammonia enable recovery of ammonia as an aqeuous solution. Isalski (1981) proposed ammonia and hydrogen recovery from the purge gas of an ammonia synthesis recycle stream by adsorbing from the purge gas and providing the regeneration gas for the ammonia adsorber from the hydrogen gas stream obtained from separating the hydrogen by cryogenic partial condensation. The ammonia adsorber could employ any suitable adsorbent in the adsorbent zones e.g activated carbon, or, preferably molecular sieves.

Speth (2003) claims an improved ammonia synthesis process by recovering the ammonia in purge gas with an adsorption agent operating at full syn-loop pressure. Suggested suitable materials are solid zeolites or materials forming complexes with ammonia such as Ni, Co, Cu or Zn which can be in the form of sulphides typically in

a carrier e.g alumina, although the only material tested in this patent was Y/SiO_2-Al_2O_3. Successful adsorption of ammonia was achieved.

Helminen et al (2000, 2001) also recognised the need to replace energy intensive cryogenic distillation in ammonia separation from gas streams in ammonia manufacture and suggested replacing it with a PSA process.. Extensive studies of ammonia adsorption were carried out on zeolite, alumina, silica gel, and activated carbon at 298K-393K and pressures below 100kPa to find which sorbent worked best. Ammonia was adsorbed most strongly on the 13X and 4A zeolites which are favourable for ammonia separation. However, regeneration becomes a difficult task. Although activated carbon had the highest working capacity, it rapidly dropped with an increase in temperature. Silica gel and alumina showed low working capacities. 13X and 4A zeolites had a lower capacity than activated carbon, but showed the same working capacity over the entire temperature range. It was therefore concluded that activated carbon could be used at 298K for an an industrial ammonia PSA sorbent and that since the zeolites had stable capacities over the temperature range tested, could be used in processes where the feed was hot. The zeolites were also found to have the ability to separate ammonia at very low concentrations.

Absorption and adsorption processes have various disadvantages however. Absorption, which can be used on small and intermediate scales for ammonia separation suffers from difficult operability, high investement costs and loss of absorbing solutions due to degradation (Helminen et al, 2000). The problems with adsorption arise from the capacity, selectivity and regeneration of the adsorbents. As ammonia is adsorbed strongly on most sorbents, regeneration of the adsorbent is crucial. Therefore regeneration could be energy intensive. These issues have accordingly driven research interests towards membrane separation processes.

2.2 Membrane Technology

Due to high energy prices, energy efficiency and energy saving have become important components of government policy globally (Daramola et al, 2012). As energy costs rise, the development of membranes is considered an important task in the introduction of new energy saving and environmentally friendly technologies. Membrane technology is therefore currently one of the most innovative and rapidly growing fields across science and engineering. In the last 20 years, membrane gas separation technology has developed into a $150million/year business (Baker, 2002). Membrane separation processes are attractive as they are considered environmentaly friendly, simple, versatile and have a low energy consumption. Conventional technologies such as cryogenic distillation, adsorption and absorption, in addition to the limitations discussed earlier, require a gas-to-liquid phase change in the gas mixture that has to be separated. This phase change adds significant energy costs to the separation cost. Membrane gas separation, on the other hand, does not require a phase change (Wenten, 2002). An overall comparison of the four relevant gas separation technologies is given in Table 2.1.

This thesis is focused on the development of a ceramic membrane and process for cost effective recovery of ammonia in ammonia synthesis plants. A reduction of the energy consumption in the process of ammonia production by eliminating the current refrigeration system would bring great benefits to the manufacture of ammonia and fertilizers.

Table 2.1: Advantages and disadvantages of gas separation technologies

Gas Separation Technologies		
Technology	Advantages	Disadvantages
Adsorption	High purity	Lower recovery Low efficiency Requires adsorbent regeneration
Absorption	High recovery	Complex process Many stages of operation
Cryogenics	High purity	Complex operations Energy intensive
Membrane	Good for bulk separation Low capital cost Simple process Energy efficient Low maintenance	Membrane design is complex Moderate product purity

2.2.1 Definition of a Membrane

A membrane can be described as a selective barrier between two phases that has the ability to separate gases or liquids with the aid of a driving force. This driving force, a difference in chemical potential, could result from differences in total pressure, partial pressure, concentration or electrical potential (Mulder, 1996). Membranes can also be classified by their morphology or structure, since membrane structure determines the separation mechanism, and hence the application (Mulder, 1996). This is discussed in more detail in section 2.3.

2.2.2 Membrane Nomenclature

Performance and efficiency of membranes are usually measured in terms of flow (or flux) through the membrane and membrane selectivity towards mixtures. The terms feed, retentate, permeate, flux and permeance are commonly used in membrane science. The feed is the stream that is fed into the membrane for separation and the retentate is the flow rejected by the membrane. The permeate is described as the flow passing through the membrane. Fluxes and permeances may be based on mass, molar or volumetric flows. The flux of a species J_i is defined as flow through the membrane per unit area and the permeance $\prod$ can be calculated from the flux by dividing by the partial pressure gradient ΔP_i:

$$\Pi_i = \frac{J_i}{\Delta P_i} \qquad \textbf{2. 1}$$

The permeance ratio (ideal selectivity or permselectivity) is commonly used to describe the performance of a membrane. This quantity is calculated from single gas permeances, measured at certain experimental conditions such as room temperature, using:

$$\alpha_{i/j} = \frac{\Pi_i}{\Pi_j} \qquad \textbf{2. 2}$$

The permeance ratio should not be confused or compared with the separation factor or separation selectivity, of a mixture. The selectivity is a measure of the difference in permeabilities i.e, the relative ease with which species can permeate, of different components. In other words, it is a measure of the membrane separation effectiveness. This separation factor $\beta_{i/j}$ of two components i and j in a mixture is defined as:

$$\beta_{i/j} = \frac{y_i / y_j}{x_i / x_j} \qquad \textbf{2. 3}$$

where y_i and y_j are the fractions of components i and j in the permeate and x_i and x_j are the fractions of the components i and j in the feed and are usually chosen so that the selectivity factor is greater than unity. If the separation factor is equal to one, there is no separation. The higher the separation factor, the more selective the membrane is towards certain species.

2.2.3 Membrane Performance

The selection of a gas separation membrane is largely determined by three parameters. The first is the permeate flux or permeability which determines the membrane area required. The second is its selectivity towards the gases to be separated. The selectivity affects the percentage recovery of the valuable gas in the feed. The third parameter is related to the membrane stability or service life, which has a strong impact on the replacement, and maintenance cost of the system (Ismail and Lai, 2003).

A major challenge is to achieve high selectivity while retaining the productivity (permeability). In addition, a superior membrane must be able to maintain its separation properties and durability in a complex and rigorous environment (Tin et al, 2003). Traditionally, there has been a trade-off between selectivity and permeability; highly selective membranes tend to exhibit less permeability and vice versa (Ismail et al, 2002). Membranes with higher permeability lead to higher productivity and lower capital costs, whereas membranes with higher selectivity lead to more efficient separations, higher recovery and lower power costs (Koros and Mahajan, 2000). Membranes that display simultaneously high values of selectivity and permeability would lead to the most economical gas separation processes. Numerous studies and efforts have therefore been centred on the development of high performance membranes for gas separation processes (Caro et al, 2000, Koros and Mahajan, 2000, Arruebo et al, 2001, Ismail and Lai, 2003, Bonhomme et al, 2003, Algieri et al, 2003, Camus et al, 2006).

2.3 Types of Membranes

As a first classification, membranes can be divided into biological and artificial membranes. Biological membranes are beyond the scope of this thesis and will not be discussed. Artificial membranes can be modified natural materials or synthetic (man-made). Synthetic membranes can be further divided into organic and inorganic membranes.

2.3.1 Organic Membranes

Organic membranes can be divided into two sub-groups: liquid and polymeric membranes. A liquid membrane is simply a thin film of liquid that is immiscible with the liquids on the retentate and permeate sides (Basu et al, 2004). The liquid film may either be self-supported or supported by a porous material that contains the liquid membrane. The membranes used in most commercial applications are polymeric solution-diffusion types. Polymeric membranes tend to be more economical than other materials and thus dominate traditional gas separations. The low cost of polymeric membranes results from their ability to be easily spun into hollow asymmetric fibers or spiral wound modules, due to their segmental flexibility and solution processability (Koros, 2002). Hollow fiber configurations are particularly popular in large scale industrial applications due to the high surface areas that can be obtained and the relatively low cost of manufacture (Bernado and Clarizia, 2013, Freemantle, 2005).

Examples of commercial polymeric membranes are the MEDAL and PRISM membranes produced, respectively, by Air Liquide and Air Products for wide-ranging gas separation applications (Stookey, 2005). Each device contains thousands of fibers. Indeed, an analysis of the history of polymeric membranes shows that it was the use of the PRISM process for hydrogen recovery in ammonia plants in the 1980s that provided the catalyst for the development and wider use of gas separation polymeric membranes (Baker, 2002, Bernado and Clarizia, 2013).

Generally, polymeric membranes are fabricated from organic polymers of varying molecular weight and cross-linking of the polymeric chains. Polymers commonly used are, among others, cellulose acetate, fluorocarbon polymers and aromatic polyamides. The preparation methods for polymeric membranes include sintering, stretching, phase inversion and sol-gel processes (Mulder, 1996, Ismail et al, 2002). Unfortunately, the efficiency of polymeric membranes decreases with time due to fouling, compaction, chemical degradation and thermal instability (Pandey and Chauhan, 2001, Bernardo and Clarizia, 2013). Compaction which is a decrease in membrane thickness over time, is often experienced in gas separation with polymeric membranes sometimes with disastrous results. Compaction and plasticization are simultaneous and competing effects in some applications. Plasticization usually leads to swelling and an increase in the permeability of glassy polymers (Freemantle, 2005). In addition to this, the limited thermal stability and susceptibility to abrasion and chemical attack have meant that polymeric membranes have not found an application in separation processes where hot reactive gases are encountered. Progress has been made recently with the introduction of free volume polymers that provide very high permebilities. Perfluoropolymers composite membranes are produced by MTR for CO2 separation with improved resistance to contaminants (Baker and Lokhandwala, 2008). Polymers with intrinsic microporosity (PIM) have shown exceptional transport properties. Although polymeric membranes continue to dominate the market because of their relatively low costs and ability to be used in a variety of applications, polymer-based membranes are increasingly facing competition from inorganic membranes which are less likely to foul (Bernardo and Clarizia, 2013).

2.3.2 Inorganic Membranes

Inorganic membranes are increasingly being explored to separate gas mixtures. Although more expensive than polymeric ones, they usually have much higher gas fluxes. They also have a well-defined pore structure in addition to their strong chemical, thermal and mechanical properties (Pandey and Chauhan, 2001). An inorganic membrane system generally consists of a macroporous support

providing mechanical strength for an overlying thin, either dense (non-porous) or porous separation membrane (Tsai et al, 2000). Their advantageous characteristics have encouraged many researchers to investigate the gas separation properties of inorganic membranes. Some studies have extended to inorganic membrane reactors (Salomon et al, 2000, Barbieri et al, 2002)

The two major categories of inorganic membrane are based on their structure. They can be identified as being either dense (non-porous) or porous. Figure 2.1 shows a breakdown of the different types of inorganic membranes. Dense membranes made of palladium and its alloys (Meinema et al, 2005), silver, nickel and stabilized zirconia have been used or evaluated mostly for separating gaseous components. Application of dense membranes is primarily for highly selective separation of hydrogen and oxygen; transport occurs via charged particles. Group V metals i.e vanadium (V), niobium (Nb) and tantalum (Ta) have the highest hydrogen permeability (Al-Mufachi et al, 2015). Vanadium in particular has the fastest transcrystalline hydrogen transfer and is therefore considered the most suitable material for hydrogen separation (Alimov et al, 2014). However, these group V metal membranes readily form oxide layers which severly hinder hydrogen dissociation and solubility (Al-Mufachi et al, 2015). Palladium (Pd) does not suffer from this and is considered a suitable alternative as a dense metal membrane. Membranes based on palladium are extensivley investigated as they are highly permeable to hydrogen (Li et al, 2015). Pervoskite membranes are also of the dense inorganic type and are selective for oxygen (Meinema et al, 2005). However, dense membranes have limited industrial application due to their low permeability compared with their porous inorganic counterparts. As a result, the commercial inorganic membrane market is currently dominated by porous membranes (Ismail and David, 2001).

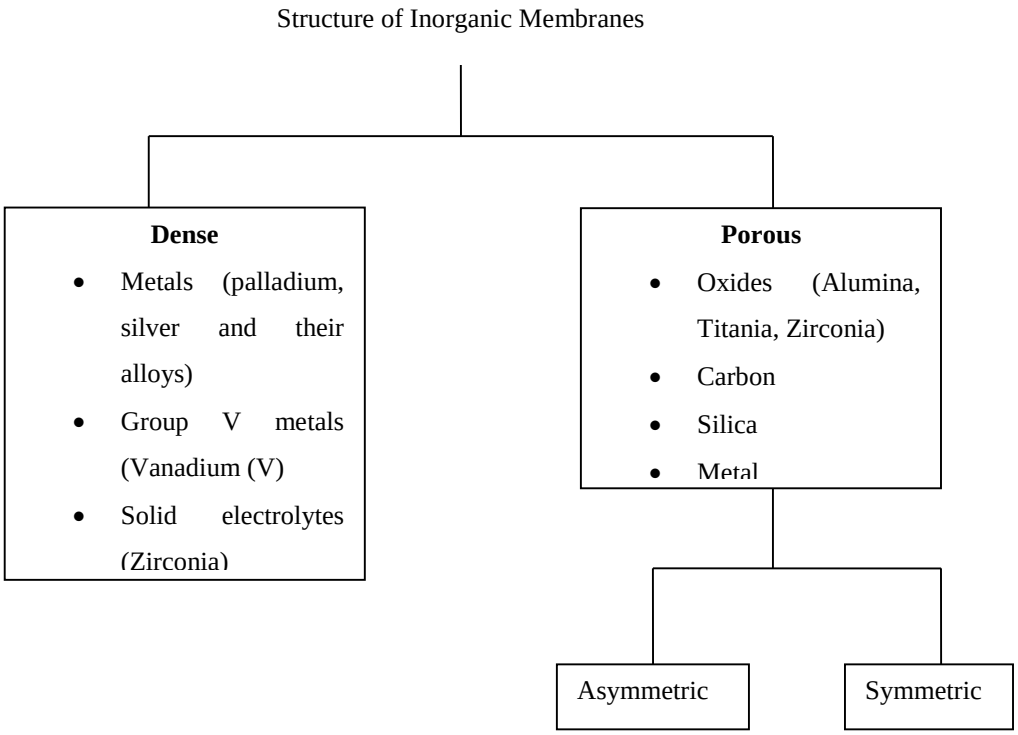

Figure 2.1: Structure of inorganic membranes (Adapted from Ismail and David, 2001)

2.3.2.1 Porous Inorganic membranes

The development of porous inorganic membranes dates from before 1945. The first porous inorganic membranes were developed for the separation of uranium isotopes, mainly used for military purposes or nuclear applications (Keizer and Verweij, 1996). Non-nuclear applications of inorganic membranes started at the beginning of the 1980s with Membralox produced by Ceraver (now Pall Corporation), Carbosep produced by SFEC (now ORELIS environment) and Ceraflo produced by Norton (now Ceraflo Pte Ltd) (Soria, 1995, Luque et al, 2008). The potential of inorganic membranes was not widely recognized until high quality porous ceramic membranes were produced for industrial usage on a larger scale (Ismail and David, 2001).

At present, interest lies in the development of porous inorganic membranes that provide better mechanical strength, thermal stability and organic solvent resistance than polymeric membranes and focus has been placed on materials that exhibit molecular sieving properties. Most of the research for gas separations is based on

silica, zeolites or carbon (Fuertes and Centeno, 1998, Ismail and David, 2001). These materials have the potential to push the upper boundary of the permeability versus selectivity trade-off relationship. Other examples of porous inorganic membranes are titania, glass and porous metals such as stainless steel and silver. Although these latter membranes are often characterised by high permeabilities but low selectivities (Caro, 2011, Pandey and Chauhan, 2001,) they, nonetheless, offer excellent potential for gas separations in process industries where operating conditions can be rather severe (Yang et al, 1999). Additional research for gas spearation has been metallic organic framweorks (MOFs), although strictly speaking these are organic-inorganic hybrids.

Porous inorganic membranes with pores of more than 0.3nm usually work as sieves for large molecules and particles. Glass, metal, alumina, zirconia, zeolite and carbon membranes are commercially used (Verweij, 2003, Soria, 1995). Other inorganic materials such as cordierite, silicon carbide, silicon nitride, titania, mullite, tin oxide and mica have also been used to produce porous inorganic membranes. The membranes vary greatly in pore size, support material and configuration and can be further classified according to the IUPAC classification of:

- Macroporous with $d > 50nm$
- Mesoporous with $2 < d < 50nm$
- Microporous with $d < 2nm$

where d is the pore diameter.

Accordingly, microporous membranes consisting of materials such as zeolites, carbon or amorphous silica with connected pores of sub nanometre dimension, can act as adsorption sites for small molecules. The size and adsorption characteristics of the micropores has led to high selectivities combined with reasonably high fluxes. Application examples include isomer separation such as p-xylene from o-xylene, separation of H_2 or CO_2 from bigger molecules and H_2O from reaction mixtures (Verweij, 2003). Microporous membranes are usually prepared as thin films on porous inorganic supports that provide the mechanical strength. The

thickness of the microporous film varies from a few tens of nanometres to a few microns (Lin et al, 2002).

The most common geometries of microporous inorganic membranes are discs and single-tubes. Hollow fibers and flat sheet geometries have also been reported (Lin et al, 2002, Luque et al, 2008). Disk-shaped membranes have limited area, however, and keeping the disks sealed inside the membrane module at the high temperatures at which membranes operate is a problem. Hollow fibers possess much larger membrane area per unit volume (Freemantle, 2005).

Commercial inorganic membranes now currently consist of three configurations: disks, tubes and multichannels/honeycombs. From an industrial point of view, tubular membranes are more suitable than plates or discs because tubes are easier to scale up than flat membranes. The multichannel monolith configuration is a great technical progression from single-tube or tube bundle geometry as it potentially offers high-mechanical strength and a higher membrane packing density (Soria, 1995).

2.4 Types of Porous Inorganic Membranes

This section concentrates on carbons, silicas and zeolites as these types of membrane have shown the most promising results in terms of application to gas separation and have consequently been studied the most. They offer excellent separation properties through various mechanisms including preferential adsorption, selective configurational diffusion or molecular sieving (Lin et al, 2002). More recently, focus has been on metallic organic frameworks (MOF's) which are considered to be an organic-inorganic hybrid that have similar properties to zeolites (Caro, 2011) and they are also discussed in this section.

2.4.1 Carbon Membranes

Carbon membranes have received great attention for gas separations ever since Koresh and Soffer (1986) successfully prepared molecular-sieving materials. In addition to being chemically and thermally stable when compared to polymer membranes, carbon membranes are also more selective. The pore system of a carbon membrane generally consists of wide openings with narrow constrictions. Separation is thereby made possible by passage of the smaller molecules of a gas mixture through the pores and hindering of the larger molecules and is known as molecular sieving (Ismail and David, 2001).

Carbon membranes can be produced by pyrolysis of a suitable polymeric precursor (e.g polyimide, polyfuryl alcohol, polyvinylidene chloride and phenolic resins) under controlled conditions (Saufi and Ismail, 2004). Molecular carbon sieves in particular are normally prepared using this method.This type of membrane can also be transformed into an adsorption-selective membrane by the carbonisation of a phenolic resin film with a short time air oxidation prior to or after carbonisation (Meinema et al, 2005).

The two major types of carbon membrane that have been developed are:

- Molecular Sieve Carbon Membranes (MSCMs): These contain pores that approach the molecular dimensions of the gases (<0.4 nm) and exhibit selectivity according to the size and shape of the molecules. They can separate gas molecules with a similar size (O_2-N_2, CO_2-N_2, CO_2-CH_4, etc).

- Adsorption Selective Carbon Membranes (ASCMs): These perform by firstly selective adsorption of certain components of the gas mixture on the pore surface followed secondly by surface diffusion of the adsorbed molecules across the membrane.

The difference between the structure of ASCMs and MSCMs involves the micropores. ASCMs have a carbon film with the micropores slightly wider than

MSCMs, in the range 0.5-0.7nm (Ismail and David, 2001). These are able to separate non-adsorbable or weakly adsorbable gases such as H_2 and N_2 from adsorbable gases like hydrocarbons (Rao and Sircar, 1993, Fuertes, 2000, Centeno et al, 2004).

A major drawback of carbon membranes is that the cost per unit area is reported to be between one and three orders of magnitude higher than for polymeric membranes. Hence, an important challenge faced by carbon membrane technology is to find a more economic material than those currently used, namely polyamides, cellulose acetate and PFA (Centeno et al, 2004). Carbon membranes can be brittle and fragile and require very careful handling, although this problem could be avoided to a certain degree by optimising precursors and preparation methods. Nonetheless it is difficult to process and expensive to fabricate carbon membranes (Ismail and David, 2001). Carbon membranes also require a very fine control of the pore sizes and require operation at an elevated temperature in order to provide acceptable fluxes for smaller molecules due to their membrane thicknesses of several microns (Rao and Sircar, 1993). Despite these disadvantages, carbon membranes have found use in a large scale application, namely in the production of low cost and high purity nitrogen from air. Other separations include separation of hydrogen from gasification and purification of methane.

2.4.2 Silica Membranes

Silica membranes have been available for more than a decade and can be used in many applications such as gas separations, liquid separation and pervaporation. Porous silica membranes with tunable pore sizes can be used potentially in a large range of gas separations. Two main types of silica membrane have been reported in the literature: those derived by sol-gel techniques (Tsai et al, 2000, Ayral et al, 2008) and those derived by chemical vapour deposition (CVD) (Gavalas et al, 1989, Ayral et al, 2008, Li et al, 2015a).

Microporous silica membranes have shown promising molecular sieve characteristics by several research groups (Li et al, 2015a). However the improvement of membrane performance (flux and selectivity), processibility, and stability remains a challenge (Tsai et al, 2000). The quality of the underlying support determines, to a large degree, the properties and the quality of the selective microporous silica membranes. These membranes are highly selective for hydrogen and CO_2 in mixtures with methane. They are therefore useful for purification of methane or for the recovery of hydrogen with particular emphasis for high temperature industrial hydrogen separation and purification (Meinema, 2005). Tsai et al (2000) studied the separation of CO_2 from a 50/50 (v/v) CO_2/CH_4 gas mixture, and for hydrogen separation from a simulated reformate gas under low temperature conditions. The dual layer microporous silica membranes reported in this study displayed high separation factors (α CO_2/CH_4 = 200-600) which was much higher than in previous studies.

Silica has long been known to exhibit reversible CO_2 adsorption at room temperature. In a study by Yildrim and Hughes (2003), a silica based composite membrane was used to determine the permeability of CO_2. It was found that the main mechanism of gas transport through a silica coated α-Al_2O_3 membrane was by Knudsen diffusion.

Although silica membranes have good gas separation properties, they suffer from water sorption sensitivity at room temperature due to the hydrophilic nature of the silica surface. Sorption of moisture for instance from air, can result in pore blocking with a large consequential impact on separation properties. Interaction of the membrane with water from process streams at higher temperatures can result in serious degradation. Because the industrial gas separations generally involve wet gas streams, the lack of stability at high temperatures especially in the presence of steam has been the main problem that prevents the large scale application of microporous silica membranes. High temperatures and humid conditions accelerate the condensation of silanol groups in the silica layer which causes the embrittlement of the silica layer and results in a decrease in gas permeance. Many

groups have therefore prioritised the development of silica membranes that are hydrothermally stable (Meinema et al, 2005, Li et al, 2015a).

De Vos et al (1999) prepared hydrophobic membranes by incorporating methyl groups. The membranes were ten times more hydrophobic than the best silica membranes, easier to handle and showed less deactivation than hydrophilic materials. This made them more suitable for applications in humid process streams. Campaniello et al (2004) also showed that incorporating methyl groups in microporous silica considerably enhances the service time in the dehydration of a butanol-water mixture. It has been suggested that alumina (3%), zirconia (10-70 mol%) or titania may be added to silica to increase the stability of the composite in high humidity environments (Morooka, 1999). Camus et al (2006) used silica membranes for the separation of ammonia from a $NH_3/H_2/N_2$ mixture. Two different silica membranes were used for comparison, one being a pure silica membrane and one a methylated silica membrane prepared from the recipe of Campaniello et al (2004). The results confirmed that for the $NH_3/H_2/N_2$ separation, the performance of a methylated silica membrane was better than a standard silica one.

Wei's group incorporated hydrophobic organic groups into the silica structure to deal with the instability of silica membranes (Wei et al, 2008 & 2014). Fluoro-carbon and perfluorodecyl were successfully incorporated into silica layers using sol-gel techniques. The modified silica membranes were transformed from hydrophilic to hydrophobic membranes. However, the membranes are only hydrothermically stable below the decomposition temperature of organic groups (Li et al, 2015a).

Another option to improve stability of pure silica membranes is by doping them with metal (Wang and Tsuru, 2011). A popular approach is to incorporate metal and metal oxide nanoparticles into the silica matrix. These metal doped silica membranes have been developed for high temperature wet gas separation processes (Li et al, 2015a). It is suggested that the incorporated nano particles might reduce the thermal-induced molecular motion of microporous silica

networks at elevated temperatures. These metal additives not only improve hydrothermal stability, but also enhance separation performance of silica membranes at high temperature. Specifically for hydrogen separation this enhanced separation is attributed to reversible hydrogen adsorption properties of metal and metal oxide nanoparticles (Battersby et al, 2009, Smart et al, 2012). Da Costa's group has successfully prepared hydrothermally stable silica membranes by embedding them with cobalt oxide (Co) (Smart et al, 2012, Wang et al, 2013, Ji et al, 2015). These membranes demonstrated good hydrothermal stability. Tsuru's group developed Nickel oxide (Ni) silica membranes (Kanezashi and Asaeda, 2005 & 2006). These Nickel doped membranes showed steady permeances for He and H_2 even after being kept in steam at 500^{o}C for 6 days. They have also developed a binary Iron (Fe)/Cobalt (Co) oxide silica membrane by sol-gel synthesis (Darmawan et al, 2015). The binary metal oxide and silica interfaces followed a molecular sieving mechanism characterised by activated transport where the permeance of the smaller gas molecules (He and H_2) increased with temperature up to 500^{o}C, whilst the permeance of larger gas molecules (CO_2 and N_2) decreased.

2.4.3 Zeolite Membranes

Zeolites are crystalline metal oxides containing micropores with a well-defined pore structure. These structures contain aluminium, silicon and oxygen in their regular framework. The zeolite framework consists of an assemblage of SiO_4 and AlO_4 tetrahedra, joined together into secondary polyhedral building units such as cubes, hexagonal prisms, octahedral and truncated octahedral forms (Ruthven, 1984, Yang, 1987). Since each oxygen is shared between tetrahedral Al or Si atoms, the stoichiometric composition of each tetrahedral unit is SiO_2 or AlO_2. The final zeolite structure consists of assemblages of the secondary units in a regular three dimensional crystalline framework (Yang 1987). The zeolite pores are made from rings in the framework and are designated by the number of oxygen atoms making up the ring (Bowen et al, 2004). Zeolites can be classified into small pore (i.e. 0.3-0.4nm with 6- and 8-membered rings), medium pore (i.e. 0.5-0.6 nm with

10-membered rings) and large pore (i.e. 0.7-0.8 nm with 12-membered rings). An example of each type of framework using ball and stick representation is shown in Figure 2.2.

Zeolites are commonly identified using a three letter code that has been assigned to confirmed framework types by the structure commission of the International Zeolite Association. This is done according to rules from an IUPAC commision of zeolite nomenclature (Bekkum et al, 2007). MFI zeolite, which was first developed by Mobil Research Development company in the early 1970's, is the IZA structure code for ZSM-5 (Zeolite Secony Mobil) and silicalite-1 (Szostak, 1998). Topological codes of some well know zeolites and their common names are displayed in Table 2.2.

Table 2.2: Topological codes and common names of zeolites (Szostak, 1998)

Topological Code	Common Name
CHA	Chabazite
FAU, X, Y	Faujasite
FER	Ferrierite
LAU	Laumontite
LTA	Linde Type A
MFI	ZSM_5 or Silicalite-1
MOR	Mordenite

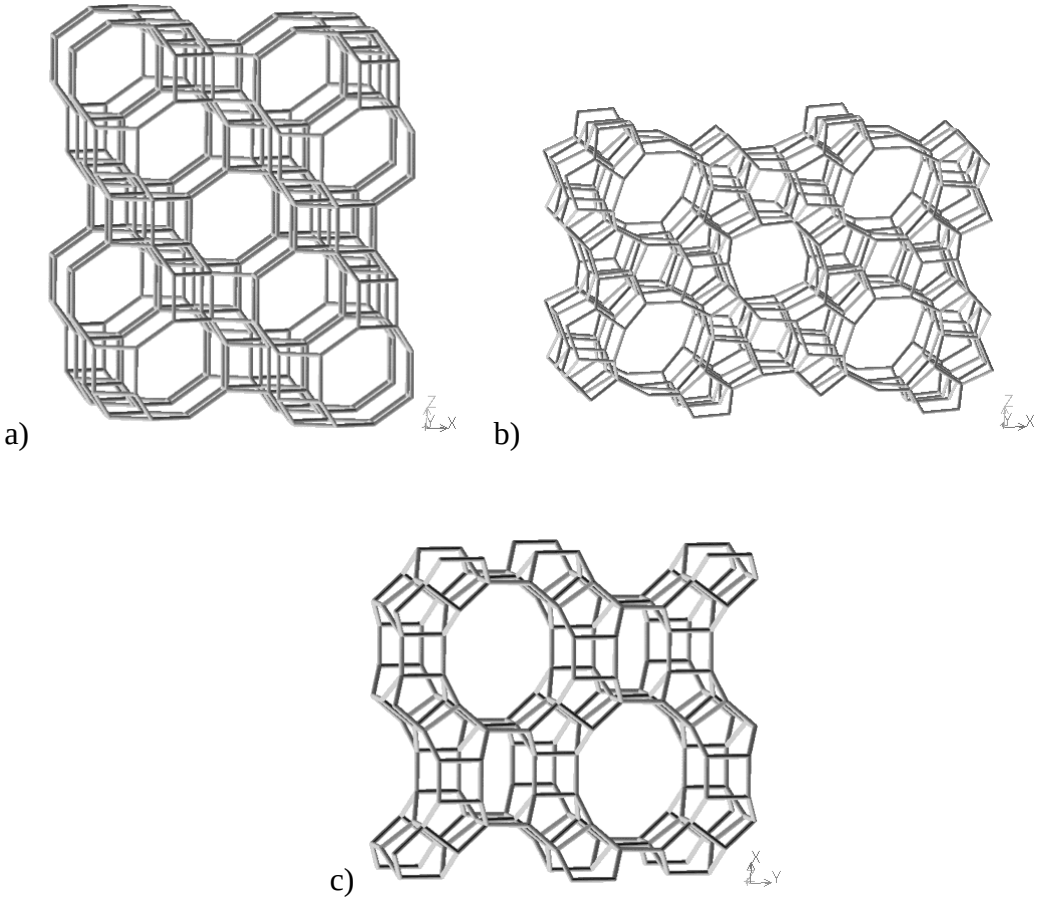

Figure 2.2: Atomic stick representations for the frameworks of a) CHA, b) MFI and c) MOR.

Traditionally, zeolites have been used as catalysts and adsorbents. However, continuous polycrystalline zeolite layers have been grown successfully and used as zeolite membranes (Bowen et al, 2004, Lin and Duke, 2013). Small pore (e.g SAPO-34 and NaA), medium pore (e.g MFI) and large pore e.g (FAU) zeolites have been successfully made into membranes (Au and Yeung, 2001, Lin and Dule 2013). Using zeolites as membrane materials is particularly advantageous due to their ordered crystalline structure when compared to disordered materials such as polymers.This means that membrane properties such as selectivity can be tailored for particular applications (Skoulidas et al, 2003). Table 2.3 shows some properties of commercially available zeolite membranes.

Zeolites can also be classified according to their silicon to aluminium (Si/Al) ratio. Generally, those containing Si/Al ratios greater than 10 are referred to as hydrophobic zeolites. They are less polar and more stable to heat and acid attack than their hydrophilic counterparts. The most frequently used framework of

zeolites for research and industry are MFI, A and FAU types and more focus has been drawn towards the synthesis of MFI (Silicalite-1 or ZSM-5) (Tavolaro and Drioli, 1999, Chiang and Chao, 2001, Lin et al, 2002, McCleary et al, 2006). In type A zeolites, access to pores is restricted by eight membered oxygen rings of free aperture and their pore diameters that range from 0.3 nm to 0.43nm. They are mostly used in size selective adsorption of relatively small molecules as well as in ion-exchange applications. Also, the Si/Al ratio is approximately1.9 making them hydrophilic. The LTA membrane was the first to find commercial application in solvent dehydration (Caro, 2011, Chiang and Chao, 2001). The Faujasite (FAU) Si/Al ratio of about 1.5-3 also makes this material hydrophilic and unsuitable for use in extreme conditions (e.g. high temperatures, acidic environments etc).

There are two main methods used in the manufacture of zeolite membranes, in-situ crsytallization method and the secondary growth method. The advantage of the in-situ method is that zeolite film growth can be completed in one step. However, reproduciblity is difficult as it is not easy to identify conditions required for supersaturation. Although the secondary method requires more steps, the zeolite membrane quality can be controlled. In addition, the secondary growth method allows one to control the structure and orientation of the crystals in the seed layer to grow oriented zeolite membranes (Lin and Duke, 2013).

Zeolite membranes have attracted much attention because of their potential to achieve gas separations under steady state operation and to be combined in reaction/separation devices such as membrane reactors (Tavolaro and Drioli 1999). Generally, conventional zeolite membranes are more thermally and chemically stable than conventional amorphous microporous inorganic membranes (Lin and Duke, 2013). Many zeolites are thermally stable to over 500^{o}C. Some are stable in an alkaline environment, while others are stable in acidic media (Tavolaro and Drioli, 1999). Kita and coworkers have reported highly stable operation of ZSM-5 zeolite membranes in acidic solution (Zhu et al, 2013). Lin's group (Wang and Lin, 2012) prepared a bilayer MFI zeolite membrane that could operate stably for H_2 separation with simulated syngas feed (equal molar of H_2, CO_2, CO and H_2O) with 500ppm H_2S at 500^{o}C .

Table 2.3: Properties of commercial zeolite membranes

Type of zeolite	Pore size (nm)	Si/Al ratio	Oxygen no. at window
CHA (SAPO-34)	0.38		8
LTA (NaA)	0.43	1-2	8
MFI (ZSM-5) (Silicalite-1)	0.53 x 0.56	10-200 ∞	10
FAU (NaX, NaY)	0.74	1.5-3	12
MOR	0.70 x 0.65	5-6	12

The crystalline nature of zeolites offers the opportunity to obtain membranes with a regular three-dimensional network of micropores at the molecular scale and they are therefore able to separate mixtures of substances on the basis of differences in molecular size and shape (Caro et al, 2000), compounds with similar molecular weights and also azeotropic mixtures (Algieri et al, 2003). Also zeolite pores are uniform in size when compared to activated carbon and silica (Daramola et al, 2012). These unique properties make them invaluable in many technical applications (Vareltzis et al, 2003).

The effective pore size distribution of a zeolite membrane, and hence its separation performance, is intrinsically governed by the choice of the zeolitic phase. This applies when molecular size exclusion or sieving is dominant and no other diffusion pathways bypass the network of well-defined zeolitic channels; otherwise viscous flow through grain boundaries would prevail. As well as zeolitic polycrystalline channels, a high quality, defect free zeolite membrane may contain intercrystalline gaps (non zeolitic pores) with sizes smaller than 2nm but larger than the zeolitic pores (<1nm) (Yu et al, 2011).

Although zeolite membrane manufacture is well established, it remains challenging to grow a consistently defect-free zeolite layer on top of a porous substrate or as an unsupported phase. The existence of any defects in the layer, such as microscopic and post-synthesis macroscopic cracks, destroys the selectivity of the membrane. In addition, the optimum thickness of the zeolite film

is always a compromise between the separation performance and overall transmembrane flux. Hence thickness should be tailored to the needs of the applications envisioned (Bonhomme et al, 2003).

Zeolite membranes can be modified to improve their performance and various methods have been used by several researchers to enhance the separation properties of these membranes. In the case of microporous intercrystalline pores formed intrinsically during zeolite membrane synthesis, these gaps can be minimized or eliminated by a template free secondary growth that avoids the template removal step (Kanezashi et al, 2006). Defects have also been eliminated by a rapid calcination method that favors condenstaion of surface hydroxyl groups on the zeolite grain boundary before template removal (Choi et al, 2009). These methods can simplify the zeolite membrane synthesis reducing the membrane costs (Lin and Duke, 2013). Other methods of post-treatment include; filling nonzeolitic pores by wet impregnation (Zhang et al, 2010), counter-diffusion chemical vapor diffusion (Kanezashi et al, 2008), or hydrolysis of organics and silica precursors (Hong et al, 2011). Post treatment methods add additional steps in membrane synthesis which adds costs (Lin and Duke, 2013).

SAPO-34 zeolite membranes with a pore size of 0.38nm have been prepared by Falconer and Noble's groups (Poshusta et al, 1998, Li et al, 2004, Hong et al, 2008, Li et al, 2010, Ping et al, 2012) for separations of light gas mixtures such as CO_2/H_2, CO_2/N_2 and CO_2/CH_4. NaA (LTA) is another type of small pore zeolite membrane (0.43nm) that has been studied mainly for pervaporation (Aoki et al, 1998, Xu et al, 2005, Kondo et al, 2010, Sorenson et al, 2011). Larger pore zeolite membranes such as NaY and NaX (FAU) have also been prepared (Kusakabe et al, 1997, Caro et al, 2009, Kumakiri et al, 2014).

The principle focus however, has been on the MFI type and this is because the pore system of this zeolite has an average pore size of 0.55 nm (medium pore size composed of 10-membered oxygen rings), which is suitable for separation of several industrially important organic molecules. MFI is also made attractive by its Si/Al ratio, which is >10 thereby making the membrane more hydrophobic, the

benefits of which have been explained above. MFI membranes can also be modified. Researchers discovered that they can improve the separation properties of MFI zeolite membranes by depositing silica in MFI zeolitic pores to reduce the effective pore size and hence improve the separation properties. Modification of MFI zeolite membranes by catalytic cracking deposition of methyldiethoxylane (MDES) has been reported in the literature (Gu et al, 2008, Tang et al, 2010, Wang and Li, 2011, Zhang et al, 2012). Selectivities of the modified membranes do improve dramatically although the permeances can decrease as the pores throughout the zeolite layer are reduced. It is important therefore that the modification process is controlled to avoid excessive deposition that can cause unacceptable loss in gas permeability. Currently, there is an increasing need for high temperature gas separation membranes that are stable in humid environments. These MDES modified MFI membranes also have better stability in high temperature humid atmospheres than molecular sieve silica membranes (Gu et al, 2008).

Separation of light gases (Hedlund et al, 1999, Van den Broeke et al, 1999, Lai and Gavalas, 2000, Bonhomme et al, 2003), close boiling hydrocarbons (Funke et al, 1996, Yang et al, 1999, Dong et al, 2000, Arruebo et al, 2001) and butane, pentane and xylene isomers (Kusakabe et al, 1997, Xomeritakis et al, 2000, Gump et al, 2000, Bernal et al, 2003, Sommer et al, 2003, Rezai et al, 2008, Tarditi et al, 2008, Zhang et al, 2012, Bayati et al, 2013) have all been reported in the literature using MFI zeolite membranes. Also a relatively large amount of information is available on their synthesis (Xomeritakis et al, 2000). These membranes have been selected for ammonia separation due to the aforementioned advantages. Accordingly a more detailed analysis of this type of membrane is therefore given later in Chapter 3.

2.4.4 Metallic Organic Framework Membranes (MOFs)

Metallic organic frameworks are organic-inorganic hybrids of crystalline structure that consist of a metal ion or cluster of metal ions linked by an organic molecule

(Caro, 2011, Zhao et al, 2013). The choice of metal and linker dictates the structure and therefore the properties of the MOF. The organic units or ligands can be either mono, di, tri or tetravalent and the metals coordination preference will have an influence on the size and shape of the pores by dictating how many ligands can bind to the metal and in which orientation (Czaja et al, 2011). This combination of organic and inorganic building blocks means that MOFs have a great flexibility in their structure, functional groups, pore sizes and porosity. As a result, MOF's have a variety of potential applications which include gas adsorption/separation, storage, catalysis and membranes (Daramola et al, 2012, Zhao et al, 2012).

MOF's have become popular in the last few years due to advances in the synthesis of nanomaterials and applications of such materials in membrane technology. They are similar to zeolites as they are crystalline porous materials with molecular dimensions, however, they are less brittle/stiff and therefore more flexible in structure. These materials are also highly porous which allows for high fluxes, and stable in extremely high temperatures (~400^{o}C) (Caro, 2011). The structure related properties of MOF's should make them good candidates for molecular sieve membranes, however, because they are structurally flexible, sharp molecular sieving is restricted (Caro, 2011).

MOF type membranes have been synthesised using the same traditional methods used to synthesise zeolite membranes. Well researched methods and techniques such as seeding, hydrothermal synthesis and use of ceramic supports as bases have been applied to the synthesis of MOF membranes (Caro, 2011). Types of MOF membranes on porous inorganic supports reported in the literature include MOF-5, H-Kust-1, MMOF, ZIFs (ZIF-7 and ZIF-8) and Mn(HCO_2) (Zhao et al, 2011). Focus has been on MOF-5 and ZIFs on supports such as alumina and silica (Gascon et al, 2012, Telfer, 2010). These membranes have a wide range of pore sizes (sometimes into the mesoporous range) which allows for the classical removal of traditional molecular separations e.g. hydrogen from other gases, removal of CO_2, separation of alkanes from alkenes, linear alkanes from branched alkanes and aromatic isomers, but would also allow for the separation of larger molecules (Telfer, 2010).

Small pore MOF membranes with a pore size <0.4nm can be effective as molecular sieves and have been prepared for the separation of small gas molecules such as H_2 and CO_2. It has been reported that high H_2 permeances up to 10^{-6} mol/(m^2.s.pa) are possible with MOF membranes which is one order of magnitude higher than that of zeolite, carbon and silica membranes (Li et al, 2015b). ZIF-7 and ZIF-8 membranes with a pore diameter of about 0.3nm and 0.34nm were grown by the seeded growth method on porous alumina supports. These membranes showed reasonable H_2/CO_2 selectivities. The synthesis of large pore MOF's with a pore size of 0.7 nm (Guo et al, 2009) have also been reported and shown to have a similar selectivity for H_2/CO_2. Zhao et al, (2012) have also prepared MOF-5 membranes by secondary growth method that offer selective permeation for CO_2 over H_2 and N_2 in CO_2/H_2 and CO_2/N_2 mixture feeds.

Because of the great intrinsic flexibility of MOFs (i.e. "gate opening"), they have the potential to be tuned for specific functions. However, this flexibility can also be a disadvantage as selectivity can be poor. For example MOF membranes still show lower CO_2/CH_4 selectivities compared to zeolites. A membrane that has a pore size of 0.34 nm can still allow a molecule of 0.38 nm to enter the pore network (Caro 2011). Recently, a ZIF-7 membrane has been shown to be able to adsorb olefins and parafins much larger than the crystallographic pore size of the structure (0.3nm). This was attributed to the "gate opening effect" due to the rotation of benzimidazole linkers in which specific threshold pressures control the rotation of the linker and therefore the uptake and release of individual molecules (reference). No sharp cut-off exists for hydrocarbons with larger frameworks, therefore selectivity is greatly reduced (Caro, 2011).

Synthesis of MOF films on porous supports can be difficult. Making continuous defect free crystalline films remains challenging and in particular, reproducibility of MOF membranes remains a formidable task due to the framework flexibility of MOF's (i.e. "gate opening"). This changing topography also means that modelling is problematic (Bux et al, 2011, Telfer, 2010). That said, the field of MOF membranes is growing rapidly and the advantages (high fluxes) and disadvantages

(low selectiveness and low reproducibility) has been identified and steps toward improvements look promising.

2.4.5 Mixed Matrix Membranes

Most membranes currently used in industry for gas separation are solution diffusion type polymeric membranes. One way of improving their separation characteristics would be to incorporate specific adsorbents such as zeolites into the polymeric matrix (Ismail et al, 2002).

A new development therefore is the formation of mixed matrix materials which consist of inorganic zeolites, carbon molecular sieves and more recently MOFs with excellent gas separation properties embedded into the matrix of a potential polymer (Caro, 2011, Ismail et al, 2002). It is suggested that mixed matrix materials have the potential to provide membranes with higher permselectivity and equivalent productivity compared with existing membrane materials (Ismail et al, 2002). Synthetic zeolite incorporation is reported to enhance the separation characteristics of rubbery polymers. The majority of the work on zeolite filled polymeric membranes utilises synthetic zeolites such as zeolite A,X,Y and silicalite-1.

Zeolite-filled rubbery polymer membranes were first investigated by Jia et al (1991, 1992). The permeation properties of various gases through poly-dimethylsiloxane (PDMS) membranes filled with silicalite-1 were studied and the permeabilities of He, H_2, O_2 and CO_2 increased with increasing silicalite-1 content while those of N_2, CH_4 and C_4H_{10} decreased. Duval et al (1993) also studied the gas separation properties of PDMS, ethylene-propylene rubber (EPDM), polychloropene (PCP) and nitrile butadiene rubber (NBR) which incorporated adsorbents. In this case, both zeolites and carbon molecular sieves were considered. Silicalite-1, zeolite 13X enhanced the separation properties of the poorly selective polymers towards a mixture of carbon dioxide/methane and this improvement increased with an increase in the volume fraction of the zeolite in the

polymer matrix. Zeolites 3A, 4A and 5A were found to be ineffective in improving the permselectivity of the rubbery polymers. Carbon molecular sieves did not improve the separation performance and this was attributed to an impervious porous structure. MOFs can also be incorporated into a polymer matrix (organic linkers couple with the polymer matrix) and have shown higher fluxes and slectivities when compared to the neat polymer (Caro, 2011, Perez et al, 2009).

2.5 Membrane Applications

There has been an increase in the number of membrane applications due to the increased efforts to achieve economical and efficient membranes, selection of new materials and improvements in membrane preparation techniques (Centeno et al, 2004).

Criteria for selecting membranes for a given application are complex. (Koros and Mahajan, 2000). Key requirements include durability, separation efficiency (selectivity) and productivity (permeation rate). However, cost is an equally important factor and must be considered in all cases (Koros and Mahajan, 2002). Ideal gas separation membranes would not only possess high permeation rates and high selectivities, but would also be thin, stable, defect free and low in cost (Baker, 2002). The membranes must also be able to maintain these requirements in aggressive environments.

Membrane applications reported in the literature are many and varied and it would be a formidable task to include all of them. Therefore, the applications selected below are those which are currently using membranes for gas separation. These membranes are mainly polymeric and are produced commercially. More than 90% of the membrane gas separation business involves the separation of inorganic gases such as nitrogen from air, carbon dioxide from methane and hydrogen from nitrogen, argon or methane (Baker, 2002). A summary of the applications is given in Table 2.4. Also included are large scale applications that currently use

polymeric membranes but which could benefit from a change to inorganic membranes such as zeolites. An excellent review of membrane applications is given by Baker (2002).

Table 2.4: Gas separation membrane application (Adapted from Ismail et al, 2002 and Stookey, 2005)

Common gas separation	Application
O_2/N_2	• Oxygen enriched air from compressed gas • Nitrogen generation from compressed air • Nitrogen enriched air from compressed air
H_2/Hydrocarbons H_2/N_2 H_2/CO	• Refinery hydrogen recovery • H_2 recovery from ammonia gas purge • CO and H_2/CO ratio adjusted syn gases • High purity hydrogen for processes
CO_2/ CH4 CO_2/Hydrocarbons CO_2/N_2 CO_2/Air	• Natural gas processing • Methane gas recovery from landfill gas and biogas • CO_2 recovery for EOR flooding • CO_2 removal from natural gas liquids • CO_2 recovery from flue gases • CO_2 separation for breathing systems
He/ Hydrocarbons He/Air	• Helium recovery and production from natural gas • Purification of air contaminated Helium
H_2S/ Hydrocarbons	• Sour natural gas processing and fuel conditioning
Hydrocarbons/ Air	• Hydrocarbons recovery • Pollution control
H_2O/ Air H_2O/Hydrocarbons	• Compressed air drying • Dehydration of natural gas • Dehydration of alcohol and solvents

One of the first large-scale commercial applications of membranes was hydrogen recovery. Separations are carried out succesfully with polymeric membranes as hydrogen has a reasonably high selectivity in most polymers when compared to other gas species (Stookey, 2005). Currently, this application competes with cryogenic, catalytic and pressure swing adsorption (PSA) processes. However,

membranes with higher selectivity and productivity as well as a developed resistance to hydrocarbons would be better suited to this application (Koros and Mahajan, 2001). This application is particularly important as hydrogen production is expected to increase due to the increase in the number of hydrogen applications e.g. fuel cells (Lin and Freeman, 2005).

Oxygen and nitrogen are the third and fifth largest bulk chemicals produced worldwide. Both gases are largely produced by the cryogenic distillation of air Currently, the major separation methods used in oxygen production are distillation (99.99% purity) and vacuum swing adsorption (95% purity) (Koros and Mahajan, 2000). Although various methods for oxygen separation from air using membranes have been investigated, none of these have achieved the level of purity required (Koros and Mahajan, 2000, Baker, 2002). For this application to be successful, higher membrane selectivities combined with equal or greater productivity are needed. Inorganic membranes have the potential to do this. Nitrogen purities of 99.5% can be economically achieved using membranes. However, transport properties of membranes currently used have not improved and better advances could be achieved with inorganic membranes (Koros and Mahajan, 2000)

Recovery of CO_2 from flue gas and natural gas is of great interest especially from the viewpoint of global warming and the energy industries. The greenhouse effect created by the accumulation of CO_2 in the atmosphere is a significant threat and continued research to efficiently separate CO_2 emitted mainly by high temperature systems is necessary (Shin et al, 2005). Polymeric membranes developed so far give relatively high CO_2 separation performances. However, they have low selectivities at higher temperatures and the plasticization effect of high CO_2 pressure and of co-existing CH_4 and other hydrocarbon vapours is a problem (Cui et al, 2004).

Besides CO_2, H_2S is often present in natural gas in appreciable concentrations. The concentration of this very toxic, highly corrosive gas has to be reduced to less than 0.2%. Removal of H_2S and CO_2 from lower hydrocarbons is essential as they can corrode pipes as well as reduce the energy content of the gas. Polymeric

membranes currently available do compete successfully with technologies such as amine scrubbing. However membranes that do not lose their productivity and have higher selectivities are required for continued growth in these markets (Koros and Mahajan, 2000).

Other applications include the separation of SO_2, CO_2 and NO_x from smoke or flue gas. Due to their relatively low concentrations at atmospheric pressure this application area is not very suitable for pressure driven operations (low driving force) but rather for membrane contactors, carrier mediated processes and membrane reactors (Mulder, 1996). These applications could sharply increase the demand for more energy-efficient, cost-effective strategies for gas separations.

A large scale application is the separation of olefins from paraffin. The current method of separation is an energy intensive distillation process with high capital costs. This separation would therefore benefit from membrane technology with its low energy consumption and simple operation (Koros and Mahajan, 2000).

Currently, several membrane applications have achieved commercial success; nitrogen production from air, hydrogen removal from ammonia purge gas, carbon dioxide removal from natural gas and in enhanced oil recovery (Bernardo and Clarizia, 2013).

2.6 Transport in Membranes

Barrer (1990) described transport through porous membranes as adsorption on the external surface, transport into the pores, intercrystalline diffusion, transport out of the pores and desorption. In general, gas transport in porous structures is more complex than non-porous systems due to the various mechanisms that work together. These mechanisms depend on the pore structure and dimensions, temperature, pressure, type of membrane and the permeating molecules.

Although non-porous membranes have shown very high selectivities for the separation of certain components of a gas mixture, the rates of transport (i.e the fluxes) of the gases through the membranes are usually very low. This is due to the solution-diffusion or solution-reaction mechanisms of transport, as explained below.

Porous membranes on the other hand can generally provide very high rates of transport for gases, but they exhibit relatively lower separation selectivity, although the situation is changing as seen in the growing number of publications and reviews (Rao and Sircar, 1993, Poshusta et al, 1999, Tavolaro and Drioli, 1999, Caro et al, 2000 &2005, Gardener et al, 2002, Bonhomme et al, 2003, Xing et al 2004, Camus et al, 2006). Membranes discriminate between molecules through differences in their rates of diffusion due to surface and configurational interactions. Configurational interactions are achieved when the pore size, or free volume, in a rigid matrix is small enough to differentiate between molecules, based on shape and/or size. Surface interactions determine the amount of pore loading and surface flow that act in parallel with other transport mechanisms. (McCarley and Way, 2001)

2.6.1 Mechanisms for Gas Separation

The main mechanisms for separation of a gas mixture through a porous membrane Knudsen diffusion, poiseuille (viscous) flow, capillary condensation, selective adsorption, molecular sieving (Rao and Sircar, 1993). Single file diffusion can also be important. A schematic of the different mechanisms is given in Figure 2.3. The relative contributions of the different mechanisms are dependent on the properties of the membranes and the gases, as well as on the operating conditions like temperature and pressure. (Pandey and Chauhan, 2001).

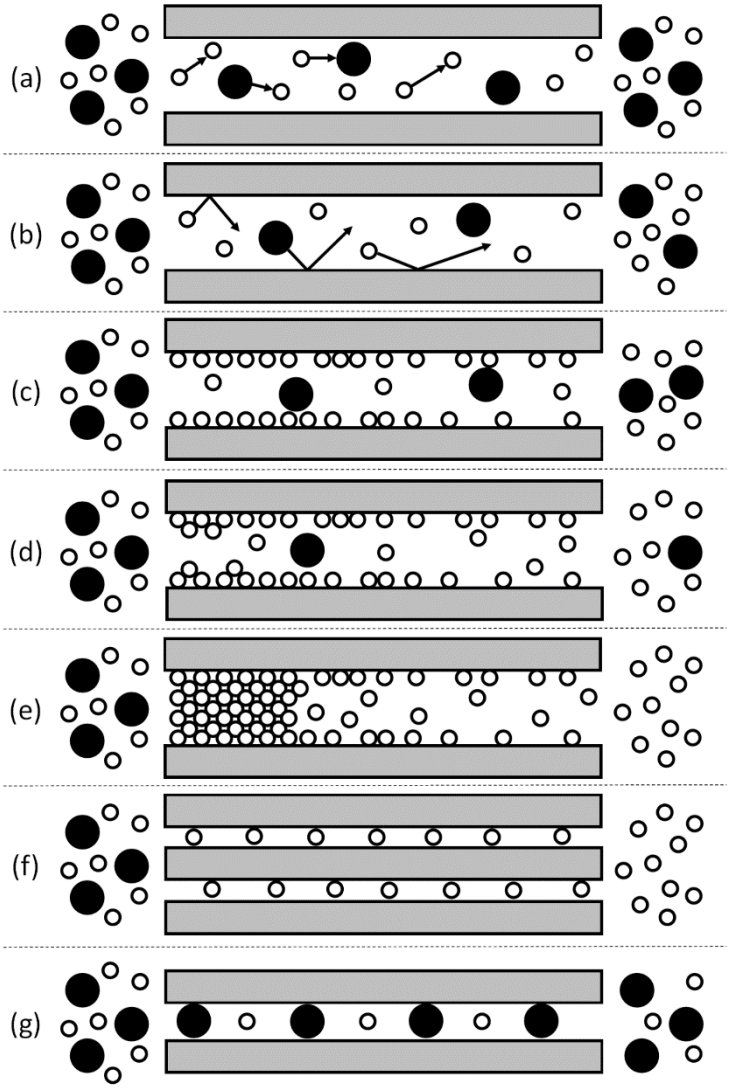

Figure 2.3: Schematic presentation of transport mechanisms through membranes a)Poiseuille flow b)Knudsen diffusion c)Surface diffusion d)Multi-layer diffusion e)Capillary condensation f)Molecular sieving g)Single-file diffusion (Adapted from Silva et al, 2008). Filled circles represent larger or weakly non-adsorbed molecules and open cirlces represent smaller or more stronlgy adsorbed molecules.

2.6.1.1 Knudsen Diffusion

This mechanism of separation is based on differences in molar masses of the components of a mixture due to Knudsen diffusion through the pores. This mode of transport occurs when the pore size of the membrane is smaller than the mean

free path of the molecules at the processing conditions (Javaid, 2005).The mean free path λ is given by:

$$\lambda = \frac{3\eta}{2P}\frac{(\pi RT)^{0.5}}{2M} \qquad \textbf{2. 4}$$

where η is the gas viscosity, R is the universal gas constant, T is the absolute temperature, M the molar mass and P is the pressure. If r/λ is much less than one (r/ λ<0.05), the collisions with pore walls are more significant than collisions with other gas molecules. The smaller number of collisions among molecules than the pore walls means that each molecule moves independently. The separation of gases is therefore achieved by the difference in velocities of different gas molecules. The gas flux in such a case is described by:

$$G_{mol} = \frac{8r(P_1 - P_2)}{3L(2\pi MRT)^{0.5}} \qquad \textbf{2.5}$$

where G_{mol} is the molecular flow of the gas, r is the pore radius, P_1 the partial pressure of the gas on the feed side, P_2 the partial pressure of the gas on the permeate side, L is the pore length, M is the molar mass, R the gas constant and T the absolute temperature.

The selectivity of separation achievable by this mechanism is generally very low and is not practical except in very special cases. (Pandey and Chauhan, 2001).

The selectivity ratio or separation factor for the Knudsen mechanism is often estimated from the square root of the ratio of molecular weights.

$$\alpha K_n = \left(\frac{i}{j}\right) = \sqrt{\frac{M_j}{M_i}} \qquad \textbf{2.6}$$

Ideal selectivities have been calculated for several gas pairs, but the actual separation factor is normally smaller. Pandey and Chauhan (2001) suggest that the

reasons for this are back-diffusion, non-separative diffusion, concentration polarisation on the feed or permeate side and the occurrence of viscous flow in large pores.

2.6.1.2 Poiseuille (Viscous) Flow

Poiseuille flow occurs when the mean free path is much smaller than the pore size of the membrane i.e. ($r/\lambda > 3$). In this case, gas diffusion occurs primarily through molecule–molecule collisions. If a pressure gradient is applied to such a pore regime, bulk or laminar flow occurs (Li, 2007). Poiseuille flow is also known as viscous flow or bulk diffusion in the literature. This phenomenon is unfavourable for gas separation membranes (Li et al, 2015). The permeability (Choi et al, 2001) is given as:

$$Q_V = \frac{J_v}{\Delta P} = \frac{\varepsilon r^2}{8\tau\mu RT} P_m \qquad \textbf{2.7}$$

where ε, τ and μ are the porosity, tortuosity factor and gas viscosity, P_m is the mean pressure. P_m is $(P_1 + P_2)/2$ and P_1 and P_2 are the inlet and outlet pressures respectively.

2.6.1.3 Capillary Condensation

Gas separation can occur through the partial condensation of one of the gases in a mixture. This happens at certain critical relative pressures such that the pore is completely filled by the condensed gas, thereby excluding the other gases. This mechanism typically requires mesoporous pores (diameter > 3nm) so that condensation of the gas mixture can take place (Pandey and Chauhan, 2001, Javaid, 2005). This type of separation can result in high selectivities, the extent of removal of that component from the gas mixture being limited by the condensation partial pressure of that component at the system temperature (which is indicated

by the Kelvin equation) as well as by the pore size and geometry of the membrane (Ulhorn, 1992). Capillary condensation can also occur in parallel with surface diffusion since conditions at which capillary condensation take place are also those under which significant surface diffusion can be expected (Coronas and Santamaria, 1999).

2.6.1.4 Selective Adsorption / Surface Diffusion

Selective adsorption of the more strongly adsorbed components of a gas mixture onto the pore surface followed by surface diffusion of the adsorbed molecules on the pore can also facilitate the separation of gases. This mechanism provides the most flexible and attractive choice for practical separation of gas mixtures because the separation selectivity is determined by preferential adsorption of certain components of the gas mixture on the surface of the membrane pores, as well as by selective diffusion of the adsorbed molecules (Pandey and Chauhan, 2001).

It has been observed that the permeance of weakly adsorbed components is radically reduced in the presence of strongly adsorbed components. A number of papers (e.g. Rao and Sircar, 1996, Piera et al, 1999, Yang et al, 1999, Ciavarella et al, 2000, Arruebo et al, 2001, Bernal et al, 2002, Algieri et al, 2003, Bonhomme et al, 2003, Sommer et al, 2003, Camus et al, 2006, Rezai et al, 2008) demonstrate the advantage of gas separation based on the surface diffusion of the strongly adsorbed components and their hindering effect on the permeance of the weakly or non-adsorbed components (Yang et al, 1999).

Also, when adsorption of the permeating gas molecules on the pore wall becomes significant, the molecules adsorbed on the surfaces may have considerable mobility. This gives rise to an additional contribution of gas transport (Kim et al, 2001). Surface diffusion rates are determined by the surface diffusion coefficient and adsorption equilibrium, both of which are related to the interactions between adsorbates and pore surfaces (Yamasaki and Inoue, 1991). Moreover, surface diffusion becomes important as the pore size becomes as small as the permeating

gas molecule, since the physicochemical interactions between the pore wall and the permeating molecules become more pronounced (Kim et al, 2001).

2.6.1.5 Molecular Sieving

Separations based on molecular sieving are caused by the passage of smaller molecules of a gas mixture through the pores while the larger molecules are hindered. In order to function as a molecular sieve, membranes must have pore diameters that are in between those of the gas molecules to be separated. If the membrane has pore sizes between the diameter of the smaller and larger molecules, then only the smaller molecule can permeate and a very high separation would be achieved. In practical situations, there will be a distribution of pore sizes in the membrane and thus the gas permeability is actually influenced by a combination of transport mechanisms (Pandey and Chauhan, 2001).

2.6.1.6 Configurational / Micropore Diffusion

This type of diffusion is considered as surface diffusion in the limit where the pore size becomes comparable to the molecular size. In this mechanism, diffusion is perceived as an "activated" process and separation is a strong function of molecular shape and size, pore size, and interactions between the pore wall and gas molecules. This type of mechanism is dominant in microporous zeolite membranes and carbon molecular sieves (Javaid, 2005).

2.6.1.7 Single File Diffusion

This mode of diffusion occurs when the pore diameter is not large enough to allow the molecules to pass one another. In finite single file systems, the effect of the boundary becomes important since only molecules at the surface are able to exchange with the ambient fluid. Single file diffusion does not allow mutual

excahnge between adjacent molecules. This only causes a problem when different molecular species (in multi-component diffusion) are considered (Schuring et al, 2007). Single file diffusion slows down the faster diffusing molecule in zeolite pores and accelerates the diffusion of the slower diffusing component.

For all mechanisms, a concentration gradient (or pressure gradient) for the diffusing species must be imposed across a porous membrane in order to provide the driving force for transport. The selectivity of separation achieved by the Knudsen mechanism is generally very low. Capillary condensation requires the pore size of the membrane to be in the mesoporous size range and a very high selectivity can be achieved by this mechanism. Molecular sieving exhibits high selectivity and high permeability for the smaller components of a gas mixture. For inorganic membranes that have pore sizes in the Knudsen range, surface diffusion may be the only mechanism that would separate gases with identical molar masses. In reality, permeation can occur through non-zeolite pores by Knudsen diffusion which adds an additional parallel contribution to the total flux through a membrane. Also if large defects are present in the zeolite layer, then the permeation of the gases may be dominated by Poiseuille flow. It can be seen from a description of the above mechanisms that both the pore size and the physiochemical nature of the pore surface play key roles in determining the separation efficiency of membranes. As a result, membrane properties can be altered by appropriate molecular engineering of their surface chemistries (Pandey and Chauhan, 2001).

2.7 Ammonia Separation using Membranes

Recovery of ammonia from mixtures with nitrogen and hydrogen using gas separation membranes has been the subject of only a limited number of studies to date even though this approach to ammonia purification requires less energy than conventional processes such as sorption and cryogenic distillation (Vorotyntsev et al, 2006). The studies are concentrated around two groups; those based on molten salts (Section 2.8.1) and those using polymer films (Section 2.8.2).

The inclusion of membranes into the ammonia separation process has been presented by various authors. Cussler and his group (e.g Bhown and Cussler, 1991, Tricoli and Cussler, 1995), have envisioned two ways in which a membrane can be incorporated into ammonia synthesis. One way is to have a new reactor and with one reactor wall made of an ammonia selective membrane. Ammonia produced in the reactor could pass through this membrane wall, but the hydrogen and nitrogen would be retained. These retained gases would then react further. Such a membrane reactor would avoid the usual constraint of equilibrium between nitrogen, hydrogen and ammonia, but would have to resist the high pressures and temperatures involved. Another way a membrane could be useful would be in the recycled gases. After these gases are cooled, some ammonia condenses, but some still remains as vapour. The gases are still at high pressure. If they were passed through a membrane module based on an ammonia selective membrane, the ammonia could be effectively removed and only the nitrogen and hydrogen would need to be reheated and recycled.

Choe et al (1995) present in their patent a specific integration of an ammonia selective membrane into both the recycle loop and the purge loop of an ammonia plant. This two-step membrane assisted process separates ammonia from the recycle stream consisting of unreacted hydrogen and nitrogen, unrecovered ammonia and other inerts in the first stage. The permeate stream is enriched in ammonia and is recycled to the reactor effluent. The non-permeate stream is enriched in hydrogen, nitrogen and the inerts, and is recycled to the reactor feed. In the second stage, the purge stream from the ammonia process (which represents the portion of the recycle stream that must be removed from the process in order to prevent the build-up of the inerts in the process) is separated in a second ammonia-selective membrane separator into a permeate stream enriched in ammonia which is recycled to the reactor feed and a non-permeate stream enriched in hydrogen, nitrogen and the inerts which can be further processed for hydrogen recovery. A key feature of this process is that a portion of the reactor feed is used to sweep the permeate side of the second membrane separator. No specifics on the type of ammonia-selective membrane are given, but suggestions include polymeric membranes as decribed by Laciak et al (1988) and Pan and Hadfield (1988)

respectively. Pan and Hadfield (1988) present a different two step process, in their patent. Ammonia is first recovered from the purge stream using an ammonia selective membrane and then hydrogen is recovered in a separate stream using a membrane that is selective to hydrogen.

This thesis is concerned with an efficient membrane system to replace the current refrigeration system as shown in Figure 1.1. The critical aspect of this design is the use of the lower pressure make-up syngas as the membrane permeate side purge (sweep gas). This collects the ammonia rich stream from the permeate side of the membrane unit. Selectivity is therefore not that critical as all of the hydrogen and nitrogen permeating with the ammonia is collected in the sweep flow, recompressed and returned to the synloop. The focus in this study is not so much on the process of ammonia recovery itself, but rather on suitable membranes that can successfully separate ammonia from hydrogen and nitrogen, and withstand the extreme operating conditions of this process.

2.7.1 Ammonia Separation using Molten Salts

Liquid membranes operate by immobilising a liquid solvent in a microporous filter or between polymer layers (Basu et al, 2004). Liquid membranes using molten salts are supported in the pores of a stainless steel mesh. Such membranes operate by a mobile carrier mechanism (Cussler, 1984, Noble et al, 1989). Studies using molten salts are made at high temperatures approaching those of ammonia synthesis (Pez et al, 1998). For example, in the case of molten zinc bromide, ammonia molecules selectively react with Zn^{2+} to form a complex which diffuses across the membrane and releases ammonia on the other side. Such carrier-assisted diffusion operates in parallel with ordinary diffusion, in which ammonia, hydrogen and nitrogen simply dissolve in the membrane and diffuse across it (He and Cussler, 1992).

Pez and Carlin (1986) achieved an effective separation of ammonia from nitrogen and hydrogen at high temperatures (250^{o}- 350^{o} C.) using a membrane consisting

of a reversibly ammonia reactive molten salt (e.g., $ZnCl_2$) immobilized in a porous metallic or ceramic support.

Sharonov and Aristov (2005) synthesized composite sorbents "chlorides of alkaline-earth metals confined to porous alumina" and tested them for ammonia removal in a fixed-bed flow adsorber at 25^{o}C-300^{o}C and a partial pressure of ammonia of 0.06bar. The modification of the alumina matrix with the salts increased its ability to adsorb ammonia and the effect grew in the sequence $BaCl_2$<$CaCl_2$<$MgCl_2$. As expected, the ammonia adsorption by the salts decreased with increasing temperature.

In the case of molten salt membranes, the selective-carrier diffusion mechanism is dominant at low gas pressures. However, at higher pressures, ordinary diffusion, which is less selective, becomes important thereby compromising the selectivity of the membrane. Although they have been shown to work well at high temperatures, their failure to be selective at high pressures means that they would not be useful at the operating pressures characteristic of ammonia synthesis (He and Cussler, 1992).

2.7.2 Ammonia Gas Separation using Polymer Films

There is considerable scientific and technological interest in the trans-membrane transport of substances interacting with polymer membranes, especially in ammonia-polymer systems (Vorotyntsev et al, 2006). Ammonia separation membranes have been fabricated from various polymers: poly(vinyltrimethylsilane) (Kulprathipanja and Kulkarni, 1986), polyamides (Semenova et al, 1997, 2000), perfluorinated sulfided cation exchangers (Tricoli and Cussler, 1995, Timashev et al, 1991), and cellulose materials (Vorotyntsev et al, 2006). Polyvinylammonium thiocayanate (Pez and Laciak, 1988, Bhown and Cussler, 1991) and perfluorinated copolymers have also received great attention for ammonia separation based on polymer films. A recent development is

poly[bis(trifluoroethoxy)phosphazene] (PTFEP) which has shown excellent results for ammonia separation (Makhloufi et al, 2012). The same group, recognising the scarcity of the permeation behaviour of ammonia through poymers, tested a broad range of materials covering a broad range of structures. Materials tested include classical amorphous polymers, (i.e polymethylsiloxane or PDMS), semi-crystalline polymers with low glass transition temperatures (i.e low density polyethylene or LDPE), semi-crystalline glassy polyolefins (i.e poly-4-methyl-pentene (TPX)), a series of fluorinated polymers; ethylene tetrafluoroethylene copolymer (ETFE), polytetrafluoroethylene (PTFE), perfluoroethyelene propylene (FEP), and amorphous glasses such as Hyflon AD40X, Hyflon AD60X, Teflon AF 1600, Teflon AF2400.

A summary of work on ammonia separation using polymeric membranes is given in Table 2.5

Table 2.5: Summary of polymeric membranes for ammonia gas separation

Type of Membrane	Purpose of Study	Comments/Findings	Study
Polyethylene	Separation of NH_3 from H_2 and N_2 in an ammonia synthesis plant.	- low permeation rate of NH_3 versus hydrogen and nitrogen and subsequently poor selectivity.	Brubaker and Kammermeyer, 1954
Multi-component silicone rubber/polyethylene glycol	Separation of polar gases from mixtures, including separation of NH_3 from H_2 and N_2	- high permeabilities and high selectivities at ambient temperatures and pressures. - not useful in high pressure systems.	Kulprathipanja and Kulkarni ,1986
Polyvinylammonium thiocyanate and polyvinylchloride	Process for separating ammonia from a mixture of gases or aqueous streams	- high NH_3 solubility and diffusivity resulting in high permeation rates. - low permeation rates of N_2 and H_2 due to their low solubility in the membranes favourable selective properties for ammonia recovery from mixtures with N_2 and H_2.	Laciak and Pez, 1988
Vinyledene fluoride-tetraflroroethylene copolymer	Ammonia gas separation	- high NH_3 selectivity/permeability properties. - prolonged contact of NH_3 with membrane may degrade the latter	Pez and Laciak, 1988
Polysulfone amide	Separation of ammonia from gas streams containing NH_3, H_2 and contaminant gases in a two-step process	- high separation of NH_3 from H_2 at temperature below 0^oC - selectivity of NH_3decreasing with increase in temperature	Pan and Hadfield, 1988

Type of Membrane	Purpose of Study	Comments/Findings	Study
Perfluosrosulfonic acid polymer hollow fibers Facilitated transport of ammonia through perfluorosulfonic acid-polymer based hollow fiber membranes in Co^{2+}, $NH4^{+}$, H^{+} and M_f^{+} ionic forms	Facilitated transport of ammonia through perfluorosulfonic acid-polymer based hollow fiber membranes in Co^{2+}, $NH4^{+}$, H^{+} and M_f^{+} ionic forms for ammonia isolation from ammonia -containing gas mixtures (e.g. ammonia industrial industries) and also from aqueous mixtures	- high ammonia permeability through hollow fibers of H+ and Mf +forms - high separation factors ($\beta \geq 10^2$-10^3) for NH_3/ H_2 - permeability of ammonia decreased with increasing temperature	Timashev et al, 1991
Composite polysulfone hollow fiber/sulfonated polysulfone	Improvement in the ammonia separation process using sulfonated polysulfone polymers coated on a porous hollow fiber polysulfone support for the separation of ammonia from gas mixtures	- high separation factors of NH_3 from NH_3/N_2, NH_3/H_2 mixtures when compared to polysulfone and cellulose acetate mixtures NH_3/H2 α =63 at 282K α =22 at 295K. - membrane performance deteriorates with increasing temperature	Bikson et al, 1991
Cellulose acetate	To determine the ammonia permeability of a cellulose acetate membrane and to determine the separation factors in the ammonia-nitrogen and ammonia-hydrogen systems.	- high permeabilities for pure NH_3 and high ideal separation factors NH_3/N_2 and NH_3/H_2 - studies restricted to single gas permeations - narrow range of usefulness with respect to temperature and pressure - degradation of membranes observed at higher temperatures and over extended use.	Vorotynstev et al, 2006a

Type of Membrane	Purpose of Study	Comments/Findings	Study
Poly(norborenylethystyrene)-b-poly(propyl styrene-sulfonate) P (N-s-S)-b-PSSP block copolymer	Develop a membrane containing 7-23 nm polystyrene sulfonate domains using a reactive block copolymer precursor that is highly selective for NH_3 vs H_2 and N_2 at modest temperatures (25^{o}C) for immediate application in existing ammonia plants.	- NH_3 permeability is >600 barrers at 25^{o}C and 2 bar - selectivity for a mixed gas feed containing NH_3 and N_2 is about the same for ideal gas selectivities at >90 - permeabilities increase with the average NH_3 pressure and retain their selectivity at higher pressure.	Phillip et al, 2009
Poly[bis(trifluoroethoxy) phosphazene](PTFEP)	Use of dense PTFEP dense membranes for ammonia gas separation from a gas mixture comprising nitrogen and hydrogen for potential application in the Haber process	- extremely high selectivities and permeabilities in favour of NH_3 - NH_3/N_2 selectivity >220 at ambient temperature - selectivity drops with increasing temperature (50^{o}C α NH_3/N_2 =59.1 to 80^{o}C $\alpha NH_3/N_2$ = 29.6) - simulations results at both temperatures studied (i.e. 50^{o}C and 80^{o}C) show reasonable membrane areas to reach the target of 2% ammonia concentration in the retentate.	Makhloufi et al, 2012

Type of Membrane	**Purpose of Study**	**Comments/Findings**	**Study**
Polydimethylsiloxane (PDMS) Polyethylene low density (LDPE) Polymethylepentene (TPX) Ethylene tetrafluoroethylene copolymer (ETFE) Polytetrafluoroethylene (PTFE) Perfluoroethylene propylene (FEP) Hyflon AD40X Hyflon AD60X Teflon AF 1600 Teflon AF 2400	Explore the solubility, diffusion coefficient and permeability of NH_3 in different polymers between 5°C and 50°C with particular emphasis on fluorinated polymers Permeation characteristics of N_2 and CO_2 determined simultaneously to highlight the potential specificities of NH_3 in comparison to the two permeants.	- lowest permeabilities of NH_3 (0.5 barrer) obtained for fluorinated polymers (PTFE, FEP) - large permeability values (up to 6500 barrer) observed for amorphous rubber polymers (PDMS) and super glassy polymers (Teflon AF 2400) - NH_3 has a higher permeability value than CO_2 in rubbery polymers (PDMS),polyolefin polymers (i.e. TPX), non-fluorinated (LDPE) and partially fluorinated (ETFE) - fluorinated polymers (FEP, PTFE, Hyflon, Teflon –AF) with a high fluorine density exhibit a reverse NH_3/CO_2 permeation selectivity	Makhloufi et al, 2013

The studies presented in Table 2.5 have demonstrated that although polymeric membranes show promising results, they may not be the best choice for ammonia gas separation from the ammonia synthesis loop. Membranes such as, polyvinylammonium thiocyanate (Bhown and Cussler, 1991), polyperfluorosulphonates (e.g Nafion) (He and Cussler (1992), and celulose acetate (Vorotynstev et al, 2006) as presented in Table 2.5 show a decline in performance stability at high pressures and high temperatures. In addition, the general problems of polymeric membranes such as fouling, chemical degradation, compaction and plasticization demonstrate the need to use materials that are best equipped to deal with these limitations (Basu et al, 2004). Inorganic membranes, as stated earlier, have the potential to overcome these problems due to their stability when exposed to adverse conditions (thermal and chemical stability as well as the ability to withstand high pressures) and their higher gas fluxes when compared to polymeric membranes. However, these membranes are generally characterised by relatively low permeances and selectivities, although the situation is changing. It has been suggested that for high pressure ammonia gas separation from a gas mixture containing hydrogen, a material that combines the stress resistance of inorganic materials and both high selectivities and permeabilities of organic polymers is highly desirable (Makhloufi et al, 2012).

Progress on improved polymeric membranes has been made by Makhloufi et al (2012) with their membrane made from a semi-crystalline inorganic polymer poly[bis(trifluoroethoxy)phosphazene] (PTFEP) which shows a high mechanical resistance to pressure (10^9 Pa), a good thermal resistance as well as good chemical resistance, particularly towards strong bases. Results of the testing are presented in Table 2.5 and show good results for ammonia separation, however selectivity drops with an increase in temperature.

Inorganic membranes are still considered as the next-generation membrane materials with the potential to break through the limitations of organic polymer separations (Iwamoto and Kawamoto, 2009). A few researchers recognized the potential for inorganic membrane use in ammonia gas separation and the studies are summarised in the next section.

2.7.3 Ammonia Gas Separation using Inorganic Membranes

Inorganic membranes, particularly microporous membranes, have been extensively studied for gas separations. One of the fundamental foundations for the future commercial application of ceramic membranes in the ammonia synthesis process is the ability to produce a defect free, ammonia-selective membrane that works at high pressure and under aggressive environments. Carbon, silica and zeolites in particular have been recognised as promising candidates.

Barrer and his group (Ash et al, 1973) studied the application of carbon membranes on ammonia gas separation. Steady state flow of the single species He, H_2, D_2, N_2 and NH_3, and binary mixtures H_2/N_2, He/NH_3, H_2/NH_3 and N_2/NH_3 through a microporous membrane of high area compressed carbon powder was investigated (Ash et al, 1973). They found that for the weakly adsorbed species (He, H_2, D_2, N_2) the permeability was independent of pressure and hence of the amount adsorbed. With the strongly sorbed ammonia, permeability increased with increased pressure and, at lower temperatures, reached a maximum and then rapidly declined. Experiments with mixtures of ammonia and a weakly sorbed gas such as hydrogen showed that sorbed ammonia could significantly block the flow of the weakly sorbed gas. The high separation factors were thought to be governed by the surface flow of ammonia and by blockage of the flow of the other gases by adsorbed ammonia. Ammonia permeated rapidly, but the weakly sorbed gases were retained on the high pressure side of the membrane. High separation factors were obtained but only at conditions close to ammonia liquefaction. The membrane, which relies on the condensation and "surface flow" of ammonia in the microporous carbon, was shown to operate effectively with an NH_3/H_2 selectivity of about 250 at conditions that are near the point of liquefaction of ammonia. Otherwise, the NH_3/H_2 selectivity decreased rapidly with increasing temperature. Therefore, this carbon membrane would not be useful in the separation of ammonia from other gases in the ammonia synthesis loop at the conditions of interest. This is in addition to the disadvantage of carbon membranes as described in section 2.4.

The introduction of MOF materials and MOF membranes looked like a promising development for ammonia gas separation using membrane technology. Supported

MOF membranes, just like zeolite membranes, are promising candidates for molecular sieving as well as separation of mixtures by adsorption and diffusion. However, it has been shown that MOFs are not stable when exposed to ammonia. Studies were done to determine ammonia adsorption properties and stabilities of MOF-5 and MOF-177 after exposure to ammonia. It was found that after exposure to ammonia, both MOF's lost their pore textures as evidenced by a drastic decrease of specific surface area and pore volume. There was also a complete loss of crystallinity. It was suggested that ammonia molecules destroy MOF frameworks by forming hydrogen bonds with ZnO_4 clusters of MOFs (Saha and Deng, 2010). Petit and Bandosz (2010) also reported that ammonia is detrimental to the MOF-5 frameworks as it behaves like the water molecule to form a hydrogen bond with the ZnO_4 unit. As a result, it is unlikely that MOF membranes could be considered suitable for ammonia gas separation.

The use of ceramic membranes for ammonia separation has been studied extensively at Bath as part of the IMPRESS project. An extensive screening programme was carried out (Camus et al, 2006) to find a suitable membrane configuration and operating conditions for the effective recovery of ammonia from the syngas loop. Three types of membranes were used:

(1) tubular MFI zeolite on a ceramic alumina support
(2) multichannel fiber MFI-type zeolite membrane
(3) tubular microporous silica

The performances of the zeolite and silica membranes were compared in terms of permeation and separation factors. Two different silica membranes were used for comparison, one being a pure silica membrane and the other being a methylated silica membrane prepared from the recipe of Campaniello et al (2004). The results confirmed that for the $NH_3/H_2/N_2$ separation, the performance of a methylated silica membrane is better than a standard silica one. A high ammonia permeance of 2.1×10^{-7} $mol.m^{-2}.s^{-1}.Pa^{-1}$ and a selectivity of NH_3/H_2 about 10 were obtained with a tubular MFI zeolite membrane. Although the methylated silica membrane had higher permeances than the zeolite, the corresponding selectivity was lower. The zeolite fiber membranes tested also showed a high selectivity at 40^oC, but the permeances obtained were lower than those for the tubular membrane. The selectivities desribed here are much lower than

those observed for polymeric membranes studied for ammonia separation. Nonetheless, these membranes are potentially highly stable at high temperatures and pressures and with increasing improvements being made in membrane synthesis, and with a better understanding of membrane transport, better selectivities could possibly be obtained.

2.7.4 Concluding Remarks

From the analysis of the literature, it is clear that if membranes are to be used in ammonia separation, several advances need to be made. It is important that the membranes should be highly selective and highly permeable to ammonia and be able to withstand the extreme conditions of the ammonia synthesis process. Microporous membranes are therefore a serious contender for this type of separation. Previous work performed at Bath has established that MFI type membranes offer the best performance characteristics (Camus et al, 2006). The study of zeolite membranes in gas separation processes, especially the MFI membrane, has continued to grow. More is known about the mechanisms of separation and reliable data is widely available. However MFI membranes are still restricted in terms of large scale application and commercial development has been slow. The successful application of MFI zeolite membranes in ammonia plants could provide a catalyst for the wider development and use of microporous ceramic membranes in other gas separation applications. A proper understanding of the $NH_3/H_2/N_2$ mixture/MFI zeolite membrane system is therefore essential.

The past three decades have seen a great increase in research on the optimal conditions for high quality membrane synthesis, understanding gas and liquid permeation/separation mechanisms, and exploration of practical separations (Dong et al, 2000, Bernado and Clarizia, 2013). Studies on MFI zeolite membranes to date have concentrated on hydrocarbon separations, particularly (C1-C4), and light (inorganic) gases (Jia et al, 1994, Bai et al, 1995, Kapteijn et al, 1995, Bakker et al, 1996, Funke et al, 1996, Bernal et al, 2002, Gump et al, 2000 Dong et al, 2000, Sommer et al, 2003). It seems that, apart from the Bath IMPRESS project (Camus et al, 2006), no one has

studied ammonia gas separation using MFI membranes. In addition, research on MFI zeolite membranes has focused on single and binary mixtures with very few studies on multi-component systems. Funke et al (1996) who studied binary and ternary systems containing n-octane, isooctane, and n-hexane found that the permeances of the components were a strong function of other components in the feed. This implies that multi-component gas permeation through a zeolite membrane cannot be predicted from single-gas or binary-gas permeation data. Piera et al, (1999) studied ternary mixtures. However these were based on water- containing mixtures (pervaporation). Dong et al, (2000) has also performed studies on a multi-component system based on a simulated refinery gas stream of eight components including hydrogen and light hydrocarbons through an alpha-alumina supported MFI-type zeolite membrane. For the successful application of zeolite membranes, permeation measurements of multi-component systems in separation conditions relevant to the industry are indispensable.

One of the limiting factors that hampers the development and use of zeolite membranes is modeling their performance (Camus et al, 2006). Modeling has not been reviewed in this Chapter as this subject will be addressed in Chapter 3. Nevertheless, it should be noted here that numerous efforts have been made to understand the mechanism and develop theoretical models for mass transport through zeolite films (Vroon et al, 1998; Bakker et al, 1997; van de Graaf et al, 1999; Krishna and van de Broeke, 1995, Kapteijn et al, 1995). The Maxwell-Stefan approach of Krishna (1990) has been identified as possibly the best theoretical description of transport through a membrane such as silicalite-1 on stainless steel supports (Krishna and van den Broeke, 1995). As with the permeation studies, most of the previous work on modeling has only dealt with single gas or binary permeation, with focus again on hydrocarbons and light inorganic gases (Dong et al, 2000). Adequate description of multi-component permeation is necessary for the design and control MFI zeolite membranes (Kapteijn et al, 1995).

In order to optimise the performance of an MFI membrane-based ammonia separation system, it is necessary to obtain a better understanding of the separation mechanism. The actual mechanism of gas permeation through an MFI-type zeolite membrane has been said to depend on the gas adsorption properties of the zeolite (Dong et al, 2000). Many authors have recognised that strongly adsorbed components can drastically

reduce the permeance of weakly adsorbed components. Preferential adsorption gives rise to highly selective separations and is therefore an advantageous quality for a membrane. Although this hinderance phenomenon is widely acknowledged, few researchers have studied it in a quantitative manner. Yang et al, (1999) proposed a simple model, the Potential Barrier Model, to describe the permeance of weakly adsorbed hydrogen in the presence of strongly adsorbed hydrocarbons. The model was successful for this system on a silicalite-1 zeolite membrane, but has not yet been tested for other systems.

2.8 Thesis Aims and Objectives

The need for an energy efficient ammonia gas separation system has been discussed, with a membrane system recognised as the best way to achieve this. This is coupled with the requirement to develop a membrane that can cope with the extreme high pressure/high temperature conditions of the ammonia process. A review of the available membrane technology has been carried out and shows inorganic membranes, particularly MFI zeolites are well suited to this type of application however. No studies based on ammonia systems with MFI zeolites seem to have been performed beyond the Bath IMPRESS project. It is therefore the aim of this investigation to further the studies on the potential of MFI zeolite membranes in ammonia gas separation. To achieve this, a number of objectives have been set:

1. Conduct single gas permeation experiments to study MFI zeolite membrane transport properties.

2. Measure the permeation and selectivity of an MFI zeolite membrane with a multi-component $NH_3/N_2/H_2$ mixture at different operating conditions with focus on feed flow rate, sweep flow rate, differential pressure and temperature.

3. Analyse the experimental results using different engineering models and compare these models.

4. Analyse the effect of operating conditions on membrane performance to confirm the mechanism of separation.

5. Examine the ability of the Potential Barrier Model to describe the hindering effect of ammonia on the permeation of hydrogen and nitrogen.

CHAPTER 3

MFI ZEOLITE MEMBRANES

3.0 Introduction

This chapter presents information on MFI zeolite membranes, their structure and how the membranes are synthesised. A discussion on mechanisms and models developed to explain transport in zeolite membranes is presented. It is important to note that there have been numerous studies on MFI-type zeolite membranes and several reviews are available (Bein et al, 1996, Coronas and Santamaria 1999, Tavolaro and Drioli, 1999, Caro et al, 2000, Lin et al, 2002, Yu et al, 2011, Lin and Duke, 2013). Therefore, it is not the intention in this chapter to provide another detailed review, but rather to highlight properties of these types of membranes that are particular to the research described in this thesis.

As explained in Chapter 2, Section 2.4.3, various types of zeolite membranes exist in the literature. Examples include SAPO-34, Faujasite and type A membranes. MFI zeolites have remained a popular choice for zeolite membrane research. The main reasons are:
(i) the accumulated knowledge in the synthesis of the MFI membrane which can be seen by the growing number of published material on their preparation (Dong et al, 1992, Geus et al, 1992, Ramsay et al, 1994, Bai et al, 1995, Yan et al, 1995, Bakker et al, 1996, Hedlund et al, 1999, Caro et al, 2000, Au and Yeung, 2001, Kalipcilar et al,

2001, Algieri et al, 2003, Mabande et al, 2004 & 2007, Noack et al, 2005, Miachon et al, 2006 & 2007, Rezai et al, 2008, Tarditi et al, 2008, Li et al, 2008, Drobek et al, 2012, Bayati et al, 2013, Sjoberg et al, 2015);
(ii) a pore diameter of 0.55nm which is attractive for industrial separations;
(iii) the relative ease of preparation;
(iv) the possible modifications in the chemical compositions including cation exchange
(v) relatively high thermal and chemical stability (Caro et al, 2000).

The different types of MFI zeolites reported in the literature are silicalite-1 and ZSM-5. Silicalite-1 is composed virtually of pure silica whereas ZSM-5 has aluminium substituted into a small fraction of the silicon sites in the crystal lattice (Gump et al, 1999). Si in the MFI framework can also be substituted with titanium for TS-1 and vanadium for VS-1 which gives MFI zeolites a wider range of chemical and catalytic properties when compared with other zeolite families. The foreign atoms in the network not only modify the chemistry but also alter the size and shape of the zeolite pores (Tuan et al, 2000, Aoki et al, 2000) thereby affecting the transport of molecules through the channel (Au and Yeung, 2001). The Si/Al ratio for silicalite-1 is >200. This zeolite has no exchangeable ions, is non-polar and shows strong hydrophobic/organophillic properties. The Si/Al ratio for ZSM-5 is in the range of 10-200 (Szostak, 1998). Aluminium affects several properties of the zeolite, and transforms the material into an acidic catalyst with hydrophilic properties (Au and Yeung, 2001, Algieri et al, 2003). MFI zeolites form a three dimensional framework of 10-membered oxygen rings that makes them more robust compared with other zeolite types.

Both ZSM-5 and silicalite-1 have the same MFI framework as shown in Figure 3.1 with two different types of channel comprising straight (0.54 x 0.56nm) and sinusoidal (0.51 x 0.55 nm) pores that run perpendicular to each other (Algieri et al, 2003).

Several groups have successfully synthesised MFI-type zeolite membranes employing different synthesis compositions, support types and materials. Methods of preparation include in-situ hydrothermal synthesis and secondary seeded growth. This subject is discussed in more detail in section 3.2.

Silicalite-1 membranes have been studied more frequently than ZSM-5 possibly due to the former's hydrophobicity which enables them to separate hydrocarbons from aqueous solutions (Chiang and Chao, 2001). An interesting development is the bi-layered Al/ZSM-5/Silicalite-1 membranes prepared by Mabande et al (2007).These membranes have the potential to expand applications even further as different functions can be combined e.g. catalytic activity/inertness, and hydrophilic/hydrophobic character.

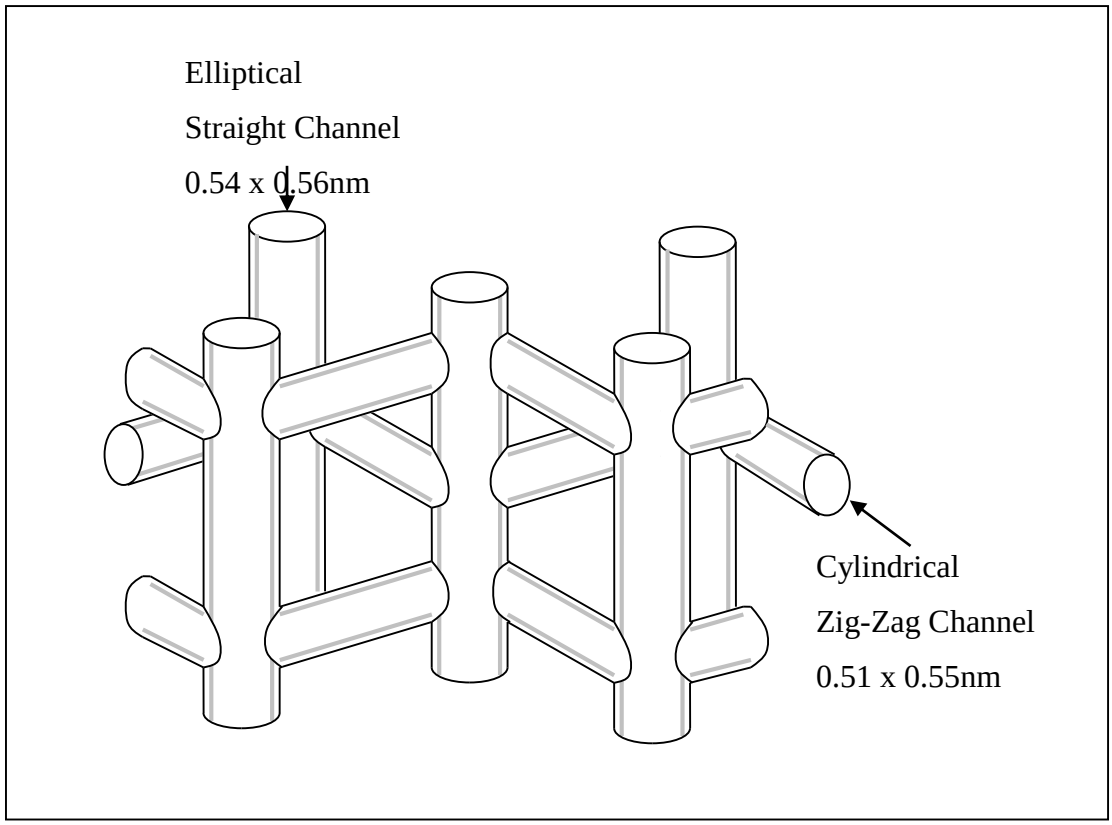

Figure 3.1*:* MFI zeolite pore structure and dimensions (Adapted from Sommer et al, 2003)

Gas permeation research on MFI membranes has mostly been focused on:

(i) the separation of branched and linear isomers of organic compounds such as C_2 - C_6 alkanes and

(ii) separation of these molecules from hydrogen. (Bai et al, 1995, Kapteijn et al, 1995, Bakker et al, 1996, Vroon et al, 1996, Coronas et al, 1997, Keizer et al, 1998, van de Graaf et al, 1998 &1999, Gump et al, 1999, Piera et al, 1999, Tuan et al, 1999, Xomeritakis et al, 1999, Yang et al, 1999, Millot et al, 2000, Ciavarella et al, 2000, Dong et al, 2000, Arruebo et al, 2001, Lai

et al, 2003, Bernal et al, 2003, Rezai et al, 2008, Tarditi et al, 2008, Deng et al, 2010, Zhang et al, 2010,Wohlrabi et al, 2011, Pham et al, 2013).

Traditionally, fewer studies have been carried out on the separation of light gas species such as H_2, N_2 and CO_2. (Poshusta et al, 1999, Au and Yeung 2001, Noack et al, 2002, Bonhomme et al, 2003, Algieri et al, 2003 Arruebo et al, 2006, Daramola et al, 2009, Nicolas et al, 2011, Zhou et al, 2014, Akhtar et al, 2015, Li et al, 2015a).This is because MFI zeolites have well defined pore sizes which make it difficult to separate gases such as H_2 from other light gases e.g. CO_2. However this changed with the introduction of MDES modified MFI zeolite membranes. Modification of MFI membranes by sylilation inside the zeolite channels showed the potential for tuning the pore size to enhance H_2 separation from small gases at high temperatures (Gu et al, 2008, Wang et al, 2012, Hong et al, 2013).

3.1 Membrane Structure

Scanning electron microscopy (SEM) characterization indicates that zeolite membranes are composed of many crystals that grow together to form a dense layer (Funke at al, 1997). The regions between the crystals can have effective pore sizes that are larger than those in the zeolite itself and are known as intercrystalline pores or defects (Funke et al, 1997). Adsorption and diffusive transport is possible both within the zeolite crystal and the intercrystalline defects. Ideally, zeolite membranes should be defect-free so that only transport through the zeolite pores takes place (Coronas and Santamaria, 1999).

Zeolite membranes could be self-supported zeolite films or a thin film of zeolite on a porous and mechanically stable support. Self-supported zeolite membranes have been reported in the literature and include both ZSM-5 (Xu et al, 1997) and silicalite-1 (Tricoli et al, 1997). However, a supported zeolite membrane is best suited for most applications. The added strength and stability provided by the support enable the preparation of a thinner zeolite membrane layer. Unsupported membranes are often

thicker resulting in a high mass transport resistance and consequently in a low flux. Very thin MFI membranes on alumina have been synthesized using hydrothermal synthesis and secondary growth and have shown high fluxes with thicknesses ranging from 0.5μm to 10 μm (Hedlund et al, 1999, Dong et al, 2000, Lai and Gavalas, 2000, Au and Yeung, 2001, Hedlund et al, 2002, Algieri et al, 2003, Bonhomme et al,2003, Lai and Tsapatsis, 2004, Bai et al, 2005,Gopalakrishnan et al, 2006, Rezai et al, 2008, Zhou et al, 2014). Large surface area MFI membranes have been fabricated with high success rates and demonstrate good permeation characteristics (Bonhomme et al, 2003).

Proper selection of the support material is important since it affects the zeolite deposition and growth (Au and Yeung, 2001). Supports include porous ceramics such as alumina (Al_2O_3), titania (TiO_2) or zirconia (ZrO_2) (Xomeritakis et al, 1999, Yang et al, 1999, Bonhomme et al, 2003, Rezai et al, 2008) as well as stainless steel (Arruebo et al, 2001, Bernal et al, 2002, Tarditi et al, 2008). Flat discs or tubular supports are frequently used. Tubular membranes may be preferable for small-scale applications because they have higher surface areas per unit volume (Kalipcilar et al, 2001) and are better for scale up (Coronas et al, 1997). Monolith type substrates have also been reported and could provide even larger surface areas per unit volume, but they present some challenges in preparing the zeolite membranes on their surfaces (Kalipcilar et al, 2001). It is important that the pore size of the support at the zeolite/support interface is sufficiently small, about 100nm. In such a case, even a thin zeolite film is sufficient to close the pores of the support. The zeolite membrane can exist either as a thin layer on top of the porous support, or the zeolite can be preferentially deposited within the porous structure of the support (Coronas and Santamaria, 1999).

The most widely used support material is alumina, mostly due to the availability of high quality micro, nano and ultra filtration ceramics with relatively smooth top surfaces and small average pore sizes reaching down to ~5 nm pore size for γ-Al_2O_3 (Mabande et al, 2004). A smooth top surface is an important requirement for the preparation of thin continuous layers. The application of porous stainless steel supports (Bernal et al, 2002, Arruebo et al, 2001) for zeolite membranes has been less popular even though they show low mass transfer resistance and are compatible with most module and packing materials (Noack et al, 2005). Stainless steel supports generally

have rougher surfaces and larger pore sizes (>100 nm) (Bernal et al, 2003). They can also be susceptible to thermally induced cracks and adhesion problems due to their higher thermal expansion coefficient compared with alumina. These factors therefore make it more difficult to produce thin, defect-free zeolite membranes directly on stainless steel compared with ceramic supports (Mabande et al, 2004). The relatively large pore size requires a thick film in order to close the pores. Despite this, MFI zeolite membranes on stainless steel supports have been prepared successfully (Bakker et al, 1996, van den Broeke et al, 1999a, b, Aoki et al, 2000, Arruebo et al, 2001, Gardener et al, 2002, Algieri et al, 2003, Bernal et al, 2003, Sommer et al, 2003, Mabande et al, 2004, Arruebo et al, 2006, Sebastian, 2007, Tarditi et al, 2008). MFI membranes have also (to a lesser extent) been prepared on carbon supports as a cheaper alternative to alumina and stainless steel (Garcia-Martinez et al, 2001, Berenguer-Murcia et al, 2003 &2007). However, these groups have reported the difficulty of growing zeolite layers on carbon substrates (discs) as they suffer from extreme surface roughness. Carbon is also hydrophobic resulting in a poor interaction between the surface and zeolite synthesis solution and therefore requires pre-treatment (Berenguer-Murcia et al, 2007).

Alumina based substrates both "α and γ" types have been used in the majority of the work reported in scientific publications (Kusakabe et al, 1996, Coronas et al, 1997, Funke et al, 1997, Keizer et al, 1998, Lin et al, 1998, Gump et al, 1999, Piera et al, 1999, Poshusta et al, 1999, Xomeritakis et al, 1999, Yang et al, 1999, Au and Yeung, 2001, Xomeritakis et al, 2001, Bernal et al, 2002, Algieri et al, 2003, Bonhomme et al, 2003, Lai and Tsapatsis, 2004, Camus et al, 2006, Miachon et al, 2006 & 2007, Rezai et al, 2008, Sebastian et al 2008, Zhang et al, 2010). The well defined pore size (>5nm for the alumina based substrate) is ideal for membrane preparation. Alumina has a better conformity in thermal expansion coefficient with the zeolite, compared with stainless steel. The α form of alumina is also relatively inert and shows low tendencies to leach aluminium into the alkaline synthesis solution. However this is not the case for the γ form, which has to be protected during synthesis (Coronas et al, 1997).

3.2 Membrane Synthesis

Efforts to prepare zeolite membranes started in the late 1980s. Initial efforts did not lead to synthesis of good quality materials. However, during the earlier years of the 1990s several research groups succeeded in preparing good quality MFI type zeolite membranes with very good permeation and separation properties. Improved techniques of membrane preparation and better choice of materials coupled with a focus on better and more environmentally-friendly processes have led this interest. As a result there has been an increasing number of papers on synthesis of MFI type zeolite membranes (Bai et al, 1995, Bakker et al, 1995, Kapteijn et al, 1995 Kusakabe et al, 1996, Funke et al, 1997, Keizer et al, 1998, Lin et al, 1998, Gump et al, 1999, Tuan et al, 1999, van den Broeke et al, 1999a,b., Aoki et al, 2000, Millot et al, 2000 Au and Yeung, 2001, Lin et al. 2001, Xomeritakis et al, 2001, Gardener et al, 2002, Algieri et al, 2003, Bernal et al, 2002 & 2003, Bonhomme et al, 2003, Sommer et al, 2003, Lai and Tsapatsis, 2004, Mabande et al, 2004, Noack et al, 2005, Arruebo et al, 2006, Miachon et al, 2006 & 2007, Mabande et al, 2007, Rezai et al, 2008, Tarditi et al, 2008, Zhang et al, 2010, Zhou et al, 2014).

Generally, zeolites are crystallised by hydrothermal treatment of a clear synthesis solution or synthesis gel containing a silica source, an alumina source and a templating agent such as tetramethylammonium (TMA^+) or the tetrapropylammonium (TPA^+) ion. Zeolite synthesis with nucleation is sensitive to experimental conditions such as synthesis solution/gel composition, concentration and viscosity, pH of the gel/solution, the source of the silica and its degree of polymerisation, as well as the temperature and duration of the reaction (Lin et al, 2002, Bonhomme et al, 2003). The zeolite crystals, films and membranes are often rinsed in some media to remove residues from the synthesis mixture. Common rinsing media are water and aqueous solutions of ammonia. The organic template molecules get trapped in the pores of the zeolite and must be removed in order to render the structure microporous. This is carried out by calcination, a procedure in which the zeolite is heated in air to decompose and burn the templating agent blocking the pores (Lin et al, 2002). A development in zeolite membrane synthesis is to use microwave heating which has been used to replace or combine conventional heating in the crystallisation step to speed up zeolite membrane synthesis (Li and Yang, 2008, Drobek et al, 2012). Microwave heating can also prevent

support dissolution and is able to consistently obtain thin defect free zeolite membranes (Sebastian et al, 2010).

Experimental conditions have to be optimised in order to obtain good quality membranes and finding the right conditions to prepare the desired zeolite membrane requires much trial and error. Preparing a synthesis mixture from different reagents can lead to variable results, even for almost the same compositions. For the preparation of MFI membranes, aerosol or colloidal silica and tetrapropylammonuim bromide (TPABr) or hydroxide (TPAOH) can be used as the silica source and the organic template respectively (Lin et al, 2002). The nature and structure of the support such as its microscopic roughness and pore size can also affect membrane formation (Tsai et al, 2000).

Different approaches to zeolite membrane formation are summarised in Figure 3.2. Composite membranes are preferred due to the added stability offered by the support and are consequently studied more frequently than self-supported films, or mixed matrix membranes. Zeolite membranes can be prepared by three main methods:

(i) in situ hydrothermal synthesis (Ramsay et al, 1994, Kapteijn et al, 1995, Yan et al, 1995, Piera et al, 1998),

(ii) secondary growth synthesis (or seeded growth) (Lai et al, 1998, Hedlund et al, 1999, Xomeritakis et al, 1999)

(iii) vapour phase transport method (Xu et al, 1990, Nishiyama et al, 1996, Kikuchi et al, 1997).

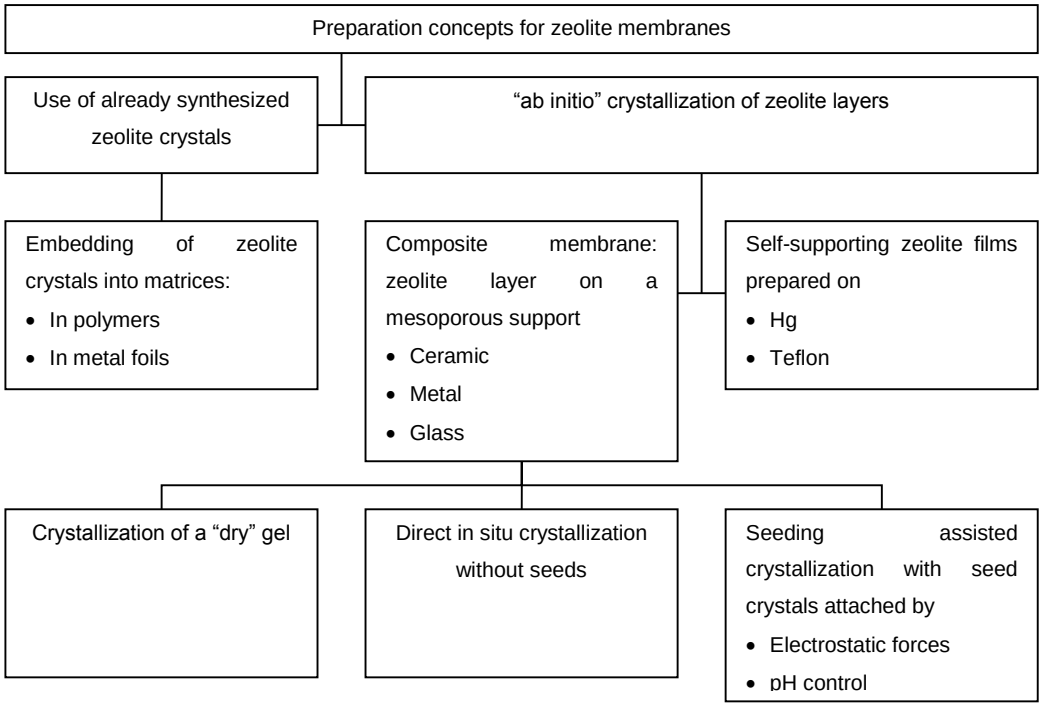

Figure 3.2: Variety of concepts for zeolite membrane preparation (Adapted from Caro et al, 2000)

3.2.1 In-Situ Crystallisation

The most common approach for the synthesis of zeolite membranes is in-situ crystallization, which consists of placing a porous support in contact with the synthesis solution or gel. Under hydrothermal conditions, small crystals are inter-grown onto macro/mesoporous substrates. MFI crystallization starts at the phase boundary between the liquid phase (as the TPA source) and the gel phase (as the Si source). The crystal grows into the gel layer consuming the gel until the growing MFI crystals reach the support. The gel for the zeolite crystallization can either form a surface layer or it can be soaked into the pore system of the support forming zeolite plugs (Ramsay et al, 1994, Piera et al, 1998). The major challenge with this approach is to identify suitable conditions so that the zeolite crystals nucleate and grow preferentially on the support surface in an interlocking fashion (Xomeritakis et al, 2000). This is difficult since the distribution homogeneity on the support depends on different parameters such as the local support surface properties which can be difficult to control (Miachon et al, 2006).

3.2.2 Secondary Seeded Growth

The second method involves the growth of seed crystals attached to a support. It is a two-step process, the first of which is nucleation. This is followed by attachment of the seeds to the support (Caro et al, 2000). The seeds are then grown under hydrothermal zeolite synthesis conditions in order to form a continuous zeolite layer on the substrate surface (Miachon et al, 2006). The aim of this is to grow a film without intercrystalline defects. Different methods for attachment to the seed surface have been proposed and include slip casting, electrostatic attraction and dip coating. Also, the seeds can be crystallised directly on the support (Mabande et al, 2004). In this method, the substrate with the zeolite layer is brought into contact with the zeolite synthesis solution and in this contact, the seed crystals grow and eventually seal the intercrystalline voids. The seeding method is considered to be better than the in-situ method since a continuous zeolite film can easily grow and cover the support under less stringent conditions. When compared with the in-situ method, the secondary growth method requires more dilute synthesis conditions, lower synthesis temperatures and shorter synthesis times (Lin et al, 2002). An important advantage of this method is that the two main steps of zeolite film formation, i.e. nucleation and growth on a support surface are separated which makes it possible to tailor the zeolite film microstructure (Xomeritakis et al, 2000).

3.2.3 Vapour Transport Method

The third method is also a two step method. Firstly, an amorphous gel that contains silica and alumina is coated on the support. In the second step, dry hydrogel is crystallised with vaporised solvent in an autoclave (Lin et al, 2002, Miachon et al, 2006). Two different vapour phase transport methods have been reported. In one method (Xu et al, 1992), the template and water are placed at the bottom of the autoclave and fed to the dry amorphous gel by saturated vapour pressure. In the other method (Sano et al, 1992), the template is mixed with the dry gel and only water is placed in the bottom of the autoclave.

An advantage of the vapour phase transport method when compared to in-situ crystallisation is that it allows 100% conversion of reaction gel. It is also possible to obtain membranes with higher Si/Al ratios than hydrothermal synthesis (Lin et al, 2002). The amount of nutrients for growing zeolite is directly controlled by the amount of gel applied. This approach has better thickness control compared with in-situ crystallization and secondary-seeded growth, since the amount of nutrient for growing zeolite is directly controlled by the amount of gel applied (Chiang and Chao, 2001). A drawback is the possibility of crack formation in the amorphous gel layer as the density of the gel is much lower than that of zeolite crystals (Chiang and Chao, 2001, Miachon et al, 2006).

Tubular or disk supports can be used with all three types of synthesis. Preparing membranes with a continuous layer on the interior surface of tubular membranes is, however, more difficult than on the surface of a disc, because maintaining the concentrations of reagents along the length of the support is more difficult during synthesis. For this reason, disc supports have been used for concept demonstration and ease of testing, whereas tubular supports have been used in industrial applications of zeolite membranes (Gascon et al, 2012). Tubular membranes are also considered better for scale-up and provide larger surface areas (Coronas et al, 1997). Monolith type supports or hollow fibers have larger surface area to volume ratios with a high packing density (Soria et al, 1999, Chiang and Chao, 2001, Camus et al, 2006, Gascon et al, 2012).

3.2.4 Pore Plugging Method

In this thesis, the membranes used were prepared by a pore-plugging method as reported by Dalmon and his group (Ramsay et al, 1994, Uzio et al, 1994, Giroir-Fendler et al, 1996). The nucleation and crystallization process is carried out under in situ hydrothermal conditions. However, rather than growing the zeolite as a film on top of the support, the zeolite crystals are grown within the pores of a ceramic α-alumina tube, until the pores are completely blocked by the zeolite material (See Figure 3.3). This results in a continuous composite zeolite-alumina membrane. The separative

layer is located within the pores of the host ceramic support (Miachon et al, 2006). This type of membrane shows different separation behaviour when compared with zeolite films and this is discussed in more detail later. The following comparison with zeolite films demonstrates the structural advantages of nanocomposite membranes as reported by Miachon et al, (2006).

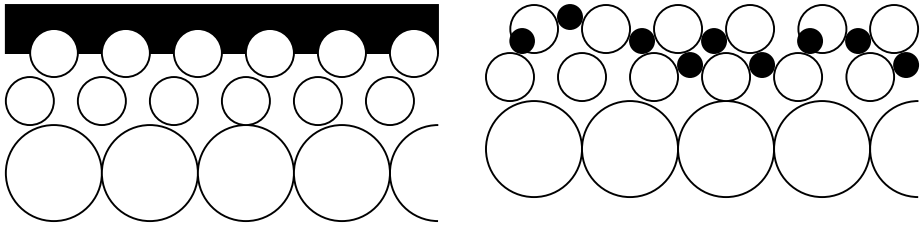

Supported Zeolite Membrane

Composite Zeolite Membrane (Pore Plugging)

Figure 3.3: Schematic comparison between film (left) and nanocomposite membrane structures (Adapted from Miachon et al, 2006)

(i) One of the problems with zeolite films is the difference in thermal expansions of the zeolite and the substrate. When the membrane is exposed to large temperature changes, long range stresses may build up and lead to the formation of cracks. However, with the nanocomposite pore-plugged membranes, the zeolite is less affected by thermal effects since the crystals are located within the substrate.

(ii) Where large membrane areas are required, the pore-plugging approach may be less challenging than other methods. If a defect is formed, it is unlikely to be larger than the pore of the host material. Scaling-up may therefore be simpler as the conditions can be less demanding (e.g. no clean room is needed).

(iii) As the membrane is located within the ceramic support, it is well protected from abrasion and shocks. Membrane handling and potting into engineering artefacts are therefore easier.

Various studies have been done on pore-plugged membranes (Coronas et al, 1997, Piera et al, 1998, Ciavarella et al et al, 2000, Camus et al, 2006, Miachon et al, 2006, Miachon et al, 2007, Alshebani et al, 2008, Deng et al, 2010, Nicolas et al, 2011) and

the concept has been used for other membrane materials, such as Pd-ceramic composite membranes (Xomeritakis and Lin, 1996, Miachon et al, 2000), V-MFI /αAl_2O_3 membranes (Julbe et al, 2003), and ZIF-8 nanocomposites (Drobek et al, 2015).

3.3 Membrane Quality Criteria

The lack of fast and reliable methods for the assessment of membrane quality has been a major issue in zeolite membrane development (Bernal et al, 2002, Chiang and Chao, 2001). Usually, the meaning of membrane quality relates to the ability of the membrane to carry out a given separation. A good membrane therefore is able to separate a mixture with high selectivity, while a low selectivity, often taken as an indication of the presence of a significant number of defects, indicates a low quality membrane. The diverse characteristics of zeolite membranes such as zeolite type, membrane thickness, concentration and size of defects etc. makes it difficult to develop a common method for membrane characterization (Bernal et al, 2002).

Zeolite membranes can be characterised by scanning electron microscopy (SEM), X-ray diffraction (XRD) and permeation/separation tests. The XRD patterns of most zeolite membranes are the same as powder zeolites, confirming that zeolite films are polycrystalline with crystals randomly oriented on substrates. The orientation of some membranes has also been reported such as a-orientation (Hedlund et al, 1999), and b-orientation (Lai et al, 2002, 2003). Good quality membranes in general have fairly small intercrystalline regions which cannot be distinguished by SEM. Transmission electron microscopy (TEM) has also been used to characterise zeolite membranes, but it is also difficult in this case to observe intercrystalline regions due to the low stability of the electron beam passing through the zeolites. These characterization techniques therefore only provide limited information on zeolite membrane characteristics. Permeation/separation tests can be more reliable methods for characterization especially in the determination of intercrystalline regions (Lin et al, 2002).

A virtually defect-free film is essential to obtain high selectivity. Zeolite membranes with defects usually have high permeances but low selectivities since the diffusivity is much higher in defects compared to the zeolite pores. Different kinds of defects exist and these include (Jareman 2004):

- Cracks
- Open-grain boundaries
- Non-closed film (pinholes)

Cracks are believed to form mainly during calcination of the synthesised film. As described in section 3.2, zeolite layers are usually formed in the presence of an organic template. Removal of this template which is incorporated in the zeolite channels is achieved by calcining the membrane. Intercrystalline gaps tend to form in the membrane due to the difference in thermal expansion between the zeolite layer and the support (Lai and Gavalas, 2000, Kanezashi et al, 2007). This is caused by stresses due to the shrinking of the zeolite layer with increasing temperature and the expansion of the support. This type of defect can be avoided by growing template-free membranes as discussed later in section 3.4. Open-grain boundaries are assumed to arise during synthesis, due to a lack of space to add another building block between two growing crystals. Defects classified as pinholes are a result of insufficient film thickness or incomplete and/or uneven seeding (Jareman 2004).

Essentially all zeolite membranes recorded so far contain intercrystalline non-zeolitic pores (Arruebo et al, 2001, Bernal et al, 2002, Bonhomme et al, 2003). Defects in zeolite membranes can be classified into macro, meso and micro defects. IUPAC defines pore sizes as follows:

- Macro-defects (usually cracks and pinholes) d_p>50nm
- Meso-defects 2nm<d_p>50nm
- Micro defects d_p <2nm

The best way to determine whether defects are present is to perform permeation/separation tests (Lin et al, 2002). The impact of defects on separations has

been studied by a number of authors (Kapteijn et al, 1995, Funke et al, 1997, Arruebo et al, 2001, Bernal et al, 2002). Although it is well accepted that reducing the number of inter-crystalline defects is the best way to increase separation selectivity, it has been shown that high selectivities could be obtained in membranes where defects are present, provided that they are small in magnitude (Coronas and Santamaria, 1999). For good quality membranes, these non-zeolitic pores should be smaller than 2nm (Lin, 2001).

The quality of zeolite membranes is generally characterized by measuring the permeance of individual gases or vapours, as well as selectivities for gas mixtures. One method involves the detection of defects before complete membrane synthesis. In the case of membranes synthesised with templates, single gas permeation through the membrane before template removal (calcination) can provide useful information about the presence of macroporous defects in the zeolite film. Before calcination, zeolitic pores are filled with TPAOH and no helium should permeate through them. Extremely low helium permeance would indicate that the membrane is pinhole or defect free. A small amount of defects may however be formed in the template removal step (Lin et al, 2002).

Various groups have suggested different methods to assess membrane quality. A well accepted method is the use of nitrogen (N_2) and sulphur hexafluoride (SF_6) due to their significant differences in diameter and diffusivities. N_2 is used due to the relative small diameter of the molecule compared with the MFI pore diameter. Hydrogen (H_2) has also been used for similar reasons (Mabande et al, 2004). SF_6 is similar in size to the MFI zeolite pores (0.55nm) and should not pass through the membrane if it is free of defects (Lin et al, 1998). A high separation factor of N_2/SF_6, much larger than the Knudsen separation factor (ratio of the square root of the molar mass), therefore indicates a good quality membrane (Lin et al, 2002). Funke et al (1997) asserted that a permselectivity between N_2 and SF_6 should be greater than 80 at room temperature in order to have a high quality MFI membrane. Lin et al (1998) argue however, that a high selectivity/separation factor of N_2/SF_6 is not necessarily indicative of a defect free membrane. Membranes prepared in their laboratory had high N_2/SF_6 selectivities, but other components larger in size than MFI zeolite pores were able to permeate through the membrane, namely iso-octane (0.62nm) and 2-2-dimethylbutane (0.62nm). This

was indicative of transport through non-zeolite pores indicating the presence of defects even though the membranes had passed the N_2/SF_6 test. Butane isomers have also been used to determine membrane quality. Kapteijn et al (1995) suggested that a good quality membrane should have a good permselectivity, (between two butane isomers), higher than 10, where n-butane is the faster permeating species.

Bernal et al (2002) stated that quality assessment methods such as measurements of ideal selectivities are often unreliable because the adsorption process plays a major role in many of the separations carried out with zeolite membranes. It was suggested that the reduction of permeation flux that takes place in the presence of suitable adsorbates could be used as a quality indicator because it relates directly to the separation selectivity of a given membrane. Miachon et al, (2006) suggested the use of an adsorbing (n-butane) and a non-adsorbing (hydrogen) component to assess the membrane quality. The presence of defects would inhibit this adsorption-based separation and would favour the transport of hydrogen. A high n-butane/H_2 selectivity would thereby indicate a good quality membrane. They also criticise the separation tests based on molecular sieving (N_2/SF_6) or diffusion separations (n/i-butane) and state that Knudsen type defects can still show some separation efficiency (N_2/SF_6) or be neutral (n/i-butane). Other organic isomers that have been used to characterize membrane include mixtures of n-hexane/DMB (Arruebo et al, 2006).

It is important to note that zeolite membranes are used under a variety of conditions which will affect membrane performance. For example, in adsorption- driven separations, a membrane may give selective separations under certain conditions (e.g. high partial pressure of the permeating compounds and low temperature) and show no selectivity under others. Membrane quality is therefore system specific and the specificity of the membrane response should be taken into account when designing tests aimed at the assessment of its quality (Bernal et al, 2002).

Generally, a membrane is considered high quality if only a small fraction of its flux is through defects, however it has been observed that for a membrane with a high concentration of defects, the traditional methods of characterization described above may not detect them and may instead indicate that the membrane is of high quality.

Zeolite membrane characterization can therefore be difficult and different characterization methods can reach different conclusions about non-zeolitic pores (Yu et al, 2007).

It has been shown that the characterization method may change membrane properties. It was found that n-hexane adsorption in MFI membranes decreased the flux through non-zeolitic pores. Therefore a method that used n-hexane, such as permporosimetry or C_6 isomer separation, may not provide accurate characterization of membrane properties (Yu et al, 2008a). It has been shown that the adsorption of n-hexane into the MFI pores swells the MFI crystals and shrinks the size of non-zeolitic pores. Yu et al, (2008a) showed that methods that use n-hexane permporosimetry and n-hexane/2,2 dimethylbutane (DMB) separation are not effective for characterization of MFI zeolite membranes. In one study, defect volume, indicated by the amount of adsorbed DMB (a molecule that adsorbs in defects but is too large to adsorb in the MFI pores) decreased by 50% when 0.7% n-hexane was added to DMB (Yu et al, 2008b). Further studies have shown adsorption of many molecules in MFI pores also expanded zeolite crystals and reduced defects size in MFI membranes and this is discussed in more detail in Section 3.4.3.

3.4 Factors Affecting Membrane Quality and Performance

Various factors can affect membrane quality and consequently the way the membrane performs a given separation. These include the presence of defects, as discussed above, membrane thickness, synthesis procedure, and Si/Al ratio.

3.4.1 Presence of Defects

Membranes with few defects have been shown to provide the most selective separations. Pre-treatment either before calcination or post-synthesis treatment after

membrane synthesis is complete, can eliminate or minimise the formation of defects. The larger (macro) defects can be eliminated by repeated crystallisation.

3.4.1.1 Pre-Treatment

Elimination of small defects may be possible by chemical vapour deposition (CVD) of silica via reaction with a silicon alkoxide or other silylation agents. Another pre-treatment that has been used involves iron oxide (Arruebo et al, 2001).

As explained previously, the presence of intercrystalline gaps in zeolite membranes affects the separation properties of a membrane. Membrane synthesis usually involves the use of a templating agent that is incorporated into the zeolite pore structure and must be removed to open up the zeolite channels (Hedlund et al, 1999, Kanezashi et al, 2006) The removal of the templating agent (TPA^+) during calcination, where temperatures can exceed 400^{o}C, results in an abrupt shrinkage of the zeolite lattice, causing substantial stress that often results in microcracks in the film (Hedlund et al, 1999, Lai and Gavalas, 2000, Kanezashi et al, 2006). Template-free synthesis can minimise these defects and/or intercrystalline gaps that form in the membranes and has been adopted by a number of authors (Mintova et al, 1998, Hedlund et al, 1999, Lai and Gavalas 2000, Li et al, 2003, Gopalakrishnan et al, 2006 and Kanezashi et al, 2006).

According to Lai and Gavalas (2000), template free synthesis not only eliminates the need for calcination, but also uses cheaper, less toxic reactants. It is also claimed that crystallization during ZSM-5 bulk synthesis is difficult since in the absence of TPA^+, crystallization is limited to a narrow range of aluminium concentration with the Si/Al ratio generally in the 140-180 range. It is suggested, however, that crystallization can be facilitated by organic additives such as alcohols, ketones, amines which can be used as, for example structure directing agents (SDAs), void fillers, host crystal stabilisers and gel chemistry modifiers (Lai and Gavalas, 2000). Selectivity results of H_2 over n-butane were above 10^4 which compared well with literature results of membranes

prepared with TPA^+, which suggests that TPA-free synthesis is effective for preparation of membranes without defects (Lai and Gavalas, 2000).

Hedlund et al (1999) treated the supports in synthesis solution free of organic template in order to grow the seed crystals into ZSM-5 films. SEM analysis indicated that the zeolite films were defect-free. Single gas selectivities for n-butane/i-butane in this study were lower than those of Yan et al (1995) and Lovallo and Tsapatsis (1996) (both used templates for membrane synthesis). It was observed during permeation experiments that the membrane did in fact contain defects due to the permeation of molecules larger than the zeolite pore sizes (xylene isomers and SF_6). In this case, it seems that not using organic templates may not have had a large effect on defect formation.

Gopalakrishnan et al (2006) prepared both a template free and a templated membrane and compared the two by performing permeation experiments. It was found that although the template-free membrane did perform better due to the absence of the calcination step, this membrane still contained some defects that were assumed to be similar in size to the zeolite pores. Therefore, preparing template-free membranes does not necessarily eliminate defects, but it does reduce them.

3.4.1.2 Post-Synthesis Treatment

Post-synthesis treatment methods can be beneficial in two ways; reducing the number of defects or intercrystalline gaps and modifying the membrane properties (Kosinov et al, 2015). Post treatment methods used to improve membrane performance include ion-exchange (Yan et al, 1995, Kusakabe et al, 1998), coking using tetraisopropylbenzene (TIPB) (Yan et al, 1997, Gump et al, 1999) and CVD using tetramethyloxosilcate (TMOS) and tetrathylosilcate (TEOS) (Lin et al, 2002). A rapid calcination method that favours the condensation of surface hydroxyl groups on the zeolite grain boundary before template removal has also been reported (Choi et al, 2009). These treatments involve a reduction of the pore openings on the external surface of the crystals and have shown a significant reduction in defects, thereby

increasing the selectivity of the membranes. However, these treatments may block access to pores or reduce pore entrance diameters and consequently decrease fluxes (Tuan et al, 1999).

The most widely adopted method to narrow the pore size, and consequently improve selectivity of MFI-type zeolite membranes is by catalytic cracking deposition (CCD) of methyldiethoxysilane (MDES). Hong et al (2005) tuned pores of B-ZSM-5 membranes by catalytic cracking deposition (CCD) of methyldiethoxysilane (MDES) and observed a significant improvement in H_2/CO_2 selectivity with a minimal decrease of H_2 permeance. In further studies, the same group (Hong et al, 2013) modifies MFI hollow fiber zeolite membranes using the same method. The membranes showed goof thermochemical stability for the separation of H_2/CO_2 gas mixtures. Tang et al (2009) observed that H_2/CO_2 selectivity increased after several consecutive CCD steps. Although H_2/CO_2 selectivity was 40 times higher, the H_2 permeance was only two times lower. Pore size tuning by deposition of molecular silica inside the zeolite pores (i.e. MDES modified MFI membranes) provide an opportunity to turn initially adsorption membranes into stable molecular sieving membranes with high selectivity towards small molecules (Kosinov et al, 2015). Another major advantage of membranes silylated by MDES is the improved thermal and hydrothermal stability (Gu et al, 2008).

3.4.2 Synthesis Methods

The method of synthesis can also seriously affect permeation behaviour. Coronas et al (1997) demonstrated that ZSM-5 membranes prepared by different procedures on porous alumina tubes can exhibit different permeation behaviours. Si/Al ratios can also make a significant contribution to membrane formation. Noack et al (2005) found that permeation properties of membranes were mainly influenced by the Al content in the MFI layers but not the type of support. Intercrystalline (non-zeolite) permeance increased with increasing Al content which gave low mixture selectivities for Al-rich membranes. Variation of Si/Al properties also caused a change in adsorption properties. A high Al content allows specific interactions with polar or polarizable

molecules, leading to their adsorptive separation from the non-polar molecules in mixtures of such substances. This is contrary to the findings of Coronas et al, (1997) who found that the differences in behaviour of those MFI membranes were not due to Si/Al ratio but were due to the presence of non zeolite pores, and different synthesis procedures which produced membranes with different relative amounts of zeolite and non-zeolite pores. Also contradictory was the fact that in this case, the Al- poor membranes showed much lower selectivities (by a factor of three) than the Al-rich membranes.

Effects of different synthesis conditions are also important. The preparation procedure, crystallization time and temperature, number of synthesis layers, gel dilution, Si source, and type of support have been investigated by various authors (Tuan et al, 1999, Aoki et al, 2000, Bernal et al, 2003, Miachon et al, 2006). Increasing crystallization time increases membrane thickness which results in less defects, but leads also to an increase in membrane transport resistance (Gardener et al, 2002, Mabande et al, 2004). For example, Mabande et al (2004) found that although permeances decreased, the ideal selectivity of H_2/SF_6 silicalite-1 increased with increasing crystallisation time and temperature. It was concluded that the high value was probably due to both the relatively high layer thickness (~10 μm according to cross-sectional SEM) and low number of defects. Xomeritakis et al (2000) observed an increase in n/i-butane selectivities on MFI with increasing membrane thickness thereby suggesting a gradual elimination of defects by growing the membranes thicker. However increasing membrane thickness after a certain point did not provide any further improvements. Au and Yeung (2001) found that H_2, He, N_2 and CH_4 displayed lower permeances with increasing ZSM-5 membrane thickness. Ideal separation ratios of H_2/n-C_4H_{10} and H_2/i-C_4H_{10} improved with increasing membrane thickness.

Location of the zeolite layer is another important factor affecting membrane performance. The MFI zeolite can either be a zeolite film on top of the support, or located within the pores (pore plugging) as shown in Figure 3.3. Both types of membrane often exhibit different separation behaviours (Coronas and Santamaria, 1999). Membranes that are plugged often have lower permeances than zeolite layer membranes but show higher selectivities (Caro et al, 2000). This is because the pore

plugging method, as mentioned before, results in membranes with less defects. Coronas et al (1997) suggest that intercrystalline pore regions are smaller for membranes plugged with zeolite than zeolite films due to a smaller increase in permeance with temperature. The nanocomposite membranes used in this thesis are therefore expected to have few defects and also have the ability to hold their selectivity at higher temperatures compared with zeolite layer membranes, as has been observed Gump et al (2000).

Although the studies described above provide an insight into the factors affecting membrane performance, care must be taken when comparing different membranes prepared in different laboratories. Precise knowledge about the measurement conditions, membrane characteristics and pre-treatments is required (Noack et al, 2005).

3.4.3 Adsorption Induced Structural Change

Characterization methods as described in section 3.3 assumed that the zeolite structure is rigid. However, recent studies have shown that MFI structures can be flexible. Defect sizes can decrease or increase when certain molecules adsorb in a zeolite pore (Yu et al, 2011).

Hydrocarbons (n-hexane, n-pentane, n-butane, n-propane) and gases such as SF_6 have been shown to swell MFI crystals when they adsorb. Apart from influencing the selection of appropriate characterization techniques for evaluating MFI membrane quality, changes in membrane microstructure due to crystal expansion also significantly affects membrane separation ability (Yu et al, 2011). Figure 3.4 shows a schematic of crystal expansion.

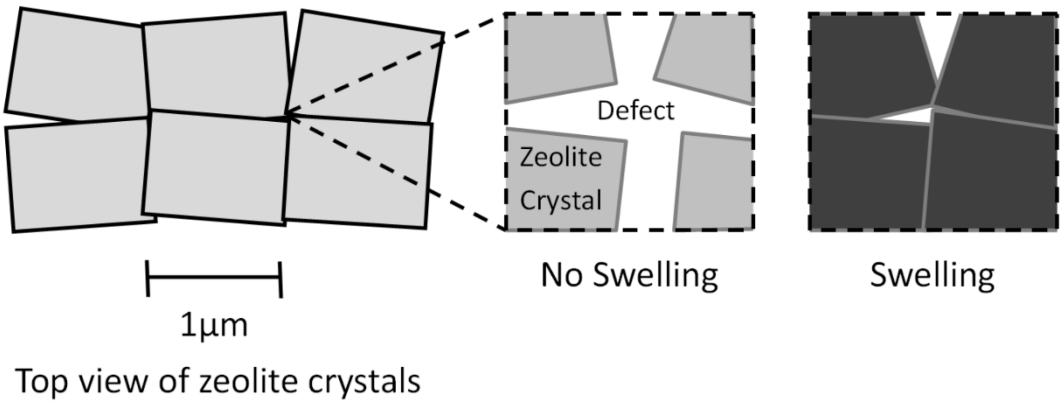

Figure 3.4: Diagram indicating impact of pore swelling on defect size (Adapted from Yu et al, 2011)

P-xylene adsorption on zeolite pores can expand the pores of the zeolite as well as the crystals. The p-xylene adsorption induced structural change can impair the separation performance of MFI zeolite for separation of a xylene isomer mixture (O'Brien-Abraham et al, 2008).

Lee et al, (2008), tested one B-ZSM-5 membrane with a relatively large number of small defects, and one silicalite-1 membrane with a smaller number of somewhat larger defects. The relative contribution of these defects to the overall flux changed dramatically in the presence of n-alkanes (n-C_3 – n-C_6) and SF_6. They found that SF_6 induced expansion stopped 99% of the flux through defects of the B-ZSM-5 membrane whereas for the silicalite-1membrane, SF_6 only decreased the flux through defects by 30%.

Sorenson et al, (2008) found that crystal expansion changed permeation and separation properties of zeolite membranes. Optical microscopy and XRD measurements performed by this group observed that silicalite-1 crystals expand when C_4-C_8 alkanes and i-butane adsorb in the MFI structure at room temperature. Crystal expansion due to n-alkane adsorption decreased the size of defects in MFI membranes. Loadings >0.5 mol/unit cell decreased the flux of isooctane through defects. Higher loadings of alkanes increased crystal expansion and further decreased the defect size which further decreased isooctane flux. It is important to note that in this study, crystal expansion was found to be reversible.

Generally, most adsorbates that have been investigated expand zeolite crystals, and it has been observed that this expansion increases monotonically with loading. However, it has also been observed that some molecules contracted crystals at low loadings, (thus increasing the size of defects), and expanded at higher loadings. Lee et al, (2009) found that adsorption of i-butane, p-xylene and benzene shrinks the size of MFI crystals in polycrystalline MFI membranes at low loadings, and expands them at higher loadings. Crystal shrinkage over different loading ranges increased the size of the defects and increased helium flux increased by as much as 44% (p-xylene loading <4 molecules per unit cell and for i-butane loading between 3 and 8 molecules per unit cell). At higher loadings (7 molecules per unit cell for p-xylene and 9 molecules per unit cell for i-butane), p-xylene expanded MFI crystals and shrank defects such that helium flow through defects decreased as much as 2 orders of magnitude (Lee et al, 2009). This phenomenon was also observed by Sorenson et al, (2010) where zeolite pores expanded or contracted upon adsorption of alkanes, thereby decreasing or increasing defect sizes. They observed that in B-ZSM-5 membranes, adsorption of n-hexane and SF_6 expanded the crystals and fluxes through defects decreased dramatically. The crystals expanded more as the loadings of the adsorbates increased. In contrast, i-butane adsorption contracted the B-ZSM-5 crystals at low loadings (increasing defect size) and expanded at high loadings (decreasing defect size).

Other studies include the separation of alcohols from water. In a study by Tokay et al (2009), a B-ZSM-5 membrane with the majority of its helium flux through defects at room temperature was used to study how MFI crystal expansion affects alcohol separations. They found that separation selectivity for 2-propanol/water was 5 orders of magnitude higher than the ideal selectivity because of crystal swelling due to alcohol adsorption. Permporosimetry measurements showed that adsorption of 2-propanol, 1-butanol and ethanol decreased helium flow through the defects because these alcohols swell MFI crystals. In contrast, neither methanol nor water adsorption appeared to affect the defect size. They concluded that both crystal swelling and preferential adsorption contributed to the separation of alcohol/water mixtures.

These studies clearly show that polycrystalline zeolite membranes are flexible and their defect sizes change due to the adsorbate-induced crystal expansion and

contraction and consequently this has a major influence on membrane quality and performance (Yu et al, 2011).

No studies have been done on the effect of ammonia adsorption on the microstructure of MFI zeolites, and therefore it is still unknown as to whether the adsorption of ammonia would decrease the defect sizes or as in some cases presented previously, increase the defect size. Most studies of ammonia adsorption on zeolite have focused on detecting the presence of acid sites, and no report has been made as to whether this adsorption causes structural changes. Studies focused on the interaction of MFI with ammonia outside acid site detection would be highly beneficial.

3.5 Separation Mechanisms

A more detailed explanation of mechanisms for gas separation through porous membranes is given in Chapter 2, Section 2.7. These same mechanisms apply to MFI zeolite membranes and are discussed further here.

Factors that play key roles in zeolite separations include the affinity of the permeating molecule toward the zeolite material and the difference between the sizes of these molecules and that of the membrane pores (Sebastian et al, 2007). Separation by zeolite membranes can therefore be due to molecular sieving and/or preferential adsorption and/or differences in diffusion rates (Rezai et al, 2008).

In zeolite pores, adsorption equilibrium and diffusion often dominate especially when the sizes of the molecules to be separated are smaller than the zeolite pore size. Molecular sieving plays a major role when some of the molecules to be separated are larger than the zeolite pore size (Sommer et al, 2003). The presence of intracrystalline and intercrystalline pores in zeolite membranes is not disputed (Kanezashi et al, 2006). As such, diffusion can also occur in the intercrystalline (non-zeolite) regions. Depending on the sizes of the non-zeolite pores and molecules, the following transport mechanisms can be important: molecular sieving (Rao and Sircar, 1993, Keizer et al,

1998), Knudsen and surface diffusion (Coronas et al, 1997, Vroon et al, 1996, Bonhomme et al, 2003). Pore blocking by adsorption (Arruebo et al, 2001, Funke et al, 1997) and capillary condensation (Coronas and Santamaria, 1999) can also be significant. Capillary condensation can take place in meso porous intercrystalline pores (defects) when present in zeolite membranes. This mechanism also occurs where significant adsorption can also be expected and therefore both processes may occur in the system, giving rise to a cooperative separation mechanism (Bernal et al, 2002).
Molecular sieving occurs when there is a significant difference between the kinetic diameters of the gases or vapours that permeate. Not many examples of this exclusion mechanism can be found in the literature since this molecular sieving mechanism requires perfect membranes (Bakker et al, 1996). However, an example is given in a study by Keizer et al (1998) where the separation of n-hexane from 2,2 dimethylbutane (0.43nm and 0.68nm kinetic diameters respectively) on an MFI ceramic membrane was attributed to molecular sieving. In most cases, this separation is actually more complicated and although in the first instance this separation could be attributed to size exclusion, detailed studies may indicate a sorption-diffusion mechanism (Caro et al, 2000).

Most separations reported with MFI zeolite membranes can be explained in terms of surface diffusion. Selective adsorption occurs when one of the components in a mixture is able to preferentially adsorb on the walls of the zeolite pores and is transported selectively, thereby blocking the membrane. This then prevents the other species in the mixture from passing through the membrane (Coronas et al, 1997). A more detailed description of this phenomenon and example studies are given in Section 3.5.2. Gaseous permeation through microporous zeolite channels can also occur via activated diffusion (Kapteijn et al, 1995, Krishna and van den Broeke, 1995).

Permeation through non-zeolitic pores occurs by Knudsen diffusion and/or viscous flow and consequently there is an additional parallel contribution to the total flux through the membrane. If large defects are present in the zeolite layer, the permeation of gases will be dominated by Poiseuille flow. If the mean free path of the diffusing molecules becomes much larger than the pore size of the membrane, the permeation will be controlled by Knudsen diffusion and the gas permeance will be proportional to the square root of the inverse of the molecular weight (Algieri et al, 2003). Adsorption

followed by surface diffusion can also occur in non-zeolite pores (of a similar size to the zeolite pores) (Gump et al, 1999).

The pathways of transport in MFI zeolite membranes can therefore be summarised as the sum of (Arruebo et al, 2001):

1. Permeation through zeolite channels which is selective
2. Permeation through non-zeolite channels which is non-selective

3.5.1 Qualitative Description of Permeation

The mechanism of single and multi-component mass transport through, or in, zeolites is still a matter of debate. Mass transport through a zeolite layer is qualitatively envisaged in Figure 3.5 by a five step model (Bakker et al, 1996)

1. Adsorption from the gas phase to the external surface
2. Mass transport from the external surface to the zeolite pores
3. Intracrystalline zeolite diffusion
4. Mass transport out of the zeolite pores to the external surface
5. Desorption from the external surface to the gas phase

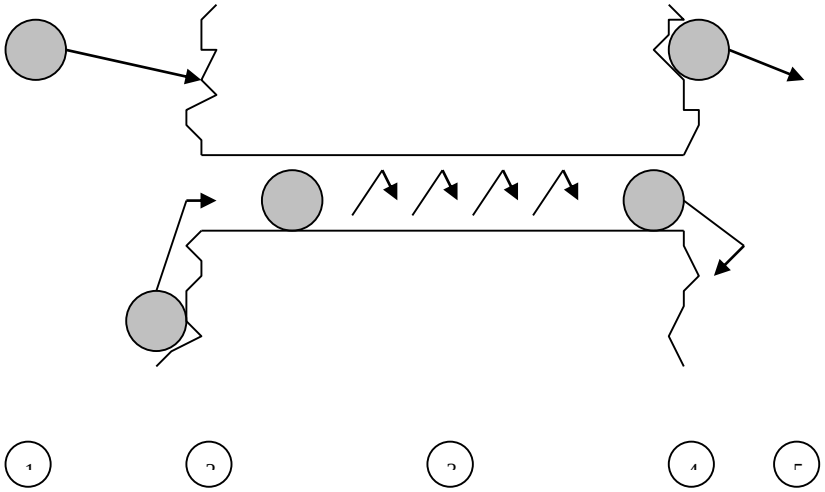

Figure 3.5: Model for mass transfer through a zeolite membrane. (Adapted from Bakker et al, 1996).

3.5.2 Gas-Phase Separations

Several studies on the mechanisms of transport, as well as on interactions and the influence of adsorbed molecules, have been performed. Preferential (selective) adsorption, where the presence of strongly adsorbed components drastically reduces the permeance of weakly or non- adsorbed components, has been observed in most of the highly selective separations on MFI-type membranes reported in the literature (Keizer et al, 1998, Yang et al, 1999, Bernal et al 2002, Bernal et al, 2003, Camus et al, 2006, Rezai et al, 2008). This effect, also known as pore-blocking, normally occurs in zeolite pores but has also been observed in non-zeolite pores (Gump et al, 1999).

Adsorption effects are strongly dependent on operating conditions such as temperature and pressure (Bernal et al, 2002). Modification of the operating conditions to enhance the selective path can result in an increase in the overall separation selectivity. The effect of operating conditions has therefore been studied extensively in order to optimise the membrane separation process (Kapteijn et al, 1995, Bakker et al, 1996, van den Broeke et al, 1999, Yang et al, 1999, Gump et al, 2000, Xomeritakis et al,

2000, Arruebo et al, 2001, Bernal et al, 2002, Sommer et al, 2003, Lai and Tsapatsis, 2004, Camus et al, 2006, Miachon et al, 2007).

It has been suggested that experimental observations of single gas permeances can be explained by the following permeation mechanisms that can occur simultaneously (van de Graaf, 1998):

- Knudsen (mesoporous defects) or Poiseuille (macroporous defects) transport is observed when permeation occurs through defects. This normally occurs for molecules that have a diameter larger than the zeolite pore or those that are weakly/non-adsorbed.
- Surface diffusion and/or activated gas diffusion which can occur in the zeolite pores for adsorbed molecules. Either of the two transport mechanisms can dominate. However, this is dependent on temperature.

Figure 3.6 shows the trend of single gas permeation of a non-adsorbing component with increasing temperature. At lower temperatures (A→B), the permeance increases with temperature as mobility of adsorbed species is enhanced. However, the amount adsorbed starts to decrease thereby reaching a maximum in permeance at point B. The amount adsorbed is much less (low occupancy) and the permeance decreases (B→C). However, at sufficiently high temperatures (C→D), the declining trend is reversed because adsorption effects become negligible and permeation is controlled by activated diffusion. This has been observed by Arruebo et al (2001) on silicalite-1 membranes for single gas permeances of hydrogen, methane and ethane.

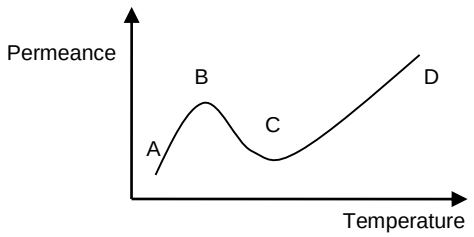

Figure 3.6: Typical permeance of a single gas through a zeolite membrane as a function of temperature. (Adapted from Coronas et al, 1999)

The permeation of mixtures is generally much more complex than single gas permeation. The behaviour of a mixture in most cases cannot be predicted purely from the permeance of its individual components (Coronas et al, 1997). It has been observed that when a strongly adsorbing component is present, the selectivity of a mixture does not reflect the ideal selectivity (ratio of pure gas permeances) (Bakker et al, 1996, Xomeritakis et al, 2000, Arruebo et al, 2001, Bernal et al, 2002). In this case, the weakly adsorbed component normally permeates faster as a single gas, but is the slower gas when contained in a mixture that contains a strongly adsorbing component (Coronas and Santamaria, 1999). The mixture selectivity can be directly related to the ideal selectivity, but only in processes where adsorption does not play a significant role (Bernal et al, 2002). For example, if a mixture contains only weakly adsorbing molecules such as H_2 and butane at 623K, the mixture selectivity resembles the ideal selectivity. The strongest adsorbing molecule is only significantly hindered if other strongly adsorbing molecules are present. The larger the difference in adsorption strength between two components, the higher is the mixture selectivity. Examples include separations of adsorbable organic compounds from non-adsorbing gases such as n-butane/H_2 mixtures (Giroir-Fendler et al, 1996, Coronas et al, 1997) and n-butane/methane (Arruebo et al, 2001). The permeance of hydrogen was lower in the mixture than as a single gas since n-butane is preferentially adsorbed, thereby hindering the hydrogen. Bakker et al, (1996) observed the permeation of weakly adsorbing hydrogen drop over orders of magnitude in the presence of strongly adsorbed i-butane on silicalite-1. Keizer et al (1998) also observed this phenomenon in separation data for N_2/O_2, H_2/CH_4, H_2/CO_2, and CH_4/n-C_4H_{10}. The results showed that methane permeance decreased by a factor of two in the CH_4/n-C4H_{10} mixture when compared to methane single gas permeance. Also at room temperature, the methane permeance was reduced in the presence of benzene, p-xylene or 2,2 dimethylbutane (DMB).

A common feature of mixtures of weakly and strongly adsorbing components is that the selectivity towards the blocking molecule decreases with increasing temperature, following the decrease in adsorption. For example, Coronas et al, (1997), found that at lower temperatures, the permeance of n-butane in the mixture is higher, due to stronger adsorption in the zeolite pores that inhibits the hydrogen permeance. As the temperature was increased, n-butane desorbed from the ZSM-5 pores and hydrogen

permeated faster, and eventually a temperature was reached where the H_2 and the n-butane permeances were equal. With a further increase in temperature, the H_2 permeance was higher than that of n-butane (Coronas and Santamaria, 1999). Similar results were obtained by Giroir-Fendler et al (1996).

When a mixture contains two adsorbable components (e.g. organic mixtures), competitive adsorption is said to occur. Most studies of such systems have been based on linear and branched alkanes (C_2 - C_6) and show very interesting behaviour. Separations of n and i-butane have been the subject of several of studies (Kusakabe et al, 1996, Coronas et al, 1997, Piera et al, 1999, Xomeritakis et al, 2000, Bernal et al, 2003, Bayati et al, 2013). This case is similar to the strongly/weakly adsorbing mixtures in the sense that one component will still be more strongly adsorbed, even though the difference in adsorption strengths might be small. For example, n-butane is preferentially adsorbed in MFI membranes and hinders the passage of i-butane through the zeolite pores (Bernal et al, 2002). Interestingly, this competitive adsorption and blockage of zeolite channels was observed on the silicalite-1 membranes of Arruebo et al (2001) even when low concentrations of n-butane were used. Coronas et al (1997 and 1998) found that a relatively small difference in adsorption strength can be sufficient enough to obtain good separations in good quality membranes.

Adsorption followed by surface diffusion can also occur in non-zeolite pores although they have to be of a similar size to zeolite pores (Gump et al, 1999). Gump et al (2000), in the separation of hexane isomers observed that the linear isomer adsorbed into and blocked the non-zeolite pores (hexane size 0.58 nm). The adsorbed n-hexane packed the non-zeolite pores, preventing the permeation of 2,2 dimethylbutane thereby resulting in high selectivities.

Many other examples of preferential/competitive adsorption as the determining factor for the separation can be found in the literature, including Funke et al (1997). They investigated the effect of adsorbed molecules on silicalite-1 using n-octane, 1,3,5 trimethylbenzene (TMB), water and impurities from the laboratory atmosphere on pure gas permeances of N_2 and SF_6 through an MFI zeolite membrane. Adsorbed molecules were found to influence the permeation of non-adsorbed molecules. For example, in one experiment, the permeance of N_2 was decreased by a factor of 18 after

the membrane had been exposed to n-octane. Strongly adsorbed n-octane blocked a significant amount of zeolite pores, thereby reducing N_2 permeance significantly. Bonhomme et al, (2003) studied separations of CO_2 from H_2 and He. CO_2 has a high affinity for the silicalite-1 membrane and was preferentially adsorbed and transported by surface diffusion.

Effects of temperature on mixtures in which both components are strongly adsorbing can be described in the same way as those containing weakly and strongly adsorbing components. In the case of n/i butane, n-butane is preferentially adsorbed at lower temperatures and prevents i-butane from permeating in the zeolite pores. At moderate increases of temperature, i-butane remains blocked and at the same time, the mobility of adsorbed n-butane increases. Consequently, the permeation flux of n-butane increases as does the selectivity. However, a further increase in temperature releases some membrane pores, leading to an increase in the i-butane permeance which results in a decrease in mixture selectivity (Bernal et al, 2002).

Adsorption is also a function of pressure which can therefore influence mixture selectivities as well. Increasing the feed-side operating pressure, for example, would increase the rate of adsorption of the strongly adsorbed component which increases the surface coverage and results in higher selectivities due to preferential adsorption (Arruebo et al, 2001). Changing the feed and permeate pressures also changes the driving force of the permeation by increasing occupancies in the membrane pores. In the separation of hexane isomers, Gump et al (1999) found that when n-hexane pressure is sufficiently low, 2,2DMB permeates through the membrane. As n-hexane pressure increases, 2,2DMB is prevented from adsorbing and therefore cannot permeate through the membrane. For higher n-hexane pressures, the adsorption coverage is higher and n-hexane was even more effective at blocking DMB.

Apart from operating conditions, support properties i.e. pore diameter, interconnectivity of pores, and porosity can affect transport modes which contribute to the overall flux in the support. Support resistance is usually not taken into account when interpreting transport data. This is because transport through the support is generally much faster than through a zeolite film. However, the flow through a support can be important and is usually dependent on the thickness of the deposited zeolite

film. Thin films on a support can result in a much slower flow through the support. Jareman and Hedlund (2005) modelled transport through supported MFI membranes taking into account the support resistance and showed that ideal selectivities for H_2/He and N_2/SF_6 increased with increasing zeolite film thickness. For 1µm or thinner films, ideal selectivities were ~1, but the selectivity increased to as high as 20 when zeolite film thickness increased to 100 µm. The thin films were not selective because the support slowed down the faster permeating molecule (H_2 or N_2) much more than the slower permeating molecule (He or SF_6). The support resistance also becomes more important as the diffusion rate increase (Gardner et al, 2007).

The complexity of gas separation is demonstrated by the different studies on MFI membranes. The separation performance of zeolite membranes has been shown to be highly dependent on operating conditions such as temperature, pressure and composition (van de Graaf et al, 1998a). A membrane can show high selectivities in some cases (low temperature, high pressure) and show no selectivity in others (high temperature). Depending on the application, a high permeance may be more important than a high selectivity and vice versa (Noack et al, 2002). However, a membrane with both high permeance and high selectivities is desirable. Knowledge of the membrane separation performance is essential for optimisation with the operating conditions (van de Graaf et al, 1999). Prediction of the separation of MFI membranes under a variety of conditions would also be useful. Models are therefore invaluable for the theoretical description of mass transfer and are discussed in section 3.6.

3.5.3 Effect of Concentration Polarisation

When a mixture is brought to a membrane surface by any driving force, there will be an accumulation of the less permeable species and a depletion of the more permeable membrane components in the boundary layer adjacent to the membrane. This causes a concentration gradient build up in the boundary layer (He et al, 1999). Using pressure as an example, the partial pressure of a faster permeating component i which is to be separated from the feed flow decreases, and the partial pressure of the slower permeating component j increases at the surface of the membrane. Because driving

force for the transport through the separative layer is provided by the partial pressure difference between the feed and the permeate side, these effects have a negative effect of the separative properties of the membrane (Ludtke et al, 1998). This phenomenon is known as concentration polarisation.

Traditionally, concentration polarisation has been studied and is well documented for liquid separation membrane processes such as ultrafiltration and reverse osmosis and it is generally believed that it does not affect gas separation processes. However, concentration polarisation is a phenomena that exists in all membrane separation processes due to the selective permeability of membranes. It has adverse effects on membranes as it reduces the overall efficiency of the separation. It has been observed that permeation rate of the more permeable gas decreases with the presence of the more permeable gas which in turn decreases the actual separation factor (He et al, 1999).

Factors that affect concentration polarisation include selectivity, permeability, mass transfer coefficient, operation pressure, gas composition and structural characteristic of the gas support (Mourgues and Sanchez, 2005). He et al (1999) preformed studies for two typical gas separation applications i.e. hydrogen and air separation with shell side feed on hollow fiber modules. They showed that the permeation rate was a dominating factor that affects concentration polarisation and increasing the feed gas velocity led to a decrease in concentration polarisation. They also found that the effect of operating pressure was limited and that the composition of feed gas did not have an effect. However, Yu et al, (2007) in studies for the separation of n-hexane from DMB and TMB found that separation factors were affected by concentration polarisation on the feed side of the membrane due to the low concentration of n-hexane in the feed. Mourgues and Sanchez (2005) also found that the permeation rate was the most important factor affecting concentration polarization.

Support properties i.e. pore diameter, interconnectivity of pores and porosity, can affect transport modes which contribute to the overall flux in the support. Flow through the support can be important, especially in the case where a thin zeolite film is deposited on the support. In mixtures where the more strongly adsorbing component preferentially permeates, the support resistance limits the flux of strongly adsorbed components more than that of the weaker adsorbing component. It has been found that

double sided membranes have the potential to have higher fluxes and selectivities than traditional single sided membranes (Gardner et al, 2007).

For mixture separation using supported thin film membranes, the mixture is fed to the zeolite side and either a lower pressure or sweep gas is applied to the support (permeate side). If the mixture is fed to the support side, concentration polarization occurs which lowers the selectivity. This is because the slower permeating components accumulate and concentrate in the support (Gardner et al, 2007). Studies by van de Graaf et al (1998) found that feeding an ethane/methane mixture to the support side of the membrane resulted in a selectivity of one. This was attributed to concentration polarisation.

Gardner et al (2007) used Maxwell-Stefan equations to model the diffusion of pure components (i-butane) through single, supported zeolite films, and membranes with films on both sides (double sided membranes). During hydrothermal synthesis of zeolite membranes, films sometimes grow on both sides of the support. They found that the flux off strongly adsorbed components can be higher through double sided membranes. In these studies, they also discovered that concentration polarisation caused by feeding a mixture to the support can be eliminated by adding a second zeolite film on the feed side. They concluded that for double sided membranes, the zeolite layer on the feed side is required to prevent concentration polarization whereas the zeolite layer on the permeate side adds to total zeolite thickness, which can increase selectivity and, in addition, it can act as a barrier to keep a sweep gas out of the support, further increasing flux.

3.6 Modelling

For practical applications of MFI zeolite membranes in industry, it is essential that the transport and separation mechanisms are properly understood and described by appropriate mathematical models (Vareltzis et al, 2003).

Diffusion in zeolites may be described either by micro or macro scale models. Micro scale models include molecular dynamics, force field simulations, Monte-Carlo simulations etc. What they have in common is that the molecules are modelled on an atomic scale and the quantum mechanical effects may be considered in the model. The major disadvantage with the microscopic approach is that the models are very cumbersome with respect to computation. Keil et al (2000) showed with simple calculations that the computing time, on a Cray Y-MP super computer, necessary for obtaining a reliable value of the self diffusivity of benzene in silicalite-1 would be about 5600h. Many groups have used the dual control volume grand canonical Monte –Carlo (DCV-GCMD) to study surface resistance on zeolite crystals. However, the DCV-GMCD require very large computational resources even for extremely thin crystals and these grow rapidly as the crystal thickness is increased (Newsome and Sholl, 2008). The other disadvantage was that they only provide information on a specific set of process conditions. Newsome and Sholl (2008) in response to this introduced the local equilibrium flux method (LEFM) to predict quickly and accurately surface resistances for large ranges of membrane operating conditions. This method allowed them to identify crystal thickness beyond which surface resistances are negligible for single component permeation of CH_4, CF_4 and C_2H_6 through silicalite membranes as a function of membrane feed and permeate pressure.

The advantage macro scale models have over the micro scale ones is their computational needs are much less demanding, although improvements are being made to reduce the computational needs of the micro scale models. The disadvantage of using macro scale models is that they consider the diffusing components to be a continuum. However, this is not the case when considering diffusion in zeolites because the pores are of molecular dimensions (Jareman et al, 2004).

Macro models are the most frequently used type when modelling diffusion in zeolites as well as zeolite membranes. The most frequently used are the Maxwell-Stefan equations, generalised Fick's Law and an activated diffusion model. In the Fickian approach, the concentration gradient in the zeolite is used as the driving force, while in the Maxwell-Stefan approach, the gradient of the thermodynamic potential is the driving force (Bakker et al, 1996). In particular, the generalised Maxwell-Stefan (GMS) equations seem to provide a good rational and theoretical basis for surface

diffusion that can be extended in a straight-forward manner from single component to multi-component systems (Wesselingh and Krishna, 1990 & 2000, Krishna 1990, 1993 and 1995).

The applicability of generalized Maxwell-Stefan (GMS) equations has been demonstrated in a number of studies (Krishna and van den Broeke, 1995, Kapteijn et al, 1995, Bakker et al, 1996, van den Broeke et al, 1999, van de Graaf et al, 1999, Ciavarella et al, 2000 Gump et al, 2000, Millot et al, 2000, Gardener et al, 2002, Krishna and Baur, 2003, Sommer et al, 2003, Martinek et al, 2006, Zhu et al, 2006, Lee 2007, Miachon et al, 2007). Krishna and van den Broeke (1995), using the Maxwell-Stefan formulation, developed a mathematical model for transient membrane mass transport to account for the isothermal permeation of lower alkanes and alkenes and alkane-alkene mixtures through a silicalite-1 membrane. The Maxwell-Stefan formulation was able to describe accurately the qualitative trends. It was found that the Fickian model failed even at the qualitative level to explain the experimental results. It was concluded that the Maxwell-Stefan model is indispensable for the description of mass transport across zeolite membranes. This model has also been adapted for steady state permeation for quantitative determination of diffusion coefficients (Kapteijn et al 1995). This study also concluded that the Fickian model was inferior to the Maxwell-Stefan model.

The generalized Maxwell-Stefan (GMS) formulation has been shown to be a convenient and general way of describing diffusion within zeolite structures and a good review on the developments of the formulation and demonstrations of how the Maxwell-Stefan approach can be incorporated into the modelling and design of practical devices such as membrane permeation units is given by Krishna and Baur (2003). For successful application of the GMS equations for descriptions of mass transfer in zeolite membranes, the adsorption equilibrium and GMS diffusivities of the molecules must be known. The adsorption of molecules in zeolites can be measured independently and there is agreement in adsorption isotherms measured in different laboratories on different samples (Chiang and Chao, 2001). Advances in molecular simulation have made it possible to simulate single component adsorption isotherms with results that are consistent with experimental data. Multi-component isotherms which are needed for mixture permeation are more difficult to obtain. However,

molecular simulation can be extended in a straight- forward manner thereby supplying much needed mixture adsorption data. Diffusion in zeolites is less straightforward than adsorption. Results for different experimental methods used to measure diffusion have not been consistent. Talu et al, (1998) compared diffusivities of small alkanes in ZSM-5 measured by different methods and found differences in orders of magnitude especially between microscopic and macroscopic measurements. Despite this, Millot et al, (2000) and van de Graaf et al, (2000) were able to back calculate zeolitic diffusivity of linear and branched alkanes from permeation data and found close agreement with the results of molecular simulation and macroscopic methods (Chiang and Chao, 2001).

In most of the studies based on GMS equations, the typical quantity used for the description of mass transport through membranes is the flux. The permeance, however, is a better quantity to consider than the flux, especially for temperature controlled experiments due to the change in concentration difference of the permeating component over the membrane (van den Broeke et al, 1999a). The permeance takes into account the change in partial pressures across the membrane which can occur especially where a sweep gas has been used. For example, when helium gas was used in studies by van den Broeke et al (1999), it was found that the helium diffused from the sweep side to the feed side and the partial pressure at the retentate side decreased. This is taken into account if the permeance is considered instead of the flux.

Atomistic methods have been widely applied to single component adsorption and diffusion in zeolites, however there has been considerably less work examining adsorbed mixtures. Skoulidas et al, (2003) directly compared detailed atomistic simulations and experimental measurements of CH_4/CF_4 mixture permeation through a silicalite membrane. The atomistic theory correctly predicted that the silicalite membrane is CF_4 selective to mixed CH_4/CF_4. They showed that although several mathematical equivalent formalisms exist for describing multi-component transport through microporous materials e.g. Maxwell-Stefan, Fickian and Onsager descriptions, there was no fundamental difference between the three. Once the relevant diffusivities or transport coefficients are known for one description, the others are also fully defined.

It has also been noted that for multi-component systems, it can be difficult to obtain an explicit expression that correlates the steady state permeation flux of each species to the feed and permeate partial pressure and temperature and numerical methods are required to solve the equations. For multi-component systems (more than two components) the Maxwell-Stefan approach becomes mathematically complex and proper correlations for diffusivities are difficult to obtain (Lin et al, 2002). All practical applications of zeolite membrane would involve the permeance of multi-component mixtures so the capability to describe transport of mixtures is a necessary requirement for any modelling method to be of value in describing these materials (Skoulidas et al, 2003). Simplified models would be preferred in the investigation of the effects of various parameters on the permeation and separation of multi-component systems by the membrane (Lin et al, 2002).

A simple but effective model for the description of membrane transport was proposed by Yang et al, (1999).Various authors, as described in Section 3.5.2, recognise the effect of adsorption on permeance and have demonstrated the advantages of gas separation based on the surface diffusion of the strongly adsorbed components and their hindering effect on the permeance of weakly or non-adsorbed components (Funke et al, 1997, Keizer et al, 1998, Van den Broeke at al, 1999, Dong et al, 2000, Gump et al, 2000, Arruebo et al, 2001, Bernal et al, 2002). However, few publications have approached the subject in a quantitative manner, resulting in a trivial understanding of the phenomenon.

Yang et al, (1999) described the hindering effect of light hydrocarbons on the permeation of hydrogen through a microporous silicalite-1 membrane. The model, known as the Potential Barrier model is an attractive method as it only requires independent data on the permeance of pure non adsorbing components and the adsorption equilibrium isotherms of the strongly adsorbing components. Although the GMS models have been used successfully to describe mass transport (flux) in zeolite membranes, it requires knowledge of the GMS diffusivity, which can vary depending on how the diffusion is measured or calculated. Also, the effective membrane thickness is required which can be difficult to determine, especially for membranes prepared by the pore-plugging method (Miachon et al, 2006). Models that require less data are therefore desirable. Yang et al's (1999) model was tested on binary experimental

systems of H_2/CH_4, H_2/C_2H_6, H_2/C_3H_8 and H_2/n-C_4H_{10}. The substantial reduction in the permeance of H_2 was described successfully over a temperature range of 20^{o}C-60^{o}C and feed pressures up to 850kPa. The model was also capable of predicting the substantial reduction in hydrogen permeance in a multi-component system of, $H_2/CH_4/C_2H_6/C_3H_8$.

The Potential Barrier model therefore presents itself as a potentially invaluable choice to quantify the hindering effect of strongly adsorbed molecules on the permeance of the non-and/or weakly adsorbing components. This may provide a better understanding of the $NH_3/H_2/N_2$ separation in MFI zeolite membranes and the extent to which adsorption affects membrane performance at different operating conditions. This information can then be used to optimise membrane performance.

CHAPTER 4

EXPERIMENTAL DETAILS

4.0 Introduction

This chapter describes the experimental techniques and equipment used to investigate the effect of operating conditions on MFI membranes in the ammonia/hydrogen/nitrogen separation. Descriptions of the membranes used and the design and method of synthesis are given. The chapter then continues with a description of the equipment used for the permeation studies.

4.1 Membranes

The membranes used in these experiments were supplied by Pall-Exekia (France, now Pall Corporation) and are ZSM-5 type membranes made by hydrothermal in-situ synthesis on α-alumina supports. The membranes were manufactured as part of the IMPRESS project and were prepared using the pore-plugging method discussed in Chapter 3, Section 3.2.4 as described by Dalmon and his group (Ramsay et al, 1994, Uzio et al, 1994, GiroirFendler et al, 1996, Miachon et al, 2006).

The membranes have a high level of aluminium incorporation which results in a high level of acidity. Increased surface acidity increases the selective adsorption of NH_3

thereby increasing its separability from the $NH_3/N_2/H_2$ mixture. Previous work (IMPRESS Report, 2004, Camus et al, 2006) demonstrated that these membranes offer the best performance for the separation of NH_3 from H_2 and N_2 compared with other membrane types such as silica or carbon membranes.

4.1.1 Membrane Synthesis

The membranes used in this project were synthesised by Pall Exekia in partnership with IRC Lyon using the pore plugging method as described previously in Chapter 3. This method involves growing the zeolite crystals within the pores of a ceramic alumina substrate, until the pore is completely blocked by the zeolite material (Ramsay et al, 1994, Uzio et al, 1994, GiroirFendler et al, 1996, Miachon et al, 2006). This results in a continuous composite alumina membrane (Miachon et al, 2006). Using this method, a continuous flawless zeolite layer can be obtained especially when considering large membrane areas. If an imperfection occurs, the defect will not be larger than the pore of the host material. Another advantage is that the separative layer is located inside the porosity of the ceramic support. Therefore, thermal cycling and occasional shocks are less likely to damage the membrane when it is incorporated within the support than when it is laid down on its exterior surface (Camus et al, 2006, Miachon et al, 2006). This makes membrane handling and module assembly easier.

Pall-Exekia developed a new support geometry known as the Multi-Channel tube (MCT). Compared to single tubes, multi-channel tubes are considered to be the best geometry for increasing support permeability and mechanical strength at the same time. The very high differential pressures the membrane will experience in the process operation (~100 bar) prevents the use of a single thin walled tube.

The multi channel tubular membranes (MCT) were made from homogenous alumina supports, one with 0.2µm pore diameter described in this thesis as MCT0.2 and the other with a 0.5µm pore diameter described as MCT0.5. These sizes refer to the pore size of the porous support in which the membrane is grown. The average pore size for ceramic α-alumina tube supports can vary and they can be homogenous or multi-

layered. Examples of multi-layered supports include Membralox T1-70 (Pall-Exekia) as described in Camus et al, (2006) and Miachon et al (2006). These supports are made of two or three layers with a pore size sequence decreasing from the outer to the inner side of the tube e.g. 12-0.8μm, 12-0.8-0.5μm or 12-0.8-0.2 μm. Pall-Exekia has also manufactured homogenous supports with pore diameters of 0.2μm and 0.5μm which are used in this study. A summary of their main characteristics is given in Table 4.1.

Table 4.1: Main characteristics of MCT membranes used in this thesis

	MCT0.2	**MCT0.5**
Geometry	Tubular	tubular
Structure of zeolite	MFI	MFI
Pore diameter of support (μm)	0.2	0.5
Length (m)	2.3×10^{-1}	2.5×10^{-1}
Outer Diameter (m)	2.4×10^{-2}	2.4×10^{-2}
Effective surface area for mass transfer (m^2)	1.73×10^{-2}	1.89×10^{-2}
Thickness of zeolite layer (μm)	Estimated 5-15	20

The precursor of the zeolite was obtained by mixing silica (Aerosil Degussa 380) and a template (TPAOH). After a three-day ageing period, the precursor was placed with the porous tube in an autoclave fitted with a PTFE insert. The hydrothermal synthesis was performed at 170^{o}C for 3 days, and then the membrane was calcined at 500^{o}C under a flow of air at 2000ml/min. Before use, the zeolite membrane was pre-treated overnight at 300^{o}C in flowing nitrogen to remove any adsorbed molecules from its pores. A detailed description of the composite membrane preparation, including the silica/TPAOH ratio and its characterization can be found elsewhere (Ramsay et al, 1994, Giroir-Fendler et al, 1996). The zeolite selective layer is located in the inner part of the 0.2 μm (MCT0.2) and 0.5 μm (MCT0.5) pore diameter support and is estimated to be 5 to 15 μm thick for MCT0.2 and 20μm for MCT0.5 respectively. A schematic of the nanocomposite membranes is shown in Figure 4.1.

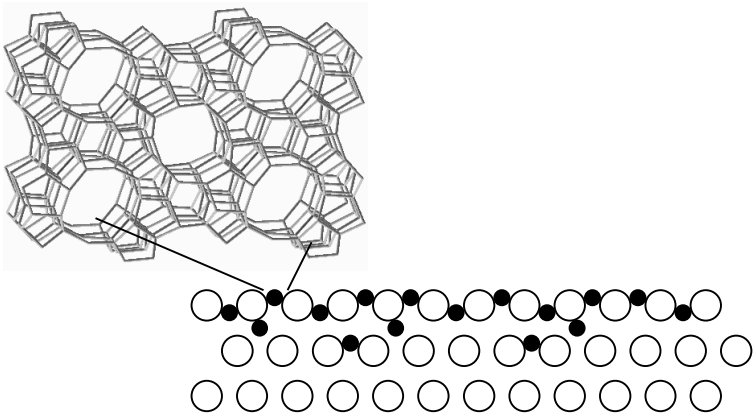

Figure 4.1: Schematic of composite membrane structures (Adapted from Miachon et al, 2006)

The membrane module design is based on the shell and tube heat exchanger configuration as shown in Figure 4.2. The zeolite layer is located on the outer diameter of the ceramic support. Flow through the membrane is counter current. The feed stream is fed through the shell side (tube wall) and the system pressure drives the molecules through the membrane located on the outer diameter of the tube. The sweep gas is fed through the lumen (tube side). Material that flows through the membrane is the permeate, and is collected on the tube side from the small channels round the periphery. The rejected material is withdrawn at the downstream end as retentate. The membrane is sealed so that there is no mixing between the permeate and the sweep. This configuration of "outside-in" was necessary due to the structure of the membrane and its geometry. If feed were to be passed through the internal channels the result would be high pressure internally and low pressure externally which creates tension and therefore mechanical instability of the membrane. Feeding on the outside eliminates this problem.

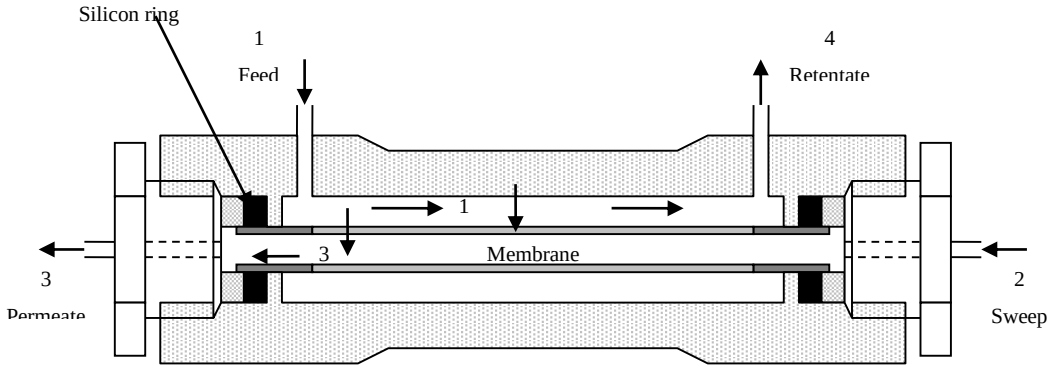

Figure 4.2: Schematic drawing of the permeation test module, showing tubular membrane and silicon seals 1) Feed stream fed through shell side 2) Sweep gas fed through the tube side 3) Permeate out of channels 4) Retentate leaving on shell side(Adapted from Miachon et al, 2007)

4.1.2 Membrane Structure

Scanning electron microscopy (SEM) can be used to visualise surface and cross sectional topography of a membrane at magnifications greater than those possible with a visible light microscope. With SEM, the shape and size of zeolite crystals and their distribution on the support, as well as a measurement of the membrane thickness and existence of inter-crystalline defects can be determined.

It was not possible to perform SEM studies on the membranes used in this study (MCT0.5 and MCT0.2). This was because it would require destruction of the membranes which could not be done until it could be confirmed that all permeation tests had been completed and that the membranes would not be required any more. Nevertheless, some SEM photographs presented in the literature (Camus et al, 2006, Miachon et al, 2006, Silva et al 2008) can provide an insight as to how the membrane would be structured.

In order to have a general understanding of the membrane structure, membranes made with the same pore-plugging techniques as described in section 4.1.1 made by Silva et al, 2008 are presented. These membranes were formed by hydrothermal synthesis following a recipe from Giroir-Fendler et al, (1995). The membrane consisted of a

three layer structure of pore size 0.2 μm-0.8 μm-10 μm. The two internal layers of the support i.e. the 0.2 μm and 0.8 μm pores were almost completely filled with zeolite. Grains of the outer layer were only partially covered with zeolite crystals. A JEOL JSM6310 model was used. A sample of the membrane was frozen in liquid nitrogen for 20-30 seconds, then sectioned using a sharp blade. A small quantity was then placed on a specimen plate and coated with a thin layer of gold for 3-5 minutes with the Edwards sputter coater (S150B). The SEM was operated in the 10-20kV range and micrographs were taken of a number of areas of a sample.

In this work, we only present the SEM micrographs that show the inner surface of the 0.2 μm layer. This is because this pore size of 0.2 μm for the inner layer matches the pore size of the homogenous support used in this work. Figure 4.3a reveals the presence of small zeolite crystallites deposited on the α-Al_2O_3 particles of the support layer. A well-defined zeolite-MFI type crystalline phase has been formed in the alumina porous tube. Figure 4.3b shows zeolite material is present in the pores of the support. Other SEM micrographs of pore-plugged membranes made by Dalmon and his group are available in various publications (Giroir-Fendler et al, 1996, Miachon et al, 2006, Camus et al, 2006).

The SEM photographs shown in Figure 4.4 (Silva et al, 2008) show the cross section images of the support in the inner layer (0.2 μm) of Pall-Exekia tubes with a three layer asymmetric structure of pore size 0.2 μm-0.8 μm-10 μm respectively. It is assumed that in the same way the inner layer of the Silva et al, (2007) 0.2 μm inner layer is filled with zeolite, the 0.2 μm homogenous support used in this work is also completely filled with zeolite. It is anticipated that the MCT0.2 membrane looks very similar internally to the one presented in Figure 4.4b.

The SEM pictures shown here are for the reader to be able to visualise what the membranes MCT0.2 and MCT0.5 might look like. It is reasonable to assume that the pores of the homogeneous substrate (0.2μm) are likely to be the same as the 0.2μm inner layer shown in Camus et al, 2006 and Silva et al 2008. The membrane is therefore likely to be plugged in the same way as the inner layers in the mentioned papers.

However, an actual representation of MCT0.2 and its characteristics can only be observed using a true SEM picture of the membrane.

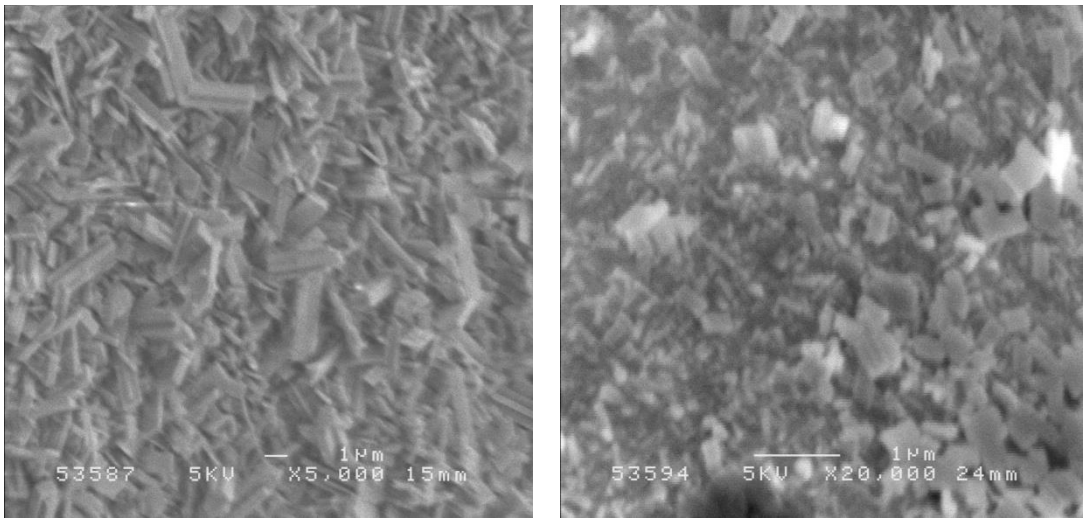

a) inner surface 5000x **b) magnified cross-section x 20000**

Figure 4.3: SEM photographs of an MFI membrane prepared by hydrothermal synthesis a) inner surface showing zeolite crystals b) magnified cross-section showing zeolite embedded in membrane (Silva et al, 2008).

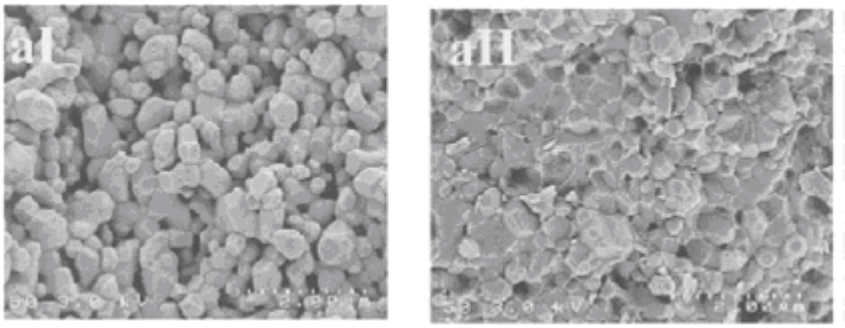

Figure 4.4: FESEM cross section images of the α-Al_2O_3 support (Pall-Exekia) a) inner layer 0.2 μm before MFI synthesis b) inner layer 0.2 μm after MFI synthesis (Silva et al, 2008).

4.2 Experimental Details

4.2.1 Materials

The membranes used are the pore-plugged homogenous multi-channel MFI zeolite membranesMCT0.2 and MCT0.5 supplied by Pall-Exekia, as described in section 4.1.1. The gases used in this study were nitrogen (N_2), hydrogen (H_2) and different compositions of ammonia gas (NH_3) supplied by BOC UK in certified-composition canisters and consisted of the following:

Single gas permeation tests

- N_2 (99.99%)
- H_2 (99.5%)
- NH_3 (99.98%)

Binary Gas permeation tests and Sweep Gas

- 75%H_2/25%N_2

Mixture Gas Permeation Tests

- 9% NH_3, 23%N_2 and 68% H_2
- 6% NH_3, 24%N_2 and 70%H_2
- 12% NH_3, 22%N_2 and 66%H_2
- 16%NH_3, 21%N_2 and 63%H_2

Argon (99.98%) was used as a carrier gas for the gas chromatography column.

4.2.2 Apparatus

The apparatus used for conducting permeability measurements consisted of the membrane module, the permeation test rig, and the gas chromatography (GC) column used for analysing the composition of the permeate gases.

4.2.2.1 Membrane Module

Two different housing modules were available for use in the permeation experiments. The module shown in Figure 4.5 was provided by Pall-Exekia. This design consists of a stainless steel module with threaded joints on each side of the module. The second module was manufactured in-house and is also a stainless steel module but instead of a threaded joint, it consists of a clamp system using bolts as shown in Figure 4.6. The threads of the first module (Figure 4.5) began to seize due to the constant tightening and opening of the module between experiments. Therefore, the membrane may not have been fully secured. Consequently, a clamp system using bolts (Figure 4.6) was deemed more suitable for membrane housing and also eliminated the seizing problem.

The membrane tubes were sealed with silicon O-rings. These were chosen because they could be used for temperatures up to 200^{o}C. The silicon O-rings provided a gas-tight seal between the upstream side (feed/retentate side) and the downstream side (permeate/sweep) as shown in the schematic in Figure 4.2. The feed side was pressurised and the permeate side was held at atmospheric pressure. A mixed sweep of H_2/N_2 in the volumetric ratio of 3:1 was used for the mixture permeation studies. The reason for this is that a critical aspect of the design of the membrane recovery process is the use of the make-up syn-gas from the ammonia synthesis production as the sweep gas. The single and binary gas experiments were performed without the use of a sweep gas.

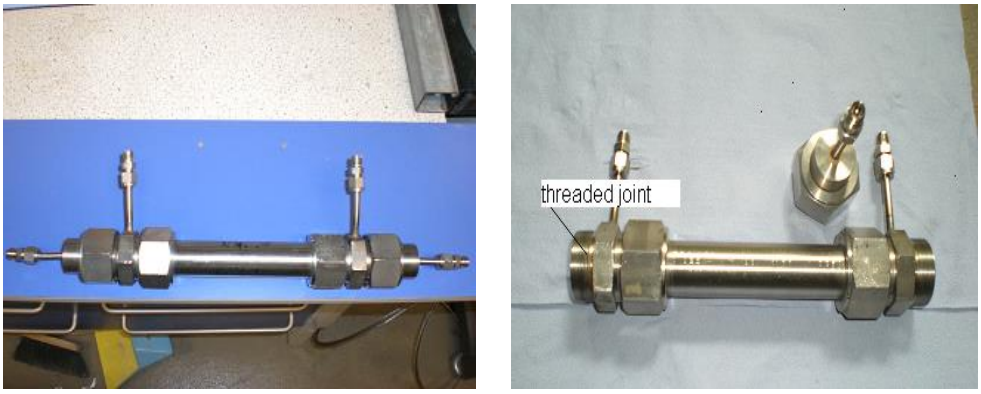

Figure 4.5: Membrane housing module (Pall-Exekia)

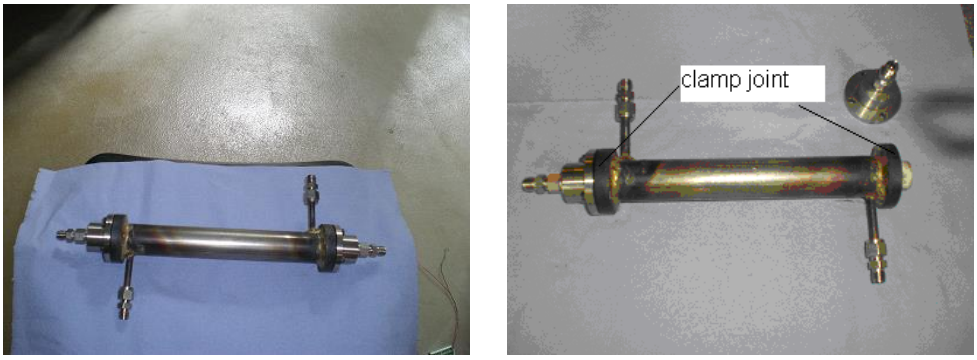

Figure 4.6: Membrane housing module (University of Bath – in-house)

4.2.2.2 Experimental Set-up

The apparatus used for the membrane separation studies is illustrated schematically in Figure 4.7. This apparatus was designed to measure the permeation of gas mixtures through a membrane under the influence of a pressure gradient. It was built to enable continuous feed mixtures of the gas to be separated into permeate and retentate streams. All the pipe work consisted of Swagelok stainless steel tubes and fittings designed to withstand pressures up to 450 bar.

Besides allowing mixed gas permeation experiments, the same set-up was used for carrying out single gas permeation experiments with minor modifications. All gases were fed from gas cylinders supplied by BOC as detailed in section 4.2.1.

Gas flow rates at the inlets were controlled by Brookes 5850 E mass flow controllers (MFC0 and MFC1) with a maximum nitrogen flow rate of 30 $l.min^{-1}$, which were pre-calibrated using a soap bubble flow meter covering a wide range of flow rates. Mass flow controller calibrations are given in Appendix I. The pressure rating for the mass flow controllers was 100 bar.

The pressures on both the feed and permeate sides were controlled using back pressure regulators (A and F). The pressures on both these streams and the retentate were recorded using digital pressure transducers EL-Press P712 C provided by Bronkhorst. The pressure rating for the transducers was 100 bar, however experiments were performed at feed pressures up to only 16 bar gauge pressure. Pressure relief valves were set up on the retentate (RV2) and permeate (RV1) lines to stop any over pressure developing in the rig. The membrane module provided by Pall-Exekia (Figure 4.5) as well as the in-house module (Figure 4.6) were both designed to withstand 110 bar differential pressure.

When performing temperature experiments, the membrane module was placed in a heating cabinet. The temperature of the heating cabinet was regulated by a controller on the heater and was measured using a Pt100 thermometer and temperatures could be monitored on a display recorder.

The feed gas from the cylinder (supplied by BOC) was introduced into the membrane module via a pressure regulator (PR2), a mass flow controller (MFC1) and a three way valve. The sweep was fed into the membrane by a gas cylinder also supplied by BOC, pressure regulator PR1 and flow rate maintained by mass flow controller MFC0. On leaving the membrane, the outlet streams i.e. the permeate and the retentate could be directed either to the GC for analysis or bubble flow meters for manual measurement via three way valves M and N respectively.

Pressure on the permeate side was kept at ambient pressure (1 bar gauge pressure) while the feed pressure was varied. The pressure drop between the feed and retentate side was assumed to be negligible at 0.04 bar.

The output signals of the pressure transducers and mass flow controllers were recorded using computer software (Advantech Ltd VisiDaq Runtime) which consisted of a multi-plexer board (Advantech Ltd PCLD 789), a data acquisition card (Advantech Ltd PCL 812 PG) and a personal computer. Once the start-up procedure was completed, all connections were tested with soap solution for leaks. Details of the experimental procedure are given in section 4.2.4.

4.2.2.3 Gas Chromatography

Valve H, connected to the rig through stream selection valve G led the streams to the gas chromatograph (GC). Gas compositions of all four streams i.e. Feed, Sweep, Permeate and Retentate were analysed using a Perkin-Elmer Autosystem gas chromatograph with both a thermal conductivity (TCD) and flame ionisation (FID) detector and a Perkin Elmer model 1020 GC Plus integrator/control computer. This was connected to the rig through a stream selection valve.

The GC was equipped with a pneumatically driven gas sampling valve, enabling the injection of a defined amount ($1cm^3$) of gaseous sample into the system. The samples were injected into an argon carrier gas stream. The gas stream was subsequently led into the column in order to separate the components. The accuracy of the GC was confirmed by calibrating with a known mixture of N_2 and H_2 before the start of each experiment. One column, a molecular sieve 5A (ALLTECH) was used in this study for the separation of hydrogen and nitrogen. The column did not detect ammonia.

On leaving the chromatograph column, the sample was led to the TCD. This detector is non-destructive and compares the thermal conductivity of the sample gas stream with the one of a reference gas (the pure carrier gas). By means of this comparison, a measure of the concentration of the components could be obtained. This detector was used for the investigation of the permanent gases.

The detector signals are led to a Perkin-Elmer model 1020 integrator and control computer. Here the signals are plotted as functions of time and the areas underneath the peaks representing components were integrated. These areas were proportional to the concentration of the components in the investigated sample. The second function of the integrator is to control the GC. The control parameters were set in the GC method. Here values such as run time, injector, oven and injector temperatures, temperature ramps, gas flow rates, sample valve opening times, signal attenuation, detector sensitivity etc. were set.

The analysis of H_2 and N_2 with the molecular sieve column and the TCD was carried out using the following conditions:
Oven temperature: 40^oC
GC column Temperature: 150^oC
Detector temperature (TCD): 200^oC
Carrier and reference gas flow rate: 30ml.min^{-1}
Calibration of the GC was carried out with a known mixture concentration of N_2 and H_2. Two calibration mixtures were used, one with a 10/90 N_2/H_2 ratio and one with a 50/50 ratio. These were mixed in-house using a mixing rig. A linear relationship exists between the peak-area and the concentration. The calibrations can be expressed linearly. The composition of both components in the four streams can be estimated using the slopes and intercepts. The remaining composition is ammonia. Calibration curves are shown in Appendix I.

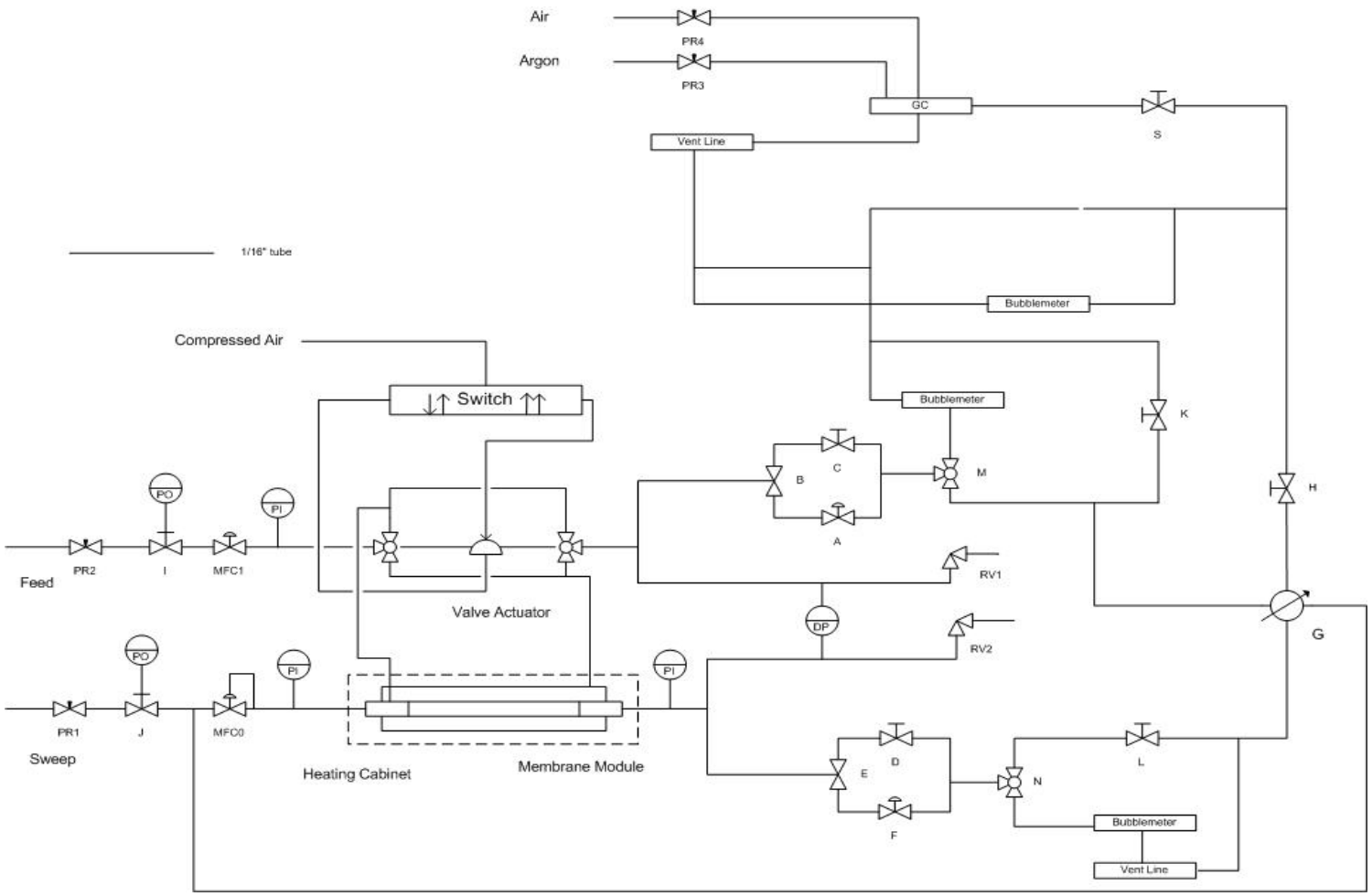

Figure 4.7: Schematic Diagram of experimental apparatus

4.2.3 Permeation Experiments

The experiments were run at steady state and the mode of operation was counter-current. The counter current set-up is generally considered to be the best configuration for permeation experiments (Mulder, 2000). This is because in the counter-current set-up, the permeate partial pressure decreases towards the (feed flow) exit of the module, resulting in a substantial driving force (partial pressure difference) as shown in Figure 4.8. This is in contrast to the co-current mode where the initial driving force is large, but decreases as permeation takes place as shown in Figure 4.9.

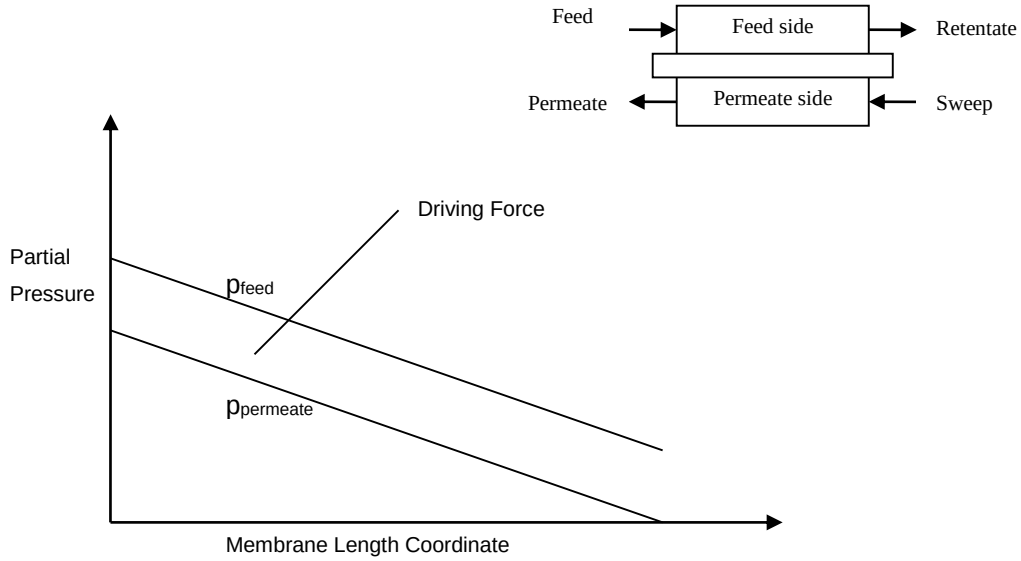

Figure 4.8: Counter current flow set–up

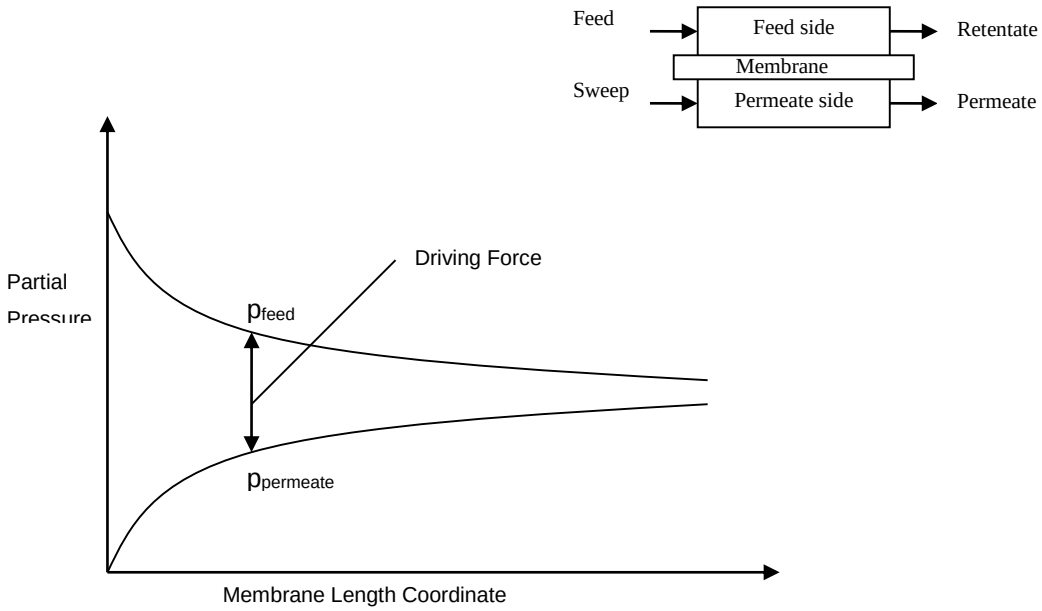

Figure 4.9: Co-current flow set-up

The feed side was pressurised and the permeate side was held at atmospheric pressure. The pressure drop along the module on both sides was relatively small at 5kPa (0.04 bar).

4.2.3.1 Single gas Measurements

Single-component permeation experiments were performed using the pure gases NH_3, N_2, and H_2 supplied by BOC (UK). The experiments were performed as a function of pressure (increasing total pressure at feed side) and temperature (for N_2 and H_2 only). The experiments were carried out using the experimental rig as shown in Figure 4.7 and the experimental procedure given in section 4.3.4. The only modification was that the sweep gas cylinder (PR1) was kept closed so that no sweep was fed into the membrane. (No sweep was used as this would render the experiment a binary system instead of a single component system).

The membrane was regenerated before the start of the experiments using nitrogen at 200^oC to remove any adsorbed substances such as water vapour etc. The pressure was varied from 3 bar to 15 bar for pure N_2 and H_2 experiments at the

feed side and the permeate side was always kept at 1 bar (gauge pressure). Temperature experiments were varied between 25^{o}C and 150^{o}C for N_2 and H_2. For pure NH_3 gas, pressure experiments were carried out up to 7 bar due to its vaporisation pressure (787kPa at 21^{o}C). Temperature experiments were not performed for this gas.

4.2.3.2 Mixture separations

Binary mixture experiments were conducted for the H_2 and N_2 (Composition 75%H_2/25%N_2 also provided by BOC UK) as a function of pressure and temperature. No sweep was used. The same procedure as the single gas experiments was used in this case. The same range of pressures, 3-15 bar feed pressure and temperatures 25^{o}C to 150^{o}C were used.

Ternary mixture permeation experiments were performed as a function of pressure, feed flow rate, sweep flow rate, temperature and ammonia feed composition. The feed for mixture permeation experiments was obtained from certified-composition gas canisters (supplied by BOC) of compositions:

- 9% NH_3, 23%N_2 and 68% H_2,
- 6% NH_3, 24%N_2 and 70%H_2,
- 12% NH_3, 22%N_2 and 66%H_2
- 16%NH_3, 21%N_2 and 63%H_2

The experimental procedure described in section 4.3.4 was used.

The feed flow rate used was in the range of 100-1500ml.min^{-1}. A Mixed sweep of 75%N_2/25%H_2 was used for mixture permeation experiments with a flow rate range of 15-150ml.min^{-1}. The reason for the 3:1 ratio of the sweep is that a critical aspect of the design of the membrane recovery process includes the use of the make-up syn-gas from the ammonia synthesis production as the sweep gas. Temperature experiments were carried out between 25^{o}C and 150^{o}C.

The permeances for mixture gas experiments were calculated using three different models for comparison:

- Well-mixed model
- Log mean pressure difference model
- Segmental model

These are discussed in more detail in Chapter 5. The separation selectivities were calculated as the ratio of the permeances. Mass balance closures based on the composition of and flow rate of the inlet and outlet streams were +/- 5% for the experiments reported in this work.

4.2.4 Experimental Procedure

The experimental procedure consisted of the following steps

1. Open gas cylinders argon (valve PR3) (delivery pressure approximately 3 bar) and allow gas flow into the GC by opening the valve O. Open valve R to the compressed air. Switch on the GC and the computer for data acquisition.
2. Open the membrane feed gas cylinder (PR2) and the sweep cylinder (PR1). Open valve Q. Switch on the mass flow controllers (flowrates<1l.min^{-1}). Set MFC's to full flow.
3. Adjust the feed pressure by closing or opening valve I.
4. Select the feed and sweep flow rates with the MFC 1 and 0 respectively, the flow rates are recorded on the computer.
5. Open valve H (see Figure 4.10 and 4.11) slowly to fix the flow rate to analytical section (< 20 ml.min^{-1}).
6. Turn on heating cabinet if necessary (T <150^{o}C).
7. Set up GC column and TCD temperatures (T_{TCD} should be 50 to 100°C higher than column) on GC.
8. Set the membrane testing rig to measure and record the parameters of the permeate (see Figure 4.11).
9. Select valves M and N to send the stream flows to the bubble meters.

10. Leave rig to stabilise (1-2 hrs).
11. While Rig is stabilising, analyse the 1st calibration mixture. Valve G (Figure 4.11) facing downwards. Inject a sample by pressing the Run key on GC for analysis.
12. Confirm that the steady state has been reached by looking at the feed pressure and retentate pressure indicators (the numbers should not be fluctuating).
13. Record the feed, permeate and retentate pressures, and the feed and sweep flow rates on the computer.
14. Determine the retentate and permeate flow rates with the bubble meters.
15. Switch valve N towards analysis section and regulate pressure at 0.018 using pressure indicator with valves L and T (T should be open completely).
16. Inject a sample in the GC by pressing the "Run" key.
17. Inject 4 more samples in GC to be sure of N_2 and H_2 concentration measurements.
18. Switch valve N to bubble meter, valve G to retentate, valve M to analysis section and regulate pressure with valve K and T (should be open completely).
19. Repeat steps 16 to 17 to get concentrations in retentate.
20. Switch valve M to bubble meter, valve G to feed and regulate pressure with valve T.
21. Repeat steps 16 to 17 in order to carry out feed analysis.
22. Return to permeate configuration for the change of experimental conditions.

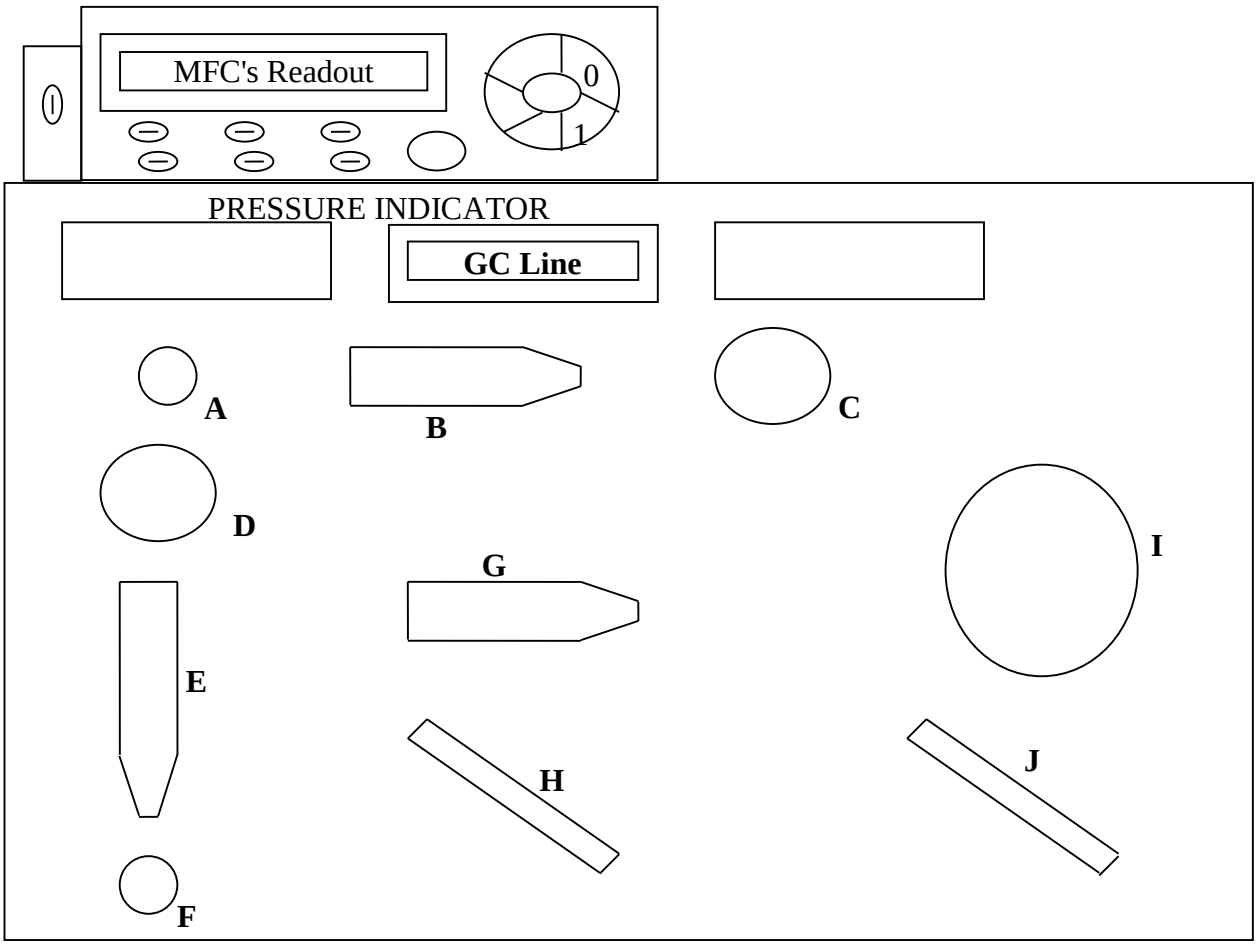

Figure 4.10: Schematic of controls for membrane separation rig

The following sections detail the procedure and valve configurations for set up of the test rig for recording the parameters of each stream.

Feed	**Permeate**	**Retentate**	**Sweep**
1. H fully closed	1. H fully closed	1. H fully closed	1. H fully closed
2. G right	2. G left	2. G up	2. G down
3. B right	3. B right	3. B right	3. B right
4. E up	4. E up	4. E up	4. E up
5. Open H slowly- monitor pressure on transducer	5. H fully open	5. Open H slowly - monitor pressure on transducer	5. H fully open

Shut down procedure

1. Run GC “cool down” program
2. Close valve H leading to analysis section
3. Fully close gas inlet valve to membrane testing rig (Valve I)
4. After GC has cooled down, turn off GC power
5. Close all gas cylinders
7. Switch off heating cabinet
8. Open valves C and D and switch valves E and B toward D and C to release the pressure.
9. Close valves O to R

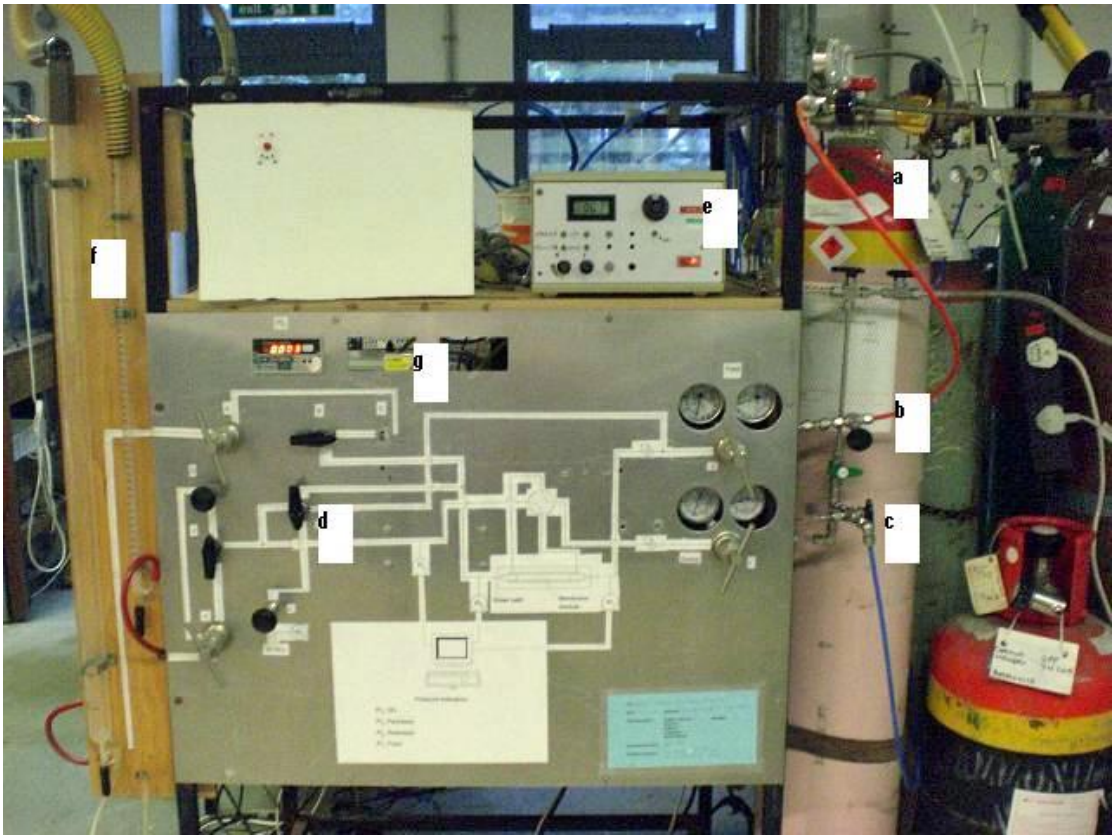

Figure 4.11: Ammonia gas separation rig a) Ammonia gas cylinder b) Feed valve c) Sweep valve d) 4 way valve for sample to GC e) Mass flow controller f) bubble meters for permeate and retentate g) Pressure Transducer

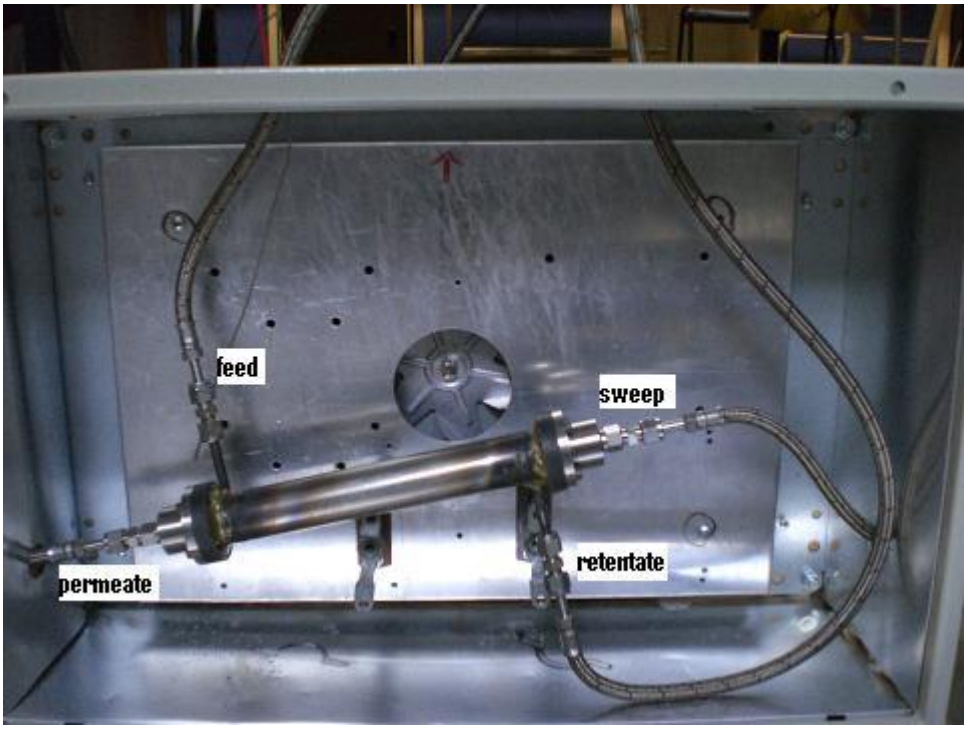

Figure 4.12: Module in heating cabinet

Figure 4.13: Gas Chromatography

Figure 4.14: Mixing Rig a) N_2 gas valve b) H_2 gas valve c) 3 way valve (gas inlet, vacuum and vent d) tube to mixture gas cylinder

CHAPTER 5

RESULTS and ANALYSIS

5.0 Introduction

In this chapter, permeation results of the membranes described in Chapter 4 are presented. Section 5.1 discusses two engineering models that can be used for data analysis, and presents a third improved model which overcomes the limitation of the first two. A detailed comparison of the models is also given. Initial screening of MCT0.2 and MCT0.5 membranes is also presented in this section. Results of gas transport through the membrane are given in Section 5.2 with the single gases and ternary mixture gas transport presented in Sections 5.2.1 and 5.2.2 respectively. A further discussion of the results including mechanisms of transport as well as the effect of operating conditions on membrane performance follows in Section 5.3 and finally concluding remarks are given in Section 5.4.

5.1 Analysis of Results

In the design of processes for membrane separation, approximate methods are needed to predict the exit compositions and area requirements in gas permeators. In order to understand the overall performance of the module, analysing the

individual permeators is required in order to predict the separation across the membrane. Different models such as the generalised Maxwell Stefan model (GMS) discussed in Chapter 3 provide clues for the development of separation techniques (for mixture diffusion within zeolites) that rely on diffusion selectivity. However, in order to design gas separation systems, engineering models are needed. Effects of various parameters can thereby be studied before embarking on a detailed design. With an engineering model, it is possible to predict the behaviour of a permeator by simulating results for a range of operating conditions, including the high pressures used in industrial ammonia production as well as predicting surface area requirements and exit compositions.

5.1.1 Mathematical Model Development

The model requirements include the ability to estimate the outlet concentrations of the gases in the permeate and retentate streams, the flow rates of these streams and the surface area of the membrane from the inlet concentrations, the sweep and feed stream flow rates, pressures and temperature and the desired amount of ammonia to be left in the retentate. This approach could be applied to different membrane separation systems.

To estimate the eight unknowns of this separation process, ten equations had to be established.

Three transmembrane fluxes, one for each component, (H_2, N_2 and NH_3)

$$J_i = \frac{P_{M_i}}{l_M}.A.\left(P_i^p - P_i^r\right) \qquad \textbf{5.1}$$

Three mass balances, one for each component

$$x_i^f F^f + x_i^s F^s = x_i^p F^p + x_i^r F^r \qquad \textbf{5.7}$$

Four mole fraction equations, one for each stream

$$\sum_i x_i^{stream} \qquad \textbf{5.8}$$

where x_i is the mole fraction of the component *i* in a stream. The superscripts *f*, *s*, *r* and *p* represent the feed, sweep, retentate and permeate stream respectively. A is the surface area, *F* is the molar flow rate, *p* is the pressure and $\frac{P_{M_i}}{l_M}$ is the permeance of component *i*.

Two methods are commonly used to calculate the permeances, namely the well-mixed model and the log mean pressure difference (LPMD) model. These are described in more detail in sections 5.1.1.1 and 5.1.1.2 respectively. An improved model is discussed in section 5.1.1.3.

5.1.1.1 Case 1: Well mixed system

The permeances can be calculated by considering well mixed behaviour on both sides of the membrane. For a well-mixed system, it is assumed that the rate of mixing on the feed-side of the permeator is so rapid, compared with the flow rate, that the gas stream has the same composition as the non-permeate stream at all points along the membrane. The same assumption is made for the permeate side. The permeation of the gases through the membrane is further assumed to be the rate controlling step. Therefore for a multi-component gas mixture, (Scott and Hughes, 1996):

$$J_i = \frac{P_{M_i}}{l_M}.A.\left(P_i^{\,p} - P_i^{\,r}\right) = (x_i Q)_{perm} \qquad \textbf{5.9}$$

This method of calculation takes no account of the concentration gradients along the membrane. Although the well-mixed assumption may be valid at high flow rates, it is particularly invalid at low flow rates where there are significant concentration changes along the length of the module. This method is therefore

most suited to situations when very small changes in concentration might occur, for example with short membrane lengths, low fluxes through the membrane or, high feed flows.

5.1.1.2 Case 2: Log Mean Pressure Difference (LMPD)

This method seeks to make allowance for gradients along the membrane by a method analogous to the log mean temperature difference approach used in heat exchanger calculations. In the log mean temperature difference approach, it is assumed that the overall heat transfer coefficient remains constant. In the same way, the LMPD model assumes that the overall mass transfer coefficient remains constant. Case 2 also takes into account all the concentrations i.e. of the feed, retentate, permeate and sweep, unlike Case 1 which only takes into account retentate and permeate concentrations. Even so, the LMPD model does not take into account the fact that there are small changes in pressure and concentration along the membrane.

$$J_i = \frac{P_{M_i}}{l_M}.A.\frac{(P_i^{perm} - P_i^{feed}) - (P_i^{sweep} - P_i^{reten})}{\ln \frac{P_i^{perm} - P_i^{feed}}{P_i^{sweep} - P_i^{reten}}} \qquad \textbf{5.10}$$

This log mean partial pressure driving force for the transport of the components across the membrane was chosen because of the uncertainty of flux variations along the membrane.

5.1.1.3 Case 3: Segmental Method

Both the well-mixed and log mean approaches have their limitations. The well-mixed system requires the concentrations to stay relatively constant between the inlets and the outlets. However, as ammonia permeates through the membrane, the feed concentration will be reduced. In the LMPD model which is analogous to the model for heat transfer (LMTD) where the overall heat transfer coefficient remains

constant, the overall mass transfer coefficient should remain constant, however it is difficult to determine whether the constant coefficient assumption is valid.

Due to these limitations, a segmental model has been used. The optimisation method recognises the fact that different concentration gradients and pressure gradients exist along the membrane. The membrane is considered to be a series of small segments as shown in Figure 5.1 for 50 such segments. McCabe et al (2001) have previously described this segmental approach to modelling membrane design and performance. If the number of segments is high enough, the variation in concentration in each segment could be negligible, allowing the equation for a well-mixed system to provide an accurate representation of each Segment.

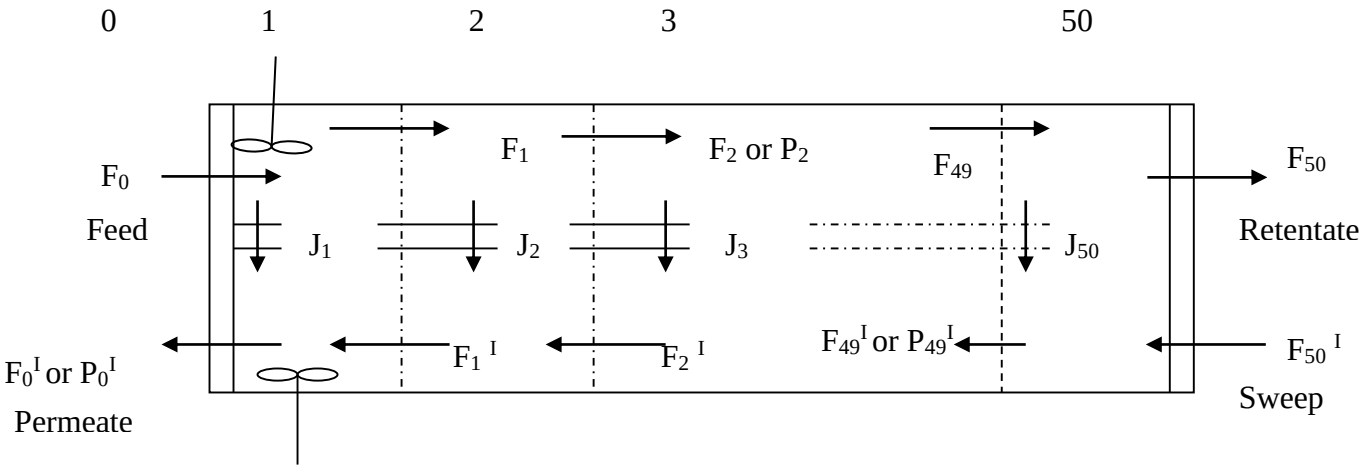

Figure 5.1: Diagram representing the membrane configuration for the segmental model

The system of equations to be solved is based on the well-mixed system applied to a volume *n* of surface area A_n. The flux across the membrane for each component y is determined by:

$$J_{n,i} = \frac{P_i}{l}.A_n(P_{n,i} - P_{n,i}{}^{I}) \qquad \textbf{5.11}$$

The permeances P_i/l are considered to be constant along the membrane. The transmembrane fluxes $J_{n,,i}$ are used to determine the flow rates for the next volume element by

$$J_{n,i} = F_{n,i} - F_{n-1,i} = F_{n,i}{}^{I} - F_{n-1,i}{}^{I} \qquad \textbf{5.12}$$

It is then possible to estimate the mole fraction of each component on both sides of the membrane and their partial pressures as follows

$$x_{n,i} = \frac{F_{n,i}}{F_n} = \frac{P_{n,i}}{P_n} \qquad \textbf{5.13}$$

With these partial pressures, the transmembrane fluxes can be estimated for the next volume element *n+1* with $A_{n+1}=A_n$/(number of segments). This process is repeated along the membrane starting from the feed/permeate end to the sweep/ retentate end as follows:

For each component in each segment the flux is determined by:

Segment 1 $$J_1 = \frac{P_{M_i}}{l_M}.A_1.(P_0 - P_0^I) \qquad F_1 = F_0 - J_1 \;\; F_1^I = F_0^I - J_1 \qquad \textbf{5. 14}$$

Where: $P_0 = P^{Feed}$ $P_0^I = P^{Perm}$ $F_0 = F^{Feed}$ $F_0^I = F^{Perm}$

Segment 2 $$J_2 = \frac{P_{M_1}}{l_M}.A_2.(P_1 - P_1^I) \qquad F_2 = F_1 - J_2 \;\; F_2^I = F_1^I - J_2 \qquad \textbf{5.15}$$

Segment 3 $$J_3 = \frac{P_{M_2}}{l_M}.A_3.(P_2 - P_2^I) \qquad F_3 = F_2 - J_3 \;\; F_3^I = F_2^I - J_3 \qquad \textbf{5. 16}$$

Segment 50 $$J_{50} = \frac{P_{M_{50}}}{l_M}.A_{50}.(P_{50} - P_{50}^I) \qquad F_{50} = F_{49} - J_{50} \;\; F_{50}^I = F_{49}^I - J_{50} \qquad \textbf{5.17}$$

The overall equation for n Segments:

$$J_n = \frac{P_{M_n}}{l_M}.A_n.(P_n - P_n^I) \qquad F_n = F_{n-1} - J_n \;\; F_n^I = F_{n-1}^I - J_n \qquad \textbf{5.18}$$

Where n = 1, 2, 3…….50

Two assumptions are made. Firstly, the permeance of each component is constant along the length of the membrane, secondly, the pressure is also constant

The set of equations 5.9-5.12 was used to determine the permeances accurately from the experimental data. The system is operated in counter-current mode and so the permeances should be calculated in a way that the sweep gas concentration (which does not contain ammonia) calculated by the model, corresponds with the experimental value. An error analysis of the segmental model was performed on a set of experimental data using 25, 50 and 100 mixed segments. It was found that a minimum of 50 segments was necessary to obtain accurate permeance values for ammonia. Whilst 25 segments gave a standard deviation of 5%, the standard deviation for the permeances was found to be around 1% with 50-100 segments. Therefore the results presented in this study have been simulated using 50 segments. All the mixture permeation results presented in this study have been obtained using the improved segmental model except where comparisons between the three models are being made.

5.1.2 Comparison of the Models

Table 5.1 shows a comparison of the permeance results obtained from the three models described in section 5.1.1. As can be seen from the table, the permeances of hydrogen and nitrogen were generally the same for all models when working with a mixed sweep, as the changes in fluxes of these components were small.
In contrast, Table 5.2 shows the variation in ammonia permeances analysed using the three models. Due to the large variation in the partial pressure of ammonia along the tubular membrane, the well-mixed model is not able to provide a meaningful value for the permeance. Generally, when the concentrations in the outlet are close to the inlet concentrations, the permeances obtained with the segmental model compare well with the well-mixed model. However, when the ammonia concentration in the outlet is much lower than that in the feed, the permeances of the LMPD model are closer to the segmental model values. These results therefore reveal the problem created by the well-mixed and LMPD models

when large changes in ammonia concentration (or partial pressure) occur along the membrane length.

Table 5.1: Comparison of permeance results from the three models for hydrogen and nitrogen

Sample Test	Membrane	H_2 Permeances			N_2 Permeances		
		Well-Mixed	LMPD	Segmental	Well-Mixed	LMPD	Segmental
1	MCT 0.5	431E-10	433E-10	445E-10	244E-10	282E-10	289E-10
2	MCT 0.5	406E-10	414E-10	447E-10	235E-10	272E-10	298E-10
1	MCT 0.2	1.02E-10	1.03E-10	1.04E-10	1.20E-10	121E-10	1.11E-10
2	MCT 0.2	2.46E-10	2.47E-10	2.67E-10	2.00E-10	2.01E-10	2.17E-10
3	MCT 0.2	1.99E-10	2.01E-10	1.96E-10	1.87E-10	1.90E-10	2.06E-10
4	MCT 0.2	1.41E-10	1.41E-10	1.52E-10	1.24E-10	1.25E-10	1.35E-10

Table 5.2: Comparison of ammonia permeance results from the three models

Sample Test	Membrane	NH_3 Feed %	NH_3 Retentate %	NH_3 Permeances		
				Well-Mixed	LMPD	Segmental
1	MCT 0.5	9	1.94	519E-10	1570E-10	1380E-10
2	MCT 0.5	9	4.53	426E-10	973E-10	3930E-10
1	MCT 0.2	9	7.5	8280E-10	7.44E-10	8.18E-10
2	MCT 0.2	9	7.6	7390E-10	7.02E-10	7.70E-10
3	MCT 0.2	16	13.8	7.53E-10	6.85E-10	30.7E-10
4	MCT 0.2	6	5.3	7.57E-10	6.85E-10	8.20E-10

5.1.3 Initial Membrane Screening

Both MCT0.5 and MCT0.2 membranes were considered suitable for ammonia separation. The difference between the two is the support pore size of 0.2μm and 0.5μm respectively as explained in Chapter 4. Test results showed that MCT0.5 had higher permeances (x1000) than MCT0.2 as shown in Tables 5.1 and 5.2, but had much lower selectivities as shown in Table 5.3. MCT0.5 also experienced high fluxes and therefore could not maintain a differential pressure higher than 300kPa. It has been noted that the zeolite pore plugging process was sensitive to pore size and that bigger support pore sizes resulted in membranes with defects. During membrane synthesis, the MCT0.5 substrate pores may not have been completely plugged with zeolite crystals giving rise to intercrystalline defects thereby resulting in the high permeance values obtained. In addition, these membranes are not selective.

MCT0.2 has a smaller support pore size and is therefore more likely to be fully plugged with zeolite (as described in Chapter 4, Section 4.2). This results in fewer defects. The support contribution to mass transfer resistances may also contribute to the lower permeances but yielding higher selectivities. For the purposes of evaluating the impact of operating conditions on membrane performance, MCT0.2 was selected due to i) the ability to test the membrane over a wider range of operating pressures ii) the higher selectivities obtained for this membrane without a significant loss to the permeability.

Table 5.3: Comparison of permeance results for MCT0.2 and MCT0.5 at 300kPa differential pressure

Sample Test	Membrane	Permeances			Selectivities	
		NH_3	H_2	N_2	NH_3/N_2	NH_3/H_2
1	MCT 0.5	973E-10	433E-10	282E-10	3.5	2.3
2	MCT 0.2	11.6E-10	1.07E-10	0.545E-10	21.3	10.8

5.2 Results

5.2.0 Error Analysis

To ensure the reliability of the experimental results, it is very important to be aware of the accuracy and repeatability of the experimental data. The sources of errors on the experimental rig include reading from the mass flow controllers and pressure transducers, and in terms of gas analysis, the GC. The errors for the measured values cause uncertainties in the calculated values which in this case are the permeance and the selectivity. In addition to this are errors such as fluctuating experiment conditions, varying environmental conditions and operator errors and biases which were difficult to quantify. Mass balances were performed for each experimental and mass balance closures were between ±5%. This was accounted for in the error analysis and the errors in the calculated values were found to be within ±10%. Detailed calculations for errors can be observed in Appendix III.

5.2.1 Single Gas Permeation

Permeation of a single gas in a zeolite membrane is normally dependent on two factors: i) the characteristic of the permeating molecule and the zeolite membrane, for example, whether the molecule is strongly or weakly adsorbed on the membrane and ii) the experimental conditions, especially the operating pressure and temperature. As such, the permeation and separation properties of the MCT0.2 membrane for the single gases hydrogen, nitrogen and ammonia were studied as a function of pressure and temperature. No sweep gas was used for these experiments as this would change the system from single component to binary. A brief discussion of gas permeation theory is given before discussion of single gas permeation results.

5.2.1.1 Gas Permeation Theory

Transport of molecules in zeolite membranes depends on the affinity of the permeating molecules towards the zeolite material and the differences in sizes of the molecules and that of the zeolite pores (Sebastian et al, 2007).

Three diffusion regimes have been identified for transport of gases through microporous zeolite membranes, namely bulk, Knudsen and configurational (surface) diffusion (Ciavarella et al, 2000, Algieri et al, 2003). Configurational diffusion is often recognised as the dominant form of transport in zeolite pores (Sommer et al, 2003). The polycrystalline structure of zeolite membranes means that a membrane may contain intercrystalline (non zeolite) regions where diffusion can also take place. Therefore, transport is usually a combination of transport through zeolite pores and transport through non-zeolitic pores which can be in series or parallel to zeolite pore diffusion (Algieri et al, 2003). Capillary condensation can also be important (Sommer et al, 2003). It has been suggested that conditions under which capillary condensation occurs are the same as those under which surface diffusion may be expected and therefore in some cases both mechanisms may exist in a given system (Coronas and Santamaria, 1999). The mechanisms are will now be discussed in more detail.

a) Bulk Diffusion

Bulk diffusion is also referred to as viscous flow or Poiseuille flow in the literature. This mechanism is predominant in macroscopic defects and cracks in the zeolite membrane layer and leads to viscous flow when a pore pressure difference is applied. Molar flux in this regime can be described by the Hagen-Poiseuille equation (Choi et al, 2001)

$$J_v = -\frac{\varepsilon r^2 p}{8\tau\mu RT}\frac{dp}{dz} \qquad \textbf{5.19}$$

where ε, τ and μ are the porosity, tortuosity factor and gas viscosity respectively. For steady state, the integration of Equation 5.14 gives the permeability (mol m^{-2} s^{-1} Pa^{-1})

$$Q_V = \frac{J_v}{\Delta P} = \frac{\varepsilon r^2}{8\tau\mu RT} P_m \qquad \textbf{5.20}$$

where P_m is the mean pressure. P_m is $(P_1 + P_2)/2$ and P_1 and P_2 are the inlet and outlet pressures respectively.

In terms of pressure dependency, viscous flow permeability is linearly proportional to the pressure. Because gaseous viscosity decreases with temperature ($\mu \sim T^{-1/2}$), permeability decreases with temperature and its dependence on temperature is $P \alpha T^{-3/2}$ (Choi et al, 2001).

b) Knudsen Diffusion

Knudsen diffusion can occur through the zeolite pores as well as the micropores created by intercrystalline grain boundaries and imperfections. Knudsen flux is said to be dependent on the molecular weight of diffusing molecules and under this mechanism, light molecules travel faster than heavy molecules under the same concentration gradient. The Knudsen equation for transport in porous media is given as (Choi et al, 2001):

$$J_K = -\frac{2}{3}\frac{\varepsilon r}{\tau}\left(\frac{8}{\pi RTM}\right)^{1/2}\frac{dp}{dz} \qquad \textbf{5.21}$$

Integration of Equation 5.16 gives the permeability as:

$$Q_k = \frac{J_K}{\Delta P} = \frac{2}{3}\frac{\varepsilon r}{\tau}\left(\frac{8}{\pi RTM}\right)^{1/2} \qquad \textbf{5.22}$$

In contrast to viscous flow which is dependent on pressure, Knudsen selectivity is independent of pressure and is proportional to the inverse square root of the molecular weight:

$$\alpha_{Kn}\left(\frac{i}{j}\right) = \sqrt{\frac{M_j}{M_i}} \qquad \textbf{5.23}$$

When this mechanism is predominant, light gases permeate faster than heavy gases (Algieri et al, 2003). The temperature dependency for Knudsen permeability is $P\alpha T^{-1/2}$.

c) Configurational Diffusion/Surface Diffusion

In the literature, this type of transport in zeolite pores is sometimes referred to as surface diffusion, configurational diffusion, intracrystalline diffusion or micropore diffusion. In this thesis and particularly in this chapter, the term configurational diffusion is used to describe the type of transport that results from an interaction between the diffusing molecules and the pore walls. Then using the descriptions as given by Xiao and Wei (1992), two types of configurational diffusion that occur in zeolite pores can be distinguished. If the molecule is strongly adsorbed, then there is a strong zeolite-adsorbate interaction and transport is by surface diffusion. If there is a weak adsorbate-zeolite interaction, transport occurs by activated diffusion which is also known as gas translational diffusion. Gas transport in zeolite membranes is exclusively controlled by configurational diffusion if the membrane is defect free.

Surface diffusion only occurs when molecules are adsorbed, provided that the surface attractive forces are strong enough to prevent surface mobility (Crittenden and Thomas, 1998). In this adsorbed phase, mass transport takes place by molecules jumping between adsorption sites. Gas translational diffusion occurs when no well-defined adsorbed phase exist in the zeolite pore, usually at high enough temperatures. The molecules retain their gaseous character, but for diffusion from site to site, molecules have to overcome an energy barrier imposed by the pore structure.

The flux J (mol m^{-2} s^{-1}) for configurational diffusion through microporous materials can be described by an equation analogous to that of the Arrhenius equation:

$$J = J_O \exp^{-E_z / RT} \qquad \textbf{5.24}$$

Permeability can also be written in the same way:

$$Q = Q_o \exp\left(\frac{-E_a}{RT}\right) \qquad \textbf{5.25}$$

where Q is the permeance, Q_o is the pre-exponential factor (mol m^{-2} s^{-1} Pa^{-1}), E_a is the activation energy ($J.mol^{-1}$), R is the gas constant (8.314 J mol^{-1} K^{-1}) and T the temperature (K).

The activation energy E_z and E_a described here is apparent as it consists of two contributions: activation energy for micropore diffusion and isosteric heat of adsorption (de Lange et al, 1995, Bai et al, 1995, Lai and Gavalas, 2000, Yoshioka et al, 2001).

d) Capillary Condensation

This transport mechanism occurs in the pores of an adsorbent at a certain critical relative pressure, where the pore gets completely filled by a gas if it is condensable. As relative pressure of the adsorbate increases, the adsorbed phase is gradually replaced by the capillary condensed phase. When saturation is approached, all pores are filled with capillary condensate (Choi et al, 2001). Theoretically, capillary condensation can achieve very high selectivities as the formation of the liquid like dense layer of the condensable gas will block and prevent the flow of the non-condensible gas (Li, 2007).

The capillary condensation mechanism is normally associated with mesopores (2nm<d<50nm) and is therefore said to occur when defects in the zeolite membrane are larger than 2nm.

5.2.1.2 Membrane Transport

Transport can occur through various combinations of the mechanisms explained above depending on various factors such as membrane quality, pore size distribution and the operating conditions. Whether bulk or Knudsen flow occurs

in the micropores is governed by the ratio of the pore radius (r) to the mean free path (λ) of the gas molecules. The mean free path is given by:

$$\lambda = \frac{RT}{\sqrt{2\pi d^2 N_a P}} \qquad \textbf{5.26}$$

where R is the universal gas constant, T is the temperature, N_a is Avogadro's number, P is pressure and d is the diameter of the gas molecule.

If $\lambda/r < 1$, the viscous (bulk) flow predominates. However if $r/\lambda < 1$, then there are more collisions with the pore walls than with other gas molecules and flow is Knudsen (Pandey and Chauhan, 2001).

Configurational diffusion has also been shown to be important when the size of the diffusing molecules approaches the zeolite pore diameter. Xiao and Wei (1992) predicted that molecules with molecular diameters larger than 60% of the pore diameter travel by configurational diffusion. This is the most common method of transport through zeolite pores and gas transport is exclusively controlled by configurational diffusion if the membrane is defect free.

In non-zeolite pores, molecules have different adsorption and diffusion properties to those in the zeolite pores. It is difficult to quantify the differences since shapes and sizes of the non-zeolite pores can be irregular. This is because non-zeolite pores can be caused by different synthesis procedures; calcination conditions etc. and they could be larger than the zeolite pores, smaller or even the same size as zeolite pores. Transport through non-zeolite pores that are larger than zeolite pores may have contributions from both surface and Knudsen diffusion and might also have viscous flow contributions (Bowen et al, 2004). In particular, if large defects are present in the zeolite layer, the permeation of the gases will be dominated by viscous flow (Algieri et al, 2003).

To confirm whether bulk or Knudsen diffusion is likely to occur in the MFI zeolite membrane, calculations of the pore diameter to mean free path ratio are presented in Table 5.4. The pore size used for MFI in this case is 0.55nm. Viscous flow of a

gas increases with pressure. However, pressure does not affect Knudsen diffusivity except when increasing the pressure increases the mean free path so that flow enters transition to viscous flow (Poshusta et al, 1999). Therefore the ratios are calculated for the pressure range used in this work.

Table 5.4: Value of mean free path for hydrogen and nitrogen

Differential Pressure	H_2	N_2
kPa	**r/λ**	**r/λ**
300	0.015	0.024
500	0.025	0.039
700	0.035	0.055
1000	0.050	0.078
1300	0.065	0.102
1500	0.075	0.118
1550	0.077	0.122

For all the gases, the ratio of r/λ is much less than one throughout the whole pressure range ruling out bulk diffusion in the micropores. Therefore diffusion in the MFI zeolite pores will either be Knudsen and/or configurational diffusion. Bulk flow should only occur in this membrane if there are large defects present (>0.55nm).

Following the description of the transport mechanisms above and their dependence on operating conditions, particularly pressure and temperature, the effects of operating conditions on single gas permeances for hydrogen, nitrogen and ammonia are analysed in order to determine which mechanisms affect their transport through MCT0.2. These results are presented in sections 5.2.1.3 and 5.2.1.4.

5.2.1.3 Effect of Pressure

The experiments with varying pressure were carried out by varying the feed pressure and keeping the permeate pressure at atmospheric. The pure gas permeances are plotted as a function of the differential pressure.

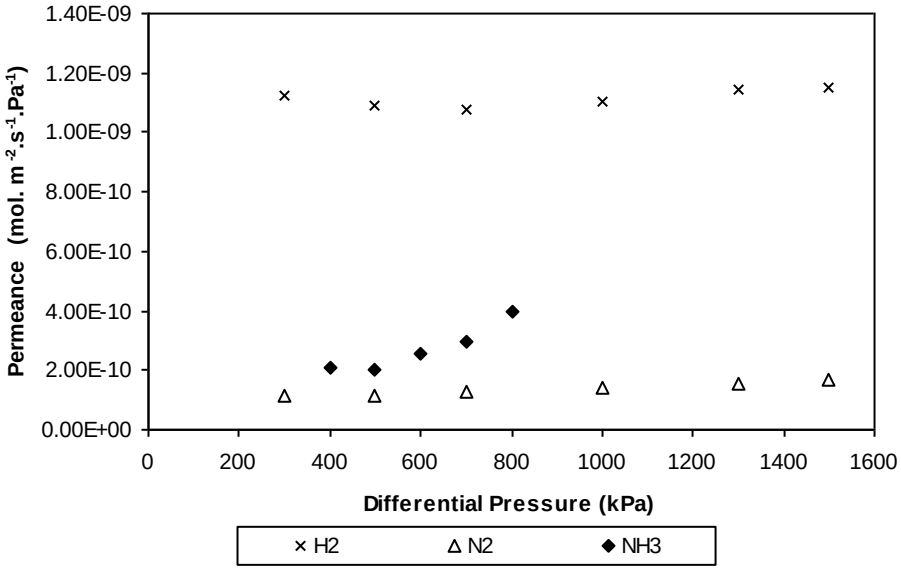

Figure 5.2: Effect of differential pressure on pure gas permeances at constant feed flow rate, 172ml min^{-1} and constant temperature, 298K.

Figure 5.2 shows the variation of permeances of the pure gases with differential pressure. For the ammonia, the maximum differential pressure that could be used was 700kPa due to the vaporisation pressure of ammonia (8.8kPa at 294K). It can be seen from the plot that the permeance of hydrogen (0.29nm) is highest, followed by ammonia (0.26nm) and then nitrogen (0.364nm). In terms of molecular size, the hydrogen molecule has a higher permeance than the smaller ammonia molecule. However, ammonia is heavier than hydrogen and the permeance of the single components in the MCT 0.2 membrane corresponds to an increase in molar mass H_2(2g.mol^{-1})<NH_3(17g.mol^{-1})<N_2(28g.mol^{-1}). This suggests that Knudsen diffusion is the transport mechanism for these molecules in MCT0.2. As mentioned in the literature, when this mechanism is predominant, light gases permeate faster than heavy gases (Algieri et al, 2003).

The permeances of hydrogen and nitrogen remain fairly constant and do not seem to be affected by an increase in differential pressure (Figure 5.3, 5.4). The ammonia however shows a small increase, then a slight decrease (Figure 5.5.).

Although bulk diffusion has been discounted for the zeolite pores (r/λ <1), it can also occur in the non zeolite pores (defects). The constant permeance with an increase in differential pressure rules out bulk diffusion as a mechanism for hydrogen and nitrogen molecules in the membrane. This is also an indication of membrane quality. As mentioned in section 5.2.1.1, bulk diffusion mainly occurs in macroporous defects and permeance in bulk diffusion is linearly dependent on the pressure. As we can see in Figure 5.2, this is not the case. Also, the ammonia permeance is not linearly proportional to the differential pressure thus indicating that the membrane does not have large defects.

It is well established from the literature that diffusion in zeolites takes place either in the Knudsen or configurational regime (Xiao and Wei, 1992, Jia et al, 1994, Bakker et al, 1996 and 1997, Choi et al, 2001, Bernal et al, 2002). According to Xiao and Wei (1992), some molecules will be in transition from Knudsen and configurational diffusion and this will depend on the properties of the molecules and those of zeolites such as such as ratio of molecular diameter to channel diameter, molecular size, zeolite structures and temperature.

In order to properly ascertain and confirm transport mechanisms in MCT0.2, figures showing the permeance and flux as a function of differential pressure are plotted for hydrogen, nitrogen and ammonia in Figures 5.3, 5.4 and 5.5 respectively.

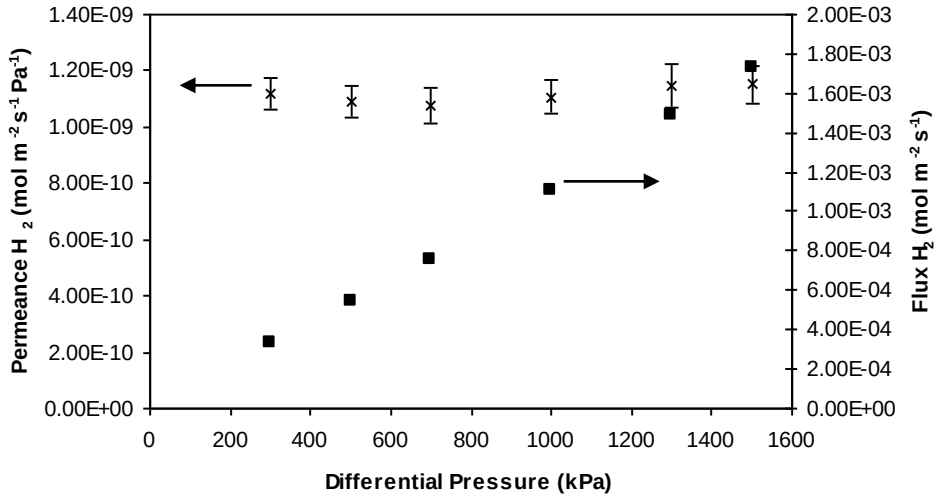

Figure 5.3: Permeation flux (squares) and permeance (crosses) of pure H_2 as a function of differential pressure at 298K and constant feed flow rate 172ml min^{-1}

Figure 5.3 shows the hydrogen permeance and flux as a function of differential pressure. It can be seen that the permeation flux is linearly related to the differential pressure thereby giving nearly constant values of the permeance. Bulk diffusion can therefore be ruled out as a possible mechanism for hydrogen transport. This is also a sign of membrane quality as any bulk diffusion would indicate defects in the membrane. As hydrogen is a weakly adsorbed component, it is unlikely that the transport mechanism would be surface diffusion. Knudsen and/or gas translational diffusion are more likely mechanisms for hydrogen transport.

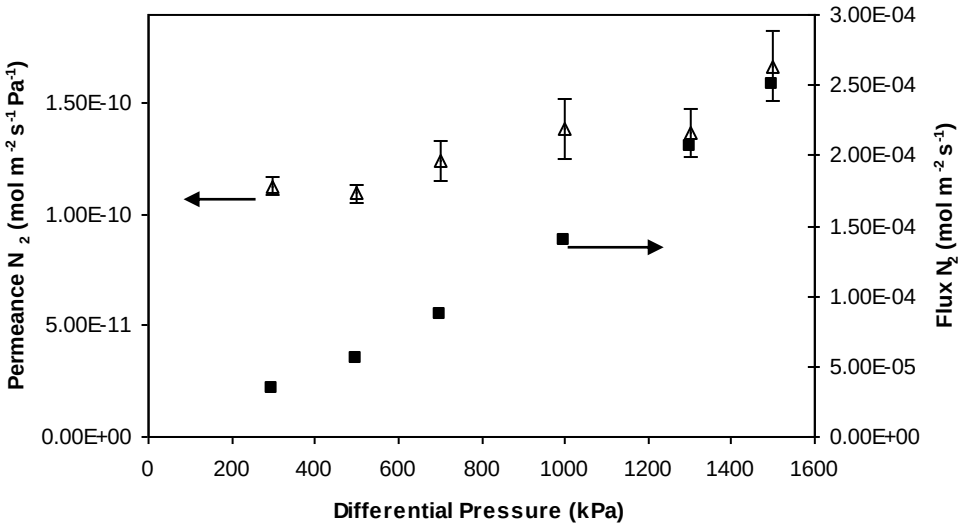

Figure 5.4: Permeation flux (squares) and permeance (triangles) of pure N_2 as a function of differential pressure at 298K and constant feed flow rate 172ml min^{-1}

Figure 5.4 shows that the nitrogen permeance does increase slightly with an increase in differential pressure. The flux increases linearly with pressure as expected. As nitrogen is also a weakly adsorbed component, it is likely that it will transport through the membrane either by Knudsen diffusion and/or gas translational diffusion.

An explanation for hydrogen and nitrogen transport could be explained with reference to their molecular size. Xiao and Wei (1992) predicted that molecules smaller than o.4nm will have little interaction with the zeolite wall and that their diffusion through zeolite channels is characterised by Knudsen flow. The sizes of hydrogen (0.29nm) and nitrogen (0.364nm) are within this range and this suggests that these molecules should permeate in the membrane via Knudsen diffusion.

The ratio of molecular diameter to channel diameter may also provide a clue. Transition from Knudsen to configurational diffusion occurs when the molecule size approaches the pore diameter (Xiao and Wei, 1992, Sommer et al, 2003) and may occur for roughly spherical molecules when the ratio of molecular diameter to channel diameter is greater than approximately 0.6-0.8. The ratio for hydrogen (0.29nm/0.55nm) is 0.53, therefore according to the stated theory, hydrogen transport is unlikely to be activated and more likely to be Knudsen. The ratio for nitrogen (0.364nm/0.55nm) is 0.66. Although Xiao and Wei (1992) found that molecules smaller than 0.4 nm would experience Knudsen diffusion in zeolites, theoretical calculations by the same group predicted that molecules with sizes between 0.3 and 0.5nm should experience increasing attraction from pore walls while passing through MFI channels (Xiao and Wei, 1992). A molecule within this range should be in transition between Knudsen and configurational diffusion. This suggests that nitrogen transport should be in the transition regime.

Another way to confirm the dominant mechanisms for hydrogen and nitrogen is to compare the permselectivity (pure gas selectivities) values with the Knudsen selectivity (Equation 5.18). If permeation is controlled by Knudsen diffusion, the

gas permeance will be proportional to the square root of the inverse of the molecular weight. When this mechanism is dominant, light gas species permeate faster than heavier gases which was observed in Figure 5.2 where hydrogen, the lightest component permeated faster than ammonia and nitrogen, and nitrogen, the heaviest molecule permeated slowest. The selectivity in the case of Knudsen diffusion is independent from pressure and is proportional to the inverse square root of the molecular weight. Table 5.5 compares the permselectivities to the Knudsen selectivity values.

Deviation from Knudsen regime for H_2/N_2 permselectivity as shown in Table 5.5 and suggests that the main mechanism for hydrogen transport is not Knudsen, another mechanism is involved. The results indicate that gas translational diffusion is a contributing factor. Also H_2/NH_3 permselectivity of 5.3 at lower pressures is higher than the Knudsen value of 2.7 but at higher pressures (700kPa), the ideal selectivity value at 2.7 is comparable to the Knudsen value. This decrease in selectivity is due to the ammonia permeance increasing with an increase in differential pressure. The transport of nitrogen should therefore be in the transition regime between Knudsen and configurational diffusion as described previously.

Table 5.5: Comparison of Knudsen selectivities and permselectivities

	Knudsen Selectivities		
	H_2/N_2	**H_2/NH_3**	**NH_3/N_2**
	3.7	2.7	1.4
Differential pressure kPa	**Permeselectivities**		
300	10.0	5.3	1.9
500	9.3	4.3	2.2
700	8.4	2.7	3.1
1000	8.0	-	-
1300	7.3	-	-
1500	6.7	-	-

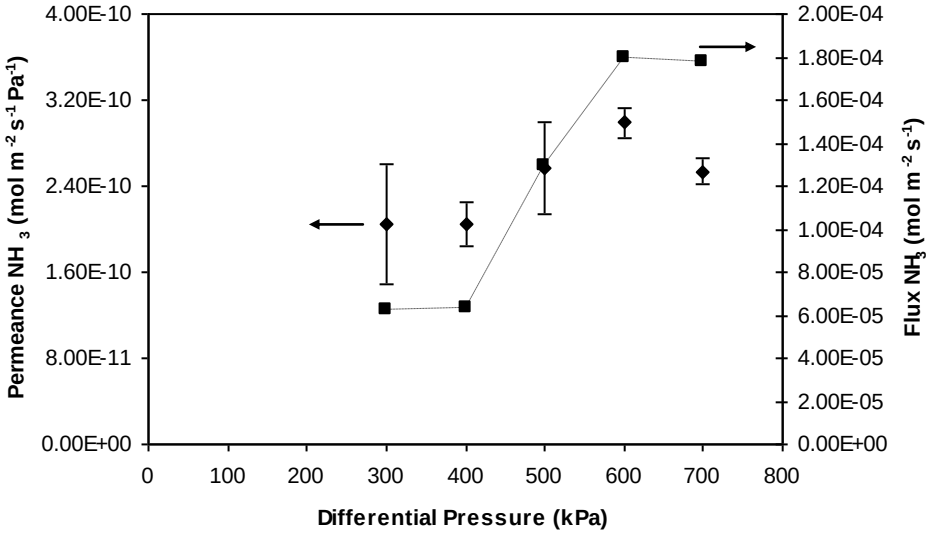

Figure 5.5: Permeation flux and permeance of pure NH_3 as a function of differential pressure at 298K and constant feed flow rate 172ml min^{-1}

The ammonia permeance with an increase in differential pressure is shown in Figure 5.5. The vapour pressure of ammonia at 294 K has been given as 888 kPa, therefore experiments were carried out at below these pressures (300-700kPa differential pressure). Ammonia permeance increases with increasing differential pressure and then decreases slightly.

Although the ammonia molecule is <0.4nm it is strongly adsorbed on MFI zeolites and will therefore have a strong adsorbate-zeolite interaction. Adsorption phenomena will play an important role in gas transport. The ammonia flux also shows a non-linear dependency with an increase in differential pressure which is expected for strongly adsorbed components. The likely mechanism for ammonia is therefore surface diffusion. Also, deviation from ideal Knudsen behaviour is observed for NH_3/N_2 permselectivity and indicates that the transport of ammonia is enhanced by surface diffusion. However, if surface diffusion were the only mechanism, then the ammonia permeance would decrease with pressure.

The surface diffusion model as described by Giroir-Fendler et al (1996), predicts that the increase in adsorbed concentration asymptotically approaches the limit as the feed pressure increases. Therefore when the adsorbed concentration of the feed side approaches saturation, a further increase in feed pressure does not

significantly change the flux across the membrane and the observed permeance decreases.

Figure 5.5 shows that at the lower pressures (300-600 kPa), the permeance of ammonia is increasing with an increase in feed pressure and the flux also increases (400-600 kPa). Increasing pressure would increase the amount adsorbed on the membrane and thereby enhance its transport. At this point, if surface diffusion is indeed the main transport mechanism, it may be assumed that the adsorbed ammonia has not yet saturated the membrane. But between 600 and 700 kPa, when the adsorbed concentration on the feed side approaches saturation, a further increase in feed pressure does not significantly change the flux. Ammonia flux reached a plateau above a feed pressure of 700 kPa (600 kPa differential pressure), suggesting that adsorption in the zeolite was saturated at this pressure. This may explain the decline in permeance with further increase in ammonia pressure. However, an ammonia adsorption isotherm on MFI zeolite measured by Mast Carbon (see Figure 5.6) shows that ammonia saturates the zeolite at 100 kPa. Therefore in this case, the membrane may already be saturated with ammonia at much lower differential pressures.

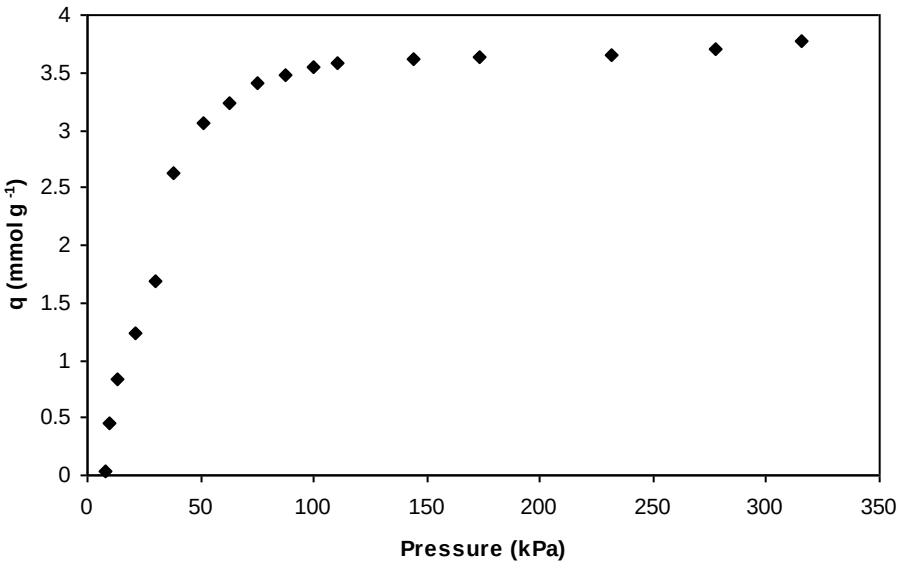

Figure 5.6: Ammonia adsorption Isotherm on H-ZSM-5 at 298K (Mast Carbon Data, 2000)

The increase in permeation may be explained by additional ammonia transport through defects/non zeolite pores. This would cause an increase in permeation with increasing differential pressure. For example, in Sebastian et al (2007), the increase for strongly adsorbed CO_2 as a function of pressure was attributed to a small contribution of Knudsen flow through intercrystalline defects. Nevertheless, this does not explain the observed decrease at 700kPa differential pressure. In addition to this, the hydrogen and nitrogen permeances confirm that the membrane does not contain a significant amount of defects. Therefore ammonia transport requires further consideration.

As ammonia is a condensable component that is strongly adsorbed, capillary condensation may also contribute to its transport across the membrane. Normally, conditions under which surface diffusion is expected are those under which capillary condensation may occur and both mechanisms may exist in a given system (Coronas and Santamaria, 1999, Bernal et al, 2002). The permeation of ammonia can be compared to Figure 5.7. As relative pressure increases, the permeability increases as a result of monolayer and multi-layer diffusion. Point 1 indicates the onset of multi-layer adsorption. Eventually, the maximum permeability is reached when all the pores are filled with liquid and capillary condensation commences. Beyond this maximum point, the permeability decreases because liquid is less permeable than the vapour (Li, 2007).

Figure 5.7: Schematic view of permeation as a function of relative pressure in the presence of capillary condensate (Adapted from Choi et al, 2001)

As mentioned previously in section 5.2.1.1, capillary condensation is normally associated with transport in mesopores (2nm<d<50nm). The observed transport of hydrogen and nitrogen as a function of pressure in this membrane dispels the presence of large defects in this membrane.

Therefore ammonia transport in MCT0.2 is probably a combination of capillary condensation in the intercrystalline pores and surface diffusion in the intracrystalline (zeolite) pores.

To summarise, pressure has a significant effect on membrane transport of hydrogen, nitrogen and ammonia in the MCT0.2 membrane. The feed pressure dependency of single gas permeation through MFI zeolite membranes has been reported in several studies (Kapteijn et al, 1995, Bakker et al, 1996, Burggraaf, 1999, van de Graaf, 1999). Generally, permeation flux of less adsorbing gases depends more linearly on the feed pressure. This was observed for hydrogen and nitrogen (Figures 5.3 and 5.4 respectively). However, it differs for ammonia. For strongly-adsorbed molecules such as ammonia, the permeation flux exhibits a nonlinear dependency on the feed pressure and this would lead to a permeance

decrease with increasing pressure (Lin et al, 2001). The observed increase in Figure 5.5 may indicate the presence of small intercrystalline pores.

In terms of transport mechanisms in zeolites at these conditions (298K), transport of weakly adsorbed hydrogen is normally attributed to Knudsen diffusion (Xiao and Wei, 1992, Hanebuth et al, 2005). However the permselectivities as shown in Table 5.5 for both H_2/N_2 and H_2/NH_3 are way above the Knudsen selectivity which indicates that the transport of these molecules is by configurational (gas translational diffusion) diffusion. Nitrogen is also a weakly adsorbed molecule, but due to its size, has a stronger interaction with the MFI zeolite pore and transport is in the transition regime between Knudsen and configurational. In the case of ammonia, being the strongly adsorbed component, the likely mechanism is surface diffusion. However, the increase in permeation with differential pressure indicates that capillary condensation in the non-zeolite (intercrystalline) pores probably makes a contribution to ammonia permeance in this membrane.

5.2.1.4 Effect of Temperature

The observed permeances for the MFI membrane as a function of temperature are presented in Figures 5.8 and 5.9. It was not possible to conduct pure ammonia gas permeances as a function of temperature.

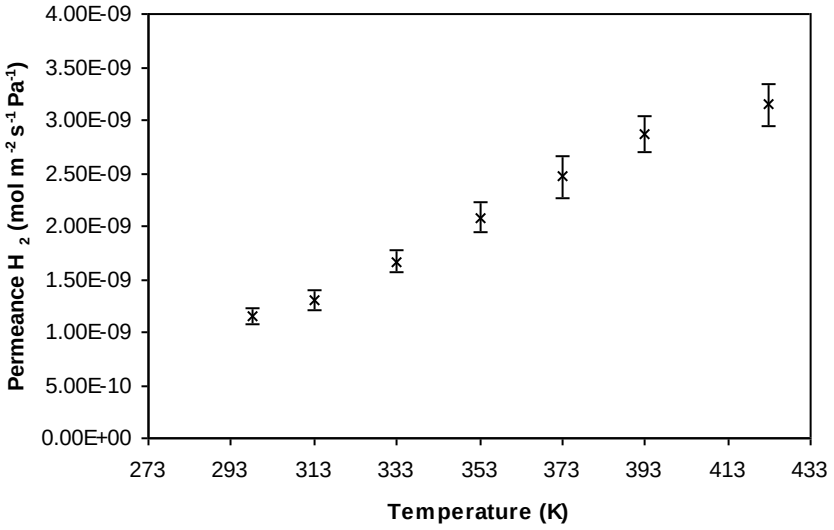

Figure 5.8: Effect of temperature on pure H_2 permeance at constant differential pressure 1500kPa and feed flow rate 172ml min^{-1}

The permeance of hydrogen increases monotonically with an increase in temperature as shown in Figure 5.8.

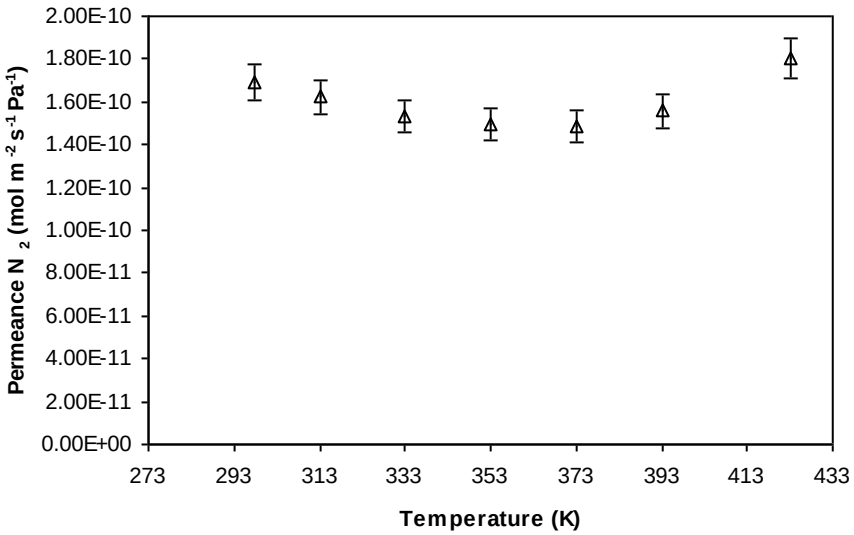

Figure 5.9: Effect of temperature on pure N_2 permeance at constant differential pressure and feed flow rate

Figure 5.9 shows the permeance of nitrogen as a function of temperature. The nitrogen permeance shows a minimum. The permeance of light gases like hydrogen and nitrogen frequently exhibit minima as a function of temperature (Bai et al, 1995, Bakker et al, 1996). The observed behaviour of nitrogen is therefore

qualitatively similar to that reported in the literature. In contrast, the hydrogen permeance increases as the temperature increases within the temperature range studied.

Prior to debating the observed dependence of hydrogen and nitrogen on temperature, a study of the typical permeance of a single gas through a zeolite membrane as a function of temperature is necessary. Figure 5.10 shows the qualitative evolution of permeance with temperature. In theory, in the region of low temperature, the permeance increases with increasing temperature because the mobility of adsorbed species is enhanced. However, at the same time, the amount of adsorbed material starts to decrease and eventually a maximum in permeance is reached (point B). From this point onwards, the decline in occupancy prevails and the permeance decreases. However at a sufficiently high temperature, the declining trend is reversed because the effect of adsorption becomes negligible, and the permeation is controlled by activated diffusion. Therefore, a minimum develops (point C), after which, there is a sustained increase of permeation with temperature.

In the ABC regime, the transport occurs mainly via adsorption, followed by surface diffusion. At higher temperatures (CD) the transport is controlled by the activated transport through the micropores (gas translation diffusion) (Algieri et al, 2003). As the adsorption strength increases, a higher temperature is required to attain the same effect; therefore a displacement of the permeance curve towards higher temperatures is expected for more strongly adsorbing compounds (Arruebo et al, 2001).

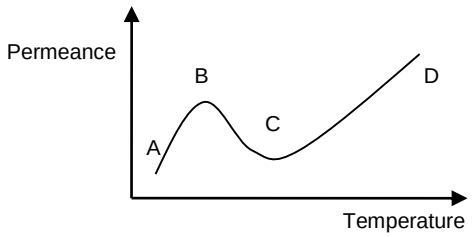

Figure 5.10: Schematic showing the qualitative evolution of permeance with temperature. (Adapted from Coronas and Santamaria, 1999)

Comparing the hydrogen (Figure 5.8) and nitrogen permeances (Figure 5.9) to Figure 5.10, hydrogen permeance is probably in the CD regime and nitrogen permeance in the C regime.

Hydrogen is a weakly adsorbed component on MFI zeolites and measurements of hydrogen adsorption on silicalite-1 crystals at atmospheric pressure showed that its adsorption is negligible above room temperature (Bakker et al, 1997, Golden and Sircar, 1994). Therefore, in the temperature range studies, hydrogen transport should be governed by activated diffusion, exponentially increasing with temperature as shown in regions C-D.

Nitrogen is also generally considered to be a weakly adsorbed component, however, studies have shown that nitrogen is more adsorbed than hydrogen and adsorption isotherms of nitrogen on both silicalite-1 and ZSM-5 at room temperature are linear and therefore in the Henry's regime (Rees et al, 1991, Dunne et al, 1996a and b, Gardner et al, 2002, Garcia-Perez et al, 2007). Henry's coefficient for nitrogen (3.16×10^{-3} mol m^{-3} Pa^{-1}) is much higher than hydrogen (2.55×10^{-4} mol m^{-3} Pa^{-1}) confirming that it is more strongly adsorbed on MFI zeolite than hydrogen (Jareman and Hedlund, 2005). Therefore nitrogen transport through the membrane should be in transition between a mode of transport governed by adsorption to one governed by activated diffusion as shown in region C of Figure 5.10.

The transport mechanisms as a function of temperature for both gases can also be confirmed through a process of elimination. As shown by Equation 5.15, if viscous flow is dominant, the permeance as a function of temperature will be dependent on $T^{-3/2}$. Therefore a plot of permeance versus $T^{-3/2}$ for both hydrogen and nitrogen is shown in Figure 5.11.

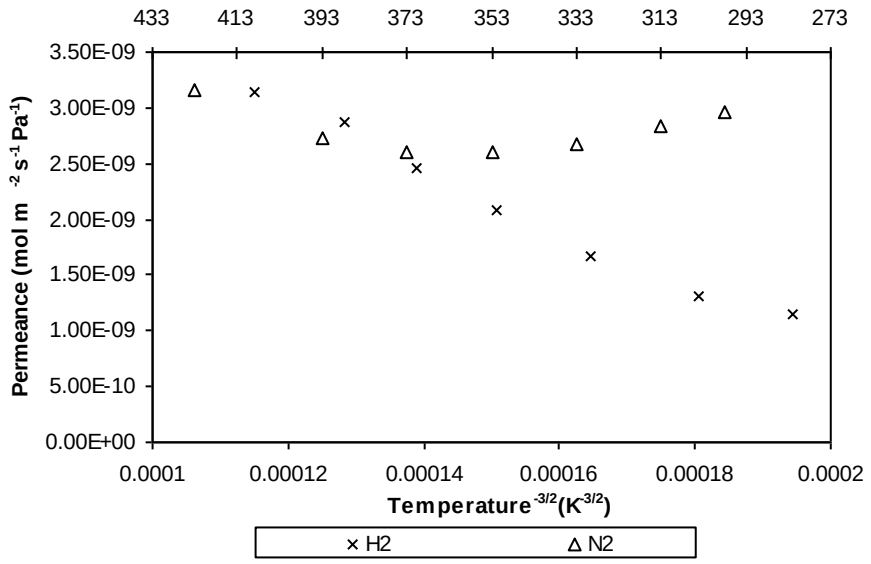

Figure 5.11: Permeance vs. Temperature $^{-3/2}$

The permeance of nitrogen shows a non-linear relationship with $T^{-3/2}$ whereas hydrogen permeance shows a negative correlation with an increase in permeance with an increase in temperature. If viscous flow was the main mechanism of transport, then the permeances would decrease with temperature. This confirms that the mechanism of transport for both molecules is not through viscous flow. This also confirms that the membrane does not contain large defects.

The next possible transport mechanism is Knudsen. It has been suggested that hydrogen transport in MFI zeolites should be by Knudsen diffusion as the molecule is weakly adsorbed (Bakker et al, 1997). Also, as suggested by Xiao and Wei (1992) transport for a molecule smaller than 0.4 nm would be primarily Knudsen. The contribution of Knudsen can be confirmed in two ways, (i) from the plot of permeance vs $T^{-1/2}$ (Equation 5.17) and (ii) from the Knudsen selectivity (Equation 5.18).

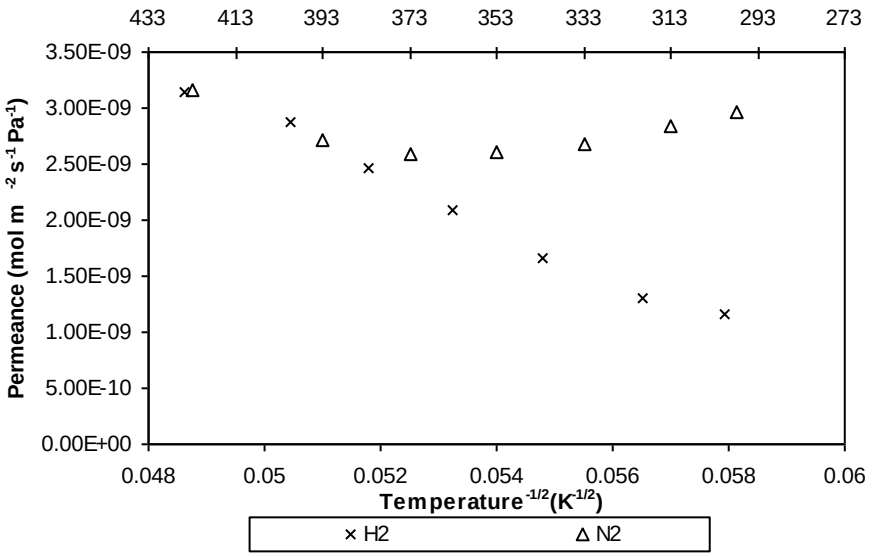

Figure 5.12: Permeance vs Temperature$^{-1/2}$

The plot of permeance vs $T^{-1/2}$ is shown in Figure 5.12 and it can be observed that nitrogen permeance has a non- linear dependence on the inverse square root of the temperature. Hydrogen has a negative correlation and shows an increase in permeance with increasing temperature. The permselectivities are shown in Table 5.6.

Table 5.6: Pure gas selectivities as a function of temperature

Temperature	Permselectivities
K	H_2/N_2
298	6.8
313	8.1
333	10.9
353	14.0
373	16.6
393	18.5
423	17.5

The Knudsen selectivity calculated using Equation 5.17 for H_2/N_2 is 3.7. This value is lower than the permselectivities in the whole temperature range. The non-linear dependence for nitrogen and the negative correlation for hydrogen on $T^{-1/2}$

and the value of permselectivity much higher than the Knudsen selectivity indicate that Knudsen is not the dominant mechanism of transport for both molecules. As the Knudsen diffusion coefficient is inversely proportional to the square root of the temperature, this would lead to a decrease in permeance with increasing temperature. This is not the case as Figure 5.8 shows a linear increase for hydrogen and Figure 5.9 shows a minimum for nitrogen.

The third mechanism of transport is configurational diffusion which is activated and occurs mainly in micropores. The activation energies of permeation were obtained by fitting the experimental gas data to an Arrhenius expression as shown in Equation 5.20 and plotting the log P vs T^{-1}.

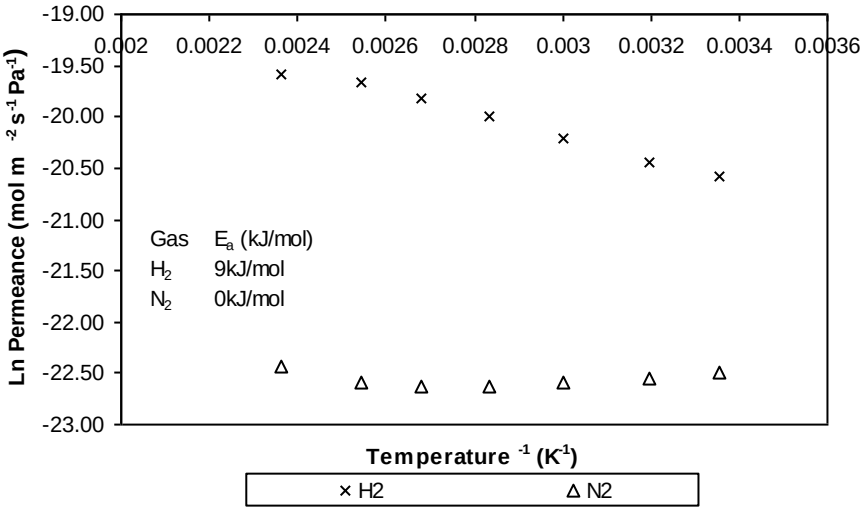

Figure 5.13: Arrhenius plot for the permeance of H_2 and N_2

The fitting results and associated parameter values are shown in Figure 5.13 and Table 5.7. The experimental data for hydrogen shows a good fit to the Arrhenius expression with an activation energy of 9 $kJ.mol^{-1}$ calculated from the plot. This confirms activated transport for this molecule. The plot for nitrogen indicates that transport is not activated (0.08 $kJ.mol^{-1}$).

The determination of which transport mechanism is dominant for hydrogen permeance in MFI membranes is not straightforward. Indeed, in the literature, hydrogen transport through an MFI zeolite membrane has been modelled via surface diffusion (Ciavarella et al, 2000), activated gas transport (Bai et al, 2005)

and Knudsen diffusion (Takata et al, 2002). Different behaviours have also been observed by some authors for hydrogen transport through MFI membranes. For example, a decrease in hydrogen permeance as a function of temperature was observed by GiroirFendler et al, (1996), Ciaveralla et al, (2000), Algieri et al, (2003), Miachon et al, (2007). Bernal et al (2002) on the other hand found an increase in hydrogen permeance with temperature, whereas Bai et al, 1995, Coronas et al, (1997) and Bakker et al, (1997) observed a minimum for hydrogen permeance. This large discrepancy in permeation behaviour with temperature has been attributed to differences in the microstructure of membranes used.

Miachon et al (2007), who observed decreases for hydrogen (and nitrogen), postulate that the temperature difference of permeation of single gases through a nanocomposite membrane for a series of gases is different from that reported in film like membranes. Indeed, most of the membranes in the literature (Giroir-Fendler et al, 1996, Ciavarella et al, 2000, Miachon et al, 2007) that experience a decrease in flux/permeance of pure gas permeances with an increase in temperature are nanocomposite membranes. They found that film-structured zeolite membranes show a reversible opening of intercrystalline pathways whereas nanocomposites membranes do not. Work done by Gualtieri et al, (2004) showed that when heated, the film like membrane MFI crystals follow the contraction also observed for MFI powder, which was translated into gap openings. For MFI crystals that were embedded into the alumina matrix, the embedded MFI followed the thermal expansion of the support. It was found that the nanocomposite membranes do not concede to intercrystalline pore opening behaviour and this was the reason one does not observe an increase in flux/permeance with an increase in temperature for nanocomposite membranes. However, this does not explain the findings of the membranes used in this thesis as shown in Figures 5.8 and 5.9. In addition, Algieri et al (2003) who observed a decrease in hydrogen permeance with an increase in temperature is a film like membrane so again the differences in behaviours may not be only about differences in thermal behaviour between the two types of membranes.

Miachon et al (2007) also suggested that differences in Si/Al ratio could account for the differences in observed behaviour. However, it is difficult to compare Si/Al

ratios as the information is not easily available in the literature. Nevertheless, this could explain why the nanocomposites used in this thesis show different behaviour to those in the literature. It is also possible that this membrane may have more intercrystalline gaps brought about during membrane synthesis.

In this work, the increases in hydrogen permeance with temperature and the calculated activated energy confirm that hydrogen transport through this membrane is activated diffusion (gas translational diffusion). The permeance increase with increasing temperature for hydrogen also suggests that the permeation through intracrsytalline pathways is dominant since permeation through mesoporous pathways would decrease with temperature according to the viscous and Knudsen flow equations.

The minimum observed in Figure 5.9 for nitrogen permeance dependency on temperature is typical of weakly adsorbed gases in zeolite MFI membranes, and has been observed by various authors (Bai et al, 1995, Coronas et al 1997, Bakker et al, 1997). Comparing the nitrogen permeance to the schematic in Figure 5.10, the trend is similar to region C. According to Bakker et al, (1997), weakly adsorbed gases only show a minimum and for strongly adsorbed gases, only a maximum is observed.

The minimum observed for nitrogen permeance has also been reported by other researchers investigating the effect of temperature permeation on weakly adsorbed gases through silicalite-1 membranes (Xiao and Wei, 1992, Bernal et al, 2004). This behaviour has been attributed to the co-existence of two different parallel diffusion mechanisms, surface diffusion and gas translational diffusion. The observed minimum can be explained by the combined temperature dependency of adsorption and diffusion for transport through a zeolite membrane (Min et al, 2003). Adsorption is more dominant at lower temperatures and therefore transport is controlled by adsorption followed by surface diffusion. Adsorption decreases with temperature and as the temperature increases, diffusion becomes more important and consequently there is a transition from adsorption based transport (surface diffusion) to diffusion based transport (gas translational diffusion). This

was also observed by Poshusta et al (1999) for temperature based single gas permeation.

This explanation for the minima as a combination of both surface diffusion and gas translational diffusion has also been confirmed by Burggraaf (1999) who showed in his calculations that the minimum in the flux could only be explained by a combination of the surface diffusion model and the gas translational model. However, in the same paper, an alternative explanation to the observed minimum for gas transport was attributed to the existence of small defects with a Knudsen contribution to the flux, parallel and in addition to gas translational flow. Therefore, when the temperature is increased, the flux decreases weakly (Knudsen flow is proportional to $I/\sqrt{TM}$) while the gas translational flow increases resulting in a minimum with the observed asymmetric shape (Burggraaf, 1999). This theory of the minimum suggesting the presence of defects has been supported by Algieri et al (2003).

Bakker et al, (1997) displayed isobars at 101K for nitrogen and hydrogen on silicalite-1 for a temperature range of 200-600K. For hydrogen no adsorption was observed above room temperature (298K) and for nitrogen, there was no adsorption above 400K. A comparison of the nitrogen permeation and the isobar showed that the minimum in the permeance occurred at the temperature where the amount adsorbed in the silicalite-1 vanishes. The fact that flux increased again at high temperatures was explained by gas translational diffusion. A similar explanation can be expected for MCT0.2. Therefore for hydrogen, as there is no adsorption on MFI zeolite above room temperature, and permeance increases monotonically with temperature, then transport is by gas translational diffusion.

For nitrogen, transport at lower temperatures (below 353K) is in the adsorbed phase, therefore nitrogen is transported by surface diffusion. As the temperature increases the adsorbed phase loading decreases with temperature and gas translational diffusion begins to take place. Activation energy for nitrogen transport calculated from Figure 5.12 is 0.08 $kJ.mol^{-1}$. This value is quite low and can be considered that the activation energy is negligible. Therefore, the nitrogen transport is probably in the intermediate region between surface and activated (gas

translational) diffusion. Further increase in temperature beyond 423K would probably give a linear dependence like that shown for hydrogen permeance. Another explanation for nitrogen transport through this membrane may be as explained by Burggraaf (1999), that there may be some transport through some intercrystalline pores and that Knudsen flow is in parallel with gas translational diffusion.

The activation energy calculated for hydrogen (9 $kJ.mol^{-1}$) in this membrane is in line with values of 8-11$kJ.mol^{-1}$ reported by Lovallo and Tsapatsis (1996), Bai et al, (1995) and Dong et al, (2000). De lange et al (1995) reports activation energies for hydrogen on MFI zeolite membranes as ranging from 5.8 $kJ.mol^{-1}$-21 $kJ.mol^{-1}$. This variation has been attributed to differences in membrane quality. It is suggested that defects (meso or micro) may give rise to a parallel flux through the defects in which transport may be determined by Knudsen and/or surface diffusion. According to these mechanisms, permeance decreases as a function of temperature and this additional contribution to transport decreases the apparent activation energy. This is supported by Lai and Gavalas (2000) in their studies of single gas permeation as a function of temperature and found high activation energies for hydrogen (24 $kJ.mol^{-1}$) and nitrogen (36 $kJ.mol^{-1}$). They postulated that these high activation energies were an indication that transport through the membrane was dominated by zeolite (intracrystalline) diffusion.

Composite MFI zeolite membranes such as those reported in Ciavarella et al, (2000) have reported an activation energy of 2.1 $kJ.mol^{-1}$ while Bakker et al, (1997) reported 1.9 $kJ.mol^{-1}$. These values seem low when compared to the range of values reported both in the literature and in this thesis. However, in the studies mentioned above, (Bakker et al, 1997, Ciavarella et al, 2000) the main mechanism for hydrogen transport in the MFI zeolite membranes was considered to be by surface diffusion only. The reason for the different observations is difficult to determine since these membranes are considered to be of high quality with minimum defects. Therefore the low activation energy may not be explained by defect presence as suggested by de Lange et al (1995) but are rather due to the different mechanism of transport through the membranes. It is also suggested that the Knudsen or viscous flow contribution of the substrate could cause the

discrepancies in activation energies reported in the literature as even the same type of membranes can be developed on substrates differing in both pore size and thickness (Labropoulus et al, 2008).

It can be concluded from the results presented in this work that single gas permeation is strongly dependent on pressure and temperature. The permeability data presented clearly indicates that the separation layer contains both zeolite channels (intracrystalline) and non zeolite (intercrystalline) channels and transport is therefore a function of both. Viscous flow is not dominant in this membrane as has been shown by the pressure dependence of hydrogen, nitrogen and ammonia and also the temperature dependence of hydrogen and nitrogen permeance which is not proportional to $T^{-3/2}$. This is also an indication of membrane quality and shows that no large defects are present in MCT0.2.

Configurational (gas translational) diffusion was found to be the dominant mode of transport for hydrogen gas both as a function of pressure and temperature. Nitrogen transport was found to be in the transition regime from Knudsen to configurational as a function of pressure and in transition between surface diffusion and gas translational diffusion as a function of temperature. Ammonia gas transport was found to be a combination of both surface diffusion and capillary condensation as a function of pressure. These mechanisms also demonstrate that transport in the MCT0.2 membrane is mainly through intracrystalline pores with some contribution from the intercrystalline pathways. It can therefore be concluded that the membrane is of good quality

5.2.2 Mixed Gas Permeation

In this section, mixed gas separation experiments were performed to determine the capability of the membrane (MCT0.2) to separate ammonia from the $NH_3/N_2/H_2$ mixture. The effect of different operating conditions on membrane performance and the steady state permeation behaviour of the mixture were studied and are

presented below. Unless otherwise stated, the concentration used was 9%NH_3; 69%H_2; 22%N_2. The sweep used was 75%H_2/25%N_2.

Error bars for hydrogen and nitrogen permeance are negligible in comparison to the error bars for ammonia. They are included in the plot for permeance with differential pressure, but it is difficult to distinguish between the hydrogen and nitrogen permeances. Therefore, error bars for these components are left out for clarity in the subsequent permeance graphs.

Generally, results for mixture gas permeances were very different compared to single gas permeances. In the observed single gas permeances (Figure 5.2), hydrogen showed the highest permeance followed by ammonia then nitrogen. The permeances coincided with an increase in molar mass (H_2>NH_3>N_2). However, in mixture gas permeances, in all cases, ammonia permeance was much higher than that of hydrogen and nitrogen as shown in Figures 5.14, 5.15, 5.16 and 5.17 (NH_3>H_2>N_2).

5.2.2.1 Effect of Pressure

Figure 5.14 shows the effect of differential pressure on the permeances of the ammonia mixture components at a feed flow rate of 172ml.min^{-1}, sweep flow rate of 15 ml.min^{-1} at a temperature of 298K.

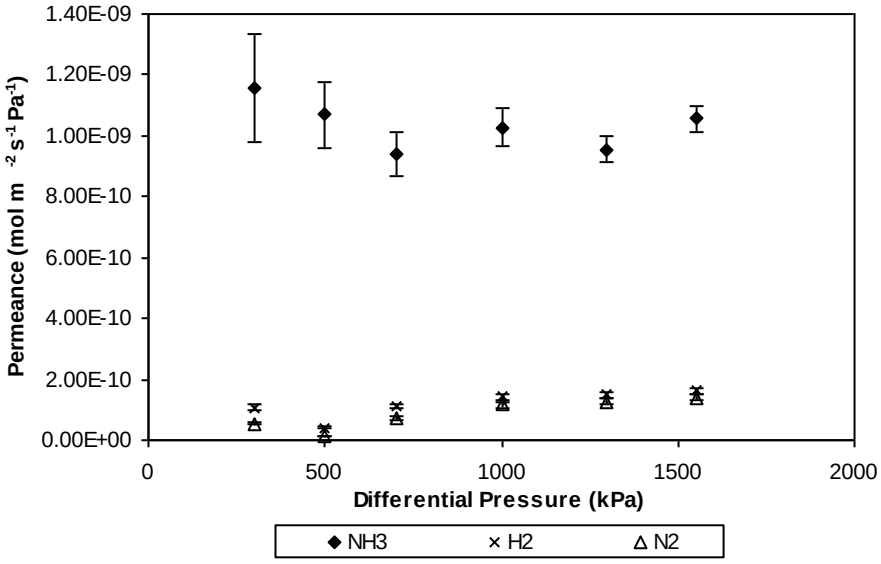

Figure 5.14: Permeance of individual components in the ternary mixture with varying differential pressure at constant feed 172ml min^{-1} and sweep 15ml min^{-1} flow rates at 298K.

Permeances of all three gases are plotted on the same graph to show the difference in permeances in the mixture when compared to that of single gases as shown in Figure 5.2. In Figure 5.2, the permeance of hydrogen was the highest followed by ammonia permeance and then nitrogen. In Figure 5.14, ammonia has the highest permeance, and that observed permeance is an order of magnitude higher than the hydrogen and nitrogen permeances. This indicates that in the mixture, ammonia is preferentially adsorbed and transported through the membrane, blocking the permeation of hydrogen and nitrogen. A comparison of the mixture permeances to the pure gas permeances shows that the hydrogen permeance has decreased by approximately 90%. The nitrogen permeance has decreased by about 50% at lower pressures, but a decrease of only about 20% is observed at higher pressures (1000-1550kPa).

Comparing Figure 5.14 with Figure 5.2, the effect of differential pressure on the ammonia permeance in the mixture is very different to that of the pure gas. The hydrogen and nitrogen permeances were hardly affected by the increase in pressure and show similar trends to those of their pure gas permeances. The trends for hydrogen and nitrogen show a small increase in the permeances. The increase is probably due to an additional contribution of Knudsen and/or configurational

diffusion in some intercrystalline pathways. Ammonia permeance remains constant probably because ammonia transport is through intracrystalline (zeolite) pores by surface diffusion.

A plot of flux (mol m^{-2} s^{-1}) versus differential pressure is shown in Figure 5.15 for further comparison. The increase in flux with increasing differential pressure for all the gases is observed in Figure 5.15 and the resulting permeances further support the fact that there is no contribution of viscous flow in gas transport through MCT0.2. The scatter of the data for ammonia permeance could be attributed to experimental errors. The dip in the nitrogen and hydrogen permeances at 500kPa is difficult to explain but is also probably be due to experimental errors.

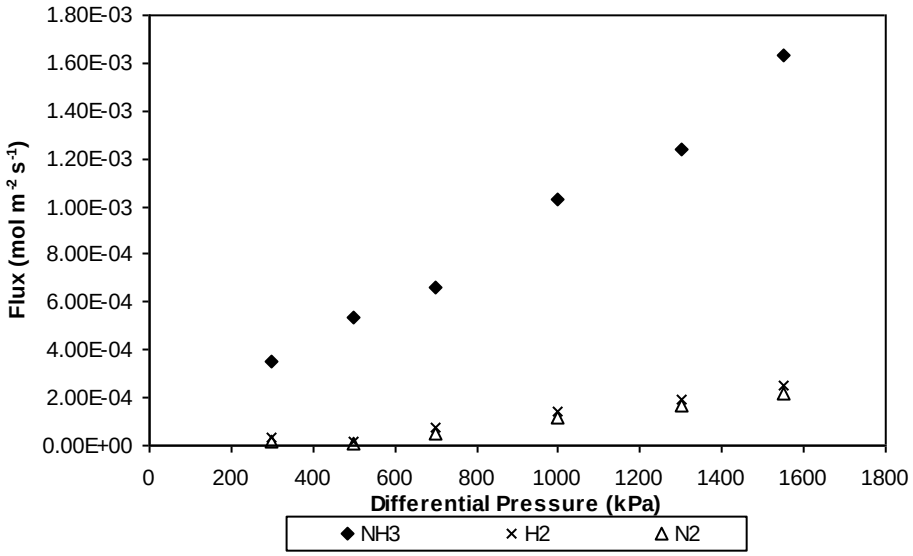

Figure 5.15: Flux of individual components in the ammonia mixture with varying differential pressure at constant feed 172ml min^{-1} and sweep 15ml min^{-1} flow rates at 298K.

A large difference in the trends can be observed for ammonia where the increase in flux is linear with differential pressure in the mixture (Figure 5.15) whereas that as a single gas is non-linear (Figure 5.5). This can be attributed to the difference in ammonia transport as a single pure gas and in the mixture. Capillary condensation has some contribution of transport for ammonia as a pure gas due to the high relative pressure of strongly adsorbed ammonia. However, in the mixture, ammonia is only at 9% and this reduces the partial pressures of ammonia significantly in the pressure range used (27-139kPa partial pressure NH_3).

Therefore it is expected that the mechanism for ammonia transport should be different in the mixture.

Surface diffusion is expected to be the main mechanism of transport for ammonia as it is the strongly adsorbed molecule. Generally, surface diffusion increases the performance of gas transport due to adsorption of adsorbing gas on the surface of the membrane pore structure (Lee et al, 2006). The gas with a high adsorption capacity preferentially adsorbs on the membrane surface thereby limiting the diffusion of the less adsorbing gas. However, capillary condensation could also be contributing to the observed ammonia transport. Therefore, in addition to blocking effects from adsorption of ammonia in zeolite pores, condensation of ammonia in the intercrystalline defects may also block nitrogen and hydrogen transport although this contribution would be small.

An increase in pressure increases the driving force and thus the fluxes would be expected to increase. This is observed for all three components. An increase in ammonia flux with increasing differential pressure is an indication of low ammonia coverage at low differential pressure. Increasing the feed side operating pressure (with a corresponding increase in the partial pressure of ammonia) would increase the rate of adsorption of ammonia onto the zeolite and increase the total surface coverage thereby enhancing ammonia transport by surface diffusion. It was found that ammonia completely saturates the zeolite when it reaches a partial pressure of 100 kPa (Camus et al, 2006). Between 1300-1550 kPa differential pressure, the partial pressure of ammonia in the feed was 117-139.5 kPa. Therefore, at higher pressures, when the pore walls are covered with ammonia at saturation, the flux should become independent of the pressure and permeance should decrease. However, this decrease was not observed, flux continued to increase and the permeance remained constant. This may be difficult to explain since the assumptions of saturation are based on the pure gas adsorption properties of ammonia, and ignore the interactions between the molecules in the mixture. These interactions probably affect adsorption and diffusion properties of each individual component in the mixture.

Selectivities as a function of differential pressure are shown in Table 5.7. The mixture selectivities are much higher than those of the permselectivities, confirming that the behaviour of gases in a mixture cannot be predicted from pure gas permeances. The high selectivities observed in Table 5.7 for mixture separations are due to the preferential adsorption of ammonia. Ammonia blocks the pores, hindering nitrogen and hydrogen diffusion across the membrane which results in higher selectivities for gas mixtures when compared to the permselectivities. The mixture selectivities decreased with an increase in differential pressure. This is due to the slight increase in hydrogen and nitrogen permeance caused by increase in diffusion pathways with increased pressure.

Table 5.7: Selectivities of both pure gas (permselectivities) and mixture as a function of differential pressure

Differential Pressure kPa	Permselectivities		Mixture Selectivities	
	NH_3/H_2	NH_3/N_2	$\alpha NH_3/N_2$	$\alpha NH_3/H_2$
300	0.02	1.9	21.2	10.8
500	0.02	2.2	71.0	26.2
700	0.04	3.1	12.7	8.4
1000			8.8	7.2
1300			7.5	6.4
1550			7.5	6.5

5.2.2.2 Effect of Sweep Flow rate

Figure 5.16 shows the effect of sweep flow rate on the permeances of gases in the mixture. The small changes in the permeance can be attributed to experimental errors. Therefore it can be assumed that the sweep flow rate has little influence on ammonia permeance.

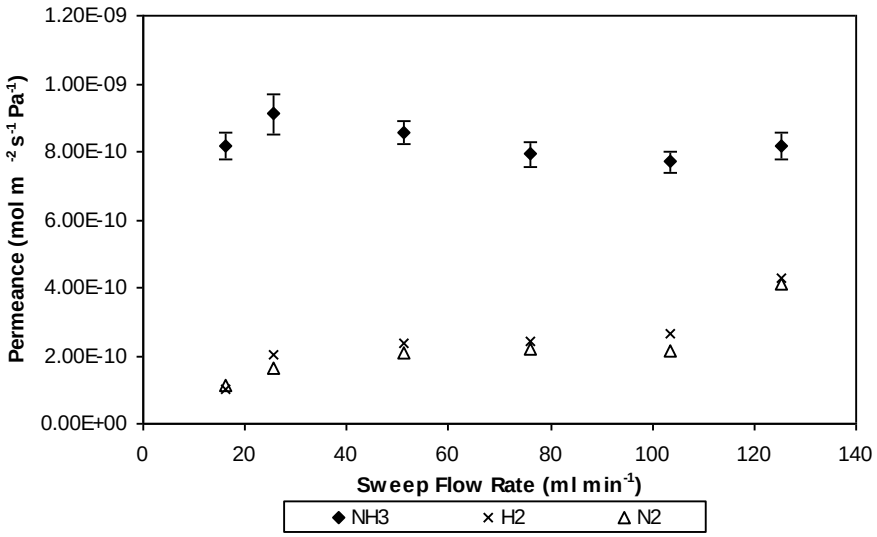

Figure 5.16: Permeance of the ammonia mixture with increasing sweep flow rate at constant feed flow rate 172ml min^{-1} and differential pressure 1550 kPa at 298K.

An increase in sweep flow rate should decrease the partial pressure of ammonia on the permeate side and thereby increase the driving force for ammonia permeance through the membrane. However, it may be that ammonia is adsorbed on the feed side of the membrane, and the extent of adsorption reduces along the length of the membrane. Accordingly an increase in sweep might well have little effect on ammonia transport.

The permeances of hydrogen and nitrogen do increase (from ~ 1 x 10^{-10} to 4 x 10^{-10} mol m^{-2} s^{-1} Pa^{-1}) with sweep flow rate and this may also be explained by the lower adsorption of ammonia on the permeate side. Hence there is easier access to the pores (as they are less blocked by ammonia) which increases their transport across the membrane. The experiment shown in Figure 5.16 was also carried out at high pressure (1550kPa) and as has been previously mentioned, at 100kPa partial pressure of ammonia, the membrane may be already saturated with ammonia on the feed side and therefore an increase in sweep flow rate (which affects partial pressures on the permeate side) may not affect the ammonia permeance. This is in contrast to Camus et al, (2006) who found that increasing the sweep flow rate improved the transport of ammonia across the membrane due to the decrease in partial pressure of ammonia on the permeate side. However, experiments performed by Camus et al, (2006) were carried out at a differential

pressure of 900kPa (partial pressure of NH_3 81kPa) and therefore the membrane was not saturated with ammonia as it was in the present case (partial pressure of NH_3 139.5).

The increase in permeances of hydrogen and nitrogen with an increase in sweep flow rate and the constant ammonia permeance could have another explanation. The mixed sweep (75% H_2: 25%N_2) increases the partial pressure of hydrogen and nitrogen on the permeate side (while decreasing ammonia partial pressure) leading to the counter diffusion of hydrogen and nitrogen thereby increasing their permeance.

The resulting selectivities are shown in Table 5.8. Gradual decreases can be observed with increasing sweep flow rate, resulting from the increase in hydrogen and nitrogen permeances and the constant ammonia permeance.

Table 5.8: Mixture gas selectivities as a function of sweep flow rate

Sweep ml.min^{-1}	$\alpha NH_3/N_2$	$\alpha NH_3/H_2$
16.24	7.4	6.3
25.51	5.5	4.5
51.13	4.1	3.6
75.91	3.6	3.3
103.58	3.6	2.9
125.42	2.0	1.9

5.2.2.3 Effect of Feed Flow rate

Figure 5.17 shows that the permeance of ammonia is fairly constant up to 1000ml.min^{-1} and then seems to decrease with a further increase in the feed flow rate. Again the explanation may be due to the partial pressure of ammonia. As the experiments were carried out at pressures where the membrane is possibly saturated with ammonia, an increase in feed flow rate is not expected to have any effect on its permeance.

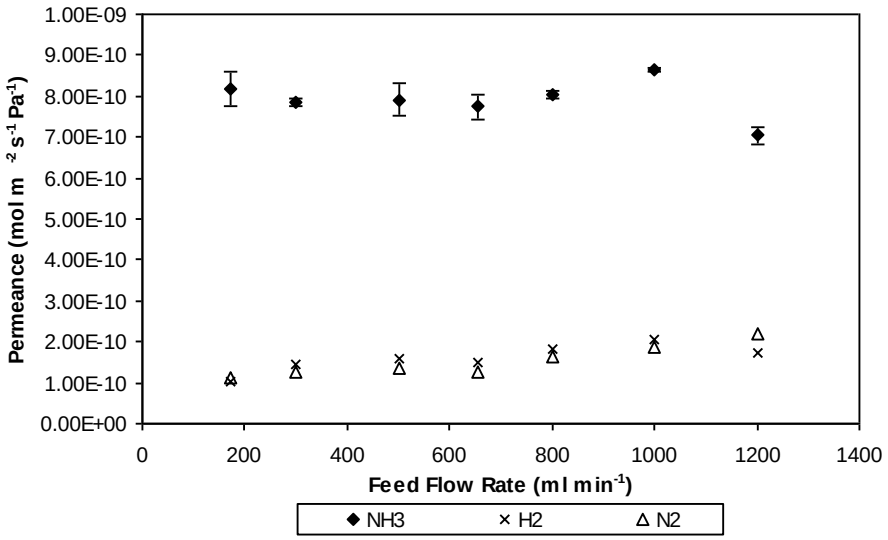

Figure 5.17: Permeance of the ammonia mixture with increasing feed flow rate at constant sweep flow rate 15ml min^{-1} and differential pressure 1550 kPa at 298K

Figure 5.17 also shows that there is a small increase in both hydrogen and nitrogen permeances with an increase in feed flow, resulting in a slight decrease in the selectivities as shown in Table 5.9. The increase shown in Figure 5.17 may be due to an increase in the driving force as more gas passes through the membrane.

Table 5.9: Mixture gas selectivities as a function of feed flow rate

Feed ml.min-1	$\alpha NH_3/N_2$	$\alpha NH_3/H_2$
172.89	7.4	6.3
301.15	6.3	5.5
499.97	5.8	5.0
653.65	6.2	5.2
800.37	4.9	4.4
1000.18	4.6	4.2
1200.76	3.2	4.1

5.2.2.4 Effect of Temperature

The effect of temperature on permeances of ammonia, hydrogen and nitrogen in the mixture is presented in Figure 5.18. Figure 5.19 shows the effect of temperature on hydrogen permeance.

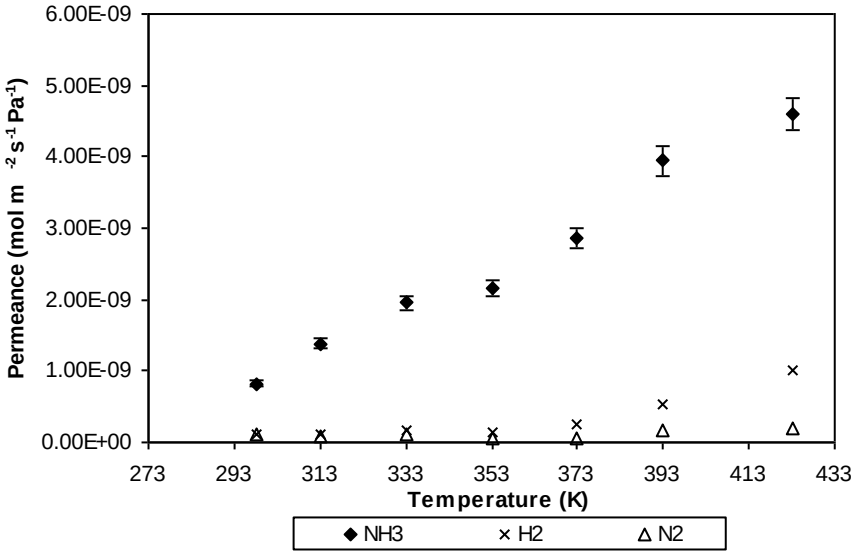

Figure 5.18: Permeance of gas mixture with increasing temperature at constant feed flow 172ml min^{-1}, sweep flow 15ml min^{-1} and Pressure 1550 kPa

Figure 5.18 shows that the permeance of ammonia increases almost linearly with an increase in temperature. The permeance of hydrogen increases in an exponential manner. This is shown more clearly in Figure 5.19. As shown in Figure 5.20, selectivities also increase steadily with temperature and reach a maximum around 353k (80^{o}C) after which they decrease.

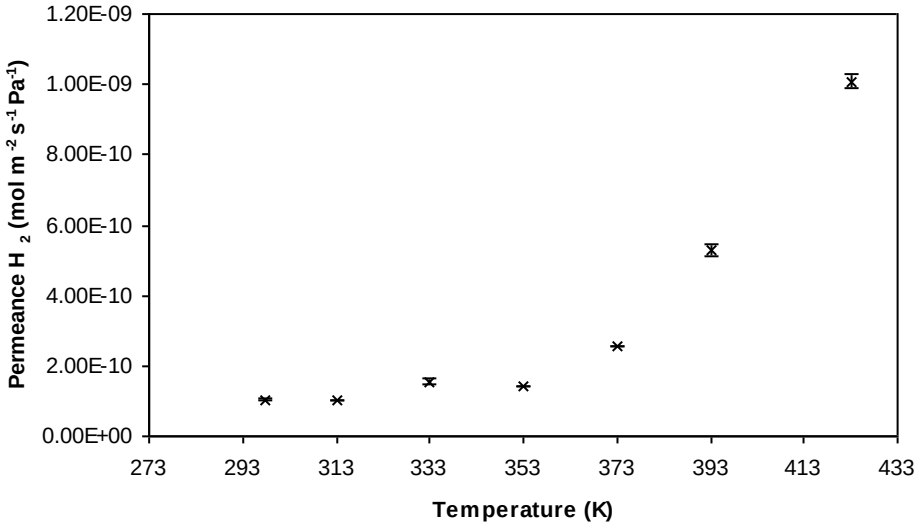

Figure 5.19: Permeance of H_2 in the ammonia mixture with an increase in temperature at constant feed 172ml min^{-1} and sweep flow rate 15ml min^{-1} and constant differential pressure 1550kPa

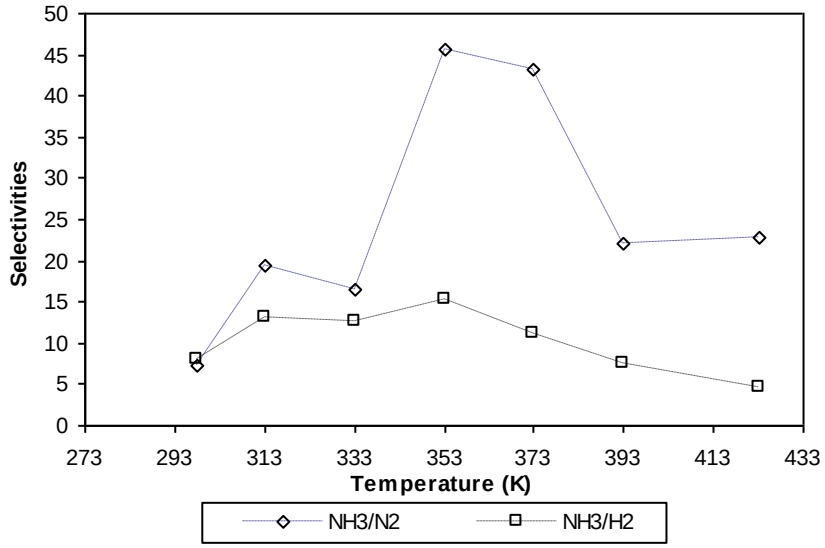

Figure 5.20: Selectivities of NH_3/N_2 and NH_3/H_2 as a function of temperature at constant feed 172ml min^{-1} and sweep flow rate 15ml min^{-1} and constant differential pressure 1550kPa

The results shown in Figure 5.18 and Figures 5.20 can be explained by the following argument. At low temperatures, ammonia adsorption is greatest and hydrogen and nitrogen are blocked out of the zeolite pores. For a moderate increase of temperature, the pores still contain adsorbed ammonia. Therefore blocking of hydrogen and nitrogen is maintained and at the same time, the mobility of ammonia increases. As a consequence, the permeation of ammonia and the

resulting selectivities increase. With a further increase in temperature, ammonia starts to desorb from the membrane pores progressively freeing pathways for hydrogen and nitrogen transport. The increase in temperature also increases hydrogen and nitrogen mobility.

The increase in hydrogen and nitrogen permeances leads to a decrease in observed selectivities, despite the continued increase in the permeance of ammonia. The trend observed in Figure 5.18 is the combined effect of strong adsorption at lower temperature, and increased diffusion at higher temperature. At higher temperatures, specifically 393K and 423K, nitrogen permeances in the mixture approach the single gas nitrogen permeances indicating that nitrogen is no longer blocked by ammonia at these temperatures. However, separation is still possible because ammonia still permeates at much higher rates than nitrogen in this membrane.

Comparing the pure gas permeances of hydrogen and nitrogen as a function of temperature in Figures 5.8 and 5.9 respectively with the mixture permeances in Figure 5.18 shows that the hydrogen permeances are reduced by about 90%, but the hydrogen permeance starts to increase after 353K and the percentage decrease is 67% at 423K. This is probably because at lower temperatures, although the mobility of ammonia has increased with temperature, there is still enough coverage to block hydrogen permeance. Ammonia inhibition is much stronger at lower temperature and therefore NH_3/H_2 and NH_3/N_2 selectivities are higher where ammonia coverage is higher. However, beyond 353K the amount of adsorbed ammonia in the pores may decrease extensively thereby freeing pathways for hydrogen transport. This, combined with increased hydrogen mobility at 353K may explain why hydrogen permeance increases causing the subsequent decrease in NH_3/H_2 selectivity.

Figure 5.21 and 5.22 compare the single gas permeances with permeances of hydrogen and nitrogen in the ternary mixture. The hydrogen permeance in the mixture is lower than the single gas and continues to remain so even at higher temperatures. The observed trend suggests that permeance of hydrogen in the mixture may be affected by factors other than ammonia adsorption.

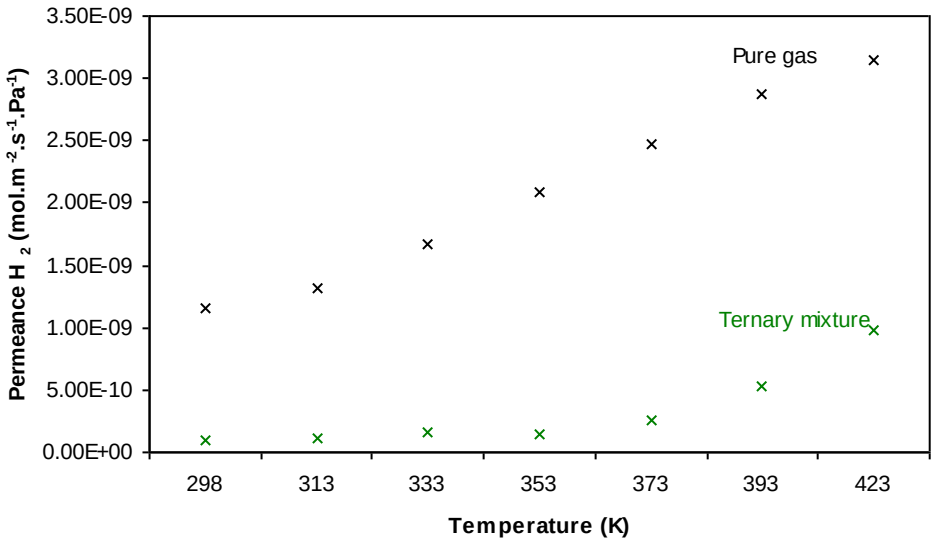

Figure 5.21: **Permeance of pure nitrogen and nitrogen in the mixture as a function of temperature differential pressure 1500kPa**

Nitrogen permeance at lower temperatures is decreased by about 50% in the presence of ammonia, but at 353K, permeance is reduced by about 68%. With a further increase in temperature, the permeance tends towards the single gas permeances.

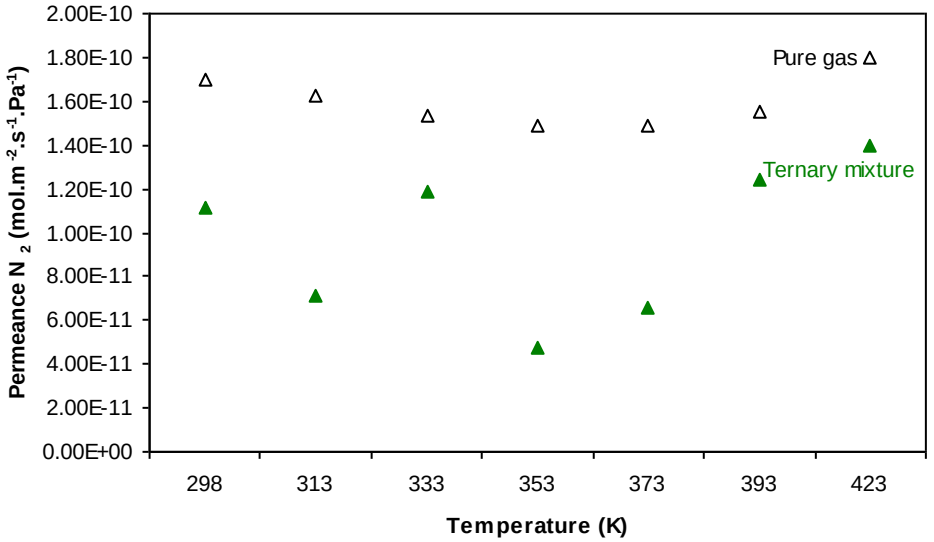

Figure 5.22: Permeance of pure nitrogen and nitrogen in the mixture as a function of temperature differential pressure 1500kPa

Studies carried out by Camus et al, (2006), also showed that the permeance of ammonia in an MFI zeolite membrane was significantly increased by an increase in temperature. It was also observed that the temperature had very little influence on the permeances of hydrogen and nitrogen and there was a subsequent increase in selectivities. A maximum in ammonia permeance was observed at 80^{o}C (353K) for both the tubular MFI zeolite membrane and the tubular silica membrane (Camus et al, 2006). However, there was no observed maximum in ammonia permeance for MCT0.2, although a maximum for selectivities was observed (selectivities decreased after 80^{o}C).

5.2.2.5 Effect of NH_3 Feed Concentration

Different feed concentrations of ammonia were studied with MCT0.2 at a temperature of 298K and the results are presented in Table 5.10. Two different sweep flows of 15 ml min^{-1}, and 50 ml min^{-1} were used.

Table 5.10: Permeances and selectivities at different ammonia feed concentrations

Sweep ml.min^{-1}	**NH_3 Feed %**	**Permeances**			**Selectivities**	
		NH_3	H_2	N_2	$\alpha NH_3/N_2$	$\alpha NH_3/H_2$
15	6	8.20E-10	1.52E-10	1.35E-10	6.1	5.4
15	9	8.18E-10	1.11E-10	1.04E-10	7.4	6.3
15	12	7.78E-10	1.90E-10	1.78E-10	4.4	4.1
15	16	7.38E-10	1.96E-10	2.06E-10	3.8	3.6
50	6	8.41E-10	2.77E-10	2.64E-10	3.2	3.0
50	9	6.67E-10	2.03E-10	1.74E-10	3.8	3.3
50	12	7.54E-10	3.20E-10	3.03E-10	2.5	2.4
50	16	7.13E-10	3.84E-10	3.78E-10	1.9	1.9

The results presented are the segmental model approximations. There was hardly any change in permeance for ammonia with an increase in percentage of ammonia in the feed. Although the permeances did not vary much, the selectivities were highest at 9% ammonia in feed. As explained previously, it seems that ammonia is completely saturating the membrane when it reaches a partial pressure of around

100kPa. This can explain the lack of variation in permeance observed at 6%, 9%, 12% and 16% ammonia (i.e. an ammonia partial pressure of 90, 135, 180 and 240 kPa respectively).

In work presented by Camus et al (2006), experiments were performed at 298K and 1000 kPa differential pressure with 2%, 9% and 16%. They found that at 2% their zeolite membrane gave much higher permeances than at 9% and 16% with hardly any change on ammonia permeances between 9% and 16%. This was because at 2%, (20 kPa partial pressure NH_3), the membrane may not have been completely saturated with ammonia allowing its easier passage across the membrane. At 9% and 16% (90 and 160kPa respectively), there was little variation and this could also be because at these partial pressures, the membrane was already saturated with ammonia (Camus et al, 2006).

5.3 General Discussion

The membrane tested (MCT0.2) has demonstrated very specific performance characteristics. The permeances of the gases in the mixture differed from their single gas permeances. In the case of the single gases, the permeances increased in the order of H_2>NH_3>N_2, despite ammonia being the smallest molecule. The permeance was found to be dependent on the molar mass rather than the size of the molecules suggesting a Knudsen mechanism of transport. But single gas selectivities for both pressure and temperature dependencies were higher than Knudsen, thereby indicating that other transport mechanisms such as configurational diffusion (both surface diffusion and gas translational diffusion) were responsible for single gas transport in MCT0.2.

In the ternary mixture however, ammonia is preferentially transported through the membrane and the separation selectivities are high even though the selectivities based on single gas permeances (permselectivities) are less than 1 in the case of NH_3/H_2 and low (between 1 and 2) in the case of NH_3/N_2. These large effects

demonstrate the strong attractions present between molecules in mixtures and thus separation behaviour cannot be readily predicted on single-gas permeances.

The results for the mixture gas indicate that the more adsorbable feed component, ammonia, was selectively adsorbed in the membrane pore structure. It is then transported as a dense adsorbed phase and this dense phase inhibits the transport of the less condensable species hydrogen and nitrogen. A combination of preferential adsorption and pore blocking at the external surface, and preferential packing of ammonia may be effective in preventing hydrogen and nitrogen from entering the pores. This phenomenon has also been observed by various authors using MFI zeolite membranes although studies have been mostly based on hydrocarbons (Bakker et, 1996 &1997, Coronas et al, 1996, Coronas and Santamaria 1999, Dong et al, 2000**)**. The net effect is that the strongly adsorbed ammonia molecules tend to permeate, leaving the weakly adsorbed molecules (nitrogen and hydrogen) at the system pressure as retentate.

Ammonia transport is achieved through the preferential adsorption in zeolite pores followed by surface diffusion and/or capillary condensation in intercrystalline pores. According to Bernal et al (2002), capillary condensation can easily take place in mesoporous intercrystalline defects when these are present in the zeolite membranes, giving rise to selective separations. Capillary condensation often occurs under conditions where a significant adsorption can also be expected, i.e. at relatively low temperatures and high partial pressures, which means that both processes may coexist in a given system resulting in a "cooperative" separation mechanism. Capillary condensation may have some contribution to ammonia pure gas transport (high ammonia pressures) in intercrystalline pores although it is highly unlikely that this is the main mechanism for ammonia transport in the mixture gas.

Ammonia gas in the mixture is preferentially adsorbed, thus blocking the zeolite pores and preventing hydrogen and nitrogen from permeating through the membrane. It should be considered that ammonia gas may also be causing the MFI zeolite crystals swell, thereby closing the intercrystalline defects (as has been shown in various recent studies on preferential adsorption of hydrocarbons, see

Fig 3.4) and thereby contributing to the prevention of hydrogen and nitrogen from permeating through the membrane. However there is no evidence currently that ammonia causes MFI crystal swelling. Looking at the single gas permeance of ammonia gas (Figure 5.5, Section 5.2.1.3), it is clear that there is some contribution of intercrystalline transport contribution. If there was no transport through intercrystalline pores, ammonia gas transport would mainly be by surface diffusion, in which case, the permeance would decrease with an increase in pressure.

It is also possible that the permeation of different components in the gas mixture may generate a boundary layer on the feed side of the membrane. In this boundary layer, the composition of the bulk feed may change as a result of different permeation rates of each component. This effect, termed concentration polarisation, may control the overall mass transfer rate to some extent. Since ammonia is withdrawn from the feed gas preferentially (it is the faster permeating component), its partial pressure decreases (while the partial pressures of the slower permeating components i.e. hydrogen and nitrogen increase) at the membrane inner surface. The concentration polarisation effect is more of a problem in liquid phase systems. However it may have some influence on the mass transfer coefficient in this gas phase system. The effect is also likely to be more significant when low feed flow rates and high concentration feeds are used (Camus et al, 2006).

The differences observed in single gas permeances with those in mixture gas permeances have been mainly attributed to the preferential adsorption of ammonia. However, diffusion of gases also plays a major role. In this work, single gas permeances were in the order H_2>NH_3>N_2. In the gas mixture, this changed to NH_3>H_2>N_2. It has been shown that the slower component in a mixture can slow down the diffusion of the component diffusing faster and at the same time accelerate the diffusion of the slow diffusing component (Cui et al, 2004). For example, nitrogen which is the slowest diffusing component could slow down hydrogen diffusion and at the same time accelerate the diffusion of ammonia.

The difference between the results obtained in these experiments compared with those of Camus et al (2006) suggest that apart from operating conditions, the type of support also has an influence on transport. Significant differences can be observed in the results for ammonia separation for the different types of membrane. In these experiments, the supports were homogeneous in nature with a pore size of 0.2 (μm) whereas those used by Camus et al (2006) were composed of three layers of α-alumina 12μm, 0.8 μm and 0.2 μm. Comparisons are shown in Table 5.11. The permeances of all three components in a 9% ammonia mixture were a factor of two lower in the MCT0.2 homogeneous membrane than the multi-layer tubular membrane. However, the selectivities were much higher. At 80°C, the permeance for ammonia in the tubular MFI membrane was 2.1 x 10^{-7} (mol m^{-2} s^{-1} Pa^{-1}) which is two orders of magnitude higher than MCT0.2 (2.16 x 10^{-9} mol m^{-2} s^{-1} Pa^{-1}). However the $\alpha NH_3/H_2$ for MCT0.2 was 15.4 compared to 10.0 for the MFI tubular membrane.

Table 5.11: Comparison of permeances and selectivities of MCT0.2 with Camus et al (2006)

Membrane	**Permeances**			**Selectivities**	
	NH_3	H_2	N_2	$\alpha NH_3/N_2$	$\alpha NH_3/H_2$
Multilayer (Camus et al 2006)	6.40E-08	2.07E-08	2.24E-08	2.8	3.1
MCT0.2 (This work)	1.03E-09	1.43E-10	1.16E-10	8.8	7.2

This selectivity value of 15.4 suggests that the MCT0.2 membrane has a much higher resistance to mass transfer than the multilayer membranes. The multilayer membranes may also have a thinner membrane layer which may explain their higher permeances. It is thought that that for pore plugged membranes, the thickness of the membranecould be determined by the support microstructure. When membranes are formed by pore plugging, because the zeolite membrane is embedded in the support to form a nanocomposite, the thickness of the zeolite membrane is likely to be the same thickness as the support. In multilayer supports the zeolite membrane is restricted to the top layer. Camus et al, (2006), Miachon

et al, (2006) and Li et al, (2008) found that the zeolitic material was mostly present within the last 0.2 μm (top) support layer. They found that for larger pore size support layers (0.5 μm and 0.8 μm top layers), the pore plugging was not complete. It has been suggested that there is a critical support pore diameter above which the crystallization inside the pore does not plug it totally and that this critical value should be higher than 0.5 μm (Miachon et al, 2006). However, for a homogenous support, the zeolite membrane can fill the whole support especially one that has a pore size lower than the critical support pore diameter. For MCT0.2, the pore size of the whole support layer is 0.2 μm and therefore the zeolite likely fills the whole support, making the MCT0.2 zeolite membrane much thicker. This could explain the lower permeances of and higher selectivities of MCT0.2 when compared to the multilayer membranes, it is similar to a double sided zeolite membrane in terms of total thickness of the separative layer. Figure 5.23 shows the schematics for a nanocomposite zeolite membrane grown in a multilayer support, a homogenous support and a double sided zeolite membrane (2 layers on each side).

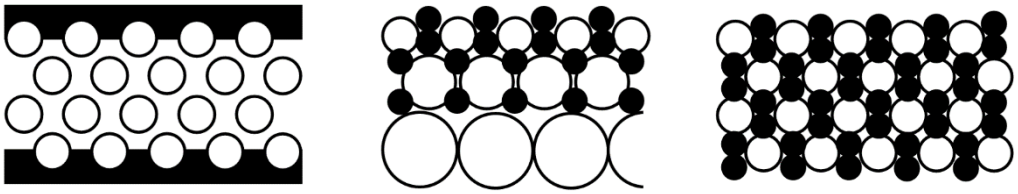

Figure 5.23: Control of membrane thickness by support design; double-sided membrane on homogeneous support, nanocompoite membrane on 3-layer support, nanocomposite membrane on homogeneous support.

Thicker membranes are usually more selective. The higher selectivity of MCT0.2 also points to another phenomenon that has been mentioned previously, i.e. concentration polarisation. It may be that because MCT0.2 is more selective to ammonia than the multilayer membranes, the hydrogen and nitrogen are left at the surface boundary and further slow down the permeance of the gas in the bulk phase. This may explain the lower permeances observed for MCT0.2 in comparison to the multilayer membranes.

It should be emphasised here that caution should be taken when comparing permeance data reported in the literature since diverse authors adopt different

experimental methods and conditions for measuring the permeation flux through membranes. The membrane thickness, the nature of support, Si/Al ratios etc. are other important factors that can affect membrane performance. The difference in single gas permeation experiments performed in this thesis with those of the same type of membrane (pore-plugged) further emphasise this point. The homogenous tubular support used in this membrane as compared to the three layered support of the membrane used in other studies may have contributed to the differences in observed behaviour.

It has been shown in these studies that membrane performance is highly dependent on the operating conditions. For the single gas permeances, it has been observed that the transport mechanism is particularly dependent on temperature. Hydrogen permeance increased monotonously with temperature suggesting that an activated diffusion process (gas translational diffusion) contributes to the mass transport through the MFI zeolite membrane, whereas nitrogen permeance showed a minimum which was attributed to a transition from surface diffusion to activated (gas translational) diffusion.

For the gas mixture, the permeances and resulting selectivities are also strongly dependent on the operating conditions, particularly pressure and temperature. Higher selectivities were obtained at lower pressures although it is important to note that the pressure experiments were performed at room temperature. A different dependency might have been observed at a different temperature. The lower selectivities at higher pressures may be because of ammonia saturating the membrane at a partial pressure of 100kpa at 298K. With an increase in temperature, ammonia adsorption is less, the membrane would not be saturated and therefore different dependencies on the pressure may be observed.

Higher selectivities in the mixture are attributed to the fact that ammonia is preferentially adsorbed into the zeolite pores thus preventing hydrogen and nitrogen from permeating. However, another phenomenon should be considered as working in parallel. As has been observed with the adsorption of hydrocarbons such as n-hexane, ammonia adsorption into MFI crystals could cause the crystals to swell and hence close any intercrystalline gaps/defects thus preventing nitrogen

and hydrogen permeation. However this phenomenon requires further investigation as there has been no evidence in the literature of ammonia causing MFI crystals to swell.

The biggest impact on membrane performance and the effective separation of ammonia gas is the effect of temperature. For mixture separations, ammonia permeance increases monotonously with temperature in the temperature range studied in this work. Hydrogen permeance increases exponentially. The nitrogen permeance shows a minimum and at higher temperatures (423K) the nitrogen permeance in the ternary mixture is approaching its single gas permeance. This suggests that ammonia hindrance to hydrogen and nitrogen transport is quite low at this temperature. However, a good separation can still be obtained since nitrogen permeates more slowly than ammonia in this MFI zeolite membrane. For hydrogen, even at the highest temperature studied, the permeance in the ternary mixture does not match the single gas permeance as shown in Figure 5.21.

Figure 5.16 suggests that hydrogen transport is also affected by the presence of nitrogen. The increase in both hydrogen and nitrogen permeances starts to occur between 353K and 373K which may indicate that ammonia is no longer adsorbed at these temperatures thereby unblocking the pores causing an increase in permeance (a shift of mechanism for ammonia from surface diffusion to activated gaseous diffusion). There is also an increase in the mobility of hydrogen and nitrogen at this temperature (353K) thereby enhancing their transport.

Another possible explanation is that an increase in thermal stress at these temperatures may have led to the enlargement of the pathways. The result is a maximum in selectivities observed at 353K. In either case, 353K (80^{o}C) could be considered as the highest temperature for optimum membrane performance for this particular type of separation.

5.4 Concluding Remarks

A segmental model has been used for data interpretation and this improved model overcomes the limitations of the well-mixed and LMPD models by taking into account concentration changes along both sides of the membrane. This can be particularly important when considering industrial applications since variations in concentration and membrane flux in the direction along the membrane are important parameters in design and analysis.

Initial membrane screening showed that MCT0.2 had lower permeances than MCT0.5 but was much more selective. The higher permeances in MCT0.5 were attributed to the presence of defects due to incomplete plugging of the zeolite into the substrate pores. MCT0.2 was therefore selected and subjected to further screening.

Results show that the single gas permeations studied cannot be used to predict the mixture gas separations. Transport mechanisms that govern transport through this zeolite membrane (MCT0.2) were confirmed and it was observed that transport through the membrane is a combination of transport through intracrystalline zeolite pores and intercrystalline pores. It was shown that permeance and selectivity are highly dependent on operating conditions particularly temperature. The highest selectivities in favour of ammonia were observed at 353K and this can be considered to be the optimum temperature for ammonia separation in this type of membrane.

The separation of ammonia from a mixture with hydrogen and nitrogen is by preferential adsorption of ammonia, which hinders the permeation of hydrogen and nitrogen. This reduction in permeance of weakly adsorbed components in the presence of a strongly adsorbed component can be qualitatively explained as has been shown in this chapter and in various permeation studies of mixtures with adsorbable and non-adsorbable components on MFI zeolite membranes. The next step is to try and explain this phenomenon quantitatively and this forms the basis of the next chapter.

CHAPTER 6

MODELLING

6.0 Introduction

In Chapter 5, it was observed that the separation of ammonia from a mixture with nitrogen and hydrogen is achieved by the preferential adsorption of ammonia thereby blocking the permeation of hydrogen and nitrogen. In this chapter, a potential barrier model is proposed to describe this hindering effect of ammonia on nitrogen and hydrogen permeation. This chapter is divided into four main sections. In section 6.1, the role of adsorption in the separation of the $NH_3/H_2/N_2$ system is discussed. Section 6.2 presents equilibrium ammonia adsorption isotherms which are fitted to empirical isotherm models such as the Langmuir and Tóth equations to obtain parameters for the ammonia-zeolite adsorption system. A detailed analysis of the errors associated with the fits to experimental data is also carried out. The results of the Potential Barrier Model are presented in Section 6.3 and the suitability of the model to describe multi-component permeation is discussed. Concluding remarks are given in section 6.4.

6.1 Role of Adsorption in Permeation

For strongly adsorbed gases, adsorption is considered as the first step in gas molecule transport through a zeolite membrane (Bakker et al, 1996). Permeation through the membrane can be controlled by adsorption followed by surface diffusion and/or activated diffusion. Which mechanism is dominant is dependent on the operating conditions such as temperature and pressure (Dong et al, 2000). The actual mechanism of gas permeation through a zeolite membrane is therefore dependent on the adsorption properties of the gas on the zeolite.

A membrane with high performance must be highly selective and have high permeances. These two characteristics, selectivity and permeance, are dictated by two fundamental characteristics of the membrane (Clark et al, 2004):

1. the relative affinities for the gas molecules to adsorb in the membrane, as described by the relevant adsorption isotherms, and
2. the relative speed with which the molecules diffuse through the membrane, as described by their respective diffusion coefficients

Both of these factors can be influenced by the operating conditions such as pressure, temperature and interaction with adsorption sites and other molecules inside the membrane (Jia and Murad, 2005). For the membrane to succeed in a given separation, the gas molecules in the mixture must have either a large difference in adsorption affinities on the membrane, a difference in their diffusivities, or both (Clark et al, 2004). In the separation of gas or vapour mixtures using zeolite membranes, the strongly adsorbing components may block the zeolitic pores by adsorption/condensation at low temperatures, and/or high partial pressures, thereby retaining the weakly adsorbed component and enriching the permeate with the strongly adsorbed component (Dong et al, 2000). High selectivities can therefore be obtained for components that differ in adsorption behaviour (Bakker et al, 1996).

Various authors recognise the effect of adsorption on permeance and have demonstrated the advantages of gas separation based on the surface diffusion of the strongly adsorbed components and their hindering effect on the permeance of weakly or non-adsorbed components (Funke et al, 1997, Keizer et al, 1998, Van den Broeke at al, 1999, Dong et al, 2000, Gump et al, 2000, Arruebo et al, 2001, Bernal et al, 2002). Even so, few publications have approached the subject in a quantitative manner, thereby resulting in only a partial understanding of the phenomenon. In addition, most of these studies have been based on the separation of hydrocarbons.

The importance of adsorption in membrane separation is best described by Jia and Murad (2005) who performed studies on different types of zeolite membrane namely Faujasite, MFI and Chabazite. They found that for mixture components with differing adsorption behaviour (using CO_2/N_2 as a test system), separation is mainly governed by adsorption and small pore zeolites separate these gases quite effectively. The results further indicated that loading (adsorption) dominates the separation of gas mixtures in small pore zeolites, such as MFI and Chabazite and that for larger-pore size zeolites such as Faujasite, although diffusion rates had some effect on gas mixture separation, adsorption was still important.

Yang et al, (1999) proposed a model to describe the hindering effect of light hydrocarbons on the permeation of hydrogen through a microporous silicalite-1 membrane. The model, known as the Potential Barrier Model is an attractive method as it only requires independent data on the permeance of pure non-adsorbing components and the adsorption equilibrium isotherms of the strongly adsorbing components. The model was tested on binary experimental systems of H_2/CH_4, H_2/C_2H_6, H_2/C_3H_8 and $H_2/n\text{-}C_4H_{10}$. The substantial reduction in the permeance of hydrogen was described successfully over a temperature range of 20^oC-60^oC and feed pressures up to 850kPa. The model was also capable of predicting the substantial reduction in hydrogen permeance in a multi-component system, $H_2/CH_4/C_2H_6/C_3H_8$. A detailed description of the model is given in section 6.3.

Analysis of the results in Chapter 5 has displayed the generally accepted notion that the permeances of weakly adsorbed components are reduced in the presence of a strongly adsorbed component. The Potential Barrier model therefore presents itself as an appropriate choice to explain quantitatively the hindering effect of strongly adsorbed ammonia on the permeance of weakly adsorbing hydrogen and nitrogen. This simplified model may provide a better understanding of the $NH_3/H_2/N_2$ separation system in MFI zeolite membranes and the extent to which adsorption affects membrane performance at different operating conditions. The information could then be used to optimise membrane performance for an effective separation.

6.1.1 Ammonia Adsorption on Zeolites

As described in the previous section, the application of the Potential Barrier Model requires independent data on the pure non-adsorbing components and the adsorption equilibrium isotherms of the strongly adsorbed components. The single permeation data for the non-adsorbing components hydrogen and nitrogen was obtained in Chapter 5. What is required therefore is the adsorption equilibrium isotherm of strongly adsorbed ammonia so that the surface coverage θ expressed as a fraction of the saturated adsorbed amount can be obtained. In this section, ammonia adsorption on MFI zeolites is discussed and corresponding isotherms from the literature and experimental work are presented.

Adsorption of ammonia on zeolites has traditionally been performed to determine the surface acidic properties for use as catalysts in the petroleum industry (Valyon et al, 1998). As a result, ammonia sorption studies have focused on chemisorption and finding suitable ammonia isotherms in the literature proved difficult. Nevertheless, some of the isotherms presented in the literature (Valyon et al, 1996, Dragoi et al, 2004) could prove useful in understanding ammonia adsorption on zeolites and extending this to studies for ammonia separation with zeolite membranes.

Valyon's group (1996, 1998) used the frequency response (FR) technique to gain a better understanding of the ammonia FR spectra by studying acidic ZSM-5 systems and to learn about the dynamics of the sorption of ammonia and thereby about the acidity of ZSM-5. Isotherms of adsorption for ammonia on H-ZSM-5 zeolite are presented. Dragoi et al, (2004) also studied the number, strength and strength distribution of the acidic sites of two amorphous silica-aluminas (Si-Al ~6.5) and three microporous zeolites H-β, H-ZSM-5 and H-MCM-22 with similar Si/Al ratios (Si-Al~13). Results were determined using microcalorimetry linked to a volumetric line using ammonia as a probe molecule. The differential heats of ammonia adsorption versus coverage and the corresponding isotherms were presented. Others who have studied ammonia adsorption on zeolites for the purpose of acid-base determination are Parillo et al, (1993, 1994), Jozefowicz et al, (1994) and Joly and Perrard, 2001.

Few studies of ammonia isotherms have been carried out in reference to ammonia gas separation as opposed to studies based on acidic properties. Only four reference sources are given for ammonia gas adsorption in Valuenzela and Myers data handbook (Valenzuela and Myers, 1989) in which the pressure and temperature approach the levels of industrial ammonia gas streams. These sources include ammonia equilibria on activated carbon (Boki et al, 1987), silica gel (Kuo et al, 1985), La Mordernite, Ru Mordernite (Coughlan and McCann, 1979) and Y zeolite in Na, La, LaH, LaCa, H and Ca forms (Shiralkar and Kulkarni, 1985). Unfortunately only a few of the above sources are relevant for design purposes because most of them do not give pure equilibrium data and/or accurate correlations.

The lack of reliable data on ammonia adsorption led to the studies by Helminen's group (Helminen et al, 2000 and 2001), who measured the adsorption equilibrium isotherms of ammonia gas over a wide range of temperatures (298K-393K) and pressures (0-100kPa) in order to determine the best sorbent for pressure swing adsorption (PSA) systems. In both studies, ammonia adsorbed most strongly on the zeolites 4A, 5A, 13X. In the first study (Helminen et al, 2000), adsorption isotherms were measured on zeolite, alumina, silica gel and activated carbons over wide temperature (298K – 393K) and pressure ranges (0-100kPa). Under these

conditions, ammonia adsorbed most strongly on 13X and 4A zeolites. The data was also fitted to five isotherm models in order to evaluate the accuracy of the correlations for design purposes.

Adsorption isotherms for ammonia separation on MFI zeolites at the required operating conditions were not available. The lack of data at higher pressures and lower temperatures (representing physisorption) led to measurements being undertaken by MAST Carbon as part of this project. The adsorption studies were however cut short by significant problems with the high pressure balance facilities. Although advised that the high pressure Sartorious balance was suitable for ammonia use, it was in fact severely damaged by the ammonia which corroded most of the bolts assembling the unit which (it transpired), were made from nickel plated brass, and not stainless steel. However, before this occurred, a partial isotherm was completed and is presented in this thesis.

6.1.2 Adsorption Theory

Adsorption occurs whenever a solid surface is exposed to a gas or liquid: it is defined as the enrichment of a material or increase in the density of the fluid in the vicinity of the interface (Roquerol and Sing, 1999). Two kinds of forces can be involved, which give rise to either physical adsorption (physisorption) or chemisorption.

Physical adsorption (physisorption) involves only relatively weak intermolecular forces (van der Waals), whilst chemisorption involves the formation of a chemical bond between the sorbate molecule and the surface of the adsorbent (Gasser, 1985). The general distinguishing features of the two types of adsorption are given in Table 6.1.

Several theories have been advanced to account for the shapes of adsorption isotherms. Assumptions are commonly made about the nature of the surface, whether it is homogenous or heterogenous, and what the gas surface interactions

are. The strength of the latter may be dependent or independent of the fractional coverage (Rouquerol and Sing, 1999).

Table 6.1: Differences between physisorption and chemisorption (Rouquerol and Sing, 1999 and Ruthven 1984)

Physisorption	**Chemisorption**
General phenomena with a relatively low degree of specificity	Dependent on the reactivity of the adsorbent and adsorptive
At high relative pressures, physisorption generally occurs as a multilayer	Chemisorbed molecules are linked to reactive parts of the surface and the adsorption is necessarily confined to a monolayer
Temperature range over which adsorption occurs is near or below the condensation point of the gas	Temperature range virtually unlimited, but a given molecule may effectively adsorb only over a small range
Low heat of adsorption, related to factors like molecular mass and polarity, typically 5-50kJ/mol	High heat of adsorption (related to chemical bond strength) typically 80-800kJ/mol
No dissociation of adsorbed species Reversible	May involve dissociation Non-reversible
Kinetics of adsorption fast, non activated	Kinetics very variable, often an activated process

The majority of isotherms observed to date are classified by the Brunauer, Deming, Deming and Teller (BDDT) classification and are shown in Fig 6.1. (Yang, 1987)

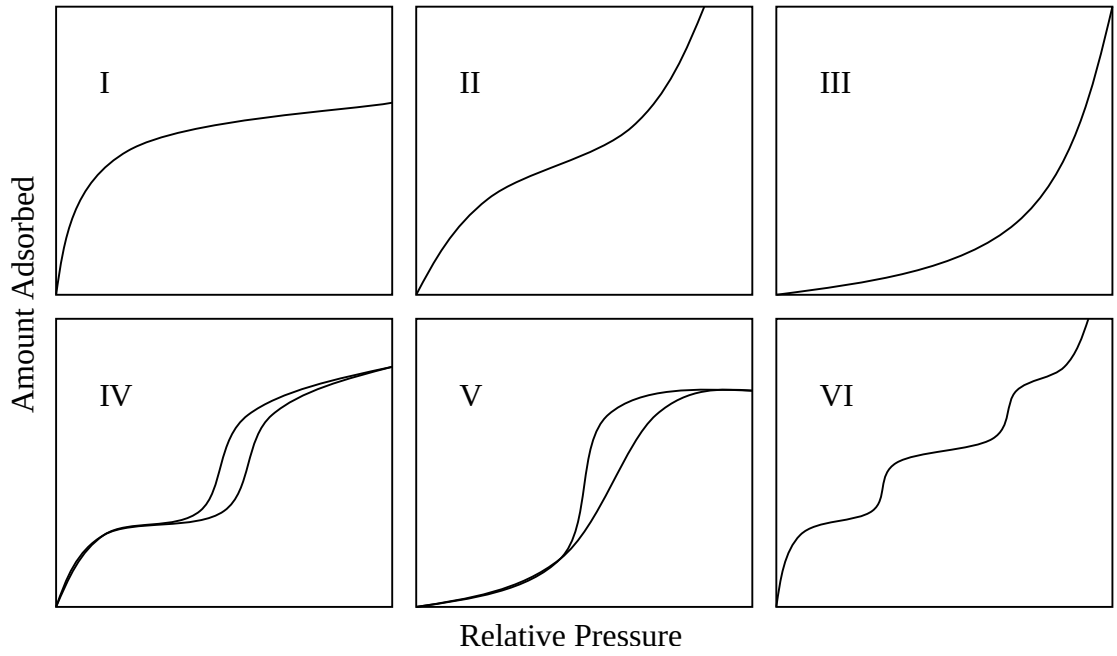

Figure 6.1: The types of adsorption isotherm according to BDDT classification

Type I isotherms are observed for the adsorption of gases on microporous solids whose pore sizes are not much larger than the molecular diameter of the adsorbate. With such adsorbents, there is a definite saturation limit corresponding to complete filling of the micropores (Ruthven, 1984). Type II and III isotherms do not have a saturation limit and are characterised by a wide range of pore sizes such that adsorption may extend from monolayer to multilayer and ultimately to capillary condensation (Tien, 1994). These isotherms are generally observed only in adsorbents in which there is a wide range of pore sizes (Ruthven, 1984). Type IV suggests that adsorption causes the formation of two surface layers, either on a plane surface or on the wall of a pore very much wider than the molecular diameter of the sorbate. Type V adsorbents are said to have irregular pore size distributions and are observed if intermolecular attraction effects are large. This type is found in the adsorption of water vapour on activated carbon. Type VI isotherms are very rare, they give an idea of the adsorption capacity. Multilayer adsorption occurs, but the filled layer has an influence on other filled layers. An example is the adsorption of noble gases such as Krypton onto “papyex” or “graphoil”.

6.1.3 Adsorption Isotherm models

Langmuir (1918) was the first to propose a coherent theory of adsorption onto a flat surface, based on a kinetic viewpoint (Do, 1998). Several empirical models have also been developed. These empirical equations have been applied to a wide range of equilibrium adsorption data with success and hence will be applied in this work. The equations are important in the fitting of experimental equilibrium data in order to obtain model parameters that can be used to reliably predict ammonia equilibria at different operating conditions for design purposes. These include the Freundlich, Langmuir-Freundlich and Toth equations and are described in detail in this section.

6.1.3.1 Langmuir

This is one of the simplest and most widely used expressions for physical adsorption (and chemisorption). The Langmuir model assumes that (Do, 1998):

- The surface is homogeneous and the adsorption energy is equal over all the sites
- The surface has a specific number of sites, each of which can adsorb one molecule, and when all these are occupied no further adsorption is possible
- All sites are equivalent and the energy of an adsorbed molecule is independent of the presence of other molecules

The Langmuir theory is based on a kinetic principle, that is, the rate of adsorption is equal to the rate of desorption.

$$q^* = \frac{q_s bp}{1 + bp} \qquad \textbf{6.27}$$

Where q* is the sorbate concentration at equilibrium, q_s the saturation limit of the sorbate concentration, b the affinity constant and p is the pressure.

At low sorbate concentrations, or when the partial pressure is very low ($bp<<1$), the Langmuir model reduces to Henry's law. This is when the amount adsorbed increases linearly with partial pressure, a constraint demanded by statistical thermodynamics (Do, 1998). When the partial pressure is sufficiently high, the amount adsorbed reaches saturation capacity, corresponding to a complete coverage of all adsorption sites with adsorbate molecules (this is called the monolayer coverage, and $\theta \rightarrow 1$). The oversimplified nature of this model, as a result of the governing assumptions, limits its application for certain adsorption systems.

6.1.3.2 Freundlich

The Freundlich equation is one of the earliest empirical equations used to describe equilibrium adsorption data and is very popular and applicable to gas phase systems that have heterogeneous surfaces. It assumes that the adsorption energy is distributed with sites having the same energy grouped into one patch and there is no interaction between patches (Do, 1998). It also assumes that on each patch, the adsorbate molecule only adsorbs onto one adsorption site making the Freundlich equation applicable to each patch.

$$q^* = Kp^n \qquad \textbf{6.28}$$

Where K is the Freundlich constant and n the empirical component (n denotes the number of sites occupied by the adsorbate)

This model is applicable when the pressure range is not too wide as the isotherm equation does not have a proper Henry's Law behaviour at low pressures and also does not have a finite limit at high pressures. It is therefore only valid in the narrow range of adsorption data.

For nonlinear equilibrium data, the simplest models are the Langmuir and the Freundlich equations because they include only two parameters.

6.1.3.3 Langmuir-Freundlich

The Langmuir-Freundlich (LF) model was proposed by Sips (1948) to overcome the problem of the continuing increase in the adsorbed amount with an increase in pressure in the Freundlich equation.

$$q^* = \frac{q_s b p^n}{1 + b p^n} \qquad \textbf{6.29}$$

The equation is similar to the Langmuir equation but with an additional parameter n. If the parameter n is unity, the equation reduces to the Langmuir equation applicable to ideal surfaces. Parameter n is therefore regarded as the parameter that characterises heterogeneity. The parameter n is usually greater than 1 and therefore the larger this parameter is, the more heterogeneous the system. The other LF parameters q_s and b represent the maximum capacity of the adsorbent and the adsorption affinity respectively. Although the LF equation has a finite saturation limit when the pressure is sufficiently high, it still does not follow the correct Henry's law limit at low pressure (Do, 1998).

6.1.3.4 Tóth

Unlike the previous equations where the Freundlich equation is not valid at the low and high ends of the pressure range and the LF equation that is not valid at the low end, the Toth equation satisfies both the two end limits in the pressure range. This equation assumes that there is an energy distribution on the surface of the adsorbent, such that its surface is energetically heterogeneous and it has the following form:

$$q^* = \frac{q_s b p}{\left[1 + (bp)^t\right]^{1/t}} \qquad \textbf{6.30}$$

Here t is a parameter that is usually less than 1. The parameters b and t are specific for adsorbate-adsorbent pairs. When t = 1, the Tóth isotherm reduces to the Langmuir equation. Hence like the LF equation, the parameter t is said to

characterize the system heterogeneity. The further t deviates from 1 the more heterogeneous the system is.

The Tóth equation is a three parameter model and can describe well many adsorption data (Do, 1998). It is normally recommended as the first choice of isotherm equation for fitting the data of many adsorbates such as hydrocarbons, carbon oxides, hydrogen sulphide, alcohols on activated carbon as well as zeolites because of its simplicity in form and its correct behaviour at low and high pressures. When behaviour in the Henry region is needed, the Tóth equation is a better choice than the LF equation.

6.2 Ammonia Adsorption Isotherms

In this section, the adsorption isotherms of ammonia on ZSM-5 both in the literature (Valyon et al, 1998, Dragoi et al, 2004) and the measured data by Mast Carbon are presented. The ideal situation would be to measure the adsorption isotherms under the experimental conditions used to obtain the membrane permeances. It was not possible to use the equipment available in the laboratory for these measurements as ammonia, due to its corrosive nature, could have affected the sensitive Intelligent Gravimetric Analyser (IGA) balance and electronic equipment. It was therefore necessary to rely on data from the literature and the partial isotherm obtained by Mast Carbon.

Isotherms of ammonia adsorption on ZSM-5 reported by Valyon et al, (1998) were determined using an all glass BET apparatus equipped with a Barocel Model 571A pressure transducer and Model 1174 electronic manometer. Adsorption isotherms of ammonia were determined up to 3.5 Torr (0.4 kPa) pressure and at temperatures in the range 373K-723K (Figure 6.2).

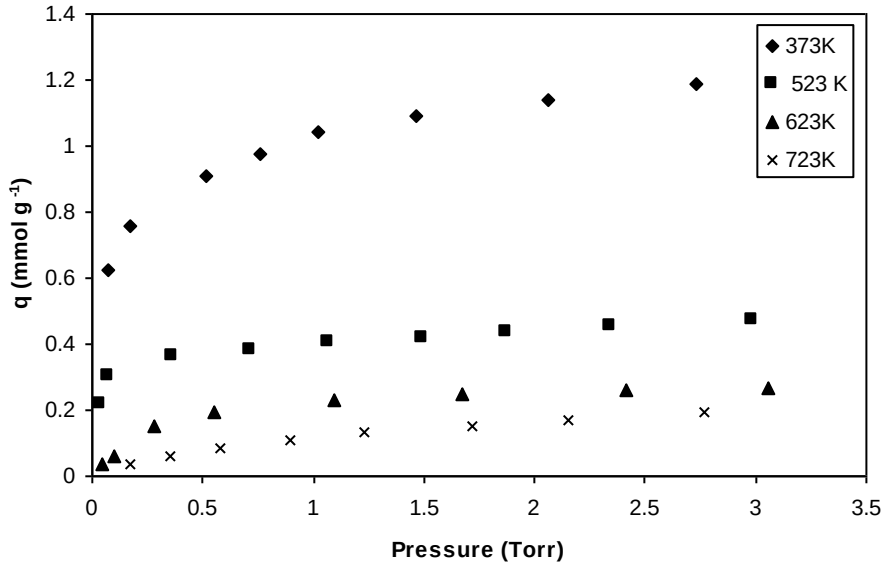

Figure 6.2: Ammonia adsorption isotherms at different temperatures on H-ZSM-5 (adapted from Valyon et al, 1998)

Dragoi et al, (2004) carried out calorimetric experiments using a Microcalorimeter of the Tian-Calvet type (C80 from Setaram) linked to a volumetric line that makes it possible to study the gas-solid interactions (Figure 6.3).

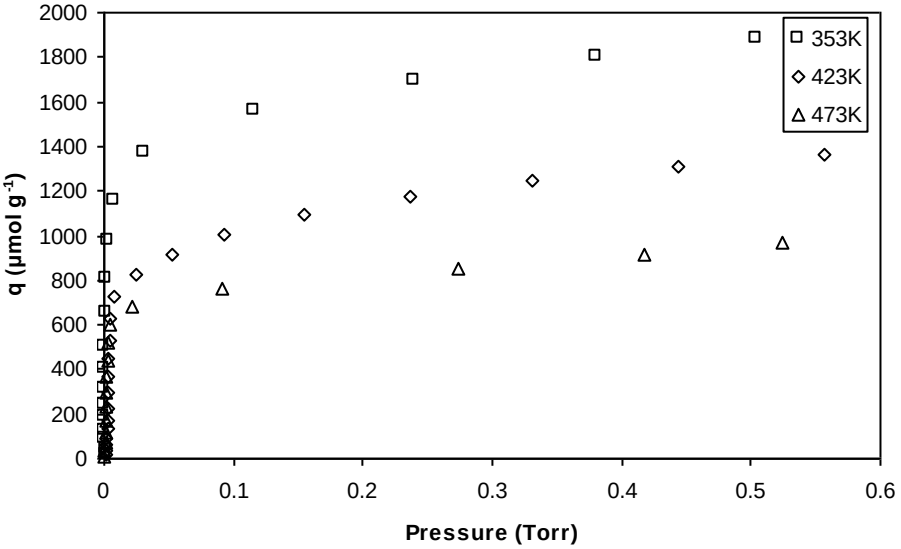

Figure 6.3: Ammonia adsorption isotherms at different temperatures on H-ZSM-5 (Dragoi et al, 2004)

Mast Carbon data was measured using a Sartorius balance at 298K and pressure range of 0-315kPa (Figure 6.4).

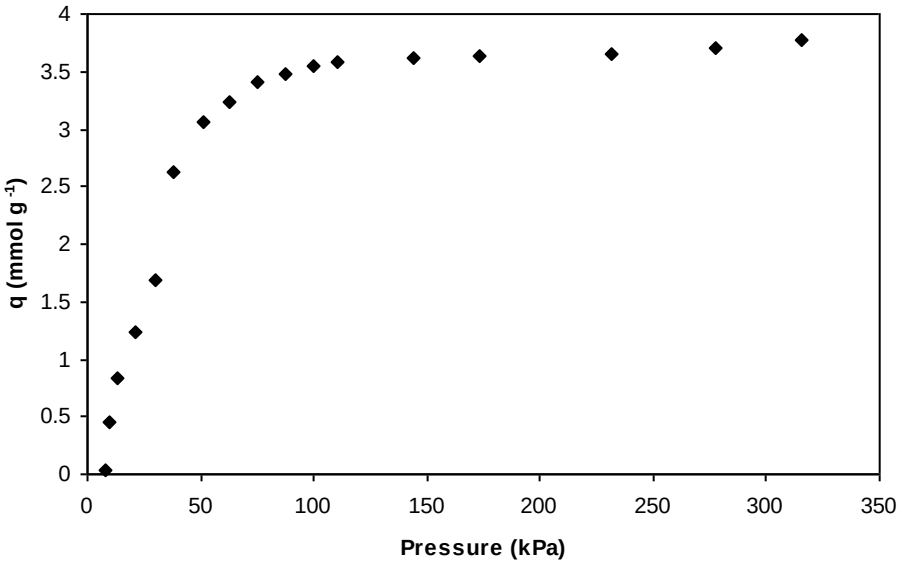

Figure 6.4: Ammonia adsorption Isotherm on H-ZSM-5 at 298K (Mast Carbon Data 2000)

According to the BDDT classification, the isotherms of this material seem to exhibit Type 1 isotherm behaviour at each of the temperatures used. The shapes of all isotherms are similar with all reaching a plateau as the pressure is increased. Figures 6.2 and 6.3, however, represent studies based on chemisorption and these isotherms generally exhibit a plateau at lower pressures than the micropore filling plateau. This limiting adsorption is due to a completion of a chemically bound monolayer (Rouquerol and Sing, 1999).

The difference in the three isotherms presented in Figures 6.2 (Valyon et al, 1998), 6.3 (Dragoi et al, 2004) and 6.4 (Mast Carbon) is evident. The pressure and temperature ranges used in each study differ considerably. The pressure ranges in the Valyon et al (1998) data (Figure 6.2) and Dragoi et al (2004) data (Figure 6.3) are far removed from the partial pressures of ammonia in the membrane separation process that range from 27-135kPa. Also, the temperature ranges (373K-723K and 353K-473K respectively) differ from those required for this thesis (298K-423K).

Although the Mast Carbon data is within the required pressure range, only one isotherm (298K) is available. In order to obtain the data in the required range, adsorption isotherms of ammonia that have been determined experimentally can be fitted with semi-empirical models to obtain the correlations and parameters

which could be used for both interpolation and extrapolation. The success of the interpolation or extrapolation however depends on the accuracy of the parameters obtained from the models. In addition, no study so far in the literature has made a comparison of isotherm models for the ammonia/ZSM-5 adsorption system. The modelling of adsorption equilibrium data and a comparison of isotherm models that could reliably predict ammonia equilibria at different conditions (of temperature and pressure) would be useful for design of ammonia separation processes.

6.2.1 Parameter Estimation Procedure

The data were fitted to the semi-empirical models described in section 6.1.3 in order to determine which model is best suited to describe ammonia adsorption on H-ZSM zeolites. It is important to note here that the study of adsorption in this chapter is not to determine the fundamental complexities of ammonia adsorption on zeolites, but rather to obtain parameters that will provide sufficiently accurate correlations for predictive purposes. This will enable the determination of the coverage of ammonia for modelling purposes as described in Section 6.3.

The most suitable model will be chosen based on the following;

- The governing assumptions of the model
- The quality (accuracy) of fit determined by visual examination, as well as residual and error analysis.

Extrapolation, for example, can be carried out only if the model is both thermodynamically consistent and its parameters are statistically accurate and reliable. Therefore the estimated parameters of all isotherm models were evaluated by established statistical methods.

The determination of accuracy of fit and error analysis has been performed using the methods to be described in section 6.2.2. The fitting of the empirical equations has been done by using a commercial graphing and data fitting software, ORIGIN. A nonlinear least square fitting (NSLF) tool incorporated into ORIGIN is used. The selected adsorption model is inserted in the tool and model parameters to be calculated are defined. The nonlinear regression method is based on the Levenberg-Marquadt (LM) algorithm, which is the most widely used algorithm in nonlinear least square fitting. It optimises the parameters of adsorption for a given set of experimental data points so that the sum of the squares of the deviation becomes minimal. The LM algorithm is an iterative procedure. First, best starting values are entered and then iterations (typically 100) are performed to give optimal values of the required parameters with minimal error.

6.2.2 Fitting of Equilibrium Ammonia Adsorption Isotherms

The Langmuir isotherm has been proposed as the simplest and still a very useful isotherm for both physical and chemical adsorption (Yang, 1987). Rouquerol and Sing (1999) recommend that chemisorption isotherms should be referred to as Langmuir isotherms, even if the mechanism involved may not be strictly in accordance with the Langmuir model. As a result, the Langmuir model is given priority in fitting the data as it should be able to fit both the chemisorption data (Valyon et al, 1996, Dragoi et al, 2004) and the physisorption data (Mast Carbon data). The fitted chemisorption isotherms are presented in Figures 6.5, 6.6 and 6.7. The Langmuir parameters q_s and b are given in Table 6.3 for Valyon data and Table 6.4 for Dragoi data.

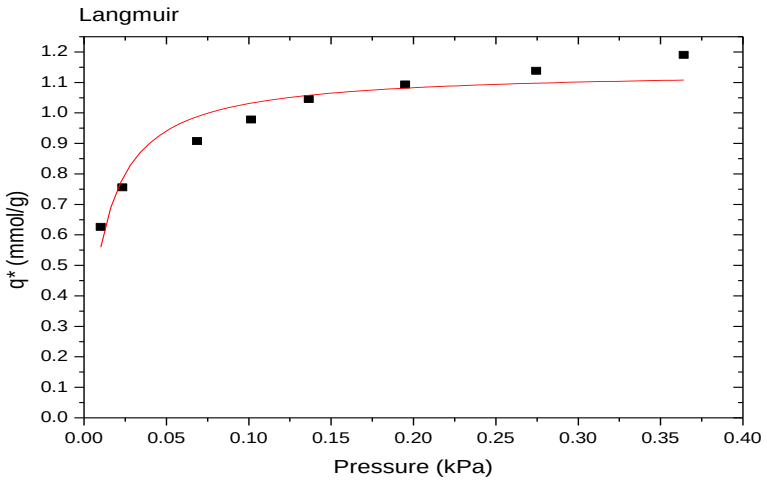

Figure 6.5: Fit of Langmuir model on Valyon et al (1996) data 373K

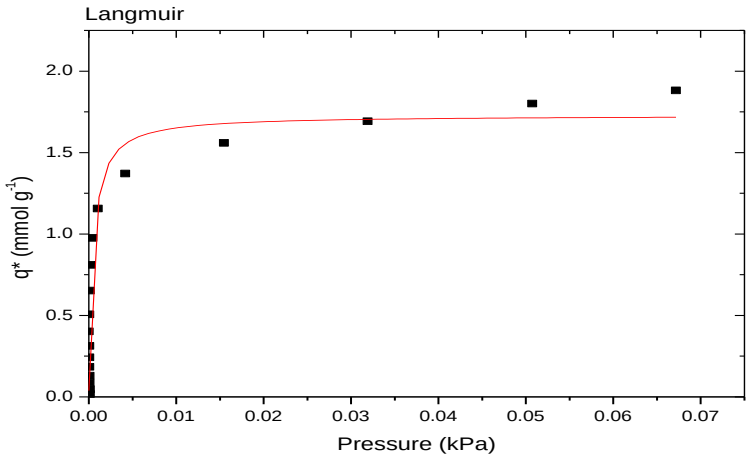

Figure 6.6: Fit of Langmuir model on Dragoi et al (2004) data at 353K

Visual assessment of the plots shows that the Langmuir isotherm models fit are poor. The sorption capacity is underestimated in the high pressure region. The Langmuir model assumes that each site can only hold one molecule and that when all the sites are covered, further adsorption cannot occur. This implies that the uptake is limited to a monolayer. The assumption that all sites are energetically equivalent and independent of each other requires that the heat of adsorption is independent of coverage (Rouquerol and Sing, 1999). The poor fit of the isotherm in this case implies that these two assumptions do not hold for the ammonia-H-ZSM-5 adsorption system. Dragoi et al, (2004) provide the differential heats of ammonia adsorption versus coverage at 353K, 423K and 473K. There is a sharp decrease of the differential heat of adsorption at low coverages, followed by a plateau near 150 $kJ.mol^{-1}$, up to a certain level of coverage (500 $\mu mol.g^{-1}$), after which it decreases to about 50 kJ/mol at each of the temperatures.

In another study, (Parillo and Gorte, 1993), the adsorption enthalpies as a function of coverage were measured at 480K on different zeolites. It was found that the heat of adsorption for ammonia on H-ZSM-5 is constant up to a level of coverage of about 100$\mu mol.g^{-1}$, above which the differential heats drop sharply. This is also observed by Jozefowicz et al, (1994) who studied the differential heats of ammonia adsorption on different forms of H-ZSM-5. An almost horizontal plateau was observed between 150$kJ.mol^{-1}$ and 145$kJ.mol^{-1}$, after which the curve drops sharply. The measured heats of adsorption are indicative of the surface

homogeneity or heterogeneity in terms of energy distribution. It is suggested that at the 150 kJ.mol^{-1} plateau, most of the sites are of a homogeneous acidic strength, but where the curve drops (150-80 kJ.mol^{-1}), there are sites which have a wide energy distribution suggesting heterogeneity at higher ammonia coverages.

The Langmuir equation shows that a saturation level is obtained in the isotherm which is characteristic of the chemisorption process and this layer is assumed to correspond to monolayer coverage. As such, one might expect that the Langmuir model would successfully fit the data. However, the discrepancies with some of the assumptions of the model as discussed above, may explain why the Langmuir isotherm does not fit the data well.

It is possible that the isotherms of ammonia can be comprised of both physisorption and chemisorption parts. Some authors have attempted to separate the contribution of chemisorption and physisorption parts, assuming the amount of chemically captured adsorbate to be a constant, whereas the physisorption part is treated by a semi-empirical method (Romm, 1996). Dragoi et al (2004) also suggested that their isotherms (Figure 6.3) consisted of two distinct parts. The vertical part was assigned to irreversible adsorption, namely chemisorption, while the horizontal part corresponded to reversible adsorption (physisorption).

The curve (Figure 6.6) shows that at low pressures (up to 0.01 Torr), chemisorption is the predominant process, and that physisorption begins above this value. Dragoi et al (2004) postulate that this behaviour is normal because chemisorption only concerns a limited number of sites, whereas reversible adsorption can occur on all types of centres. In addition to this, referring to the differences between physisorption and chemisorption as described in Table 6.1, the differential heats for ammonia adsorption on H-ZSM-5 are different at different coverages of ammonia. At coverages up to 500 μmol/g, the differential heat is given as 150kJ/mol, which suggests chemisorption but after this coverage, the heat of adsorption decreases to about 50 kJ/mol which suggests physisorption at higher coverages.

Jozefowicz et al (1994) also observed a similar trend for ammonia adsorption on H-ZSM-5. The plots of differential heats of adsorption against amount of adsorbed

ammonia show that at low coverages (100 μmol/g) a few sites evolve high heats of adsorption. A horizontal plateau is observed between 100 and 400 μmol/g and the heat of adsorption is given as 150-145kJ/mol, after which the curve drops sharply to ≈50kJ/mol. In this work, it is suggested that in the 80kJ/mol region, heats that are evolved from H-ZSM-5 zeolites tend to be representative of physisorption (Jozefowicz et al, 1994). Therefore the use of other semi-empirical models not necessarily linked to chemisorption could provide better fits of the data.

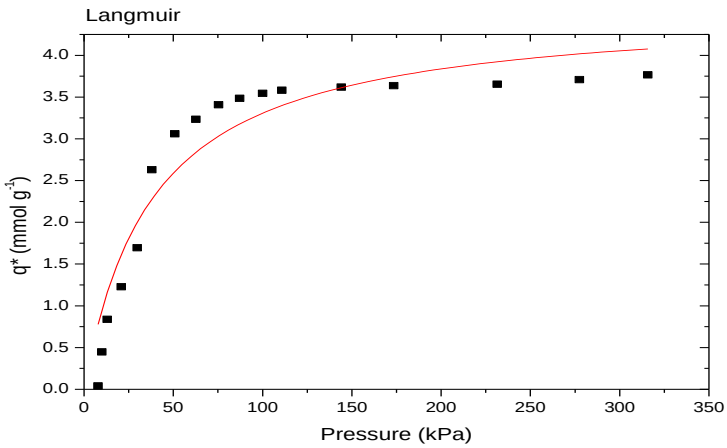

Figure 6.7: Fit of the Langmuir model to Mast Carbon data (298K)

Fig 6.7 shows the fit of the Langmuir model to the physisorption data provided by Mast Carbon. Langmuir parameters for Mast Carbon data are given in Table 6.2.

Rouquerol and Sing, (1999) recommend that the term Langmuir isotherm should not be used in the context of physisorption by microporous solids. This statement can be regarded to be true in this case since the Langmuir model is also a poor fit of the Mast Carbon data. Poor fits of the Langmuir isotherm have also been observed for ammonia adsorption (physisorption) on other zeolites namely 4A, 5A and 13X. According to Helminen et al, (2001), the Langmuir model does not usually give an accurate prediction for the ammonia equilibrium data for inorganic sorbents. The actual isotherm equation contains only two parameters, which evidently is not sufficient. Moreover, the Langmuir model does not take into account non-idealities such as intermolecular attractions and surface heterogeneity, whose contribution is substantial in the adsorption of ammonia on inorganic sorbents.

Following the failure of the Langmuir model to provide a good fit, the other three popular semi-empirical models presented in section 6.1.4 have been used to fit the data (Figures 6.8-6.10).

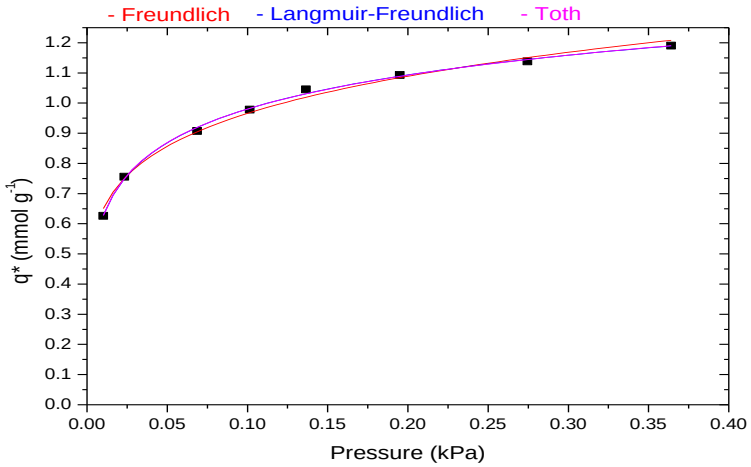

Figure 6.8: Freundlich, Langmuir-Freundlich and Toth fits of Valyon et al data at 373K

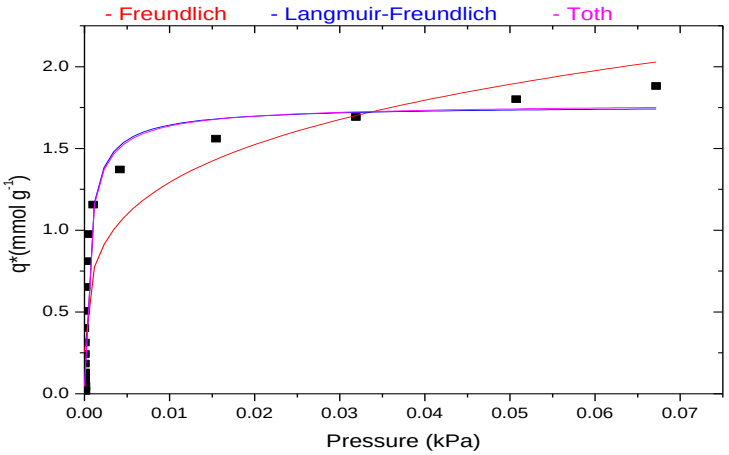

Figure 6.9: Freundlich, Langmuir-Freundlich and Toth fits of Dragoi et al data at 353K

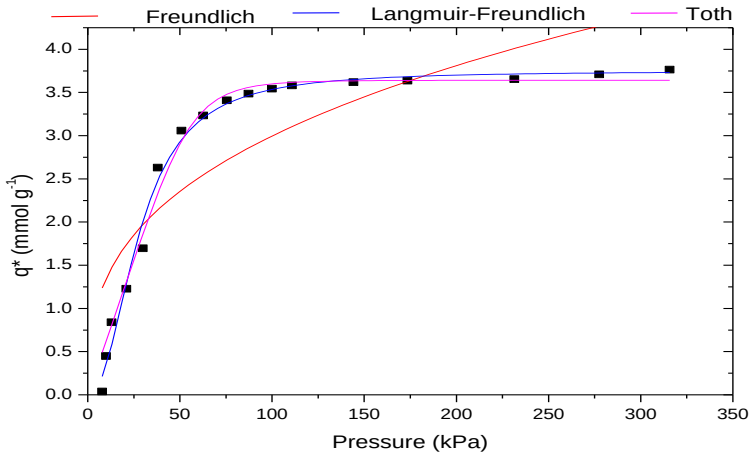

Figure 6.10: Freundlich, Langmuir-Freundlich and Toth fits of Mast Carbon data at 298K

The Freundlich model gives a poor fit for all three sets of data and tends to underestimate the adsorption capacity at lower pressures and overestimates at higher pressures. As mentioned previously, the Freundlich model is only valid within a limited pressure range as it does not show the appropriate Henry's law behaviour at low pressures and, in addition, it does not show a finite saturation limit at higher pressures which explains the inadequacy of this model in fitting the experimental data.

The quality of fit obtained using the Langmuir-Freundlich (LF) and Tóth equations is an improvement on the other two models. In this case, both models are very close in their fits. In Figure 6.8, the fits of Tóth and LF overlap each other and neither can be distinguished from each other. This may be as a result of having three parameters instead of two. The LF gives the best fit visually, and, although the model is heterogeneous, it does not reduce to Henry's law at low pressures. In contrast, the Tóth model reduces to Henry's law at low pressures and has a finite limit at higher pressures. However, reliance on visual fits of the model should be done with caution as a model may give a good fit but give parameters that are not thermodynamically correct. Further analysis is therefore required.

6.2.3 Accuracy of Fit and Error Analysis

In order to ascertain the suitability of fitting of the experimental data, an accuracy of fit and error analysis must be performed. This allows for the determination of model parameters with some degree of certainty especially if the models are to be used for extrapolation purposes. At first glance, a visual examination of the fit to the experimental data would provide preliminary information on the quality of fit. However, special attention should be paid to correct statistics. Statistical evaluation of the isotherm model accuracy, for example by the average relative error or the coefficient of determination (R^2) provided by ORIGIN is not sufficient. The error of the entire model can be small, although the errors in single parameters can be large. Therefore, the model parameters must also make "thermodynamic sense" in addition to being statistically accurate and reliable. The accuracy of fit was evaluated on the basis of various standard statistical values, including the coefficient of determination (R^2), the residual r, the residual sum of squares (RSS) and the root mean square error (RMSE).

6.2.3.1 Residual

The residual r from a fitted model is defined as the difference between the experimental observation and the predicted observation obtained from the model. This is given by:

$$r = q^* - q_i^* \qquad \textbf{6.31}$$

Here q* is the experimental observation (mmol/g) and q^*_i is the model prediction. If the model used is a good representation of experimental data, the residual will be an approximation of the random errors associated with the fit. However, the appearance of a systematic pattern in the observed residual indicates a bias of fit. Figure 6.11 shows the residual plots for the different adsorption models fitted to the Mast data. The residual appears randomly distributed around zero for the LF and Tóth fits. The residuals of the Langmuir and Freundlich model are

systematically positive for much of the data range implying that these models are a poor fit for the data.

6.2.3.2 RSS

The parameters were estimated with non-linear regression by minimising the weighted sum of residual squares, that is, the differences between the experimental and estimated equilibrium sorbate concentration.

$$RSS = \sum (q^* - q_i^*)^2 \qquad \textbf{6.32}$$

6.2.3.3 The Root Mean Square Error (RMSE)

The RMSE is also known as the fit standard error or the standard error of regression. It is calculated using equation 6.7 :

$$RMSE = \sqrt{\frac{\sum \left(q^* - q_i^*\right)^2}{N_d - N_p}} \qquad \textbf{6.33}$$

The denominator in the above equation refers to the degrees of freedom, where N_d is the number of data points to be fitted and N_p is the number of parameters in the model equation used.

Statistical data are presented in Tables 6.2, 6.3, and 6.4 for the Mast Carbon, Valyon et al (1996) and Dragoi et al, (2004) data respectively.

Table 6.2: Tables showing the model parameters of Mast Carbon data

Isotherm Model	Isotherm Parameters			R^2 %	RSS	RMSE
	Symbol	Value	Error			
Langmuir	q_s (mmol.g^{-1})	4.57113	±0.29254	91.63	2.227	0.385
	b (kPa^{-1})	0.02615	±0.0056			
Freundlich	K	0.605043		75.371	6.552	0.661
	N	0.34734	±0.06589			
Langmuir-Freundlich	q_s (mmol.g^{-1})	3.74831	±0.0631	99.05	0.253	0.134
	b (kPa^{-1})	0.00062	±0.00036			
	N	2.21343	±0.17622			
Toth	q_s (mmol.g^{-1})	3.6418	±0.07042	98.45	0.412	0.172
	b (kPa^{-1})	0.01716	±0.00098			
	T	5.14514	±1.87925			

For the Langmuir model, the R^2 values, and the RSS and RMSE values are poor. This further ascertains that the Langmuir model does not give an accurate prediction of the ammonia equilibrium data for inorganic sorbents. The Freundlich model gives the worst fit, with a very low R^2 value and a very high RSS value which indicates that it gives a very poor correlation with the data. The residual plot shows a definite negative at lower pressures followed by a definite positive bias for the Langmuir and Freundlich models. It can therefore be concluded that the parameters obtained from using these two models can be considered inaccurate.

As expected, the three parameter LF and Tóth models give the best fits. It is evident that both these models provide good fits to the data without a bias in the fit such that the residuals are evenly distributed evenly around zero. However, the LF model has a higher R^2 value. The R^2 value of 99% is regarded as a limit of superior

correlation. In addition, the LF model has somewhat lower RSS and RMSE values, which means the LF model provides a better fit.

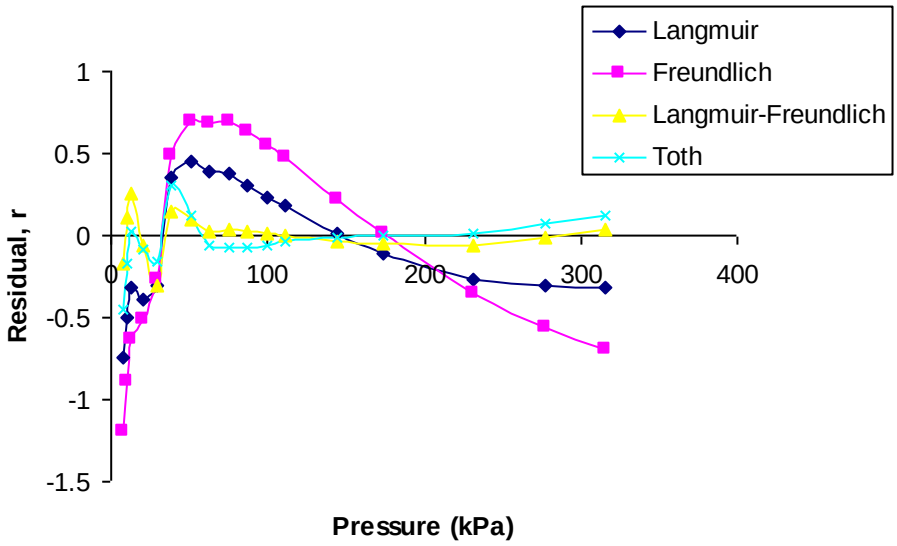

Figure 6.11: Residual plot of Mast Carbon data

Table 6.3: Tables showing the model parameters for Valyon et al (1998) data at different temperatures

Langmuir Model	**Isotherm Parameters**			**R^2 %**	**RSS**	**RMSE**
Valyon Data	**Symbol**	**Value**	**Error**			
373K	q_s (mmol.g^{-1})	1.14398	±0.03515	91.22	0.023296	0.062311
	b (kPa^{-1})	93.15529	±18.67329			
523K	q_s (mmol.g^{-1})	0.42624	±0.01052	93.01	0.00565	0.02841
	b (kPa^{-1})	234.6869	±42.49148			
623K	q_s (mmol.g^{-1})	0.29377	±0.00643	99.44	0.000318	0.007282
	b (kPa^{-1})	24.92952	±2.21848			
723K	q_s (mmol.g^{-1})	0.28667	±0.01408	99.40	0.000128	0.00462
	b (kPa^{-1})	5.25667	±0.54184			

Freundlich Model	**Isotherm Parameters**			**R^2 %**	**RSS**	**RMSE**
Valyon Data	**Symbol**	**Value**	**Error**			
373K	K	1.439489	±7.3E11	99.27	0.001945	0.018006
	N	0.1733	±0.00733			
523K	K	0.534896	±2.0E12	96.11	0.001692	0.015549
	N	0.14164	±0.0144			
623K	K	0.392735	±6.8E12	91.72	0.004725	0.028063
	N	0.33462	±0.06013			
723K	K	0.343677	*	99.58	0.000089	0.003848
	N	0.55597	±0.0202			

Langmuir-Freundlich Model	Isotherm Parameters			R^2 %	RSS	RMSE
Valyon Data	**Symbol**	**Value**	**Error**			
373K	q_s (mmol.g^{-1})	2.03155	±0.28798	99.82	0.000486	0.009863
	b (kPa^{-1})	1.95468	±0.72629			
	n	0.32129	±0.03915			
523K	q_s (mmol.g^{-1})	0.56996	±0.1401	97.24	0.00167	0.016685
	b (kPa^{-1})	5.35371	±6.45645			
	n	0.37257	±0.1548			
623K	q_s (mmol.g^{-1})	0.28083	±0.00889	99.61	0.000224	0.006693
	b (kPa^{-1})	43.99427	±17.71826			
	n	1.1383	±0.09864			
723K	q_s (mmol.g^{-1})	0.48703	±0.10203	99.58	0.0000252	0.002248
	b (kPa^{-1})	1.38395	±0.54224			
	n	0.74436	±0.05516			

Toth Model	Isotherm Parameters			R^2 %	RSS	RMSE
Valyon Data	**Symbol**	**Value**	**Error**			
373K	q_s (mmol.g^{-1})	2.73669	±0.77172	99.81	0.000492	0.009923
	b (kPa^{-1})	102003.6	±240998.1			
	t	0.17566	±0.04639			
523K	q_s (mmol.g^{-1})	0.60496	±0.19564	97.38	0.00134	0.014946
	b (kPa^{-1})	16104.14	±63186.7			
	t	0.28029	±0.17344			
623K	q_s (mmol.g^{-1})	0.27781	±0.01077	99.58	0.000238	0.006897
	b (kPa^{-1})	21.79082	±2.64658			
	t	1.24079	±0.20117			
723K	q_s (mmol.g^{-1})	0.933522	±0.52213	99.89	0.000017	0.001834
	b (kPa^{-1})	3.97755	±0.72212			
	t	0.39404	±0.10882			

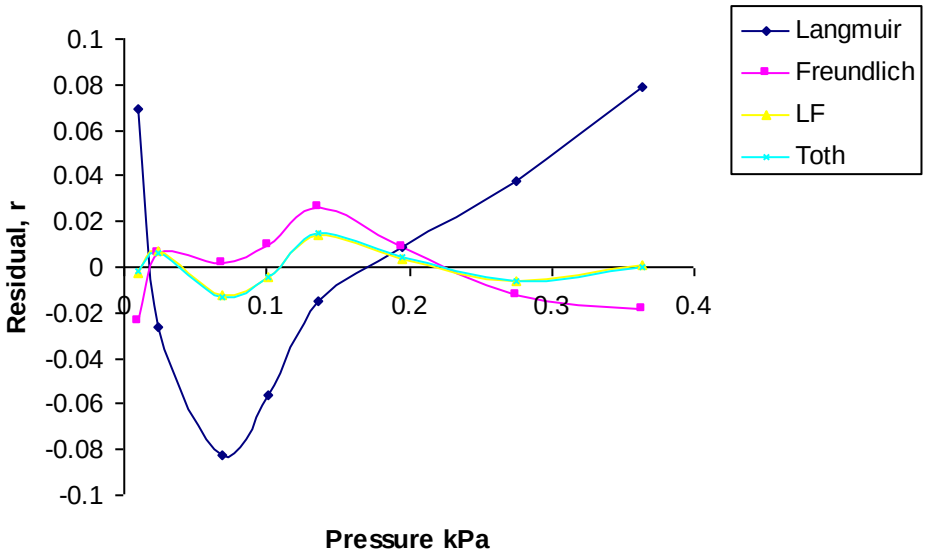

Figure 6.12: Residual plot for Valyon et al (1996) isotherm data

The R^2 values of the different models shown in Table 6.3 are interesting as they differ with temperature. At lower temperatures (373K-523K), the R^2 values are low at 91% and 93% respectively. At higher temperatures, this value increases to 99%. The Freundlich model R^2 values also differ with temperature with values as high as 99%, and as low as 91% at 623K. The R^2 values for the LF and Toth model are almost identical (R^2 drops to 97% at 523K for both).

Figure 6.12 shows the residual plot for Valyon et al (1996) data at 373K. The Langmuir model in this case gives a negative bias at lower pressures and a positive bias at higher pressures. The residuals for the LF and Tóth models are without bias and are almost identical indicating that both these models provide good fits. In the Tóth fit, the parameter b decreases as the temperature of adsorption increases which is intuitively correct. This is because the larger the affinity constant, b, the more the surface of the adsorbent is covered with adsorbate molecules as a result of the stronger affinity of the adsorbate molecules to the surface of the adsorbent. This is verified by the decrease in the amount of ammonia adsorbed as the adsorption temperature increased as observed from the equilibrium data shown in Figures 6.2 and 6.3.

Table 6.4: Tables showing the model parameters for Dragoi et al (2004) data at different temperatures

Langmuir Model	**Isotherm Parameters**			**R^2 %**	**RSS**	**RMSE**
Dragoi Data	**Symbol**	**Value**	**Error**			
353K	q_s (mmol.g^{-1})	1.72894	±0.10418	89.68	0.756685	0.217469
	b (kPa^{-1})	2126.795	±527.5381			
423K	q_s (mmol.g^{-1})	1.15099	±0.06666	92.41	0.242067	0.112873
	b (kPa^{-1})	870.1615	±156.1216			
473K	q_s (mmol.g^{-1})	0.89281	±0.04482	92.87	0.11416	0.090301
	b (kPa^{-1})	1948.924	±342.6238			

Freundlich Model	**Isotherm Parameters**			**R^2 %**	**RSS**	**RMSE**
Dragoi Data	**Symbol**	**Value**	**Error**			
353K	K	3.845259	5.97E14	83.04	0.671615	0.20488
	n	0.23671	±0.03295			
423K	K	4.008545	8.92E14	82.04	0.216583	0.106767
	n	0.32386	±0.04406			
473K	K	1.837526	*	80.38	0.155785	0.105487
	n	0.22155	±0.03425			

Langmuir-Freundlich Model	**Isotherm Parameters**			**R^2 %**	**RSS**	**RMSE**
Dragoi Data	**Symbol**	**Value**	**Error**			
353K	q_s(mmol.g^{-1})	1.76133	±0.13924	89.74	0.435002	0.170294
	b (kPa^{-1})	1870.22	±787.4836			
	n	0.90214	±0.23214			
423K	q_s (mmol.g^{-1})	0.95229	±0.04234	95.23	0.022819	0.035605
	b (kPa^{-1})	1546.727	±137.5674			
	n	2.24946	±0.43525			
473K	q_s (mmol.g^{-1})	0.83674	±0.03084	96.19	0.155785	0.01766
	b (kPa^{-1})	2947	±228.9845			
	n	2.20814	±0.39006			

Toth Model	Isotherm Parameters			R^2 %	RSS	RMSE
Dragoi Data	Symbol	Value	Error			
353K	q_s (mmol.g^{-1})	1.7833	±0.16713	89.79	0.748762	0.223422
	b (kPa^{-1})	2527.825	±1327.224			
	t	0.81374	±0.33769			
423K	q_s (mmol.g^{-1})	1.03704	±0.06231	93.11	0.398101	0.148717
	b (kPa^{-1})	726.0383	±126.117			
	t	1.96907	±1.08361			
473K	q_s (mmol.g^{-1})	0.83636	±0.03753	94.32	0.090969	0.083652
	b (kPa^{-1})	1371.582	±175.7682			
	t	4.1997	±5.06055			

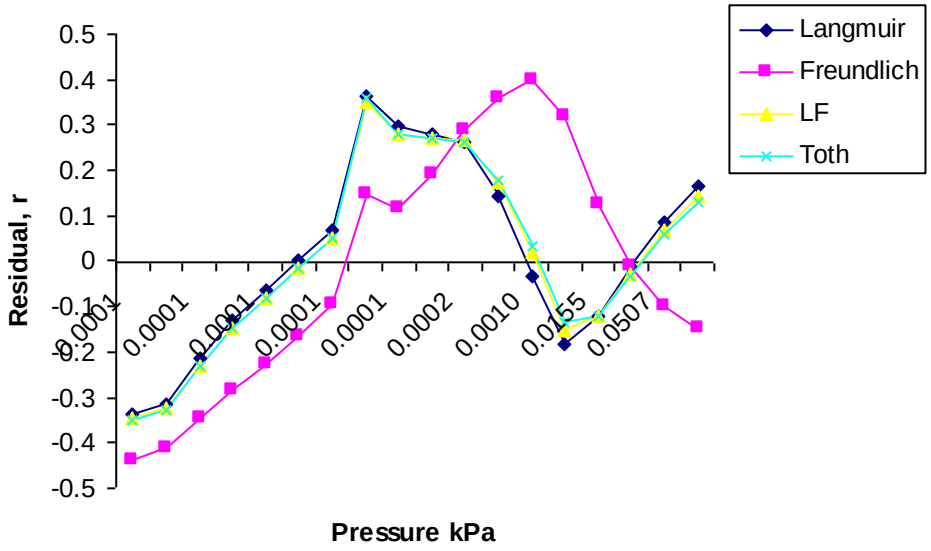

Figure 6.13: Residual plot of Dragoi et al (2004) isotherm data

Table 6.4 shows that the fitted data for Dragoi et al (2004) is very poor with low R^2 values for each empirical isotherm model. A plot of the residual (Figure 6.13) shows a definite positive bias for all the models. Thus the models provide a poor fit for the data. It is not clear at this point why the empirical models used here do not provide a good fit for this data and it may need further investigation. However, this is beyond the scope of this thesis.

Currently, only a few comparisons of ammonia isotherm models have been published. Kuo et al, (1985), for example, fitted the ammonia equilibria data for silica gel for a temperature range of 298-333K and a pressure range of 2.7 to 27

kPa to the Langmuir and potential theory models. It was found that the potential theory model correlated considerably better than the Langmuir model. Helminen et al, (2000), fitted 16 different isotherm models by modifying three main approaches; the Langmuir approach, the Gibbs approach and the potential theory approach. In the Langmuir approach, experimental ammonia adsorption data were fitted to the Langmuir and Langmuir-Freundlich equations with five temperature dependent models. The Henry Isotherm model and the vacancy solution (VS) theory isotherm models were treated in the Gibbs approach. In the potential theory approach, the Dubinin-Astakhov model was considered. The Langmuir models and the vacancy solution models failed with ammonia adsorption on zeolite, alumina and silica gel sorbents.

The Langmuir-Freundlich models, with a temperature dependent adsorption equilibrium constant from the van't Hoff equation generally provided the best fit on all inorganic solvents (Helminen et al, 2000). In a further study, the same group (Helminen et al, 2001), used the Langmuir, Freundlich, Langmuir-Freundlich, and Toth isotherm models to fit experimental data measured on 5A and 13X zeolites. It was found that the three parameter Langmuir-Freundlich and Toth models were the best for most sorbents including alumina, all silica gels and zeolites, especially if the equilibrium data contained a saturation level. The Langmuir model did not give the best fit for any of the sorbents even though this model is generally considered to be more thermodynamically reliable.

The studies presented by Helminen et al, (2000, 2001) as well as the research in this thesis using the Mast, Valyon et al, (1998) and Dragoi et al, (2004), adsorption data show that the adsorption isotherms of ammonia on zeolites do not follow the Langmuir isotherm quantitatively. However according to Valyon et al, (1998), it provides a more accurate description of the adsorption over a definite type of sorption site. This is feasible since as was discussed previously, at low coverages, there are a few sites which evolve high heats of adsorption. These sites have been associated with Lewis sites of a homogeneous energy distribution. The Langmuir assumption of surface homogeneity may therefore hold, but is specific for this site.

In this section, the Langmuir, Freundlich, Langmuir-Freundlich and Toth models have been fitted to different data on the adsorption of ammonia. Parameters were calculated from these models and analysed using the goodness of fit and error analysis described in section 6.2.3. The three parameter models Langmuir-Freundlich and Tóth provided the best fits and are in practice equally accurate for both the Mast Carbon data and the Valyon et al (1996) data. This is in line with the results of Helminen et al, (2000, 2001). The semi-empirical models presented in this work provided poor fits for the Dragoi et al (2004) data.

To reiterate, the main purpose of this study was to obtain the coverage θ of ammonia, expressed as a fraction of the saturated adsorbed for the Potential Barrier Model described in section 6.3. The isotherm produced by Mast Carbon as part of this research would seem to provide a suitable option for obtaining θ. However, as the isotherm was only carried out at one temperature and no further studies could be performed, it would be useful to compare this isotherm with others in the literature since they cover a wider temperature range. This has proven to be difficult. Figure 6.14 shows the comparison of the Valyon et al (1998) and Dragoi et al, (2004) isotherms.

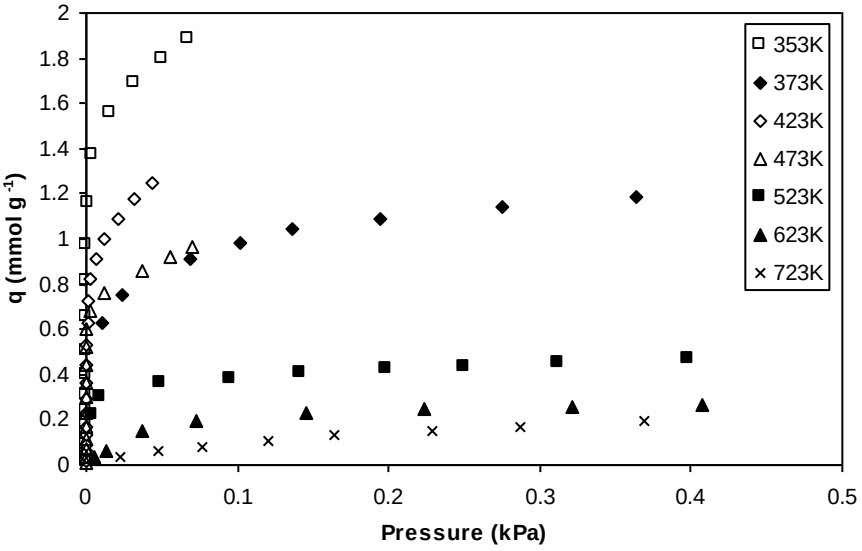

Figure 6.14: Comparison of Valyon et al, 1998 (closed symbols) with Dragoi et al, 2004 (open symbols) isotherms

Figure 6.14 clearly shows the marked differences in the data with Dragoi et al data (2004) displaying a higher affinity for ammonia at all the temperatures studied.

Both studies were concerned with studying the acidic properties of H-ZSM-5 for catalysis. According to Dragoi et al (2004), one of the major factors influencing acid properties of zeolites is the Si/Al ratio. It has been shown (Dondur et al, 2005) that the amount of strongly adsorbed ammonia decreases as the Si/Al ratio increases. The lower the Si/Al ratio, the more acidic the zeolite (due to an increase in Al) and therefore the more ammonia will adsorb. This is clearly the case above since the Si/Al ratios for Dragoi et al, (2004) and Valyon et al, (1998) were 13 and 34 respectively. Due to this difference, and a lack of ammonia adsorption isotherms on H-ZSM-5 in the literature, the data should not be used for interpolation or extrapolation purposes. In addition, extrapolation from such low pressures (0.0001-0.07kPa and 0-0.4kPa) to the pressures used in the current permeation experiments (partial pressure of ammonia 36-144kPa) would probably create very large errors, especially, as in the case of the Dragoi et al (2004) data, if the parameters are not accurate.

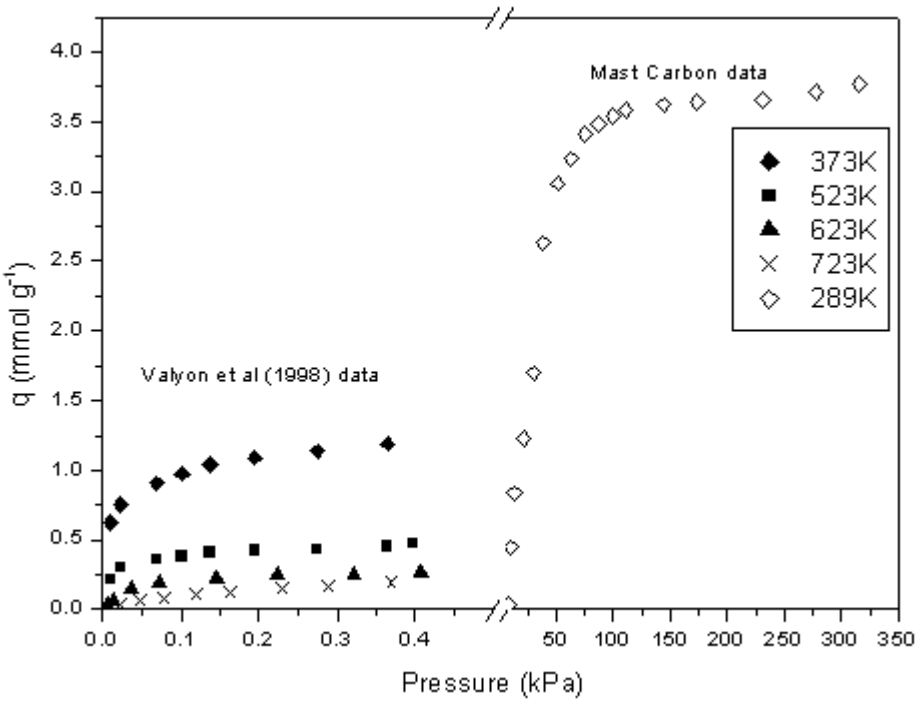

Figure 6.15: Comparison of Valyon adsorption data (1998) with Mast Carbon Data

A comparison of the Valyon et al (1998) adsorption isotherm with the one obtained using Mast Carbon data is shown in Figure 6.15. The figure shows the large difference in the equilibrium pressures which were used in the two studies. It was therefore decided that the Mast Carbon data would be best suited as it was

performed at the correct pressure range for the permeation measurements. This data shows that physical adsorption in the zeolite reached saturation at around 100 kPa. Comparison with ammonia adsorption data on other zeolites namely 4A, 5A and 13X, (Helminen et al, 2000, 2001) at 298K showed similar saturation at low pressures. In order to obtain ammonia isotherms at higher temperatures, extrapolation is necessary. This requires the temperature dependence of the fitted semi-empirical model (LF in this case) together with the heat of adsorption. Details are presented in section 6.2.4.

6.2.4 Heat of Adsorption

The heat of adsorption provides a measure of the change in enthalpy before and after adsorption and is therefore a quantitative description of the interaction strength between the surface of the adsorbent (ZSM-5) and the adsorbate (ammonia) molecules (Do, 1998). The measurement of the heat of adsorption can provide information about the surface heterogeneity of ZSM-5 zeolite. Such materials can exhibit sites that have a distribution of adsorption energies. The magnitude of this energy (heat of adsorption) is indicative of the adsorption process taking place i.e. physical or chemical. The different heats of adsorption measured for ammonia adsorption on H-ZSM-5 have been discussed in Section 6.2.2 and generally, high heats of adsorption (150-145kJ.mol^{-1}) have been attributed to chemisorption and lower heats of adsorption (<80kJ.mol^{-1}) have been attributed to physisorption.

Several definitions of the heat of adsorption are presented in the literature and these include: isosteric, differential, integral and equilibrium heats of adsorption. The most relevant of these is the isosteric heat of adsorption. Knowledge of the isosteric heat of adsorption is important in the study of adsorption kinetics and the temperature dependency of equilibrium adsorption. For the purposes of this study, the isosteric heat is important as it allows extrapolation of the adsorption of ammonia to temperatures at which the permeation studies were performed. The

isotherms at different temperatures were simulated using the Langmuir-Freundlich parameters of the fitted Mast Carbon data using ORIGIN.

6.2.4.1 Temperature Dependence of the Langmuir-Freundlich Isotherm Model

The temperature dependence of the LF equation for the affinity constant b is as follows:

$$b = b_o \exp\left[\frac{Q}{R_T T_o}\left(\frac{T_o}{T} - 1\right)\right] \qquad \textbf{6.34}$$

Where b is the adsorption affinity constant at a particular temperature T, and b_o is at some reference temperature T_o. The temperature dependence of the affinity constant b is taken from that of the Langmuir equation. Unlike Q in the Langmuir equation, where it is the isosteric heat, i.e. invariant with the surface loading, the parameter Q in the LF equation is only the measure of adsorption heat.

The heat of adsorption of a basic molecule on an acidic site is claimed to be a characteristic of the strength of the site (Dragoi et al, 2004). To obtain an acid strength distribution from the heat of adsorption as a function of coverage, the sample temperature has to be sufficiently high to assure that the probe molecule reaches the sorption equilibrium on the sites being probed (Dragoi et al, 2004). This explains why ammonia adsorption in the literature (Onyestak et al, 1996, Valyon et al, 1998) has been carried out at very high temperatures since the purpose of the studies has been to obtain the number, strength and strength distribution of acid sites.

The heat of adsorption of ammonia has been determined by various authors and a summary is given in Table 6.5.

Table 6.5: Measured differential heats of adsorption of ammonia on zeolites

Sample	Si/Al ratio	Method of measurement	-ΔH (kJ/mol)	Reference
H-ZSM-5 (480K)	>30	TPD-TGA microcalorimetry	150	Parillo and Gorte, 1993
H-ZSM-5	Not given	Microcalorimetry	140-120	Auroux et al, 1994
H-ZSM-5	33.7 20.9 13.9	Microcalorimetry	150-145	Jozefowicz et al, 1994
H-ZSM-5	22.5 33.4	Microcalorimetry	163-155 141-134 153-138	Onyestak et al, 1996
MFI			145-155	Derouane et al, 2000
H-Y		TPD	150-120	Joly et al, 2001
H-ZSM-5	13	Microcalorimetry	150	Dragoi et al, 2004

The values given in the table are representative of the high energy sites that are thought to be responsible for the high heats of adsorption (Jozefowicz et al, 1994) and are typical of chemisorption. For example in the studies by Dragoi et al, (2004), a plot of differential heats with amount adsorbed show three regions in the case of H-ZSM-5. A sharp decrease of the differential heat at low coverages indicates the presence of a small concentration of very strong Lewis type acid sites. A plateau of constant heats of adsorption follows and results from adsorption of ammonia on the Brønsted acid sites. The corresponding heat of adsorption is 150kJ.mol^{-1} which is the value given above. After all the Brønsted acid sites have been covered, the differential heat decreases again sharply. This decrease to 50kJ.mol^{-1} indicates that there is a transition from chemisorption to physisorption

(once all the acid sites are filled, then adsorption can occur on all other sites). This decrease in differential heats is also observed by Jozefowicz et al (1994). At low coverages, a few sites evolved high heats upon adsorption of ammonia (180kJ.mol^{-1}). A plateau was observed at 150-145kJ.mol^{-1} for coverages at 0.1-0.3mmol.g^{-1}. At slightly higher coverages (0.3-0.5 mmol.g^{-1}) the heats were approximately 80kJ.mol^{-1}. It is suggested in this work (Jozefowicz et al, 1994) that in the 80kJ.mol^{-1} region, the heats that are evolved from H-ZSM-5 zeolites tend to be representative of physisorption and indicate the interaction of silanol groups and cations with ammonia. At about 0.6 mmol.g^{-1}, the value of differential heat is approximately 55kJ.mol^{-1}. Evolution of the heat of adsorption with coverage is typical of a heterogeneous surface, in that it decreases from a very high value down to a low value.

The heats of adsorption presented in Table 6.5 therefore only represent the differential heats evolved when the acid sites (Brønsted) have been filled and represent chemisorption. As a result, the value of 150kJ.mol^{-1} as the heat of adsorption will not be used in this thesis. The interest in this case is based on the physisorption of ammonia due to the conditions under which the permeance experiments were carried out. The isosteric heat allows the evaluation of the temperature dependence of the equilibrium adsorption. In order to obtain the isosteric heat of adsorption, the curves of pressure as a constant value of the amount adsorbed can be plotted. The slope of each curve corresponds to the isosteric heat.

The Mast Carbon adsorption isotherm (Figure 6.4) is more in line with the experimental conditions used in this work. However, the isosteric method involves the measurement of at least two isotherms for the given system at different temperatures. As a result, it was not possible to obtain the isosteric heat of adsorption from this data.

As the Mast Carbon data represents physisorption of ammonia (high pressures), it may be possible to use a different set of data based on ammonia physisorption to obtain the isosteric heat of adsorption. The ammonia adsorption studies performed by Dragoi et al, (2004) postulate that chemisorption is the predominant process at

low pressures (up to 0.01 torr), and that physisorption begins above this value. This is not surprising since chemisorption concerns only a limited number of sites, namely the stronger sites, whereas reversible adsorption can occur on all types of sites. The corresponding isosteres for surface coverages included in the physical adsorption range of the isotherms (800-900μmol) were plotted for H-ZSM-5. The adsorption isosteres were obtained by plotting ln (p) versus 1/T. From the slopes of these lines, isosteric heats of adsorption, Q_{st} were evaluated in accordance with the Clausius-Clapeyron equation.

$$Q_{st} = RZ\left(\frac{\partial \ln p}{\partial(1/T)}\right)_n \qquad \textbf{6.35}$$

Where *p* and *T* are the equilibrium pressure and absolute temperature respectively, *R* is the universal gas constant, *Z* is the compressibility coefficient (with *Z*=1 for an ideal gas phase), and n is the adsorbate coverage. A value of 55kJ/mol was obtained for H-ZSM-5. This low value is more in line with physisorption and would therefore be more suitable in the simulation of Mast Carbon data. Helminen et al (2000) also calculated the isosteric heat with the Clausius-Clapeyron equation at 298K and 323K and pressure values of 0-100Pa. The isosteric heat for the 4A zeolite was found to be 47.2kJ.mol^{-1}. This is in line with the value calculated by Dragoi et al, (2004). The value of 55kJ.mol^{-1} was therefore used to simulate variation of adsorption capacity of ammonia with temperature. The results are shown in Figure 6.16. This figure will be used to calculate the ammonia coverage at different temperatures for the potential barrier model in section 6.3.2.2.

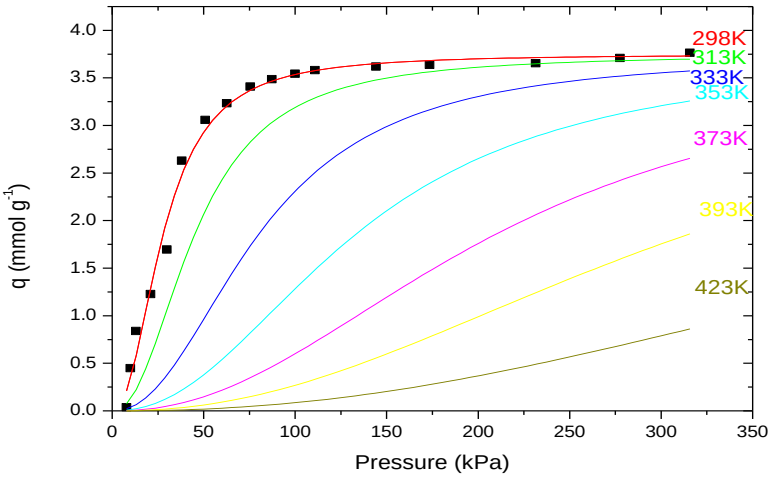

Figure 6.16: Simulation of adsorption isotherms with LF isotherm at different temperatures (Qst =55kJ.mol^{-1}). The squares represent the isotherm data by Mast Carbon at 298K and the lines are the simulated curves at different temperatures.

6.3 The Potential Barrier Model

6.3.1 Theoretical Background

Yang et al (1999) suggested that the presence of adsorbed molecules form a barrier to the diffusion of non-adsorbed molecules, and thereby hinder their transport across the membrane. This barrier can be considered to be a potential barrier, regardless of its physical nature. As a result, only those molecules with energy levels higher than the barrier can pass through the membrane pores. The model follows the assumption that the molecules of the non adsorbed gas follow the Boltzmann distribution. Therefore, the mole fraction of the molecules whose energy levels are higher than that of the potential barrier will be proportional to a factor equal to exp (-E/RT). The permeance can, as a result, be expressed by the following equation:

$$P = P_0 \exp(-E / RT) \qquad \textbf{6.36}$$

Where, P_0 is the permeance of pure adsorbed gas and E the potential barrier.
E is related to the surface coverage of the adsorbed gas (θ) as follows:

$$E = E_{0,i}\theta \qquad \textbf{6.37}$$

Where $E_{0,i}$ is the potential barrier introduced by a pure component i at its condition of saturated adsorption and θ is expressed as a fraction of the saturated adsorption amount ($\theta = q/q_{max}$). $E_{0,i}$ can then be calculated firstly by obtaining the adsorption isotherm for the given pure compound (ammonia in this case) from the general literature and secondly by calculating the coverage θ from the isotherm using the feed partial pressure, then the permeate partial pressure. The average of these two coverages is then obtained. In this work, both arithmetic and logarithmic averages have been considered and a comparison is made in section 6.3.2.1.

It is generally assumed that there is no variation in adsorption occupancy along the membrane module length, however, it is not known how the coverage varies over the membrane thickness (there is variation in adsorption coverage unless the membrane is saturated with adsorbed species). Kapteijn et al, (1995) described a linear change of ln (1- θ), rather than a linear change of θ with membrane thickness as follows:

$$\ln(1-\theta) = kx + \ln(1-\theta_0) \qquad \textbf{6.38}$$

where θ is the coverage at any thickness, θ_0 is the coverage at the feed side x is thickness of membrane and k is a constant.
Hence

$$\theta = 1-(1-\theta_0)\exp kx \qquad \textbf{6.39}$$

The boundary condition is $\theta = \theta_{1,0}$ when $x=x_0$, the constant can be expressed as:

$$k = \left(\frac{1}{x_0}\right)\ln\left[(1-\theta_{1,0})/(1-\theta_0)\right] \qquad \textbf{6. 40}$$

The average coverage is given by

$$\bar{\theta} = \frac{1}{x_0}\int_0^{x0} \theta dx \qquad \textbf{6.41}$$

and hence by

$$\bar{\theta} = 1 - \frac{\theta_0 - \theta_{1,0}}{\ln\left[\left(1-\theta_{1,0}\right)/\left(1-\theta_0\right)\right]} \qquad \textbf{6.42}$$

The value of $E_{0,i}$ is found from a plot of ln P against θ. The slope of the plot is ($-E_{0,i}/RT$) the experiment having been carried out at constant temperature.

Once the value for $E_{0,i}$ has been found, E can be calculated using Equation 6.11, and substituting the value for E in Equation 6.10 to calculate the permeance.

The permeance of the non-adsorbing component (in this case hydrogen and nitrogen) represented by P_o in Equation 6.10, is temperature dependent.

6.3.2 Model Results and Discussion

The potential barrier model has been applied to describe the hindering effect of strongly adsorbed ammonia on the permeation of weakly/non-adsorbed hydrogen and nitrogen through the MCT0.2 zeolite MFI membrane. Adsorption effects are strongly dependent on the operating conditions, mainly temperature and pressure. The results have therefore been analysed as a function of these conditions and are presented in sections 6.3.2.1 and 6.3.2.2.

6.3.2.1 As a Function of Pressure

In order to demonstrate the hindrance effect of ammonia on hydrogen and nitrogen permeances, the permeances of pure gases are plotted on the same graph as their

permeances in the 9% $NH_3/N_2/H_2$ mixture and are presented in Figures 6.17 and 6.18 respectively.

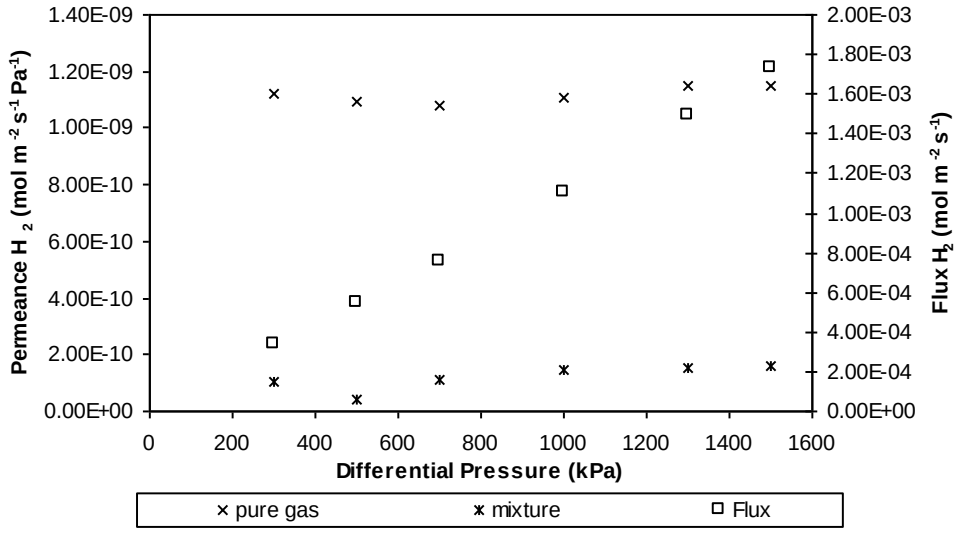

Figure 6.17: Permeance of pure hydrogen and hydrogen in the mixture with permeation flux as a function of pressure (T 298K)

Figure 6.17 shows the substantial reduction in the permeance of hydrogen in the multi-component $NH_3/H_2/N_2$ system. The hydrogen permeance is reduced by ≈ 90%. This can be explained qualitatively as described in the results section in Chapter 5 (section 5.2.2.1) where the presence of ammonia is inhibiting hydrogen permeation.

The nitrogen permeance decreases by about 50% at lower pressures, but at higher differential pressures (1000-1550kPa), the nitrogen permeance in the mixture is only 20% lower than as a pure gas. The reduction in hydrogen and nitrogen permeances in the presence of ammonia can be explained by the following. The adsorption of ammonia on the membrane pores effectively reduces the open void space and significantly alters the permeation of non-adsorbed molecules through the void space. This has also been observed by Camus et al, (2006) on MFI membranes.

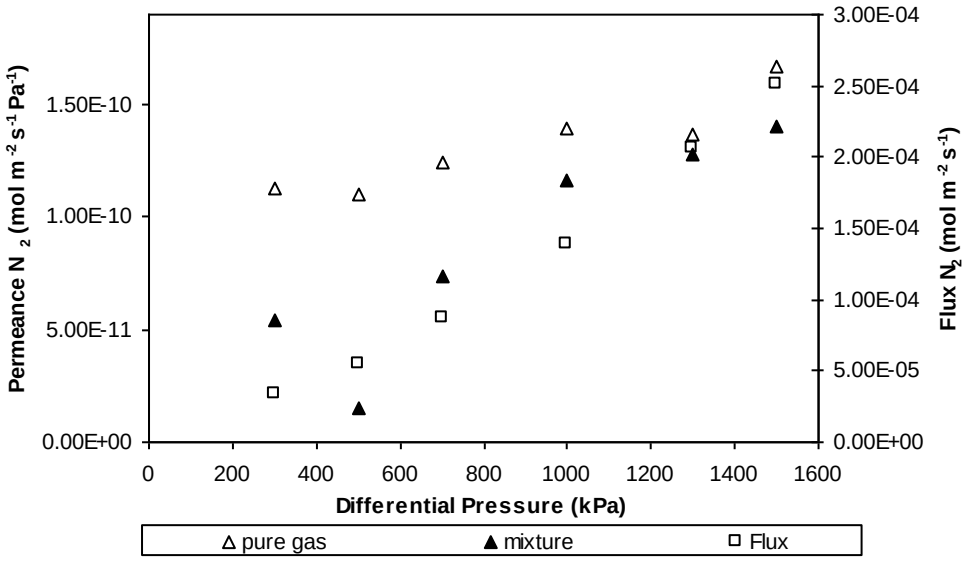

Figure 6.18: Permeance of pure nitrogen and nitrogen in the mixture with permeation flux as a function of pressure (T 298K)

The ammonia coverage was calculated from the isotherm provided by Mast carbon (Figure 6.4) as described by equations 6.12-6.16. Example values of the arithmetic average are compared with the logarithmic average calculated from Equation 6.16 for ammonia adsorption coverage, is shown in Table 6.6. It can be seen that there is a significant variation in the values and use of the arithmetic average may introduce some errors.

Table 6.6: Comparison of calculation procedures for average adsorption coverages

Logarithmic average $\overline{\theta}$	Arithmetic average $\overline{\theta}$
0.374	0.324
0.522	0.422
0.607	0.467
0.687	0.510

The predicted multi-component gas permeances from the Potential Barrier Model are displayed in Tables 6.7 and 6.8 respectively and are calculated as described by Equations 6.10 to 6.16.

Table 6.7: Comparison of the measured and calculated permeance of H_2 in the ternary mixture with logarithmic average coverage as a function of pressure.

FP (kPa)	PP (kPa)	$\bar{\theta}$	H_2 Permeance ($mol.m^{-2}.s^{-1}.Pa^{-1}$) Pure gas P_o	H_2 Permeance ($mol.m^{-2}.s^{-1}.Pa^{-1}$) Calculated	H_2 Permeance ($mol.m^{-2}.s^{-1}.Pa^{-1}$) Measured
400	100	0.374	11.21E-10	5.35E-10	1.07E-10
600	100	0.522	10.91E-10	3.89E-10	0.41E-10
800	100	0.609	10.77E-10	3.25E-10	1.12E-10
1100	100	0.688	11.06E-10	2.85E-10	1.43E-10
1400	100	0.738	11.46E-10	2.67E-10	1.50E-10
1650	100	0.758	11.52E-10	2.58E-10	1.63E-10

Table 6.8: Comparison of the measured and calculated permeance of N_2 in the mixture with logarithmic mean coverage as a function of pressure

FP (kPa)	PP (kPa)	$\bar{\theta}$	N_2 Permeance ($mol.m^{-2}.s^{-1}.Pa^{-1}$) Pure gas P_o	N_2 Permeance ($mol.m^{-2}.s^{-1}.Pa^{-1}$) Calculated	N_2 Permeance ($mol.m^{-2}.s^{-1}.Pa^{-1}$) Measured
400	100	0.374	1.12E-10	0.20E-10	0.55E-10
600	100	0.522	1.10E-10	0.78E-10	1.49E-10
800	100	0.609	1.24E-10	0.45E-10	0.74E-10
1100	100	0.688	1.39E-10	0.80E-10	1.17E-10
1400	100	0.738	1.37E-10	0.94E-10	1.28E-10
1650	100	0.758	1.67E-10	1.06E-10	1.40E-10

Table 6.7 shows that the calculated hydrogen permeances in the multi-component $NH_3/H_2/N_2$ system predicted using the potential barrier model are much higher than the measured experimental values. In contrast, the predicted values for nitrogen shown in Table 6.8 are lower than the measured values. A comparison of calculated permeances and measured permeances of hydrogen and nitrogen are shown in Figures 6.19 and 6.20 respectively.

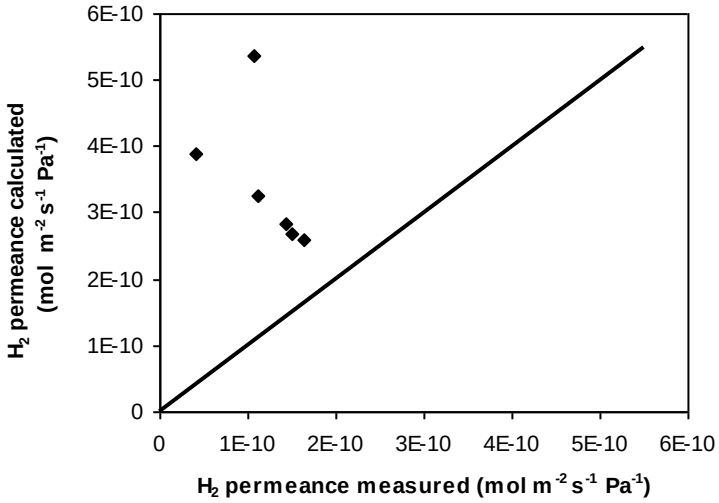

Figure 6.19: Comparison of the measured and calculated values of the hydrogen permeance in the ternary mixture using logarithmic average ammonia coverage

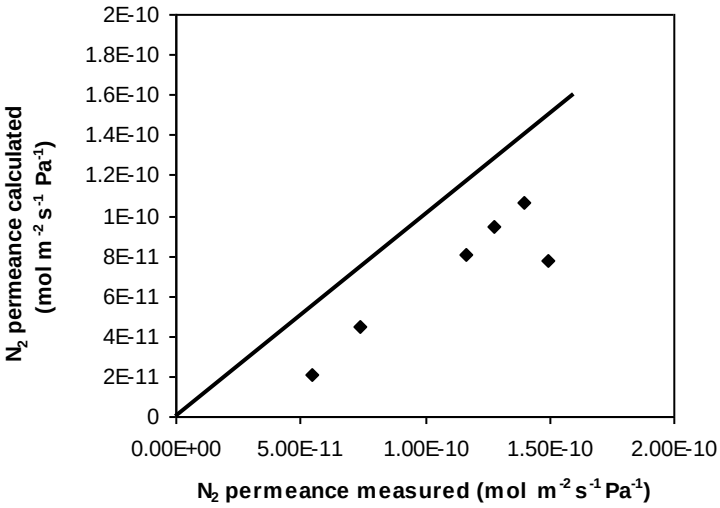

Figure 6.20: Comparison of the measured and calculated values of the nitrogen permeance in the ternary mixture using logarithmic average ammonia coverage.

The predictions deviate quite significantly from the measured values. The model over predicts the hydrogen permeances which suggests that ammonia adsorption should not hinder hydrogen permeance as much as what is observed experimentally. The under prediction of nitrogen permeances suggests that the nitrogen permeance should be hindered to a greater extent than has been observed in the experiments.

One of the reasons for these deviations could be the average coverage of ammonia. In the potential barrier model, the logarithmic average coverage which considers the coverage on the feed side and the coverage of the permeate side of the membrane is used. In Chapter 5, it was suggested that adsorption of ammonia may be much higher on the feed side with hardly any coverage at the permeate side. A schematic of ammonia adsorption is shown in Figure 6.21.

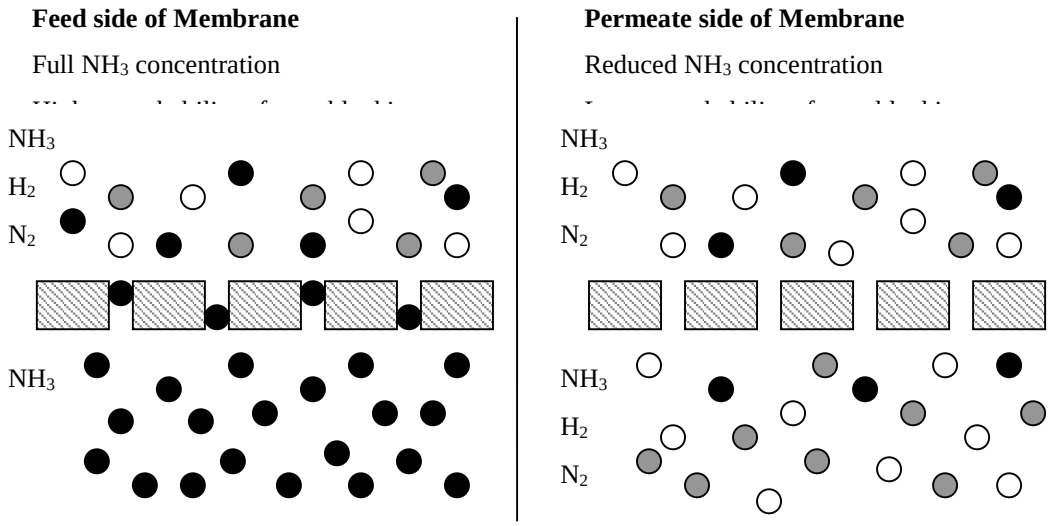

Figure 6.21: Representation of ammonia adsorption along the membrane

The potential barrier model calculations for both hydrogen and nitrogen were repeated, replacing average coverage with coverage on the feed side. The results for predicted hydrogen and nitrogen permeances are presented in Tables 6.9 and 6.10 Figures 6.22 and 6.23 respectively.

Table 6.9: Comparison of the measured and calculated permeance of H_2 in the mixture with feed side coverage as a function of pressure

FP (kPa)	PP (kPa)	θ_F	H_2 Permeance ($mol.m^{-2}.s^{-1}.Pa^{-1}$) Pure gas P_o	H_2 Permeance ($mol.m^{-2}.s^{-1}.Pa^{-1}$) Calculated	H_2 Permeance ($mol.m^{-2}.s^{-1}.Pa^{-1}$) Measured
400	100	0.633	11.21E-10	3.50E-10	1.07E-10
600	100	0.809	10.91E-10	2.47E-10	0.41E-10
800	100	0.889	10.77E-10	2.11E-10	1.12E-10
1100	100	0.942	11.06E-10	1.96E-10	1.43E-10
1400	100	0.965	11.46E-10	1.95E-10	1.50E-10
1650	100	0.974	11.52E-10	1.93E-10	1.63E-10

Table 6.10: Comparison of the measured and calculated permeance of N_2 in the mixture with feed side coverage as a function of pressure

FP (kPa)	PP (kPa)	θ_F	N_2 Permeance ($mol.m^{-2}.s^{-1}.Pa^{-1}$) Pure gas P_o	N_2 Permeance ($mol.m^{-2}.s^{-1}.Pa^{-1}$) Calculated	N_2 Permeance ($mol.m^{-2}.s^{-1}.Pa^{-1}$) Measured
400	100	0.633	1.12E-10	0.26E-10	0.55E-10
600	100	0.809	1.10E-10	0.90E-10	1.49E-10
800	100	0.889	1.24E-10	0.89E-10	0.74E-10
1100	100	0.942	1.39E-10	1.11E-10	1.17E-10
1400	100	0.965	1.37E-10	1.30E-10	1.28E-10
1650	100	0.974	1.67E-10	2.11E-10	1.40E-10

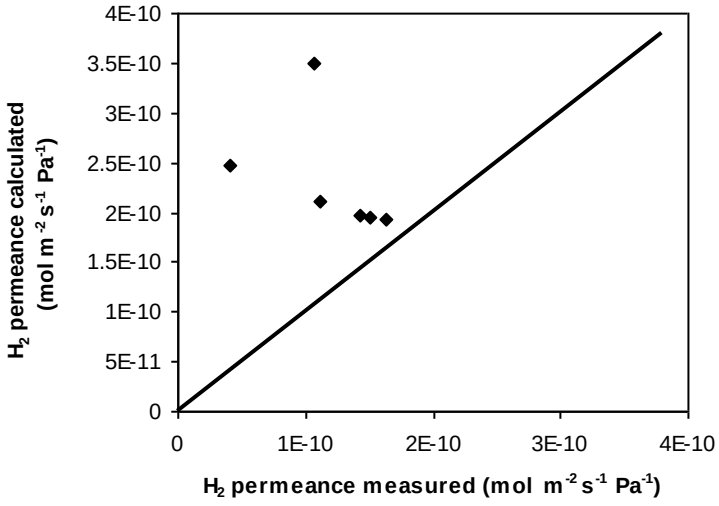

Figure 6.22: Comparison of the measured and calculated values of the hydrogen permeance using ammonia coverage on the feed side.

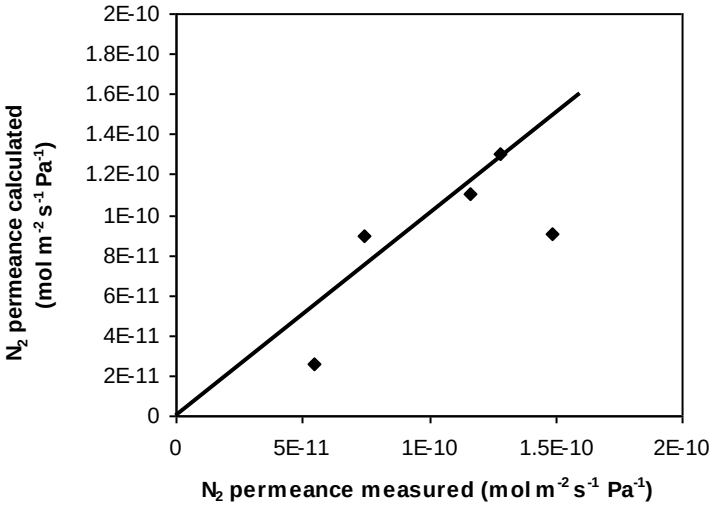

Figure 6.23: Comparison of the measured and calculated values of the nitrogen permeance using ammonia feed coverage.

An improvement in the correlations of measured and calculated permeances can be observed in Figures 6.22 and 6.23 when using ammonia coverage on the feed side. However, model predictions for hydrogen are still higher than the experimental values. There could be a number of reasons why this is the case. It may be that some of the parameters used in the calculation are not completely accurate. The average coverage of ammonia was calculated from one isotherm and no comparison at the same temperature was available. If this parameter was inaccurate, it would seriously affect the model predictions. Another reason could be that the observed (measured) permeances may be affected by factors other than the hindering effect of adsorbed ammonia. The predictions of nitrogen permeance are generally better and give good predictions. The scatters could be attributed to experimental error especially for the value at 600kPa feed pressure.

The potential barrier model only considers the hindering effect of the strongly adsorbed component (NH_3) on the permeance of the weakly adsorbed component (H_2 or N_2). However, the model fails to predict this phenomenon for the $NH_3/H_2/N_2$ system. This suggests that in this case, the interaction between the weakly adsorbed components (H_2 and N_2) may also significantly affect their transport through the membrane.

6.3.2.2 As a Function of Temperature

Figures 6.24 and 6.25 show the inhibiting effects of ammonia on hydrogen and nitrogen permeance as a function of temperature.

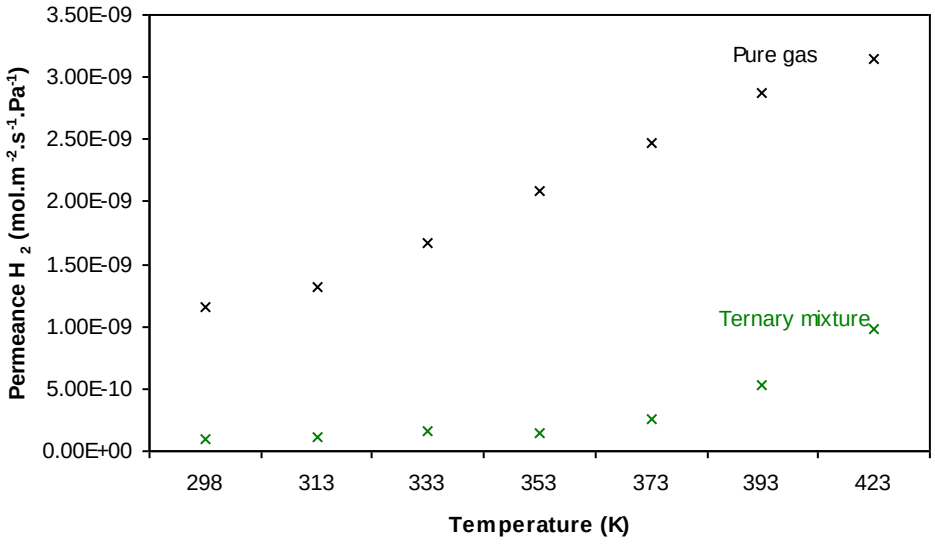

Figure 6.24: Permeance of pure hydrogen and hydrogen in the mixture as a function of temperature, differential pressure 1500 kPa

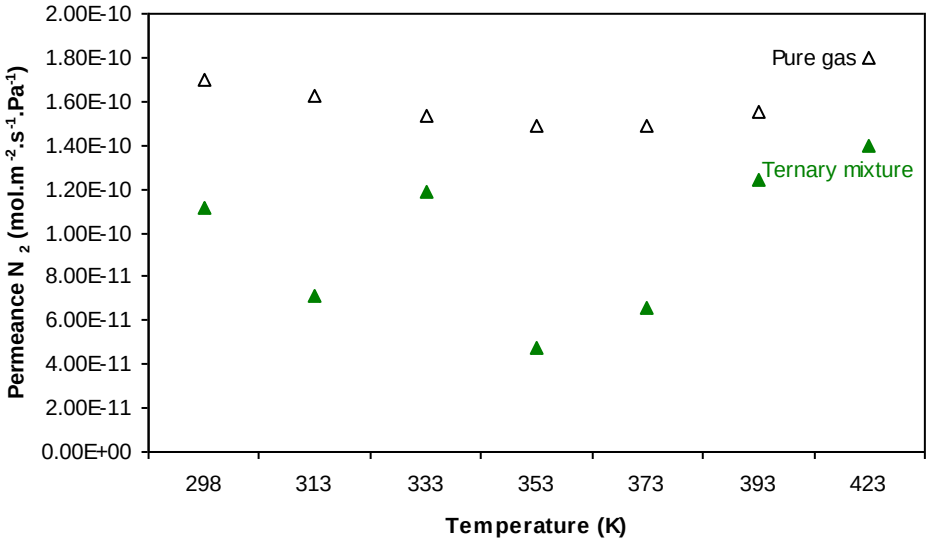

Figure 6.25: Permeance of pure nitrogen and nitrogen in the mixture as a function of temperature differential pressure 1500kPa

Pure hydrogen gas permeance is higher than that of hydrogen in the ternary mixture over the entire temperature range and both permeances (pure gas and ternary mixture) increase with temperature although the trends are somewhat different. The pure gas permeance of hydrogen is around 10 times higher that of the hydrogen in the mixture at the lower temperatures. However, the ratio decreases as the temperature increases. Although ammonia is still blocking hydrogen permeance, this effect seems to decrease with increasing temperature. This is not surprising as the amount of ammonia adsorbed is decreasing with increasing temperature (see Table 6.11). It might be expected that the hydrogen permeance in the mixture would approach pure hydrogen permeance values due to the decrease in ammonia adsorption. This is not the case however, which indicates that factors other than ammonia adsorption alone, may affect hydrogen permeance in the ternary mixture.

Nitrogen on the other hand shows a different trend. While the permeance of pure nitrogen in the membrane is generally higher than that in the ternary mixture, the permeances of nitrogen tend towards the single gas permeance values at higher temperatures (393K and 423K). This is not surprising, given that at these temperatures, ammonia adsorption is very low (Figure 6.16) therefore the hindrance effect of adsorbed ammonia on the nitrogen permeance is expected to be much lower. The permeance of pure nitrogen is only 2-3 times higher than that in the mixture indicating that nitrogen permeance is less affected by ammonia adsorption than hydrogen. Both the permeance of nitrogen in the mixture and the pure nitrogen permeance display a minimum although the minimum in the mixture is more pronounced. The trend at higher temperatures for the nitrogen permeance in the mixture may be the result of a combined effect of decreased ammonia adsorption and an increase in nitrogen diffusion.

The adsorption of ammonia decreases with increasing temperature (Tables 6.11-6.14) and it would be expected that the hindrance effect of adsorbed ammonia would decrease with temperature. As a result, permeances of hydrogen and nitrogen should increase gradually, approaching their pure gas permeance values. The potential barrier model is applied in this case to predict permeances of hydrogen and nitrogen in the ternary mixture as a function of temperature.

Results from model predictions are presented in Tables 6.11 to 6.14. The coverage of ammonia at different temperatures was calculated from the simulated Mast Carbon isotherm as shown in Figure 6.16 using a heat of adsorption of 55kJ/mol. The calculated permeances were obtained from the pure gas permeances at different temperatures using Equations 6.10 and 6.16.

Tables 6.11 and 6.13 show a comparison of the experimental data with the model predictions using the average ammonia coverage. The model predictions are not in good agreement with the experimental data for both hydrogen and nitrogen. Using the feed ammonia coverage (Tables 6.12 and 6.14) instead of the average does not improve the situation. At lower temperatures (298-333K), the model predicts much lower permeances than those observed in the experimental data suggesting that the amount of adsorbed ammonia should block the hydrogen permeance more than has been observed in the experiments. At higher temperatures (353-423K) the model predicts much larger permeances than the experimental work, suggesting that ammonia hindrance should be much lower than that observed in experiments. Plots for the comparison of measured data with the calculated are shown in Figures 6.26 and 6.27.

Table 6.11: Comparison of the measured and calculated permeance of H_2 in the mixture with logarithmic average coverage as a function of temperature

Temperature (K)	$\bar{\theta}$	**H_2 Permeance (mol.m^{-2}.s^{-1}.Pa^{-1}) Pure gas P_o**	**H_2 Permeance (mol.m^{-2}.s^{-1}.Pa^{-1}) Calculated**	**H_2 Permeance (mol.m^{-2}.s^{-1}.Pa^{-1}) Measured**
298	0.769	11.52E-10	0.04E-10	1.04E-10
313	0.661	13.11E-10	0.11E-10	1.05E-10
333	0.492	16.65E-10	0.60E-10	1.54E-10
353	0.305	20.84E-10	2.99E-10	1.40E-10
373	0.159	24.65E-10	9.48E-10	2.55E-10
393	0.076	28.76E-10	18.6E-10	5.29E-10
423	0.025	31.44E-10	27.5E-10	9.73E-10

Table 6.12: Comparison of the measured and calculated permeance of H_2 in the mixture with coverage on the feed side as a function of temperature

Temperature (K)	θ_F	H_2 Permeance ($mol.m^{-2}.s^{-1}.Pa^{-1}$) Pure gas P_o	H_2 Permeance ($mol.m^{-2}.s^{-1}.Pa^{-1}$) Calculated	H_2 Permeance ($mol.m^{-2}.s^{-1}.Pa^{-1}$) Measured
298	0.976	11.52E-10	0.00E-10	1.04E-10
313	0.927	13.11E-10	0.02E-10	1.05E-10
333	0.781	16.65E-10	0.09E-10	1.54E-10
353	0.537	20.84E-10	0.68E-10	1.40E-10
373	0.298	24.65E-10	4.10E-10	2.55E-10
393	0.147	28.76E-10	12.4E-10	5.29E-10
423	0.050	31.44E-10	24.2E-10	9.73E-10

Table 6.13: Comparison of the measured and calculated permeance of N_2 in the mixture with logarithmic average coverage as a function of temperature

Temperature (K)	$\overline{\theta}$	N_2 Permeance ($mol.m^{-2}.s^{-1}.Pa^{-1}$) Pure gas P_o	N_2 Permeance ($mol.m^{-2}.s^{-1}.Pa^{-1}$) Calculated	N_2 Permeance ($mol.m^{-2}.s^{-1}.Pa^{-1}$) Measured
298	0.769	1.70E-10	0.24E-10	1.11E-10
313	0.661	1.62E-10	0.33E-10	0.71E-10
333	0.492	1.53E-10	0.50E-10	1.18E-10
353	0.305	1.49E-10	0.78E-10	0.47E-10
373	0.159	1.48E-10	1.08E-10	0.66E-10
393	0.076	1.56E-10	1.34E-10	1.24E-10
423	0.025	1.8E-10	1.72E-10	1.40E-10

Table 6.14: Comparison of the measured and calculated permeance of N_2 in the mixture with coverage on the feed side as a function of temperature

Temperature (K)	θ_F	N_2 Permeance ($mol.m^{-2}.s^{-1}.Pa^{-1}$) Pure gas P_o	N_2 Permeance ($mol.m^{-2}.s^{-1}.Pa^{-1}$) Calculated	N_2 Permeance ($mol.m^{-2}.s^{-1}.Pa^{-1}$) Measured
298	0.976	1.70E-10	0.14E-10	1.11E-10
313	0.927	1.62E-10	0.17E-10	0.71E-10
333	0.781	1.53E-10	0.26E-10	1.18E-10
353	0.537	1.49E-10	0.47E-10	0.47E-10
373	0.298	1.48E-10	0.81E-10	0.66E-10
393	0.147	1.56E-10	1.17E-10	1.24E-10

423	0.050	1.8E-10	1.65E-10	1.40E-10

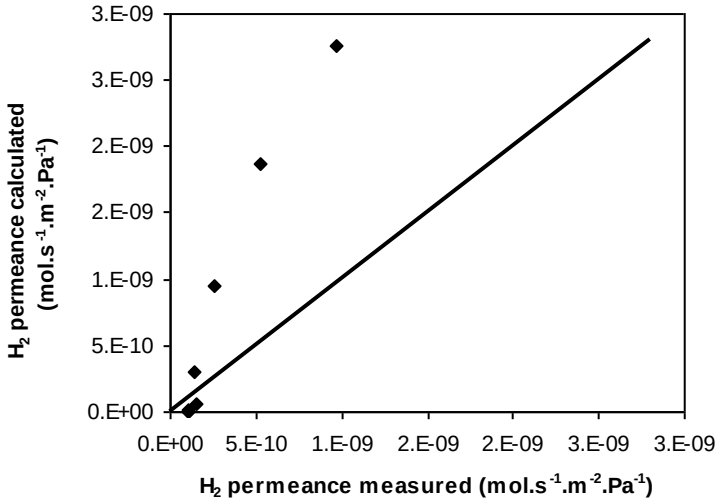

Figure 6.26: Comparison of the measured and calculated values of the hydrogen permeance using average ammonia coverage.

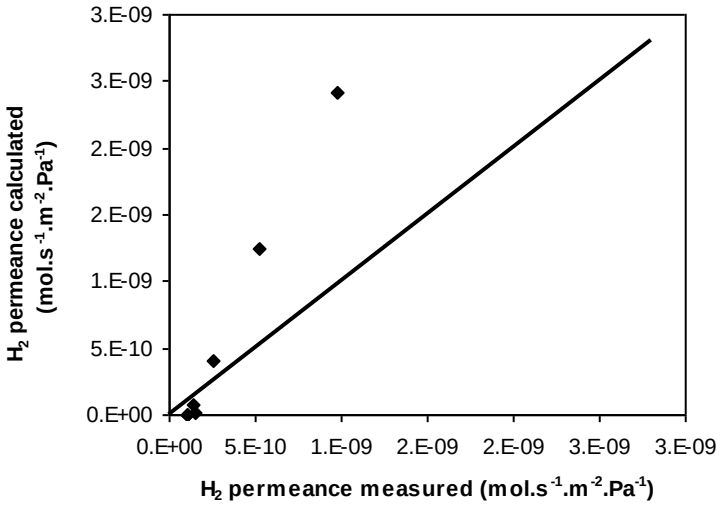

Figure 6.27: Comparison of the measured and calculated values of the hydrogen permeance using ammonia coverage on the feed side.

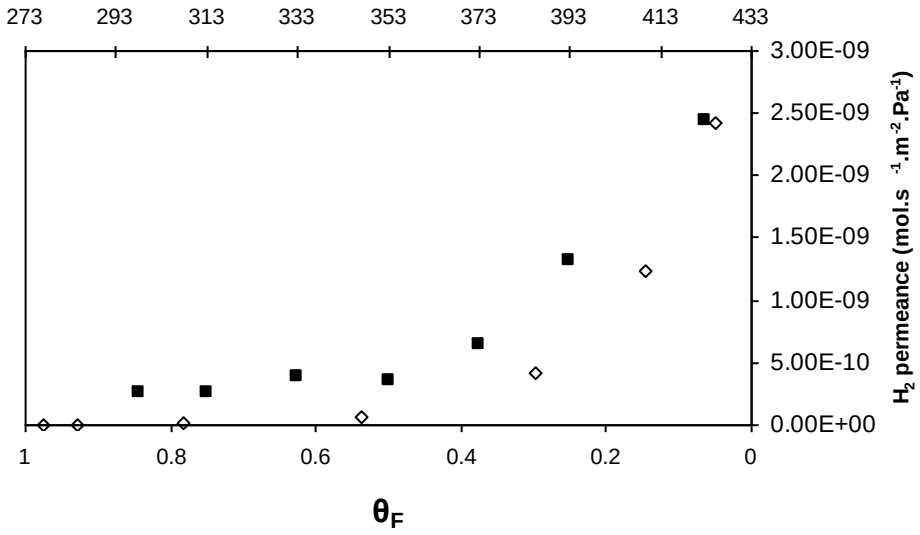

Figure 6.28: Plot of H_2 permeance against the logarithmic average adsorbed amount of NH_3 in the ternary mixture. Closed symbols represent the measured values and open symbols represent the calculated values.

Although there is poor agreement between predicted and calculated data, the trends are similar as shown in Figure 6.28. The expected trend would be that as the temperature increases, the mean adsorbed amount of ammonia decreases, reducing the hindrance effect and resulting in an increase in the permeance of hydrogen in the mixture. At lower temperatures between 298K and 353K, although there is a decrease in amount of adsorbed ammonia, the hydrogen permeance seems to remain constant or increase only slightly. Therefore, hydrogen is still hindered by ammonia at these temperatures. However, with further increase, at about 353K (80^{o}C), the hydrogen permeance starts to increase monotonically with increasing temperature. This is expected since the ammonia coverage (both average and at the feed side) drops drastically after 353K. Therefore, ammonia hindrance to hydrogen (and nitrogen) permeation should be quite low.

Comparing the permeance of hydrogen in the ternary gas mixture to that of the pure gas (Figure 6.24), it can be seen that permeance of pure gas increases throughout the whole temperature range, whereas hydrogen permeance in the ternary gas mixture increases from 353K, when amount of ammonia adsorbed (Tables 6.10-6.14) has decreased significantly. It would be expected that as the hindrance by adsorbed ammonia to hydrogen permeation is decreasing, the hydrogen permeance in the

mixture would approach the pure hydrogen gas permeance values. However, this is not the case as seen in Figure 6.22. This may be caused by other interactions of the hydrogen molecules with the other molecule (NH_3 and N_2) in the mixture. Another reason could be the increase in mobility of components with an increase in temperature. Temperature affects gas permeances by influencing both adsorption and diffusion (Lin et al, 2002). As a result, the potential barrier model is not able to predict hydrogen permeance values in the ternary mixture as it only takes into account the effect of ammonia adsorption.

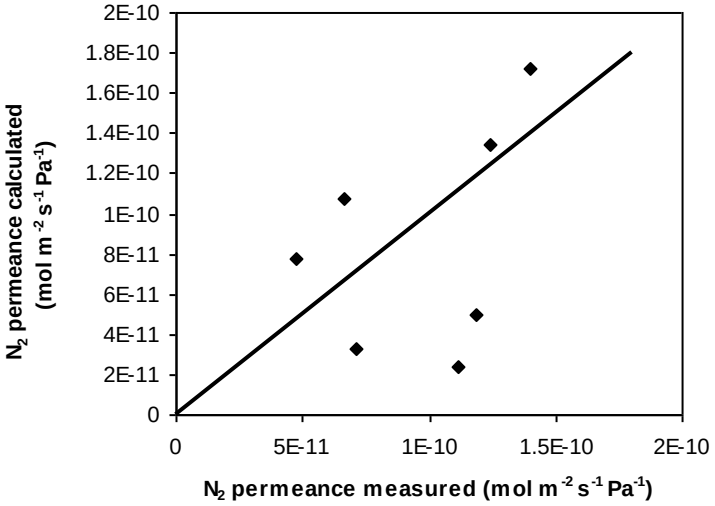

Figure 6.29: Comparison of the measured and calculated values of nitrogen permeance using average ammonia coverage.

Comparing the measured and calculated data for nitrogen (Tables 6.13 and 6.14), there is poor correlation using the logarithmic average coverage (Figure 6.29). Using the feed side coverage, the model does not predict correctly the nitrogen permeances at lower temperatures (Figure 6.30). It is interesting that at higher temperatures, particularly from 353K, the predictions are almost accurate. This suggests that at higher temperatures, nitrogen is only affected by adsorbed ammonia, therefore as ammonia adsorption decreases, nitrogen is no longer hindered and permeates freely. This also explains the nitrogen permeance in the ternary mixture approaching its single gas permeances. In the case of nitrogen, the predicted trend is not similar to the measured permeance trend. The predicted permeances do not show the minimum that

was observed at around 353K for both the single gas and the ternary mixture permeances.

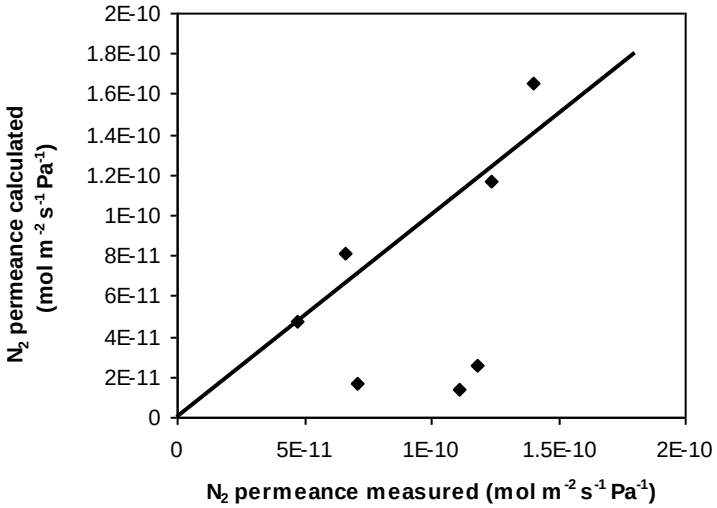

Figure 6.30: Comparison of the measured and calculated values of the nitrogen permeance using coverage of ammonia on the feed side.

From the results of the model predictions for both hydrogen and nitrogen permeances as a function of temperature, it can be said that the potential barrier model generally did not predict the permeances well. One of the reasons for the model failure could be due to inaccuracies in the values that were calculated for ammonia coverage at different temperatures. Due to lack of isotherms at different temperatures, the isotherms were extrapolated as shown in Figure 6.16. Also, the value of heat of adsorption extracted from Dragoi et al (2004) data may not be accurate. Both of these factors would result in permeance values with significant errors.

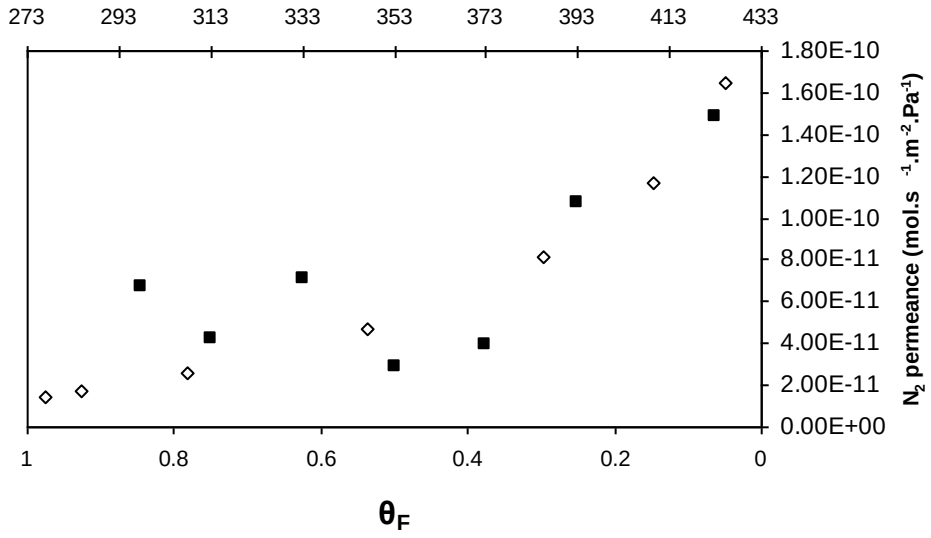

Figure 6.31: Plot of N_2 permeance against the logarithmic average adsorbed amount of NH_3 in the ternary mixture. Closed symbols represent the measured values and open symbols represent the calculated values.

6.3.2.3 Model Evaluation

Although the model predictions were not accurate, they have shown that there are other factors apart from adsorption that could be affecting membrane transport. In particular, the influence of the three molecules on their permeation and separation behaviour is not considered in the model. The potential barrier model only takes into account the effect of the strongly adsorbed component (ammonia) and the single gas permeance to predict the permeance of the weakly adsorbing component in the mixture. However, it may be that the interactions between the two weakly adsorbing components (H_2/N_2) and the strong/weakly adsorbed components (NH_3/N_2 and or NH_3/H_2) could also influence their transport in the membrane.

Generally, the permeation and separation behaviour in mixed component permeation can be explained based on the synergistic effects of preferential adsorption, molecular sieving and diffusion effects (Cui et al, 2004, Rezai et al, 2008). However, transport could be dominated by either mechanism. Molecular sieving is not relevant in this case since all three molecules are smaller than the MFI pore size. Gas molecules with a

higher adsorption capacity (NH_3) preferentially adsorb on the surface and limit the diffusion of the less adsorbing gas molecule (H_2 and N_2) into the pores. Diffusion effects may include single file diffusion, which slows down the faster diffusing molecule in zeolite pores and accelerates the diffusion of the slower diffusing component.

In Chapter 5, it was observed that hydrogen was the fastest moving component and nitrogen was the slowest. It has been shown in various studies (Geus et al, 1992, Cui et al, 2004, Hong et al, 2008) that the slower moving species may reduce the mobility of the faster moving species. Therefore, the observed decrease in hydrogen permeance observed in the ternary mixture may be caused by both the hindering effect of adsorbed ammonia and reduced mobility caused by slower moving nitrogen. This may explain why predicted permeances for hydrogen were higher than the measured values since the potential barrier model only considers ammonia adsorption as the hindering factor.

In the same way that faster moving molecules may be slowed by slower moving species, the slower moving species can be accelerated by the faster moving species. For nitrogen, the predicted permeances were lower than the measured values. This suggests that nitrogen should be hindered to a greater extent than observed. Therefore, the observed nitrogen permeances in the ternary mixture could be attributed to the effect of both the hindering effect of ammonia and the increased mobility caused by faster moving hydrogen and/or ammonia.

It is clear from the results presented in this section that there may be some diffusion effects in the ternary mixture permeation that have not been previously discussed and have not been catered for in the model. In order to give a better understanding of the transport properties, binary mixture experiments ($25\%H_2/75\%N_2$) were conducted and compared to single and ternary mixture permeances to determine whether interactions between the molecules affects the transport properties of these molecules. This is presented in section 6.3.3.

6.3.3 Binary Mixture Permeation

The results obtained from the ternary mixture (9%NH_3/69%H_2/22%N_2) experiments have shown that ammonia is preferentially adsorbed and hinders the permeation of both hydrogen and nitrogen. When compared to the pure gas permeances, hydrogen in the ternary mixture was more affected by the presence of ammonia than nitrogen (H_2 and N_2 permeances were reduced by ≈ 90% and 50% respectively). A binary experiment with 75%H_2 and 25%N_2 (close to the 69% H_2 and 22%N_2 used in the mixture experiments) was carried out to observe how these components interact and transport through the membrane. Figure 6.32 shows the hydrogen permeance as a single gas, in the binary mixture (H_2 and N_2) and in the ternary mixture with ammonia.

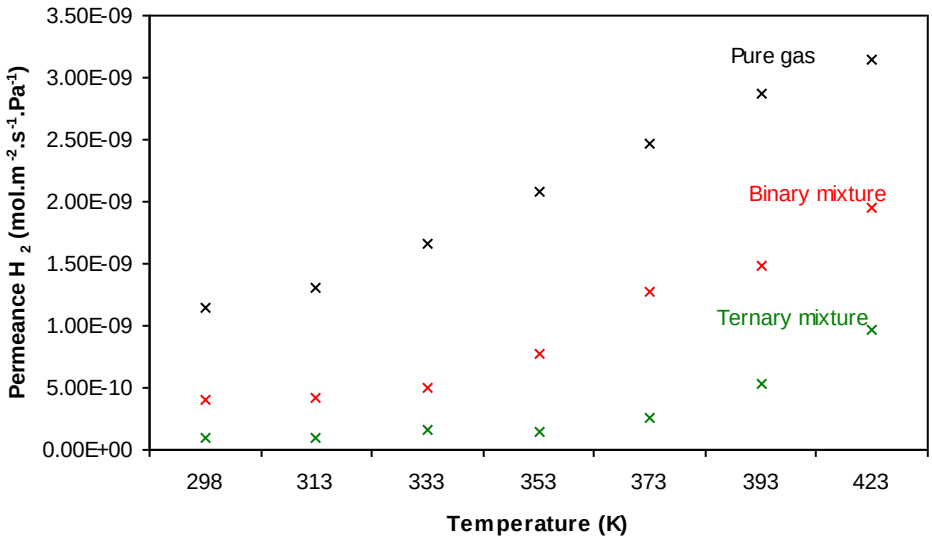

Figure 6.32: Permeance of hydrogen in MCT0.2 as a pure gas, in the binary mixture 75%N_2/25%H_2 and ternary mixture 9%NH_3/69%H_2/22%N_2.

From the results in Figure 6.32, it can be seen that hydrogen permeance in the binary mixture is lower than the single gas permeance. This is as expected since generally, for binary gas mixtures that are both weakly adsorbing, the permeance values in the mixture are somewhat lower than their single gas permeances (Lin et al, 2002). The results therefore confirm that nitrogen does affect hydrogen permeation. In the binary mixture, the hydrogen permeance is decreased by ≈ 60%, suggesting that nitrogen has more influence on hydrogen transport than was previously thought. From the single gas permeances, hydrogen permeates much faster than nitrogen. In the case of the

binary mixture, the slower diffusing molecule, nitrogen, may be slowing down the diffusion of the faster diffusing component, hydrogen. This phenomenon has often been observed in zeolite membranes and is referred to as single file diffusion, where the diffusion of the component diffusing faster in zeolite pores is slowed down, and the diffusion of the component diffusing slowly is accelerated (Cui et al, 2004).

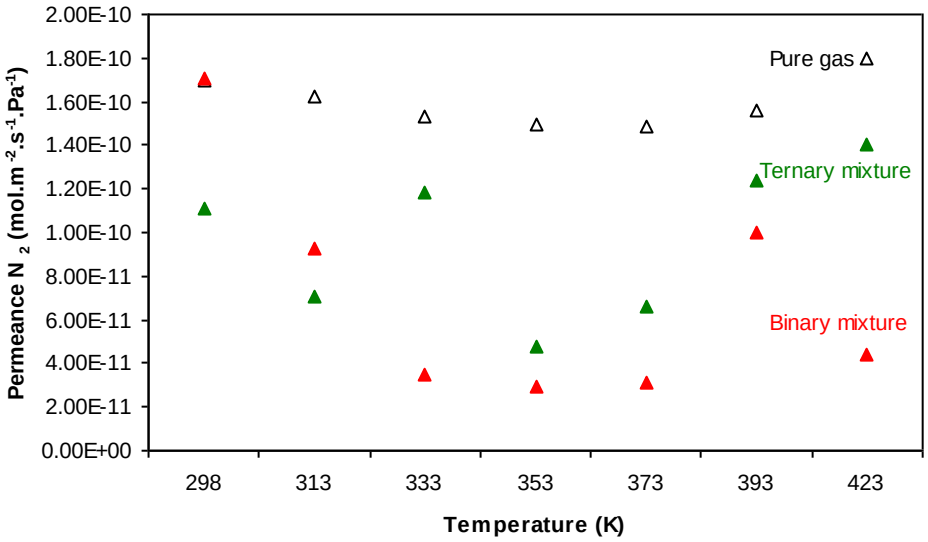

Figure 6.33: Permeance of nitrogen in MCT0.2 as a pure gas, in the binary mixture 75%N_2/25%H_2 and ternary mixture 9%NH_3/69%H_2/22%N_2.

In the case of nitrogen, the permeation of this component in the binary mixture is lower than that in the ternary mixture. It is not completely clear why this is the case. One explanation could be that the transport pathways are different for both mixtures. As was explained earlier, in the ternary mixture, the zeolite pores are blocked by adsorbed ammonia thereby hindering the hydrogen and nitrogen permeation. However as the temperature increases, ammonia desorbs and frees pathways for nitrogen and hydrogen which results in an increase in their permeances. In addition to this, it may be that both gases were permeating through the few intercrystalline defects present.

In the binary mixture, without ammonia blocking the pores, the nitrogen and hydrogen permeation is through zeolite pores. Therefore because the transport for nitrogen in the ternary mixture is a result of both transport through the zeolite pores and non-zeolite

pores, the resulting permeances (as temperature increases) are higher than those in the binary mixture. On the other hand, it could be that ammonia and hydrogen, both of which diffuse faster than nitrogen are enhancing its transport across the membrane.

The binary mixture results show that the interactions between the non-adsorbed molecules are a very important factor when considering the transport properties of a mixture containing one strongly adsorbed component in zeolite membranes. In the case of hydrogen, it was deduced from observing the single gas and ternary mixture permeances that the reduced hydrogen permeance observed in the $NH_3/H_2/N_2$ mixture compared to those of the single gas were due to ammonia adsorption resulting in a hindering effect. Hydrogen permeances in the mixture were reduced by 90% as has been mentioned previously and this decrease was assumed to be dependent only on the ammonia adsorbing and blocking hydrogen permeance. However, use of the potential barrier model, did not give good correlations. When binary mixture H_2/N_2 experiments were performed, it was found that the hydrogen permeances in the binary mixture reduced by ≈60% when compared to single gas permeance.

The hydrogen permeance in the ternary mixture is therefore a combination of both a) the slower diffusing nitrogen slowing down the faster diffusing hydrogen and b) the stronger adsorbing ammonia blocking pores and inhibiting hydrogen transport. For nitrogen, the binary mixture permeances were lower than that in the ternary mixture suggesting that the slower moving nitrogen may be enhanced by the presence of ammonia and hydrogen.

The potential barrier model could still be useful however. Better prediction of the permeances of hydrogen and nitrogen in the ternary mixture permeation could be obtained from the use of the binary mixture permeation for predictions, instead of pure gas permeations as described in Equation 6.10. For example, hydrogen permeance in the binary mixture is lower than that in the single gas. This has been attributed to the slower diffusing nitrogen slowing down hydrogen transport. Hydrogen permeation in the ternary is mixture is also lower than both the single gas and binary mixture permeances. This could be attributed to both the nitrogen “slowing effect” and the ammonia “adsorbing effect”. Therefore, the permeance of hydrogen and nitrogen in the binary mixture permeance could be used for ternary mixture prediction in place of

single gas permeances since the effect of both components in the binary mixture on each other (H_2 and N_2) has already been accounted for. Results from the potential barrier model are presented in sections 6.3.3.1 and 6.3.3.2.

6.3.3.1 As a function of Pressure

The results are presented using binary gas permeation of hydrogen and nitrogen respectively as P_o (Equation 6.10) and feed side coverage as described in section 6.3.1.

Table 6.15: Comparison of the measured and calculated permeance of H_2 in the mixture with feed side coverage as a function of pressure.

FP (kPa)	PP (kPa)	θ_F	H_2 Permeance (mol.m^{-2}.s^{-1}.Pa^{-1}) Binary gas P_o	H_2 Permeance (mol.m^{-2}.s^{-1}.Pa^{-1}) Calculated	H_2 Permeance (mol.m^{-2}.s^{-1}.Pa^{-1}) Measured
400	100	0.633	3.85E-10	1.2E-10	1.07E-10
600	100	0.809	4.80E-10	1.09E-10	0.41E-10
800	100	0.889	6.73E-10	1.31E-10	1.12E-10
1100	100	0.942	9.98E-10	1.77E-10	1.43E-10
1400	100	0.965	11.9E-10	2.03E-10	1.50E-10

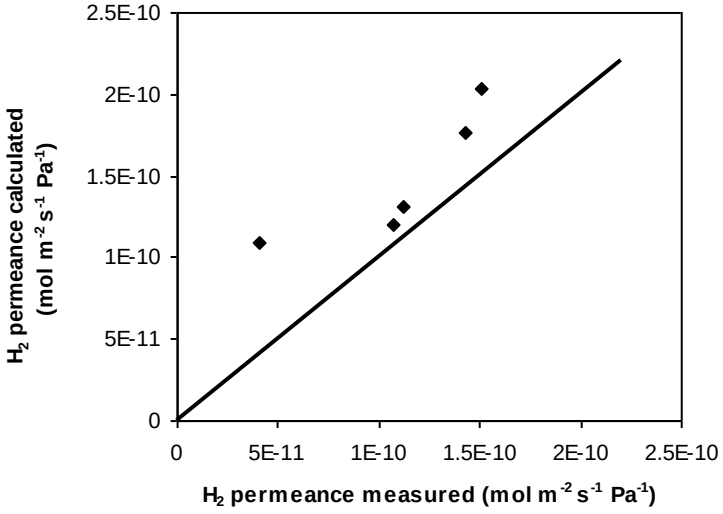

Figure 6.34: Comparison of the measured and calculated values of hydrogen permeance using ammonia coverage on the feed side

Table 6.16: Comparison of the measured and calculated permeance of N_2 in the mixture with feed side coverage as a function of pressure

FP (kPa)	PP (kPa)	θ_F	N_2 Permeance ($mol.m^{-2}.s^{-1}.Pa^{-1}$) Binary gas P_o	N_2 Permeance ($mol.m^{-2}.s^{-1}.Pa^{-1}$) Calculated	N_2 Permeance ($mol.m^{-2}.s^{-1}.Pa^{-1}$) Measured
400	100	0.633	1.03E-10	0.26E-10	0.55E-10
600	100	0.809	5.17E-10	0.91E-10	1.49E-10
800	100	0.889	6.08E-10	0.90E-10	0.74E-10
1100	100	0.942	8.43E-10	1.11E-10	1.17E-10
1400	100	0.965	10.4E-10	1.30E-10	1.28E-10

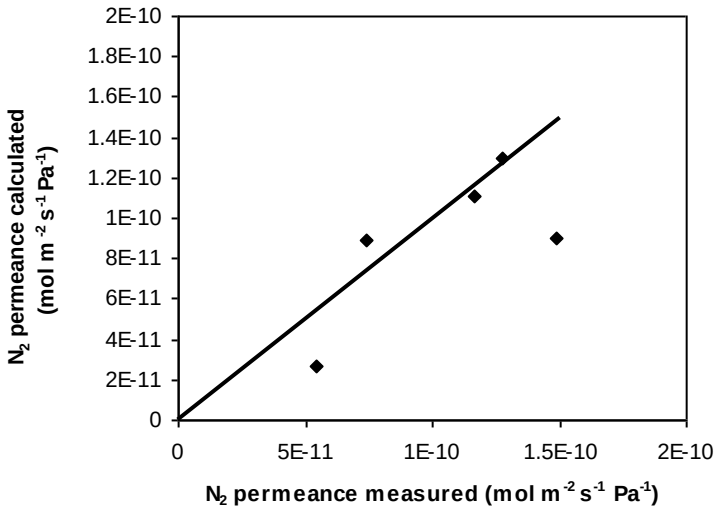

Figure 6.35: Comparison of the measured and calculated values of nitrogen permeance using ammonia coverage on the feed side.

Measured and calculated results for both hydrogen and nitrogen are compared in Tables 6.15 and 6.16 respectively. Using binary mixture permeation results of the individual components shows that there is improved correlation between experimental and calculated results. Figures 6.34 and 6.35 reveal a much better fit of the data by the model. The deviations observed for both hydrogen and nitrogen at 600kPa FP may be attributed to an error in the experimental values.

It may be concluded that the use of binary mixture permeation results of the components, and feed side coverage results in smaller discrepancies between

experimental values and calculated values than for the case using the single gas permeation results. Although there is some scatter in the data as shown in Figures 6.34 and 6.35, the prediction is generally acceptable. However, the agreement is still not perfect. What is needed is a model that includes diffusion effects. Also, interactions during multi-component separation are complex. Therefore, knowledge of multi-component adsorption and diffusion is needed to explain multi-component transport.

6.3.3.2 As a Function of Temperature

Table 6.17: Comparison of the measured and calculated permeance of H_2 in the mixture with coverage on the feed side as a function of temperature

Temperature (K)	θ_F	H_2 Permeance ($mol.m^{-2}.s^{-1}.Pa^{-1}$) Binary gas P_o	H_2 Permeance ($mol.m^{-2}.s^{-1}.Pa^{-1}$) Calculated	H_2 Permeance ($mol.m^{-2}.s^{-1}.Pa^{-1}$) Measured
298	0.976	3.98E-10	0.002E-10	1.04E-10
313	0.927	4.19E-10	0.005E-10	1.05E-10
333	0.781	5.03E-10	0.03E-10	1.54E-10
353	0.537	7.69E-10	0.25E-10	1.40E-10
373	0.298	12.7E-10	2.1E-10	2.55E-10
393	0.147	14.9E-10	6.42E-10	5.29E-10
423	0.050	19.5E-10	15.0E-10	9.73E-10

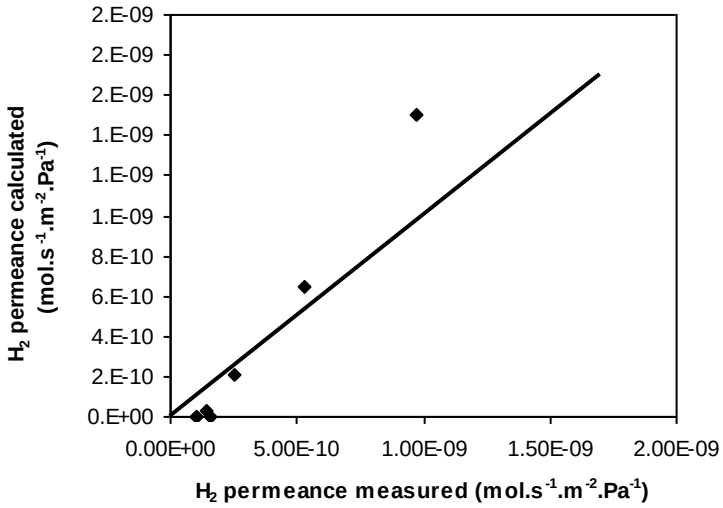

Figure 6.36: Comparison of the measured and calculated values of hydrogen permeance using ammonia coverage on the feed side.

Table 6.18: Comparison of the measured and calculated permeance of N_2 in the mixture with coverage on the feed side as a function of temperature

Temperature (K)	θ_F	N_2 Permeance ($mol.m^{-2}.s^{-1}.Pa^{-1}$) Binary gas P_o	N_2 Permeance ($mol.m^{-2}.s^{-1}.Pa^{-1}$) Calculated	N_2 Permeance ($mol.m^{-2}.s^{-1}.Pa^{-1}$) Measured
298	0.976	1.70E-10	0.14E-10	1.11E-10
313	0.927	0.92E-10	0.09E-10	0.71E-10
333	0.781	0.35E-10	0.05E-10	1.18E-10
353	0.537	0.30E-10	0.09E-10	0.47E-10
373	0.298	0.31E-10	0.17E-10	0.66E-10
393	0.147	1.00E-10	0.76E-10	1.24E-10
423	0.050	0.44E-10	0.40E-10	1.40E-10

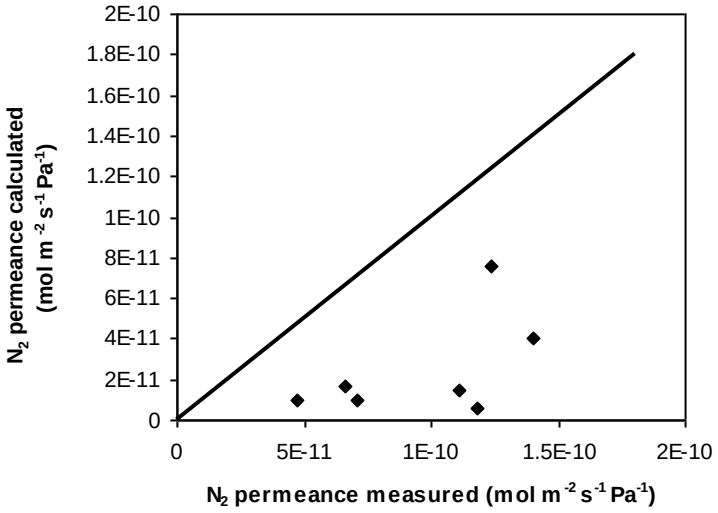

Figure 6.37: Comparison of the measured and calculated values of nitrogen permeance using ammonia coverage on the feed side.

The results shown in Tables 6.17 and 6.18 and Figures 6.36 and 6.37 as a function of temperature for hydrogen and nitrogen respectively deviate from the measured values. The deviation for nitrogen is the worst of the two. As has been discussed in section 6.3.2.2, the temperature affects gas permeances by influencing both adsorption and diffusion. The increase in mobility as a result of an increase in temperature has not been accounted for in the model and may explain why the model does not predict the permeances well, even when binary mixture permeation values are used. Other reasons for failure of the model include the extrapolation of isotherms at different temperatures which may contribute significantly to errors in the predictions.

6.4 Concluding Remarks

The potential barrier model fails to predict the permeances of hydrogen and nitrogen in a $NH_3/H_2/N_2$ mixture using pure gas permeances. Although it is well recognized that the presence of adsorbed molecules may significantly hinder the transport of a non-adsorbed component across a membrane, the diffusion effects of the weakly adsorbed components cannot be ignored. The model in its simplicity only requires data on the permeance of the pure adsorbing component (H_2 and N_2) and the adsorption equilibrium isotherms of the strongly adsorbing component. However as has been confirmed by the results of the model, this is not enough to predict the permeances in the ternary mixture.

The use of the binary mixture permeances gave much better correlations since the effects of hydrogen and nitrogen on each of the components' transport are taken into account. Using hydrogen as an example, it was observed in the ternary mixture that hydrogen permeance was reduced by about 90% when compared to single gas permeances. As ammonia is the strongly adsorbed component, it had been assumed that this reduction in hydrogen permeance was solely due to the hindrance effect of adsorbed ammonia. However, when binary mixture (H_2/N_2) permeance measurements were carried out, it was shown that hydrogen permeances were 50% lower than the pure gas permeances, which suggested that the hydrogen transport was slowed down by slower diffusing nitrogen. Therefore, the decrease in permeance for hydrogen observed in the ternary ($NH_3/H_2/N_2$) mixture is a result of both adsorption (ammonia blocking the pores and hindering permeation) and single file diffusion (nitrogen slowing down hydrogen).

It is also important to emphasize here that the isotherms at different temperatures were extrapolated and the corresponding coverage calculated from parameters obtained from the Langmuir-Freundlich isotherm model and a heat of adsorption calculated in Dragoi et al, (2004). The errors incurred here may pass on to the calculated coverages and may therefore not be truly representative of ammonia adsorption and its change with temperature. Measurements of ammonia adsorption isotherms at different

temperatures are therefore needed in order to obtain accurate values for adsorption coverage.

The results presented in Chapter 5 and the modelling in this chapter show that although membrane performance is strongly dictated by adsorption characteristics of the membrane, the diffusion effects cannot be ignored. The permeation and separation behaviour of the multi-component mixture ($NH_3/H_2/N_2$) in this MFI zeolite membrane can therefore be explained by the synergistic effects of preferential adsorption which enhances ammonia transport and reduces the permeation of weakly adsorbed hydrogen and nitrogen, and single file diffusion.

CHAPTER 7

CONCLUSIONS

7.0 Introduction

In this Chapter, the conclusions drawn from the work described in this thesis are presented. This chapter is divided into three main sections. Section 7.1 is a summary of the thesis findings. Overall conclusions are highlighted in section 7.2 and suggestions for future work are discussed in section 7.3.

7.1 Summary

The application of multi-channel tubular MFI zeolite membranes in the separation of ammonia from the synthesis loop in ammonia plants has been explored in this work. It has been highlighted that understanding the mechanisms of separation and obtaining reliable data on membrane performance is essential for the successful application of MFI zeolite membranes in ammonia plants. Single gas and mixture permeation tests have been performed in order to identify and understand the mechanisms of separation of this ammonia-membrane system. The influence of operating conditions (pressure, temperature, sweep gas flow etc.) has been studied experimentally and consequently, conditions for the optimum performance on this membrane (MCT0.2) for ammonia separation have been identified. In addition, the Potential Barrier Model has been

tested to determine its ability to describe the hindering effect of adsorbed ammonia on the permeation of weakly/non adsorbed hydrogen and nitrogen through a multi-channel tubular (MCT) MFI zeolite membrane.

The findings from this study are summarised as follows:

- Three models were compared for data analysis, the well mixed model, log mean pressure difference (LMPD) model and an improved model, the segmental model. The segmental was found to give the best representation of the behaviour of the membrane for all experimental conditions. In industrial application, the variations in concentrations and membrane fluxes in the direction along the membrane are important in design and analysis. The well-mixed and LMPD models cannot properly account for these important variations and therefore the segmental model is used for data analysis.

- Initial membrane screening showed that the MCT0.2 membrane had lower permeances than MCT0.5 but was much more selective. It was postulated that the higher permeances and lower selectivities of MCT0.5 were due to the presence of defects caused by incomplete plugging of the zeolite pores. Consequently, MCT0.2 was selected for further screening.

- Single (pure) gas permeance results showed that the permeances of single components in the MCT0.2 membrane correspond to an increase in molar mass. The light gases permeated faster than the heavier gases in the order H_2(2g/mol)>NH_3(17g/mol)>N_2(28g/mol).

- It has also been observed that the overall transport through the membrane is a combination of transport through zeolite (intracrystalline) pores and transport through small non-zeolite (intercrystalline) pores and that permeance and selectivity are highly dependent on operating conditions.

- Increase in differential pressure has little effect on pure gas permeances of the weakly adsorbing gases hydrogen and nitrogen. This also confirms membrane

quality as the presence of large defects would lead to an increase in permeance with differential pressure.

- In terms of transport mechanisms for single gases at these conditions (298K), the permselectivities for both H_2/N_2 (9.5 -6.9) and H_2/NH_3 (5.33) are higher than the Knudsen selectivity (3.74 and 2.65 respectively) which indicates that the transport of these molecules involve configurational diffusion. Nitrogen is also a weakly adsorbed molecule, but due to its size, has a stronger interaction with the MFI zeolite pore and transport is in the transition regime between Knudsen and configurational.

- Ammonia is the strongly adsorbed component, and the likely mechanism of transport in this membrane as a single gas is surface diffusion. However, the observed behaviour in ammonia permeance with increase in differential pressure suggests that another mechanism, capillary condensation occurs in the intercrystalline pores. Therefore, the transport of ammonia in this membrane is by surface diffusion in the intracrystalline (zeolite) pores in parallel with capillary condensation in the intercrystalline (non-zeolite) pores.

- Pure gas permeances have been shown to be highly dependent on temperature. Hydrogen pure gas permeance increases monotonically with temperature and transport is dominated by activated diffusion. An activation energy of 9 kJ/mol was calculated which is in line with values reported in the literature by Lovallo and Tsapatsis (1996) and Bai et al, (1995) for similar membranes. Nitrogen pure gas permeance shows a minimum and is not activated (Ea = 0.08kJ/mol). This has been attributed to transition from surface diffusion to activated gaseous diffusion.

- The separation of ammonia from a mixture with hydrogen and nitrogen is by preferential adsorption of ammonia, which hinders the permeation of weakly adsorbed hydrogen and nitrogen. The permeances increased in the order $NH_3>H_2>N_2$. Ammonia permeances in the mixture increased by ≈ 80% when

compared to ammonia single gas permeances. Hydrogen permeances decreased by ≈ 90% and N_2 by ≈ 50%.

- In the mixture gas separation experiments, differential pressure has only relatively small effects on the permeances in the pressure range evaluated in this work. No significant change was observed for ammonia permeance with an increase in differential pressure. The permeances of hydrogen and nitrogen increased slightly. This was attributed to extra flow through some intercrystalline pores. As a result, selectivities decreased with an increase in differential pressure.

- Increase in sweep flow rate has little effect on ammonia gas permeance, but hydrogen and nitrogen permeances increase. It has been suggested that an increase in partial pressure due the use of a mixed sweep (3:1 N_2/H_2) of nitrogen and hydrogen increases their driving force and thus increases their permeances. This leads to a decrease in selectivities ($\alpha NH_3/N_2$ and $\alpha NH_3/H_2$). The optimum sweep flow rate for the highest selectivities at 298K and 1550 Kpa ($\alpha NH_3/N_2 = 7$ and $\alpha NH_3/H_2 = 6$) was found to be 15ml min^{-1}.

- Increase in feed flowrate also has little effect on ammonia permeance however, a decrease in permeance was observed at 1200 ml min^{-1}. The nitrogen and hydrogen permeance increase due to an increase in the driving force and therefore the selectivities decrease with increasing feed flow rate.

- Membrane performance was found to be highly dependent on temperature. Ammonia permeance in the mixture increases linearly with temperature. Hydrogen increased exponentially and the increase is observed from 353K. Nitrogen displays a minimum but starts to increase after 353K. The increase in permeance for ammonia is due to an increase in mobility with an increase in temperature. The increase in hydrogen and nitrogen permeance after 353K is due to the fact that the amount of ammonia adsorbed at this temperature (353K) reduces significantly and therefore hindrance to hydrogen and nitrogen permeation is reduced. There is also an increase in mobility of the two

components with an increase in temperature. Therefore a maximum selectivity is obtained at 353K ($\alpha NH_3/N_2$ = 46 and $\alpha NH_3/H_2$ = 15) and is the optimum temperature for membrane performance.

- From both the single gas permeation and ternary mixture gas permeation results, it has been concluded that transport through the membrane is a combination of transport through zeolite (intracrystalline) pores which is mostly selective and transport through small non-zeolite (intercrystalline) pores (<2nm) which is largely non-selective and that permeance and selectivity are highly dependent on operating conditions, especially temperature and pressure.

- Although the potential barrier model can describe the hindering effects of strongly adsorbed ammonia on weakly adsorbed nitrogen and hydrogen permeances, it failed to correctly predict hydrogen and nitrogen permeances in the ternary mixture using pure gas (H_2 and N_2) permeances. The model over predicted hydrogen permeance in the mixture and under predicted nitrogen permeances.

- Binary mixture permeation H_2/N_2 showed that there are diffusion effects (single file diffusion) that have not been taken into account in the Potential Barrier Model. The hydrogen permeance in the binary mixture was lower than that as a pure gas. Therefore it was suggested that slower diffusing nitrogen is slowing down faster diffusing hydrogen. The observed decrease in hydrogen permeance in the ternary mixture is therefore a result of both the nitrogen slowing effect and ammonia adsorption hindrance effect.

- The results from the binary mixture permeation experiments explain why pure gas permeances cannot be used to predict permeances in the ternary gas mixture as the Potential Barrier Model does not take into account the diffusion effects described. When permeances of the individual components in the binary mixture are used instead of the pure gas permeances, there is a much better agreement between experimental and predicted results.

- The results confirm that permeation and separation in this MCT0.2 membrane is a function of both preferential adsorption and single file diffusion effects. The preferential adsorption of ammonia and the resulting hindrance of hydrogen and nitrogen is the main mechanism for separation, however, it has been shown that diffusion effects, i.e. the slowing down of hydrogen and nitrogen could be responsible for the reduction in hydrogen permeance observed in the ternary mixture.

7.2 Overall Conclusions

Permeation data has been presented which gives an overview of the permeation and separation mechanisms of a homogeneous α-alumina supported MFI zeolite membrane. This membrane can successfully separate ammonia from its multi-component mixture with nitrogen and hydrogen. This is achieved because ammonia is transported preferentially over hydrogen and nitrogen due to its strong adsorption. The results have also added to the fundamental understanding of multi-component transport in nanocomposite multi-channel tubular membranes.

The highest permeance obtained for this membrane was 2.16×10^{-9} mol m^{-2} s^{-1} Pa^{-1} and a selectivity $NH_3/H_2 = 15$ at 80°C. Compared to the project target of 2.4×10^{-7} mol m^{-2} s^{-1} Pa^{-1} and selectivity $NH_3/H_2 > 15$, the selectivities are high and within the target but a significant improvement of ammonia permeance is needed. Nevertheless, several advantages can be accrued with this homogeneous MCT0.2 membrane. It possesses good separation qualities and has a high selectivity for ammonia. This research has therefore paved the way for selective membrane systems for separation and recovery of ammonia and also the possible application of this type of membrane to other industrial applications. In the present form, this membrane is more suitable in cases where selectivity is more important than permeance.

7.3 Future Work

The work carried out in this investigation has led to a series of interesting observations. The following suggestions are proposed as interesting future directions for this work:

- Preparation of more defect free MCT0.2 type membranes. Reproducibility of both the membranes and permeation results is needed to justify use in industrial applications.

- Precise measurement of ammonia adsorption on ZSM-5 membranes. For mixture permeation, multi-component isotherms are needed. It has been found that adsorption properties in membrane may vary greatly from those in the bulk e.g. because of differences in composition such as Si/Al ratio, therefore it would be desirable to measure adsorption characteristics of sorbates on a functioning membrane.

- Diffusive properties of these individual molecules i.e. ammonia, nitrogen and hydrogen and also the multi-component mixture in the membrane need to be studied extensively and factors that affect diffusion examined. The effect of single file diffusion in the multi-component system in particular needs to be explored further.

- Extension and/or modification of the Potential Barrier model to be able to predict mixture permeances from single gas permeances.

REFERENCES

(1996) Terminology for membranes and membrane processes (IUPAC Recommendation 1996). *Journal of Membrane Science,* **120,** 149-159.

Aguado, S., Polo, S.A.C., Bernal, M.P., Coronas, J., Santamaria,J. (2004). Removal of pollutants from indoor air using zeolite membranes. *Journal of Membrane Science*. **240**, 159-166.

Algieri, C., Bernardo, P., Golemme, G., Barbieri, G. & Drioli, E. (2003) Permeation properties of a thin silicalite-1 (MFI) membrane. *Journal of Membrane Science,* **222,** 181-190.

Alimov, V., Busnyuk, A., Notkin, M., Livshits, A. (2014) Pd–V–Pd composite membranes: Hydrogen transport in a wide pressure range and mechanical stability. *Journal of Membrane Science*, **457**, 103-112.

Al-Mufachi, N., Rees, N., Steinberger-Wilkens, R. (2015) Hydrogen selective membranes: A review of palladium-based dense metal membranes. *Renewable and Sustainable Energy Reviews*, **47**, 540-551.

Alshebani, A.; Pera-Titus, M.; Yeung, K.; Miachon, S.; Dalmon, J. (2008) Influence of desorption conditions before gas separation studies in nanocomposite MFI–alumina membranes. *Journal of Membrane Science*, **314**, 143-151.

Akhtar, F., Sjöberg, E., Korelskiy, D., Rayson, M., Hedlund, J., Bergström, L. (2015) Preparation of graded silicalite-1 substrates for all-zeolite membranes with excellent CO2/H2 separation performance. *Journal of Membrane Science*, **493**, 206-211.

Anderson, M. W., Pachis, K. S., Shi, J. & Carr, S. W. (1992) Synthesis of self – supporting films. *Journal of Materials Chemistry*, **2,** 255-256.

Aoki, K., Kusakabe, K. & Morooka, S. (1998) Gas permeation properties of A-type zeolite membrane formed on porous substrate by hydrothermal synthesis. *Journal of Membrane Science,* **141,** 197-205.

Aoki, K., Tuan, V. A., Falconer, J. L. & Noble, R. D. (2000) Gas permeation properties of ion-exchanged ZSM-5 zeolite membranes. *Microporous and Mesoporous Materials,* **39,** 485-492.

Anantharaman, B., Hazarika S., Ahmad, T., Nagvekar, M., Ariyapadi, S., Gualy, R. (2012) Coal gasification technology for ammonia plants. *Nitrogen & Syngas Conference,[Online] 20-23rd February, Athens, Greece* pp 1-10 [Accessed January 20th, 2015] Available from: http://kbr.com/%2FNewsroom%2FPublications%2FWhitepapers%2FCoal-Gasification-Technology-for-Ammonia-Plants.pdf

Arruebo, M., Coronas, J., Menendez, M. & Santamaria, J. (2001) Separation of hydrocarbons from natural gas using silicalite membranes. *Separation and Purification Technology,* **25,** 275-286.

Arruebo, M., Falconer, J. L. & Noble, R. D. (2006) Separation of binary C5 and C6 hydrocarbon mixtures through MFI zeolite membranes. *Journal of Membrane Science,* **269,** 171-176.

Asaeda, M. & Yamasaki, S. (2001) Separation of inorganic/organic gas mixtures by porous silica membranes. *Separation and Purification Technology,* **25,** 151-159.

Ash, R., Barrer, R. M. & Lowson, R. T. (1973) Transport of single gases and of binary gas mixtures in a microporous carbon membrane. *Journal of the Chemical Society-Faraday Transactions I,* **69,** 2166-2178.

Au, L. T. Y. & Yeung, K. L. (2001) An investigation of the relationship between microstructure and permeation properties of ZSM-5 membranes. *Journal of Membrane Science,* **194,** 33-55.

Auroux, A., Muscas, M., Coster, D. J. & Fripiat, J. J. (1994) Distribution of acid sites and differential heat of NH3 chemisorption on some aluminas and zeolites. *Catalysis Letters,* **28,** 179-186.

Avila, A., Funke, H., Zhang, Y., Falconer, J., Noble, R. (2009) Concentration polarization in SAPO-34 membranes at high pressures. *Journal of Membrane Science*, **335**, 32-36.

Ayral, A., Julbe, A., Roussac,V., Roualdes,S., Durand, J. (2008) Microporous silica membranes: Basic principles and recent advances. *Membrane Science and Technology*, **13**, 33-79.

Bai, C., Jia, M.-D., Falconer, J. L. & Noble, R. D. (1995) Preparation and separation properties of silicalite composite membranes. *Journal of Membrane Science,* **105,** 79-87.

Baker, R. W. (2002) Future directions of membrane gas separation technology. *Industrial & Engineering Chemistry Research*, **41,** 1393-1411.

Bakker, W. J. W., Kapteijn, F., Poppe, J. & Moulijn, J. A. (1996) Permeation characteristics of a metal-supported silicalite-1 zeolite membrane. *Journal of Membrane Science,* **117,** 57-78.

Bakker, W. J. W., Van Den Broeke, L. J. P., Kapteijn, F. & Moulijn, J. A. (1997) Temperature dependence of one-component permeation through a silicalite-1 membrane, AIChE Journal**, 43,** 22034-2214.

Barbieri, G., Marigliano, G., Golemme, G. & Drioli, E. (2002) Simulation of CO_2 hydrogenation with CH_3OH removal in a zeolite membrane reactor. *Chemical Engineering Journal,* **85,** 53-59.

Barrer, R. M. (1990) Porous Crystal Membranes. *Journal of the Chemical Society. Faraday Transactions,* **86,** 1123-1130.

Basu, A., Akhtar, J., Rahman, M. H. & Islam, M. R. (2004) A review of separation of gases using membrane systems, *Petroleum Science and Technology.* **22,** 1343-1368.

Battersby, S., Tasaki, T., Smart, S., Ladewig, B., Liu, S., Duke, M.; Rudolph, V.; Diniz da Costa, J. (2009) Performance of cobalt silica membranes in gas mixture separation. *Journal of Membrane Science,* **329**, 91-98.

Bayati, B., Belbasi, Z., Ejtemaei, M., Charchi Aghdam, N., Babaluo, A., Haghighi, M., Drioli, E. (2013) Separation of pentane isomers using MFI zeolite membrane. *Separation and Purification Technology*,**106**, 56-62.

Bein, T. (1996) Synthesis and applications of molecular sieve layers and membranes. *Chemistry of Materials,* **8,** 1636-1653.

Bernado, P., Clarizia, G. (2013) 30 years of membrane technology for gas separation. *Chemical Engineering Transactions*,**32**,1999-2004. DOI:10.3303/CET1332334

Berenguer-Murcia, A., Gora, L., Zhu, W., Jansen, J.C., Kapteijn, F., Cazorla-Amoros, D., Linares-Solano, A. (2007) Synthesis and Permeation Properties of Silicalite-1/Carbon Membranes. *Industrial and Engineering Chemistry Research,* **46**, 3997-4006.

Bernal, M. P., Coronas, J., Menendez, M. & Santamaria, J. (2002) Characterization of Zeolite Membranes by Measurement of Permeation Fluxes in the Presence of Adsorbable Species. *Industrial & Engineering Chemistry Research,* **41,** 5071-5078.

Bernal, M. P., Coronas, J., Menendez, M. & Santamaria, J. (2003) On the effect of morphological features on the properties of MFI zeolite membranes. *Microporous and Mesoporous Materials,* **60,** 99-110.

Beuscher, U., Gooding, C.H. (1998) The permeation of binary gas mixtures through support structures of composite membranes. *Journal of Membrane Science*, **150**, 57-73.

Bhown, A. & Cussler, E. L. (1991) Mechanism for selective Ammonia Transport through Poly(vinylammonium thiocyanate) Membrane. *Journal of the American Chemical Society,* **113,** 742-749.

Boki, K., Tanada, S.,Nobuhiro, O., Tsutsui, S.,Yamasaki, R., Nakamura, M. (1987) Adsorption of Polar and Non-polar Gases of Different Sizes on Nitrogen-Containing Activated Carbon. *Journal of Colloid Interface Science*, **120**, 286−288

Bonhomme, F., Welk, M. E. & Nenoff, T. M. (2003) CO2 selectivity and lifetimes of high silica ZSM-5 membranes. *Microporous and Mesoporous Materials,* **66,** 181-188.

Bowen, T.C., Noble, R.D., Falconer, J.L. (2004) Fundamentals and applications of pervaporation through zeolite membranes. *Journal of Membrane Science*, **245**, 1-33.

Brubaker, D.W., Kammermeyer, K (1954) Separation of gases by plastic membranes – permeation rates and extent of separation. *Industrial & Engineering Chemistry Research,* **46 ,** 733-739.

Burggraaf, A. J. (1999) Single gas permeation of thin zeolite (MFI) membranes: theory and analysis of experimental observations. *Journal of Membrane Science,* **155,** 45-65.

Bux, H., Chmelik, C., Krishna, R., Caro, J. (2011) Ethene/Ethan separation by MOF membrane ZIF-8: Molecular correlation of permeation, adsorption, diffusion. *Journal of Membrane Science*, **369**, 284-289.

Campaniello, J., Engelen, C. W. R., Haije, W. G., Pex, P. & Vente, J. F. (2004) Long-term pervaporation performance of microporous methylated silica membranes. *Chemical Communications***, 7**, 834-835.

Camus, O., Perera, S., Crittenden, B., Van Delft, Y. C., Meyer, D. F., Pex, P., Kumakiri, I., Miachon, S., Dalmon, J. A., Tennison, S. & Chanaud, P. (2006) Ceramic membranes for ammonia recovery. *Aiche Journal,* **52,** 2055-2065.

Caro, J. (2011). Are MOF membranes better in gas separation than those made of zeolites? *Current Opinion in Chemical Engineering* [*Online*]. **1**, 77-83 Available from: www.sciencedirect.com. [10th January 2015].

Caro, J., Noack, M. & Kolsch, P. (2005) Zeolite Membranes: From the Laboratory Scale to Technical Applications. *Adsorption,* **11,** 215-227.

Caro, J., Noack, M., Kolsch, P. & Schafer, R. (2000) Zeolite membranes - state of their development and perspective. *Microporous and Mesoporous Materials,* **38,** 3-24.

Centeno, T. A., Vilas, J. L. & Fuertes, A. B. (2004) Effects of phenolic resin pyrolysis conditions on carbon membrane performance for gas separation. *Journal of Membrane Science,* **228,** 45-54.

Chiang, A. S. T. & Chao, K.-J. (2001) Membranes and films of zeolite and zeolite-like materials. *Journal of Physics and Chemistry of Solids,* **62,** 1899-1910.

Choe, J. S., Lyndon, J. & Kellog, J. (1995) Membrane-assisted process to produce ammonia. USA, Air Products and Chemicals, Inc.

Choi, J.G., Do, D.D., Do, H.D. (2001) Surface diffusion of adsorbed molecules in porous media: monolayer, multilayer, and capillary condensation regimes. *Industrial & Engineering Chemistry Researc*h, **40**, 4005-4031.

Choi, J., Jeong, H., Snyder, M., Stoeger, J., Masel, R., Tsapatsis, M. (2009) Grain Boundary Defect Elimination in a Zeolite Membrane by Rapid Thermal Processing. *Science*, **325**, 590-593.

Ciavarella, P., Moueddeb, H., Miachon, S., Fiaty, K. & Dalmon, J.-A. (2000) Experimental study and numerical simulation of hydrogen/isobutane permeation and separation using MFI-zeolite membrane reactor. *Catalysis Today.* **56,** 253-264.

Clark, T. E., Deckman, H. W., Cox, D. M. & Chance, R. R. (2004) In situ determination of the adsorption characteristics of a zeolite membrane. *Journal of Membrane Science.* **230,** 91-98.

Cornelius, C., Hibshman, C. & Marand, E. (2001) Hybrid organic-inorganic membranes. *Separation and Purification Technology.* **25,** 181-193.

Coronas, J., Falconer, J. L. & Noble, R. D. (1997) Characterization and permeation properties of ZSM-5 tubular membranes. *AIChE Journal.* **43,** 1797-1812.

Coronas, J., Noble, R. D. & Falconer, J. L. (1998) Separations of C4 and C6 isomers in ZSM-5 tubular membranes. *Industrial & Engineering Chemistry Research,* **37,** 166-176.

Coronas, J. & Santamaria, J. (1999) Separations using zeolite membranes. *Separation and Purification Methods,* **28,** 127-177.

Coughlan, B. & Mccann, W. A. (1979) Adsorption properties of zeolitic ruthenium and of chromium, iron and lanthanum mordenites. Part 1.—Equilibria and Affinities. *Journal Of The Chemical Society, Faraday Transactions 1: Physical Chemistry In Condensed Phases***, 75,** 1969-1983.

Crittenden, B.D. & Thomas, W.I., 1998, *Adsorption Technology and Design*, Butterworth-Henemann, Oxford.

Cui, Y., Kita, H. & Okamoto, K. (2004) Preparation and gas separation performance of zeolite T membrane. *Journal of Materials Chemistry,* **14,** 924-932.

Cussler, E.L., (1984). *Diffusion,* London: Cambridge University Press.

Daramola, M.O., Aransola, E.F., Ojumu, T.V. (2012) Potential applications of zeolite membranes in reaction coupling separation processes. *Materials* [*Online*]. **5**, 2101-2136. Available from: www.mdpi.com/journal/materials. [13th Jan 2015]

Darmawan, A., Motuzas, J.; Smart, S., Julbe, A., Diniz da Costa, J. (2015) Temperature dependent transition point of purity versus flux for gas separation in Fe/Co-silica membranes. *Separation and Purification Technology*, **151**, 284-291.

Davis, S. P., Borgstedt, E. V. R. & Suib, S. L. (1990) Growth of zeolite crystallites and coatings on metal-surfaces. *Chemistry of Materials,* **2,** 712-719.

De Lange, R. S. A., Keizer, K. & Burggraaf, A. J. (1995) Analysis and theory of gas transport in microporous sol-gel derived ceramic membranes. *Journal of Membrane Science,* **104,** 81-100.

De Vos, R. M., Maier, W. F. & Verweij, H. (1999) Hydrophobic silica membranes for gas separation, *Journal of Membrane Science.* **158,** 277-288.

Deng, Z.; Nicolas, C.; Daramola, M.; Sublet, J.; Schiestel, T.; Burger, A.; Guo, Y.; Giroir-Fendler, A.; Pera-Titus, M. (2010) Nanocomposite MFI-alumina hollow fiber membranes prepared via pore-plugging synthesis: Influence of the porous structure of hollow fibers on the gas/vapour separation performance. *Journal of Membrane Science*, **364**, 1-8.

Derouane, E. G. & Chang, C. D. (2000) Confinement effects in the adsorption of simple bases by zeolites, *Microporous and Mesoporous Materials.* **35-36,** 425-433.

Drobek, M., Bechelany, M., Vallicari, C., Abou Chaaya, A., Charmette, C., Salvador-Levehang, C., Miele, P., Julbe, A. (2015) An innovative approach for the preparation of confined ZIF-8 membranes by conversion of ZnO ALD layers. *Journal of Membrane Science*, **475**, 39-46.

Dondur, V., Rakic, V., Damjanovic, L. & Auroux, A. (2005) Comparative study of the active sites in zeolites by different probe molecules. *Journal of Serbian Chemical Society,* **70,** 457-474.

Do, D., (1998). *Adsorption Analysis: Equilibria and Kinetics*, London: Imperial College Press.

Dong, J. L., Lin,Y.S., Wei, L. (2000) Multicomponent Hydrogen/Hydrocarbon Separation by MFI-Type Zeolite Membranes. *AIChE Journal*, **46,** 1957-1966.

Dong, J. X., Dou, T., Zhao, X. G. & Gao, L. H. (1992) Synthesis of membranes of zeolites ZSM-5 and ZSM-35 by the vapor-phase method. *Journal of the Chemical Society-Chemical Communications***, 15,** 1056-1058.

Doshi, K. J. (1978) Recovery of hydrogen and nitrogen from ammonia plant purge gas Union Carbide Corporation (New York, NY)

Dragoi, B., Gervasini, A., Dumitriu, E. & Auroux, A. (2004) Calorimetric determination of the acidic character of amorphous and crystalline aluminosilicates. *Thermochimica Acta*, **420,** 127-134.

Drobek, M., Motuzas, J., van Loon, M., Dirrix, R., Terpstra, R., Julbe, A. (2012) Coupling microwave-assisted and classical heating methods for scaling-up MFI zeolite membrane synthesis. *Journal of Membrane Science*, **401-402**, 144-151.

Duke, M. C., Da Costa, J. C. D., Lu, G. Q. & Gray, P. G. (2006) Modeling hydrogen separation in high temperature silica membrane systems. *AIChE Journal*, **52,** 1729-1735.

Dunne, J.A., Mariwala, R., Rao, M., Sircar, S, Gorte, R.J & Myers, A.L (1996a) Calorimetric Heats of Adsorption and Adsorption Isotherms. 1. O2, N2, Ar, CO2, CH4, C2H6, and SF6 on Silicalite . *Langmuir*, **12**, 5888-5895

Dunne, J.A., Rao, M., Sircar, S, Gorte, R.J & Myers, A.L. (1996b) Calorimetric Heats of Adsorption and Adsorption Isotherms. 2. O2, N2, Ar, CO2, CH4, C2H6, and SF6 on NaX, H-ZSM-5, and Na-ZSM-5 Zeolite, *Langmuir*, **12**, 5896-5904.

Duval, J. M., Folkers, B., Mulder, M. H. V., Desgrandchamps, G. & Smolders, C. A. (1993) Adsorbent filled membranes for gas separation. Part 1. Improvement of the gas separation properties of polymeric membranes by incorporation of microporous adsorbents. *Journal of Membrane Science,* **80,** 189-198.

Farooq, S. & Karimi, I. A. (2001) Modeling support resistance in zeolite membranes. *Journal of Membrane Science,* **186,** 109-121.

Foote, H. W. & Hunter, M. A. (1920) Equilibrium in the system ammonia-ammonium thiocyanate. *Journal of the American Chemical Society,* **42,** 69-78.

Forni, L., Vatti, F. P. & Ortoleva, E. (1995) Temperature-programmed desorption-diffusion of ammonia in molecular sieves V. ZSM-5 zeolite. *Microporous Materials.* **3,** 367-375.

Freemantle, M. (2005) Membranes for gas separation. *Chemical & Engineering News[Online]*, **43**, 49-57. Available from: http://pubs.acs.org/cen/coverstory/83/8340membranes.html [August 2007].

Fuertes, A. B. (2000) Adsorption-selective carbon membrane for gas separation. *Journal of Membrane Science,* **177,** 9-16.

Fuertes, A. B. & Centeno, T. A. (1998) Carbon molecular sieve membranes from polyetherimide. *Microporous and Mesoporous Materials,* **26,** 23-26.

Funke, H. H., Argo, A. M., Baertsch, C. D., Falconer, J. L. & Noble, R. D. (1996) Separation of close-boiling hydrocarbons with silicalite zeolite membranes. *Journal of the Chemical Society-Faraday Transactions,* **92,** 2499-2502.

Funke, H. H., Frender, K. R., Green, K. M., Wilwerding, J. L., Sweitzer, B. A., Falconer, J. L. & Noble, R. D. (1997) Influence of adsorbed molecules on the permeation properties of silicalite membranes. *Journal of Membrane Science,* **129,** 77-82.

Garcia-Martinez, J., Cazorla-Amoros, D., Linares-Solano, A., & Lin, Y.S. (2001) Synthesis and characterisation of MFI-type zeolites supported on carbon materials. *Microporous and Mesoporous Materials*, **42**, 255–268.

Gardner, T. Q., Flores, A. I., Noble, R. D. & Falconer, J. L. (2002) Transient measurements of adsorption and diffusion in H-ZSM-5 membranes, *AIChE Journal*. **48,** 1155-1167.

Gardner, T., Martinek, J., Falconer, J., Noble, R. (2007) Enhanced flux through double-sided zeolite membranes. *Journal of Membrane Science*, **304**, 112-117.

Gascon, J., Kapteijn, F., Zornoza, B., Sebastian, V., Casado, C., Coronas, J. (2012). Practical approach to zeolitic membranes and coatings: state of the art, opportunities, barriers and future perspectives. *Chemistry of Materials* [Online], **24**, 2829-2844. Available from: http://pubs.acs.org/doi/abs/10.1021/cm301435j Accessed on 15th Jan, 2015.

Gasser, R.P.H (1985) An Introduction to Chemisorption and Catalysis by Metals. Oxford science publications.

Gavalas, G. R., Megiris, C. E. & Nam, S. W. (1989) Deposition of H2 permselective SiO2 films. *Chemical Engineering Science*, 44**,** 1829.

Geus, E. R., Denexter, M. J. & Vanbekkum, H. (1992) Synthesis and characterization of zeolite (mfi) membranes on porous ceramic supports, *Journal of the Chemical Society-Faraday Transactions*. **88,** 3101-3109.

GiroirFendler, A., Peureux, J., Mozzanega, H. & Dalmon, J. A. (1996) Characterization of a zeolite membrane for Catalytic Membrane Reactor application. *11th International Congress on Catalysis - 40th Anniversary, Pts A and B.*

Gonzales, M. R., Sharma, S. B., Chen, D. T. & Dumesic, J. A. (1993) Thermogravimetric and microcalorimetric studies of ZSM-5 acidity, *Catalysis Letters*. **18,** 183-192.

Gopalakrishnan, S., Yamaguchi, T., Nakao, S. (2006) Permeation Properties of Templated and Template-free ZSM-5 membranes, *Journal of Membrane Science.* **274**, 102-107.

Gualtieri, L.M., Gualtieri, A.F, Hedlund, J., Jareman, J.,Sterte, M.,Dapiaggi, M. (2004) Accurate measurement of the thermal expansion of MFI zeolite membranes by in situ HTXRPD, *Studies in Surface Science and Catalysis*, **154A**, 703-709.

Guizard, C., Bac, A., Barboiu, M. & Hovnanian, N. (2001) Hybrid organic-inorganic membranes with specific transport properties: Applications in separation and sensors technologies. *Separation and Purification Technology*, **25,** 167-180.

Gump, C. J., Lin, X., Falconer, J. L. & Noble, R. D. (2000) Experimental configuration and adsorption effects on the permeation of C4 isomers through ZSM-5 zeolite membranes. *Journal of Membrane Science*, **173,** 35-52.

Gump, C. J., Noble, R. D. & Falconer, J. L. (1999) Separation of Hexane Isomers through Nonzeolite Pores in ZSM-5 Zeolite Membranes. *Industrial & Engineering Chemistry Researc*h, **38,** 2775-2781.

Hanebuth, M., Dittmeyer, R., Mabande, G. T. P. & Schwieger, W. (2005) On the combination of different transport mechanisms for the simulation of steady-state mass transfer through composite systems using H2/SF6 permeation through stainless steel supported silicalite-1 membranes as a model system, *Catalysis Today.* **104,** 352-359.

Hasegawa, Y., Ikeda, T., Nagase, T., Kiyozumi, Y., Hanaoka, T. & Mizukami, F. (2006) Preparation and characterization of silicalite-1 membranes prepared by secondary growth of seeds with different crystal sizes, *Journal of Membrane Science.* **280,** 397-405.

He, G., Mi, Y., Lock Yue, P.,Chen, G. (1999) Theoretical Study On Concentration Polarization In Gas Separation Membrane Processes, *Journal of Membrane Science*, **153**, 243-258.

He, Y. & Cussler, E. L. (1992) Ammonia permeabilities of perfluorosulfonic membranes in various ionic forms, *Journal of Membrane Science.* **68,** 43-52.

Hedlund, J., Noack, M., Kolsch, P., Creaser, D., Caro, J. & Sterte, J. (1999) ZSM-5 membranes synthesized without organic templates using a seeding technique. *Journal of Membrane Science,* **159,** 263-273.

Hedlund, J., Sterte, J., Anthonis, M., Bons, A. J., Carstensen, B., Corcoran, N., Cox, D., Deckman, H., De Gijnst, W., De Moor, P. P., Lai, F., Mchenry, J., Mortier, W. & Reinoso, J. (2002) High-flux MFI membranes. *Microporous and Mesoporous Materials,* **52,** 179-189.

Heffer, P., Prud'homme, M. (2008) Outlook for World Fertilizer Demand, Supply and Supply/Demand Balance, *Turkish Journal of Agriculture and Forestry.* **32**, 159-164.

Helminen, J., Helenius, J., Paatero, E. & Turunen, I. (2000) Comparison of sorbents and isotherm models for NH3-gas separation by adsorption, *AIChE Journal.* **46,** 1541-1555.

Helminen, J., Helenius, J., Paatero, E. & Turunen, I. (2001) Adsorption Equilibria of Ammonia Gas on Inorganic and Organic Sorbents at 298.15 K. *Journal of Chemical Engineering Data,* **46,** 391-399.

Hong, M., Shiguang, L. Falconer, J.L., Noble, R.D.(2008) Hydrogen purification using a SAPO-34 membrane. *Journal of Membrane Science*, **307**, 277-283.

Hong, M., Falconer, J., Noble, R. (2005) Modification of zeolite membranes for H 2 separation by catalytic cracking of methyldiethoxysilane. *Industrial & Engineering Chemistry Research*, **44**, 4035-4041.

Hong, Z., Sun, F., Chen, D., Zhang, C., Gu, X., Xu, N. (2013) Improvement of hydrogen-separating performance by on-stream catalytic cracking of silane over

hollow fiber MFI zeolite membrane. *International Journal of Hydrogen Energy*, **38**, 8409-8414.

Hong, Z., Zhang, C., Gu, X., Jin, W., Xu, N.(2011) A simple method for healing nonzeolitic pores of MFI membranes by hydrolysis of silanes. *Journal of Membrane Science*, **366**, 427-435.

Isalski, W. (1981) Recovery of Hydrogen and Ammonia from Purge gas. Petrocarbone Development Limited.

Ismail, A. F. & David, L. I. B. (2001) A review on the latest development of carbon membranes for gas separation. *Journal of Membrane Science,* **193,** 1-18.

Ismail, A. F. & Lai, P. Y. (2003) Effects of phase inversion and rheological factors on formation of defect-free and ultrathin-skinned asymmetric polysulfone membranes for gas separation. *Separation and Purification Technology,* **33,** 127-143.

Ismail, A. F., Ridzuan, N. & Rahman, A. (2002) Latest development on the membrane formation for gas separation. *Songklanakarin Journal of Science and Technology*, **24**, 1025-1042.

Iwamoto, Y., Kawamoto, H. (2009) Trends in research and development of nanoporous ceramic separation membranes – Saving energy by applying the technology to the chemical synthesis process. *Science and Technology Trends*, Quarterly review **32**, 43-57 .

Jareman, F., Hedlund, J., Sterte, J. (2004) Effects of aluminium content on the separation properties of MFI membranes. *Separation and Purification Technology*, **32**, 159-163.

Jareman, F., Hedlund, J., Creaser, D. & Sterte, J. (2004) Modelling of single gas permeation in real MFI membranes. *Journal of Membrane Science,* **236,** 81-89.

Jareman, F., Hedlund, J. (2005) Permeation of H2, N2, He and SF6 in real MFI membranes. *Microporous and Mesoporous Materials*, **83**, 326-332.

Javaid, A. (2005) Membranes for solubility-based gas separation applications. *Chemical Engineering Journal*, **112,** 219-226.

Javaid, A., Hughey, M. P., Varutbangkul, V. & Ford, D. M. (2001) Solubility-based gas separation with oligomer-modified inorganic membranes. *Journal of Membrane Science,* **187,** 141-150.

Ji, G., Smart, S., Bhatia, S., Diniz da Costa, J. (2015) Improved pore connectivity by the reduction of cobalt oxide silica membranes. *Separation and Purification Technology*, **154**, 338-344.

Jia, M.-D., Chen, B., Noble, R. D. & Falconer, J. L. (1994) Ceramic-zeolite composite membranes and their application for separation of vapor/gas mixtures. *Journal of Membrane Science,* **90,** 1-10.

Jia, M.-D., Pleinemann, K.-V. & Behling, R.-D. (1992) Preparation and characterization of thin-film zeolite-PDMS composite membranes. *Journal of Membrane Science,* **73,** 119-128.

Jia, M., Peinemann, K.-V. & Behling, R.-D. (1991) Molecular sieving effect of the zeolite-filled silicone rubber membranes in gas permeation. *Journal of Membrane Science,* **57,** 289-292.

Jia, W. & Murad, S. (2005) Separation of gas mixtures using a range of zeolite membranes: A molecular-dynamics study. *The Journal Of Chemical Physics,* **122,** 234708-1 - 234708-11.

Jiang, L., Chung, T.-S., Li, D. F., Cao, C. & Kulprathipanja, S. (2004) Fabrication of Matrimid/polyethersulfone dual-layer hollow fiber membranes for gas separation. *Journal of Membrane Science,* **240,** 91-103.

Joly, J. P. & Perrard, A. (2001) Determination of the heat of adsorption of ammonia on zeolites from temperature-programmed desorption experiments. *Langmuir,* **17,** 1538-1542.

Jozefowicz, L. C., Karge, H. G. & Coker, E. N. (1994) Microcalorimetric investigation of h-zsm-5 zeolites using an ultrahigh-vacuum system for gas adsorption. *Journal of Physical Chemistry,* **98,** 8053-8060.

Julbe, A., Farrusseng, D., de Ménorval, L., Guizard, C. (2003) Characterization of MFI/αAl2O3 and V-MFI/αAl2O3 composite membranes by 129Xe NMR. *Separation and Purification Technology*, **32**, 165-173.

Kalipcilar, H., Falconer, J. L. & Noble, R. D. (2001) Preparation of B-ZSM-5 membranes on a monolith support. *Journal of Membrane Science,* **194,** 141-144.

Kanezashi, M., Asaeda, M. (2005) Stability of H2-permeselective Ni-doped silica membranes in steam at high temperature. *Journal of Chemical Engineering Japan,* **38**, 908-912.

Kanezashi, M., Asaeda, M. (2006) Hydrogen permeation characteristics and stability of Ni-doped silica membranes in steam at high temperature. *Journal of Membrane Science,* **271**, 86-93.

Kanezashi, M., O'Brien, J., Lin, Y.S. (2007) Template-free synthesis of MFI-type zeolite membranes: Permeation characteristics and thermal stability improvement of membrane structure. *Journal of Membrane Science,* **194,** 213-222.

Kapteijn, F., Bakker, W. J. W., Zheng, G., Poppe, J. & Moulijn, J. A. (1995) Permeation and separation of light hydrocarbons through a silicalite-1 membrane: Application of the generalized Maxwell-Stefan equations. *The Chemical Engineering Journal and the Biochemical Engineering Journal,* **57**, 145-153.

Kawai, T., Lee, Y. M., Higuchi, A. & Kamide, K. (1997) Separation of mixed gases through porous polymeric membranes. *Journal of Membrane Science,* **126,** 67-76.

Keil, F. J., Krishna, R. & Coppens, M. O. (2000) Modeling of diffusion in zeolites. *Reviews in Chemical Engineering,* **16,** 71-197.

Keizer, K., Verwiej, H. (1996) Progress in inorganic membranes. *Chemtech,* 37.

Keizer, K., Burggraff, A. J., Vroon, Z. A. E. P. & Verwiej, H. (1998) Two component permeation through thin zeolite MFI membranes. *Journal of Membrane Science,* **147,** 159-172.

Kikuchi, E., Yamashita, K., Hiromoto, S., Ueyama, K. & Matsukata, M. (1997) Synthesis of a zeolitic thin layer by a vapor-phase transport method: appearance of a preferential orientation of MFI zeolite. *Microporous Materials,* **11,** 107-116.

Kim, Y. K., Lee, J. M., Park, H. B. & Lee, Y. M. (2004) The gas separation properties of carbon molecular sieve membranes derived from polyimides having carboxylic acid groups. *Journal of Membrane Science,* **235,** 139-146.

Kim, Y. S., Kusakabe, K., Morooka, S. & Yang, S. M. (2001) Preparation of microporous silica membranes for gas separation. *Korean Journal of Chemical Engineering,* **18,** 106-112.

Koresh, J. E., Soffer, A. (1986) Mechanism of permeation through molecular-sieve carbon membrane. Part 1. The effect of adsorption and the dependence on pressure. *Journal of the Chemical Society., Faraday Transactions I,* **82,** 2057-2063.

Koros, W. J. (2002) Gas separation membranes: Needs for combined materials science and processing approaches. *Macromolecular Symposia,* **188,** 13-22.

Koros, W. J. & Mahajan, R. (2000) Pushing the limits on possibilities for large scale gas separation: which strategies? *Journal of Membrane Science,* **175,** 181-196.

Krishna, R. (1990) Multicomponent surface diffusion of adsorbed species: a description based on the generalized Maxwell--Stefan equations. *Chemical Engineering Science,* **45,** 1779-1791.

Krishna, R. (1993) Problems and pitfalls in the use of the fick formulation for intraparticle diffusion. *Chemical Engineering Science,* **48,** 845-861.

Krishna, R. & Baur, R. (2003) Modelling issues in zeolite based separation processes. *Separation and Purification Technology,* **33,** 213-254.

Krishna, R. & Paschek, D. (2000) Permeation of hexane isomers across ZSM-5 zeolite membranes. *Industrial & Engineering Chemistry Research,* **39,** 2618-2622.

Krishna, R., Paschek, D. & Baur, R. (2004) Modeling the occupancy dependence of diffusivities in zeolites. *Microporous and Mesoporous Materials,* **76,** 233-246.

Krishna, R. & Van Den Broeke, L. J. P. (1995) The Maxwell-Stefan description of mass transport across zeolite membranes. *The Chemical Engineering Journal and the Biochemical Engineering Journal,* **57,** 155-162.

Krovvidi, K. R., Kovvali, A. S., Vemury, S. & Khan, A. A. (1992) Approximate solutions for gas permeators separating binary mixtures. *Journal of Membrane Science,* **66,** 103-118.

Kondo, M., Kita, H. (2010) Permeation mechanism through zeolite NaA and T-type membranes for practical dehydration of organic solvents. *Journal of Membrane Science,* **361**, 223-231.

Kosinov, N., Gascon, J., Kapteijn, F., Hensen, E.J.M. (2015) Recent developments in zeolite membranes for gas separation. *Journal of Membrane Science*. ***In Press, Accepted Manuscript.***

Kulprathipanja, S. & Kulkarni, S. S. (1986) *Separation of polar gases from nonpolar gases.* US 4608060 A.

Kuo, S-L., Pedram E, O., Hines, A.L. (1985) Analysis of Ammonia Adsorption on Silica Gel using the Modified Potential Theory. *Journal of Chemical Engineering Data,* **30**, 330-332.

Kusakabe, K., Kuroda, T. & Morooka, S. (1998) Separation of carbon dioxide from nitrogen using ion-exchanged faujasite-type zeolite membranes formed on porous support tubes. *Industrial and Engineering Chemistry Research,* **36,** 649-655.

Kusakabe, K., Yoneshige, S., Murata, A. & Morooka, S. (1996) Morphology and gas permeance of ZSM-5-type zeolite membrane formed on a porous [alpha]-alumina support tube. *Journal of Membrane Science,* **116,** 39-46.

Laciak, D. V. & Pez, G. P. 1988 *Ammonia separation using ion exchange polymeric membranes and sorbents*. US Patent 4,758,250.

Lai, R. & Gavalas, G. R. (1998) Surface seeding in ZSM-5 membrane preparation. *Industrial & Engineering Chemistry Research,* **37,** 4275-4283.

Lai, R. & Gavalas, G. R. (2000) ZSM-5 membrane synthesis with organic-free mixtures. *Microporous and Mesoporous Materials,* **38,** 239-245.

Lai, Z. P., Bonilla, G., Diaz, I., Nery, J. G., Sujaoti, K., Amat, M. A., Kokkoli, E., Terasaki, O., Thompson, R. W., Tsapatsis, M. & Vlachos, D. G. (2003) Microstructural optimization of a zeolite membrane for organic vapor separation. *Science,* **300,** 456-460.

Lai, Z. P. & Tsapatsis, M. (2004) Gas and organic vapor permeation through b-oriented MFI membranes. *Industrial & Engineering Chemistry Research,* **43,** 3000-3007.

Langmuir, I. (19I8) The evaporation of small spheres. Physical Review, **12**, 368-370.

Lavie, R. (1985) *Process for the Manufacture of Ammonia*. US 4537760.

Lawson, K. W., Hall, M. S. & Lloyd, D. R. (1995) Compaction of microporous membranes used in membrane distillation. I. Effect on gas permeability. *Journal of Membrane Science,* **101,** 99-108.

Lee, H-J., Yamauchi, H., Suda, H., Haraya, K. (2006) Influence of adsorption on the gas permeation performances in the mesoporous alumina ceramic membrane. *Separation and Purification Technology,* 49 49-55.

Lee, J. M., 1996. *Process for ammonia recovery in ammonia production*. US 5484582A.

Lee, J., Funke, H., Noble, R., Falconer, J. (2009) Adsorption-induced expansion of defects in MFI membranes. *Journal of Membrane Science*, **341**, 238-245.

Lee, J., Funke, H., Noble, R., Falconer, J. (2008) High selectivities in defective MFI membranes. *Journal of Membrane Science*, **321**, 309-315.

Lee, D., Zhang, L., Oyama, S.T., Niu,S., Saraf, R.F. (2004) Synthesis, characterization, and gas permeation properties of a hydrogen permeable silica membrane supported on porous alumina. *Journal of Membrane Science*, 231, 117-126.

Ley, V., Kruzic, A. P. & Timmons, R. B. (2003) Permeation rates of low molecular weight gases through a plasma synthesized allyl alcohol membrane. *Journal of Membrane Science,* 226**,** 213-226.

Li, G., Kikuchi, E., Matsukata, M. (2003) ZSM-5 zeolite membranes prepared from a clear template-free solution. *Microporous and Mesoporous Materials*, 60, 225-235.

Li, H., Haas-Santo, K., Schygulla, U., Dittmeyyer, R. (2015b) Inorganic microporous membranes for H2 and CO2 separation – Review of experimental and modelling programs. *Chemical Engineering Science,* **127**, 401-417.

Li, K. (2007) *Ceramic Membranes for Separation and Reaction.* Chichester: John Wiley & Sons.

Li, P., Wang, Z., Qiao, Z., Liu.,Y., Cao, Y., Wen, L., Wang, J, Wang., S. (2105a) Recent developments in membranes for efficient hydrogen purification. *Journal of Membrane Science*, **495**, 130-168.

Li, S.G., Falconer, J.L., Noble, R.D. (2004) SAPO-34 membranes for CO2/CH4 separation. *Journal of Membrane Science*, **241**, 121.

Li, Y., Pera-Titus, M., Xiong, G., Yang, W., Landrivon, E., Miachon, S., Dalmon., J.A (2008). Nanocomposite MFI-alumina membranes via pore plugging synthesis: Genesis of the zeolite material. *Journal of Membrane Science*, **325**, 973-981.

Lin, Y., Duke, M. (2013) Recent progress in polycrystalline zeolite membrane research. *Current Opinion in Chemical Engineering,* **2**, 209-216.

Li, Y., Yang, W. (2008) Microwave synthesis of zeolite membranes: A review. *Journal of Membrane Science* 2008, *316*, 3-17.

Lin, H. & Freeman, B. D. (2005) Materials selection guidelines for membranes that remove CO2 from gas mixtures. *Journal of Molecular Structure,* **739,** 57-74.

Lin, X., Falconer, J. L. & Noble, R. D. (1998) Parallel Pathways for Transport in ZSM-5 Zeolite Membranes. *Chemistry of Materials,* **10,** 3716-3723.

Lin, Y. S. (2001) Microporous and dense inorganic membranes: Current status and prospective. *Separation and Purification Technology,* **25,** 39-55.

Lin, Y. S., Kumakiri, I., Nair, B. N. & Alsyouri, H. (2002) Microporous inorganic membranes. *Separation and Purification Methods,* **31,** 229-379.

Lochmuller, C. H., Dwyer, E. & Spiller, L. (1985) Chemically-modified ion-exchange membranes as sampling devices for gas-phase ammonia. *Analytical Letters Part A - Chemical Analysis,* **18,** 423-428.

Lonyi, F. & Valyon, J. (2001) On the interpretation of the NH3-TPD patterns of H-ZSM-5 and H-mordenite. *Microporous and Mesoporous Materials,* **47,** 293-301.

Lovallo, M. C., Gouzinis, A. & Tsapatsis, M. (1998) Synthesis and characterization of oriented MFI membranes prepared by secondary growth. *AIChE Journal*, **44,** 1903-1913.

Lovallo, M. C., Gouzinis, A. & Tsapatsis, M. (1996) Preferentially Oriented Submicron Silicalite Membranes. *AIChE Journal*, **42**, 3020-3029.

Lüdtke, O., Behling, R., Ohlrogge, K. (1998) Concentration polarization in gas permeation. *Journal of Membrane Science*, **146**, 145-157.

Luque, S., Gòmez, D., Alvarez, J.R. (2008) Industrial applications of porous ceramic membranes (Pressure driven processes). *Membrane Science and Technology*, **13**, 177-216.

Mabande, G. T. P., Noack, M., Avhale, A., Kolsch, P., Georgi, G., Schwieger, W. & Caro, J. (2007) Permeation properties of bi-layered Al-ZSM-5/silicalite-1 membranes. *Microporous and Mesoporous Materials*, **98,** 55-61.

Mabande, G. T. P., Pradhan, G., Schwieger, W., Hanebuth, M., Dittmeyer, R., Selvam, T., Zampieri, A., Baser, H. & Herrmann, R. (2004) A study of Silicalite-1 and Al-ZSM-5 membrane synthesis on stainless steel supports. *Microporous and Mesoporous Materials,* **75,** 209-220.

Marriott, J. I., Sorensen, E. & Bogle, I. D. L. (2001) Detailed mathematical modelling of membrane modules. *Computers & Chemical Engineering,* **25,** 693-700.

Martinek, J. G., Gardner, T. Q., Noble, R. D. & Falconer, J. L. (2006) Modeling transient permeation of binary mixtures through zeolite membranes. *Industrial & Engineering Chemistry Research,* **45,** 6032-6043.

Makhloufi, C., Belaissaoui, B., Roizard, D., Favre, E. (2012) Interest of Poly[bis(trifluoroethoxy)phosphazene] membranes for ammonia recovery–potential application in haber process. *Procedia Engineering*, **44**, 143-146.

Makhloufi, C., Roizard, D., Favre, E. (2013) Reverse selective NH3/CO2 permeation in fluorinated polymers using membrane gas separation. *Journal of Membrane Science*, **441**, 63-72.

McCabe, W.L., Smith, J.C., Harriott, P. (2001) *Unit Operations of Chemical Engineers*. 6th Edition. McGraw Hill: London.

Mccarley, K. C. & Way, J. D. (2001) Development of a model surface flow membrane by modification of porous [gamma]-alumina with octadecyltrichlorosilane. *Separation and Purification Technology,* **25,** 195-210.

McKinley, J. J. (1970) *Ammonia analysis system*. US 3545931.

Mcleary, E. E., Jansen, J. C. & Kapteijn, F. (2006) Zeolite based films, membranes and membrane reactors: Progress and prospects. *Microporous and Mesoporous Materials,* **90,** 198-220.

Meinema, H. A., Dirrix, R. W. J., Brinkman, H. W., Terpstra, R. A., Jekerle, J. & Kosters, P. H. (2005) Ceramic Membranes for Gas Separation - Recent Developments and State of the Art. *Interceram*, **54,** 86-91.

Meixner, D. L. & Dyer, P. N. (1998) Characterization of the transport properties of microporous inorganic membranes. *Journal of Membrane Science,* **140,** 81-95.

Miachon, S., Ciavarella, P., Van Dyk, L., Kumakiri, I., Fiaty, K., Schuurman, Y. & Dalmon, J. A. (2007) Nanocomposite MFI-alumina membranes via pore-plugging synthesis: Specific transport and separation properties. *Journal of Membrane Science,* **298**, 71-79.

Miachon, S., Landrivon, E., Aouine, M., Sun, Y., Kumakiri, I., Li, Y., Prokopova, O. P., Guilhaume, N., Giroir-Fendler, A., Mozzanega, H. & Dalmon, J. A. (2006) Nanocomposite MFI-alumina membranes via pore-plugging synthesis: Preparation and morphological characterisation. *Journal of Membrane Science,* **281,** 228-238.

Miachon, S., Mazuy, A., Dalmon, J.A. (2000) Catalysis of palladium salt reduction in a gas-liquid membrane reactor. *Studies in Surface Science and Catalysis, **130**,* 2693-2698.

Millot, B., Methivier, A., Jobic, H., Moueddeb, H. & Dalmon, J. A. (2000) Permeation of linear and branched alkanes in ZSM-5 supported membranes. *Microporous and Mesoporous Materials,* **38,** 85-95.

Mintova, S., Hedlund, J., Valtchev, V., Schoeman, B.J., Sterte, J. (1998) ZSM-5 films prepared from template free precursors. Journal of Material Chemistry, **8**, 2217-2221.

Molinari, R., Gagliardi, R. & Drioli, E. (1995) Methodology for estimating saving of primary energy with membrane operations in industrial processes. *Desalination,* **100,** 125-137.

Morooka, S. & Kusakabe, K. (1999) Microporous inorganic membranes for gas separation. *MRS Bulletin,* **24,** 25-29.

Mourgues, A., Sanchez, J.(2005) Theoretical analysis of concentration polarization in membrane modules for gas separation with feed inside the hollow-fibers. *Journal of Membrane Science*, **252**, 133-144.

Mulder, M. (Ed.) (1996) *Basic principles of membrane technology.* Kluwer Academic Publishers: Netherlands.

Nenoff, T.; Dong, J. (2009) Chapter 14 – Highly Selective Zeolite Membranes. In *Ordered Porous Solids Recent Advances and Prospects*; Valtchev, V.; Mintova, S.; Tsapatsis, M., Ed.; Elsevier: Oxford; pp. 365-386.

Newsome, D., Sholl, D. (2008) Atomically detailed simulations of surface resistances to transport of CH4, CF4, and C2H6 through silicalite membranes. *Microporous and Mesoporous Materials*, **107**, 286-295.

Nicolas, C.; Pera-Titus, M. (2012) Nanocomposite MFI-Alumina Hollow Fiber Membranes: Influence of NO x and Propane on CO 2 /N 2 Separation Properties. *Industrial & Engineering Chemistry Research*, **51**, 10451-10461.

Nicolas, C., Sublet, J., Schuurman, Y., Pera-Titus, M. (2011) Role of adsorption and diffusion pathways on the CO2/N2 separation performance of nanocomposite (B)-MFI-alumina membranes. *Chemical Engineering Science*, **66**, 6057-6068.

Nishiyama, N., Ueyama, K. & Matsukata, M. (1996) Synthesis of defect-free zeolite-alumina composite membranes by a vapor-phase transport method. *Microporous Materials,* **7,** 299-308.

Noack, M., Kolsch, P., Schafer, R., Toussaint, P. & Caro, J. (2002) Molecular sieve membranes for industrial application: Problems, progress, solutions (Reprinted from Chem. Ing. Tech., vol 73, pg 958-967, 2001). *Chemical Engineering & Technology,* **25,** 221-230.

Noack, M., Kolsch, P., Schafer, R., Toussaint, P., Sieber, I. & Caro, J. (2001) Preparation of MFI membranes of enlarged area with high reproducibility. *Microporous and Mesoporous Materials*, **49,** 25-37.

Noack, M., Kolsch, P., Seefeld, V., Toussaint, P., Georgi, G. & Caro, J. (2005a) Influence of the Si/Al-ratio on the permeation properties of MFI-membranes. *Microporous and Mesoporous Materials,* **79,** 329-337.

Noack, M., Mabande, G. T. P., Caro, J., Georgi, G., Schwieger, W., Kolsch, P. & Avhale, A. (2005b) Influence of Si/Al ratio, pre-treatment and measurement conditions on permeation properties of MFI membranes on metallic and ceramic supports. *Microporous and Mesoporous Materials,* **82,** 147-157.

Noble, R. D., Koval, C. A. & Pellegrino, J. J. (1989) Facilitated transport membrane systems. *Chemical Engineering Progress,* 85, 58-78.

O'Brien-Abraham, J., Kanezashi, M., Lin, Y. (2008) Effects of adsorption-induced microstructural changes on separation of xylene isomers through MFI-type zeolite membranes. *Journal of Membrane Science*, **320**, 505-513.

Onyestyak, G., Shen, D. & Rees, L. V. C. (1996) Frequency-response NH3 sorption study of acidic sites in H-ZSM-5 catalysts. *Journal of the Chemical Society, Faraday Transactions,* 92**,** 307-315.

Pan, C. Y. & Hadfield, E. M. (1988) *Permeation Processes for Separating Ammonia from a Gas Mixture*. US 4793829 A.

Pan, M., Lin, Y.S. (2001) Template-free secondary growth synthesis of MFI type zeolite membranes Microporous and Mesoporous Materials, **43**, 319-327.

Pandey, P. & Chauhan, R. S. (2001) Membranes for gas separation. *Progress in Polymer Science*, **26,** 853-893.

Parillo, D.J., Gorte, R.J. (1993) Characterization of acidity in H-ZSM-5, H-ZSM-12, H-Mordenite, and H-Y using microcalorimetry, *Journal of Physical Chemistry*, **97**, 8786-8792.

Parrillo, D. J., Gorte, R. J. & Farneth, W. E. (1993) A calorimetric study of simple bases in H-ZSM-5: a comparison with gas-phase and solution-phase acidities. *Journal of the American Chemical Society*, **115,** 12441-12445.

Parrillo, D. J., Lee, C. & Gorte, R. J. (1994) Heats of adsorption for ammonia and pyridine in H-ZSM-5: evidence for identical Bronsted-acid sites. *Applied Catalysis A: General*, **110,** 67-74.

Pereira, C. C., Nobrega, R., Peinemann, K. V. & Borges, C. P. (2003) Hollow fiber membranes obtained by simultaneous spinning of two polymer solutions: a morphological study. *Journal of Membrane Science,* **226,** 35-50.

Petit, C., Bandosz, T.J. Enhanced adsorption of ammonia on metal-organic framework/graphite oxide composites: Analysis of surface interactions. *Advanced Functional Materials*, **20** (1), 111-118.

Pez, G. P. & Laciak, D. V. Air Products and Chemicals Inc (1988). *Ammonia Separation using semipermeable membranes*. EP 0293737 B1.

Pham, T., Nguyen, T., Yoon, K. (2013) Gel-Free Secondary Growth of Uniformly Oriented Silica MFI Zeolite Films and Application for Xylene Separation. *Angewandte Chemie*, **125**, 8855-8860.

Phillip, W., Martono, E., Chen, L., Hillmyer, M., Cussler, E. (2009) Seeking an ammonia selective membrane based on nanostructured sulfonated block copolymers. *Journal of Membrane Science*, **337**, 39-46.

Piera, E., Bernal, M. P., Salomon, M. A., Coronas, J., Menendez, M. & Santamaria, J. (1999a) Preparation and permeation properties of different zeolite tubular membranes. *Porous Materials in Environmentally Friendly Processes*, **125**, 189-196.

Piera, E., Coronas, J., Menendez, M. & Santamaria, J. (1999b) High separation selectivity with imperfect zeolite membranes. *Chemical Communications***, 14**, 1309-1310.

Piera, E., Salomon, M. A., Coronas, J., Menendez, M. & Santamaria, J. (1998) Synthesis, characterization and separation properties of a composite mordenite/ZSM-5/chabazite hydrophilic membrane. *Journal of Membrane Science,* **149,** 99-114.

Pina, M., Mallada, R., Arruebo, M., Urbiztondo, M., Navascués, N., de la Iglesia, O., Santamaria, J. (2011) Zeolite films and membranes. Emerging applications. *Microporous and Mesoporous Materials*, **144**, 19-27.

Ping, E., Zhou, R., Funke, H., Falconer, J., Noble, R. (2012) Seeded-gel synthesis of SAPO-34 single channel and monolith membranes, for CO2/CH4 separations. *Journal of Membrane Science*, **415-416**, 770-775.

Poshusta, J. C., Noble, R. D. & Falconer, J. L. (1999) Temperature and pressure effects on CO2 and CH4 permeation through MFI zeolite membranes. *Journal of Membrane Science,* **160,** 115-125.

Prokop, Z. & Setinek, K. (1974) Sorption of gaseous ammonia on sulfonated macroreticular ion-exchangers. *Journal of Polymer Science Part a-Polymer Chemistry*, 12**,** 2535-2543.

Ramsay, J., Giroir-Fendler, A., Julbe, A. & Dalmon, J. A. (1994) *Materiau inorganique poreux, notament sous forme de membrane, et procede d'obtention d'un tel materiau*. WO 1995029751 A1.

Rao, M. B. & Sircar, S. (1993) Nanoporous carbon membranes for separation of gas mixtures by selective surface flow. *Journal of Membrane Science,* **85,** 253-264.

Rao, M. B. & Sircar, S. (1996) Performance and pore characterization of nanoporous carbon membranes for gas separation. *Journal of Membrane Science,* **110,** 109-118.

Rao, V. U. S. (1983) The role of metal-zeolite interactions in indirect liquefaction catalysis. *Physica Scripta*, **1983,** 71-78.

Rees, L.V.C., Brickner, P., Hampson, J. (1991) Sorption of N2, CH4 &CO2 in Silicalite-1. *Gas Separation & Purification*, **5**, 67-75.

Rezai, S.A.S., Lindmark, J., Andersson, C., Jareman, F., Moller, K., Hedlund, J. (2008) Water/hydrogen/hexane multicomponent selectivity of thin MFI membrane with different Si/Al ratios. *Microporous and Mesoporous Materials* **108**, 136-142.

Rice, R. D. & Busa, J. V. (1984) Recovering NH3 by the phosam-w process. *Chemical Engineering Progress,* **80,** 61-63.

Romm, F. (1996) Derivation of the equations for isotherm curves of adsorption on microporous gel materials, *Langmuir,* 12 (14) 3490-3497

Rouquerol, F., Rouqerol, J., Sing, K. (1999) *Adsorption by Powders and Porous Solids, Principles, Methodology and Applications*. London, Academic Press: UK.

Ruthven, D.M., (1984) *Principles of Adsorption Processes* J Wiley & Sons Inc.: Canada.

Saha,D., Deng, S. Ammonia adsorption and its effects on framework stability of MOF-5 and MOF-177. *Journal of Colloid and Interface Science,* **348** (2), 615-620

Salomon, M. A., Coronas, J., Menendez, M. & Santamaria, J. (2000) Synthesis of MTBE in zeolite membrane reactors. *Applied Catalysis A: General,* **200,** 201-210.

Saufi, S. M. & Ismail, A. F. (2004) Fabrication of carbon membranes for gas separation-A review. *Carbon,* **42,** 241-259.

Schuring, D., Koriabkina, A. O., De Jong, A. M., Smit, B. & Van Santen, R. A. (2001) Adsorption and diffusion of n-hexane/2-methylpentane mixtures in zeolite silicalite: experiments and modeling. *Journal of Physical Chemistry B,* **105,** 7690-7698.

Schuring, A., Fritzche, S., Vasenkov, S. (2007) A new type of of diffusional boundary effect at the edges of single-file channels. In *From Zeolites to Porous MOF materials-the 40th Anniversary of International Zeolite Conference*; Studies in Surface Science, 1000-1007.

Scott, K., Hughes, R. (1996) *Industrial Membrane Separation Technology*. Blackie Academic and Professional: UK

Sebastián, V., Kumakiri, I., Bredesen, R., Menendez, M. (2007) Zeolite membrane for co2 removal:operating at high pressure physical. *Journal of Membrane Science,* **292,** 92-97.

Sebastian, V., Mallada, R., Coronas, J., Julbe, A., Terpstra, R., Dirrix, R. (2010)Microwave-assisted hydrothermal rapid synthesis of capillary MFI-type zeolite–ceramic membranes for pervaporation application. *Journal of Membrane Science*, **355**, 28-35.

Semenova, S. I., Ohya, H. & Smirnov, S. I. (1997) Physical transitions in polymers plasticized by interacting penetrant. *Journal of Membrane Science,* **136,** 1-11.

Semenova, S. I., Smirnov, S. I. & Ohya, H. (2000) Performances of glassy polymer membranes plasticized by interacting penetrants. *Journal of Membrane Science,* **172,** 75-89.

Sharonov, V. E. & Aristov, Y. I. (2005) Ammonia adsorption by MgCl2, CaCl2 and BaCl2 confined to porous alumina: The fixed bed adsorber. *Reaction Kinetics and Catalysis Letters,* **85,** 183-188.

Shin, D. W., Hyun, S. H., Cho, C. H. & Han, M. H. (2005) Synthesis and CO2/N2 gas permeation characteristics of ZSM-5 zeolite membranes. *Microporous and Mesoporous Materials,* **85,** 313-323.

Shiralkar, V. P. & Kulkarni, S. B. (1985) Sorption of ammonia in cation-exchanged Y zeolites: Isotherms and state of sorbed molecules. *Journal of Colloid and Interface Science,* **108,** 1-10.

Sklari, S. D. & Zaspalis, V. T. (2007) A novel system of Al100P60Oz microporous ceramic membrane for hydrogen separation from hydrogen/propane mixtures. *Microporous and Mesoporous Materials,* **99,** 176-180.

Silva, L., Plaza, A., Romero, J., Sanchez, J., Rios, G.M. (2008) Characterization of MFI zeolite membranes by means of permeability determination of near critical and supercritical CO_2. *Journal of the Chilean Chemical Society*, **53**,1415-1421.

Sjöberg, E., Barnes, S., Korelskiy, D., Hedlund, J. (2015) MFI membranes for separation of carbon dioxide from synthesis gas at high pressures. *Journal of Membrane Science* 2015, **486**, 132-137.

Skoulidas, A. I., Bowen, T. C., Doelling, C. M., Falconer, J. L., Noble, R. D. & Sholl, D. S. (2003) Comparing atomistic simulations and experimental measurements for CH4/CF4 mixture permeation through silicalite membranes. *Journal of Membrane Science,* **227,** 123-136.

Smart, S., Vente, J., Diniz da Costa, J. (2012) High temperature H2/CO2 separation using cobalt oxide silica membranes. *International Journal of Hydrogen Energy*, **37**, 12700-12707.

Smith, S. W., Hall, C. K., Freeman, B. D. & Rautenbach, R. (1996) Corrections for analytical gas-permeation models for separation of binary gas mixtures using membrane modules. *Journal of Membrane Science,* 118**,** 289-294.

Smil, V., (2001*) Enriching the Earth: Fritz Haber, Carl Bosch and the Transformation of World Food Production*. MIT Press: Cambridge Mass.

So, J.-H., Yang, S.-M. & Bin Park, S. (1998) Preparation of silica-alumina composite membranes for hydrogen separation by multi-step pore modifications. *Journal of Membrane Science,* **147,** 147-158.

Sommer, S., Melin, T., Falconer, J. L. & Noble, R. D. (2003) Transport of C6 isomers through ZSM-5 zeolite membranes. *Journal of Membrane Science,* **224,** 51-67.

Sorenson, S., Payzant, E., Gibbons, W., Soydas, B., Kita, H., Noble, R., Falconer, J. (2011) Influence of zeolite crystal expansion/contraction on NaA zeolite membrane separations. *Journal of Membrane Science*, **366**, 413-420.

Sorenson, S., Payzant, E., Noble, R., Falconer, J. (2010) Influence of crystal expansion/contraction on zeolite membrane permeation. *Journal of Membrane Science*, **357**, 98-104.

Soria, R. (1995) Overview on industrial membranes. *Catalysis Today,* **25,** 285-290.

Speth, C. (2003) *Ammonia recovery from purge gas.* US 5114694 A.

Spiewak, B. E., Handy, B. E., Sharma, S. B. & Dumesic, J. A. (1994) Microcalorimetric studies of ammonia adsorption on γ-Al2O3, HNa-Y zeolite, and H-mordenite. *Catalysis Letters,* **23,** 207-213.

Stainer, M., Hardy, L. C., Whitmore, D. H. & Shriver, D. F. (1984) Stoichiometry of formation and conductivity response of amorphous and crystalline complexes formed between poly(ethylene oxide) and ammonium salts – POEX NH4 AND PEOX.NH4SO3CF3. *Journal of the Electrochemical Society,* **131,** 784-790.

Stephan, W., Noble, R. D. & Koval, C. A. (1995) Design methodology for a membrane/distillation column hybrid process. *Journal of Membrane Science,* **99,** 259-272.

Stookey, D. J. (2005). Membranes: Gas Separation Applications. Ullmann's Encyclopedia of Industrial Chemistry [Online] *22* Available from http://onlinelibrary.wiley.com/doi/10.1002/14356007.j16_j02/abstract (Accessed 15 April 2007)

Szostak, R. (1998) *Molecular Sieves: Principles of Synthesis and Identification.* Blackie Academic and Professional: London.

Talu, O. (1992) Cleveland State University *Gas Separation Process*. US 5160512.

Talu, O., Sun, M.S., Shah, D.B (1998) Diffusivities of N-alkanes in silicalite by steady-state single-crystal membrane technique. *AIche Journal*, **44**, 681-694.

Takata, Y., Tsuru, T., Yoshioka, T., Asaeda, M. (2002) Gas permeation properties of MFI zeolite membranes prepared by the secondary growth of colloidal silicalite and application to the methylation of toluene. *Microporous and Mesoporous Materials*, **54**, 257-268.

Tang, Z., Kim, S., Reddy, G., Dong, J., Smirniotis, P. (2010) Modified zeolite membrane reactor for high temperature water gas shift reaction. *Journal of Membrane Science*, **354**, 114-122.

Tarditi, A.M., Lombardo, E.A., Avila, A.M. (2008) Xylene permeation through Composite Ba-ZSM-5/SS Tubular Membranes: Modeling the Steady-State Permeation. *Industrial & Engineering Chemistry Research*, **47**, 2377-2385.

Tavolaro, A. & Drioli, E. (1999) Zeolite Membranes. *Advanced Materials*, **11,** 975-996.

Telfer, S.G. (2010) What are these things called MOFs? *Chemistry in New Zealand* [*Online*] Available from: http://nzic.org.nz/CiNZ/articles/CiNZ_jan10_telfer.pdf [15th January 2015].

Terzyk, A. P., Chatlas, J., Gauden, P. A., Rychlicki, G. & Kowalczyk, P. (2003) Developing the solution analogue of the Toth adsorption isotherm equation. *Journal of Colloid and Interface Science,* 266**,** 473-476.

Tien, C. (1994). *Adsorption calculations and modeling*. Butterworth-Heinemann: Newton Mass. USA

Timashev, S. F., Vorobiev, A. V., Kirichenko, V. I., Popkov, Y. M., Volkov, V. I., Shifrina, R. R., Lyapunov, A. Y., Bondarenko, A. G. & Bobrova, L. P. (1991) Specifics of highly selective ammonia transport through gas-separating membranes based on perfluorinated copolymer in the form of hollow fibers. *Journal of Membrane Science,* **59,** 117-131.

Tin, P. S., Chung, T. S., Liu, Y., Wang, R., Liu, S. L. & Pramoda, K. P. (2003) Effects of cross-linking modification on gas separation performance of Matrimid membranes. *Journal of Membrane Science,* **225,** 77-90.

Tomita, T., Nakayama, K. & Sakai, H. (2004) Gas separation characteristics of DDR type zeolite membrane. *Microporous and Mesoporous Materials,* **68,** 71-75.

Tokay, B., Falconer, J., Noble, R. (2009) Alcohol and water adsorption and capillary condensation in MFI zeolite membranes. *Journal of Membrane Science* 2009, *334*, 23-29.

Tricoli, V. & Cussler, E. L. (1995) Ammonia selective hollow fibers. *Journal of Membrane Science,* **104,** 19-26.

Tricoli, V., Sefcik, J., Mccormick, A.V. (1997) Synthesis of oriented zeolite membranes at the interface between two fluid phases. *Langmuir*, **13**, 4193-4196.

Tsai, C.-Y., Tam, S.-Y., Lu, Y. & Brinker, C. J. (2000) Dual-layer asymmetric microporous silica membranes. *Journal of Membrane Science,* **169,** 255-268.

Tsikoyiannis, J. G. & Haag, W. O. (1992) Synthesis and characterization of a pure zeolitic membrane. *Zeolites,* **12,** 126-130.

Tuan, V. A., Falconer, J. L. & Noble, R. D. (1999) Alkali-free ZSM-5 membranes: Preparation conditions and separation performance. *Industrial & Engineering Chemistry Research,* **38,** 3635-3646.

Tuan, V. A., Falconer, J. L. & Noble, R. D. (2000) Isomorphous substitution of Al, Fe, B, and Ge into MFI-zeolite membranes. *Microporous and Mesoporous Materials,* **41,** 269-280.

Uhlhorn, R. J. R., Keizer, K. & Burggraaf, A. J. (1992) Gas transport and separation with ceramic membranes. Part I. Multilayer diffusion and capillary condensation. *Journal of Membrane Science,* **66,** 259-269.

Uzio, D., Peureux, J., Giroirfendler, A., Dalmon, J. A. & Ramsay, J. D. F. (1994) Formation and pore structure of zeolite membranes. *Characterization of Porous Solids III. Studies in Surface Science and Catalysis,* ***87****,* 411-418.

Valenzuela, D.P., Myers, A.L. (1989) *Adsorption Equilibrium Data Handbook*. Prentice Hall, Englewood Cliffs: New Jersey.

Valyon, J., Onyestyak, G. & Rees, L. V. C. (1998) Study of the dynamics of NH3 adsorption in ZSM-5 zeolites and the acidity of the sorption sites using the frequency-response technique. *Journal of Physical Chemistry B,* **102,** 8994-9001.

Valyon, J., Onyestyak, G. & Rees, L. V. C. (2000) A Frequency-Response Study of the Diffusion and Sorption Dynamics of Ammonia in Zeolites. *Langmuir,* **16,** 1331-1336.

Van De Graaf, J. M., Kapteijn, F. & Moulijn, J. A. (1999) Modeling permeation of binary mixtures through zeolite membranes. *AIChE Journal,* **45,** 497-511.

Van De Graaf, J. M., Kapteijn, F. & Moulijn, J. A. (2000) Diffusivities of light alkanes in a silicalite-1 membrane layer. *Microporous and Mesoporous Materials,* **35-36,** 267-281.

Van De Graaf, J. M., Van Der Bijl, E., Stol, A., Kapteijn, F. & Moulijn, J. A. (1998) Effect of operating conditions and membrane quality on the separation performance of composite silicalite-1 membranes. *Industrial & Engineering Chemistry Research,* **37,** 4071-4083.

Van Den Broeke, L. J. P., Bakker, W. J. W., Kapteijn, F. & Moulijn, J. A. (1999a) Transport and separation properties of a silicalite-1 membrane-I. Operating conditions. *Chemical Engineering Science,* **54,** 245-258.

Van Den Broeke, L. J. P., Kapteijn, F. & Moulijn, J. A. (1999b) Transport and separation properties of a silicalite-1 membrane-II. Variable separation factor. *Chemical Engineering Science,* **54,** 259-269.

Vareltzis, P., Kikkinides, E. S. & Georgiadis, M. C. (2003) On the optimization of gas separation processes using zeolite membranes. *Transactions of the IChemE,* **81,** 525-536.

Verweij, H. (2003) Ceramic membranes: Morphology and transport. *Journal of Material Science,* **38,** 4677-4695.

Verweij, H., Lin, Y. S. & Dong, J. (2006) Microporous silica and zeolite membranes for hydrogen purification. *MRS Bulletin,* **31,** 756-764.

Vieira-Linhares, A. M. & Seaton, N. A. (2003a) Non-equilibrium molecular dynamics simulation of gas separation in a microporous carbon membrane. *Chemical Engineering Science,* **58,** 4129-4136.

Vieira-Linhares, A. M. & Seaton, N. A. (2003b) Pore network connectivity effects on gas separation in a microporous carbon membrane. *Chemical Engineering Science,* **58,** 5251-5256.

Vorotyntsev, I. V., Drozdov, P. N. & Karyakin, N. V. (2006a) Ammonia permeability of a cellulose acetate membrane. *Inorganic Materials,* **42,** 231-235.

Vorotyntsev, I. V., Drozdov, P. N., Shablikin, D. N. & Gamajunova, T. V. (2006b) Ammonia separation and purification by absorbing pervaporation. *Desalination,* **200,** 379-380.

Vroon, Z., Keizer, K., Gilde, M. J., Verweij, H. & Burggraaf, A. J. (1996) Transport properties of alkanes through ceramic thin zeolite MFI membranes. *Journal of Membrane Science,* **113,** 293-300.

Vroon, Z. A. E. P., Keizer, K., Burggraaf, A. J. & Verweij, H. (1998) Preparation and characterization of thin zeolite MFI membranes on porous supports. *Journal of Membrane Science,* **144,** 65-76.

Wang, H., Lin, Y. (2012) Synthesis and modification of ZSM-5/silicalite bilayer membrane with improved hydrogen separation performance. *Journal of Membrane Science*, **396**, 128-137.

Wang, H.; Lin, Y. (2011) Effects of synthesis conditions on MFI zeolite membrane quality and catalytic cracking deposition modification results. *Microporous and Mesoporous Materials*, **142**, 481-488.

Wang, D., Teo, W. K. & Li, K. (2002) Preparation and characterization of high-flux polysulfone hollow fiber gas separation membranes. *Journal of Membrane Science,* **204,** 247-256.

Wang, D., Motuzas, J., Diniz da Costa, J., Smart, S. (2013) Rapid thermal processing of tubular cobalt oxide silica membranes. *International Journal of Hydrogen Energy*, **38**, 7394-7399.

Wang, J., Tsuru, T. (2011) Cobalt-doped silica membranes for pervaporation dehydration of ethanol/water solutions. *Journal of Membrane Science,* **369**, 13-19.

Wei, Q., Ding, Y., Nie, Z., Liu, X., Li, Q. (2014) Wettability, pore structure and performance of perfluorodecyl-modified silica membranes. *Journal of Membrane Science,* **466**, 114-122.

Wei, Q., Wang, F., Nie, Z., Song, C., Wang, Y., Li, Q. (2008) Highly Hydrothermally Stable Microporous Silica Membranes for Hydrogen Separation. *The Journal of Physical Chemistry B,* **112**, 9354-9359.

Wenten, I. G. (2002) Recent development in membrane science and its industrial applications. *Songlanakarin Journal of Science and Technology,* **24,** 1009-1024.

Wesselingh, J. A., Krishna, R. (1990) *Mass transfer.* Ellis Horwood: Chichester.

Wesselingh, J. A., Krishna, R. (2000) *Mass transfer in multicomponent mixtures.* Delft University Press: The Netherlands.

Whitlock, D. R. (1999) *Method for ammonia production*. US 5968232 A.

Wohlrab, S.; Meyer, T.; Stöhr, M.; Hecker, C.; Lubenau, U.; Oßmann, A. (2011) On the performance of customized MFI membranes for the separation of n-butane from methane. *Journal of Membrane Science,* **369**, 96-104.

Xiao, J. & Wei, J. (1992) Diffusion mechanism of hydrocarbons in zeolites--I. Theory. *Chemical Engineering Science,* **47,** 1123-1141.

Xing, W., Da Costa, J. C. D., Lu, G. Q. & Yan, Z. F. (2004) Zeolite membranes for environmental separation and reactions. *Encyclopedia of Nanoscience and Nanotechnology,* **2**, 1157-1166.

Xomeritakis, G., Gouzinis, A., Nair, S., Okubo, T., He, M. Y., Overney, R. M. & Tsapatsis, M. (1999) Growth, microstructure, and permeation properties of supported zeolite (MFI) films and membranes prepared by secondary growth. *Chemical Engineering Science,* **54,** 3521-3531.

Xomeritakis, G., Lai, Z. P. & Tsapatsis, M. (2001) Separation of xylene isomer vapors with oriented MFI membranes made by seeded growth. *Industrial & Engineering Chemistry Research,* **40,** 544-552.

Xomeritakis, G. & Lin, Y. S. (1996) Fabrication of a thin palladium membrane supported in a porous ceramic substrate by chemical vapor deposition. *Journal of Membrane Science,* 120**,** 261-272.

Xomeritakis, G., Nair, S. & Tsapatsis, M. (2000) Transport properties of alumina-supported MFI membranes made by secondary (seeded) growth. *Microporous and Mesoporous Materials,* 38**,** 61-73.

Xomeritakis, G., Tsai, C.-Y. & Brinker, C. J. (2005) Microporous sol-gel derived aminosilicate membrane for enhanced carbon dioxide separation. *Separation and Purification Technology,* 42**,** 249-257.

Xu, W. Y., Dong, J. X., Li, J. P., Li, J. Q. & Wu, F. (1990) A novel method for the preparation of zeolite ZSM-5. *Journal of the Chemical Society-Chemical Communications***, 10,** 755-756.

Xu, X., Bao, Y., Song, C., Yang, W., Liu, J & Lin, L. (2005) Synthesis, characterization and single gas permeation properties of NaA zeolite membrane. *Journal of Membrane Science,* **249**, 51-64.

Xu, H.H., Shah, D.B., Talu, O. (1997) Synthesis of ZSM-5 films at elevated gravity. *Zeolites* **19**, 98-217.

Yamasaki, A. & Inoue, H. (1991) surface-diffusion of organic vapor mixtures through porous-glass. *Journal of Membrane Science,* **59,** 233-248.

Yan, Y., Davis, M. E. & Gavalas, G. R. (1995) Preparation of Zeolite ZSM-5 Membranes by In-Situ Crystallization on Porous .alpha.-Al2O3. *Industrial & Engineering Chemistry Research,* **34,** 1652-1661.

Yan, Y., Davis, M. E. & Gavalas, G. R. (1997) Preparation of highly selective zeolite ZSM-5 membranes by a post-synthetic coking treatment. *Journal of Membrane Science,* **123,** 95-103.

Yang, M., Crittenden, B. D., Perera, S. P., Moueddeb, H. & Dalmon, J. A. (1999) The hindering effect of adsorbed components on the permeation of a non-adsorbing component through a microporous silicalite membrane: the potential barrier theory. *Journal of Membrane Science,* **156,** 1-9.

Yang, R.T., (1997) Gas separation by Adsorption Processes. *Imperial College Press: London*

Yildirim, Y. & Hughes, R. (2003) An experimental study of CO2 separation using a silica based composite membrane. *Transactions of the IChemE,* **81,** 257-262.

Yu, F. D., Luo, L. A. & Grevillot, G. (2002) Adsorption Isotherms of VOCs onto an Activated Carbon Monolith: Experimental Measurement and Correlation with Different Models. *Journal of Chemical & Engineering Data*, **47,** 467-473.

Yu, M., Noble, R., Falconer, J. (2011) Zeolite Membranes: Microstructure Characterization and Permeation Mechanisms. *Accounts of Chemical Research*, **44**, 1196-1206.

Yu, M., Falconer, J., Noble, R. (2008) Characterizing non-zeolitic pore volume in zeolite membranes by temperature-programmed desorption. *Microporous and Mesoporous Materials*, **113**, 224-230.

Yu, M., Falconer, J., Noble, R. (2008) Characterizing Nonzeolitic Pores in MFI Membranes. *Industrial & Engineering Chemistry Research*, **47**, 3943-3948. (a)

Yu, M., Wyss, J., Noble, R., Falconer, J. (2008) 2,2-Dimethylbutane adsorption and diffusion in MFI zeolite. *Microporous and Mesoporous Materials*, **111**, 24-31.

Zhang, Y., Avila, A., Tokay, B., Funke, H., Falconer, J., Noble, R. (2010) Blocking defects in SAPO-34 membranes with cyclodextrin. *Journal of Membrane Science*, **358**, 7-12.

Zhang, Y., Wu, Z., Hong, Z., Gu, X., Xu, N.(2012) Hydrogen-selective zeolite membrane reactor for low temperature water gas shift reaction. *Chemical Engineering Journal*, **197**, 314-321.

Zhang, C., Hong, Z., Chen, J., Gu, X., Jin, W., Xu, N. (2012) Catalytic MFI zeolite membranes supported on α-Al2O3 substrates for m-xylene isomerization. *Journal of Membrane Science*, **389**, 451-458.

Zhao, Z., Ma, X., Li, Z., Lin,Y.S.(2011) Synthesis and Characterisation of MOF-5 Membranes. *Journal of Membrane Science*, **382**, 82-90.

Zhao,Z., Ma, X., Kasik, A., Li, Z., Lin, Y.S. (2013) Gas separation properties of metal organic framework (MOF-5) Membranes. *Industrial and Chemical Engineering Research*, **52**, 1102-1108.

Zhou, W., Yoshino, M., Kita, H. & Okamoto, K.-I. (2003) Preparation and gas permeation properties of carbon molecular sieve membranes based on sulfonated phenolic resin. *Journal of Membrane Science,* **217,** 55-67.

Zhou, H., Korelskiy, D., Sjöberg, E., Hedlund, J. (2014) Ultrathin hydrophobic MFI membranes. *Microporous and Mesoporous Materials*, **192**, 76-81.

Zhu, W., Hrabanek, P., Gora, L., Kapteijn, F. & Moulijn, J. A. (2006) Role of adsorption in the permeation of CH4 and CO2 through a silicalite-1 membrane. *Industrial & Engineering Chemistry Research*, **45,** 767-776.

Zhu, M., Kumakiri, I., Tanaka, K., Kita, H. (2013) Dehydration of acetic acid and esterification product by acid-stable ZSM-5 membrane. *Microporous and Mesoporous Materials*, **181**, 47-53.

Zivkovic, T., Benes, N. E. & Bouwmeester, H. J. M. (2004) Gas transport efficiency of ceramic membranes: comparison of different geometries. *Journal of Membrane Science,* **236,** 101-108.

APPENDIX I

Calibration of GC and Mass Flow Controllers

GC Calibration

The accuracy of the GC was confirmed by calibrating twice with a known mixture of N_2 and H_2 before the start of each experiment. One column, a molecular sieve 5A (ALLTECH) was used in this study for the separation of hydrogen and nitrogen. The ammonia was not detected.

The analysis of H_2 and N_2 with the molecular sieve column and the TCD was carried out using the following conditions:
Oven temperature: 40^oC
GC column Temperature 150^oC
Detector temperature (TCD) 200^oC
Carrier and reference gas flowrate: 30ml/min

Calibration of the GC was carried out with a known mixture concentration of N_2 and H_2. Two calibration mixtures were used, one with a 10/90 N_2/H_2 ratio and one with a 50/50 ratio. A linear relationship exists between the peak-area and the concentration. The calibrations can be expressed linearly. The composition of both components (N_2 and H_2) in the four streams can then be estimated using the slopes and intercepts. The remaining composition is NH_3.

An example of the calibration graphs is given in Figures A1-A3.

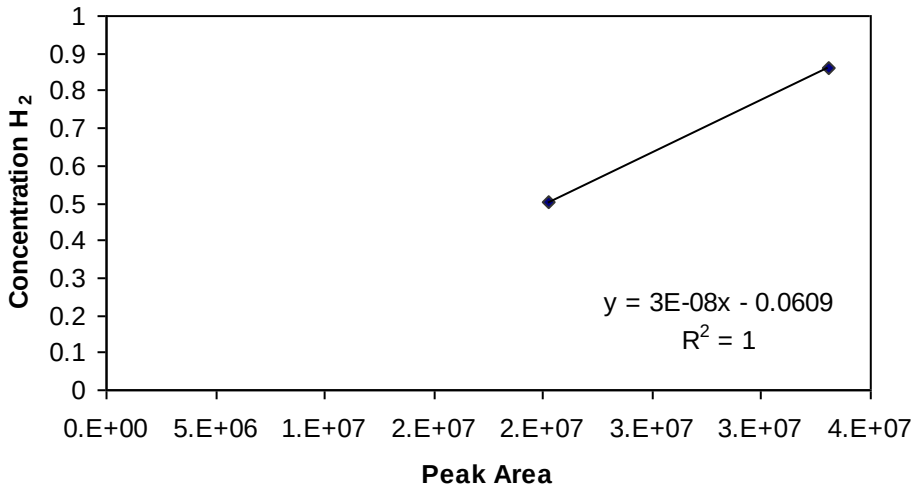

Figure A1: Gas Chromatograph Calibration for Hydrogen Gas

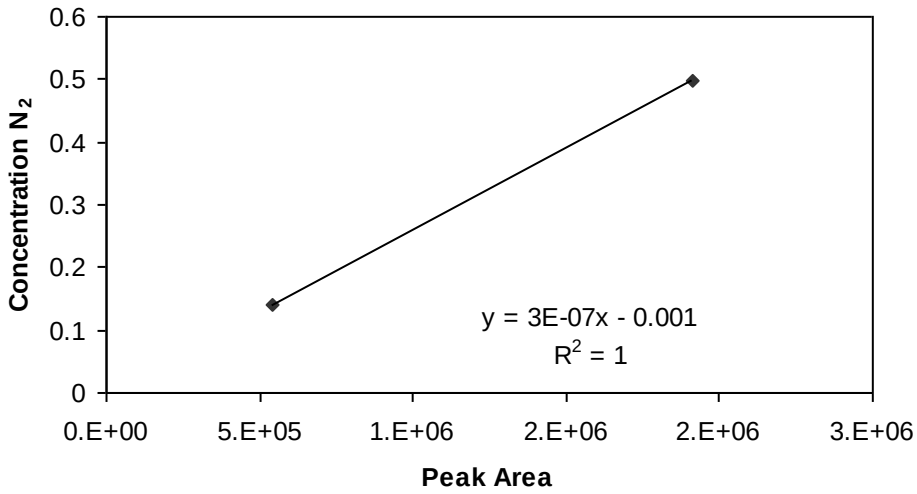

Figure A2: Gas Chromatograph Calibration for Nitrogen Gas

Another example is given of a 3 point calibration. It can be seen that there is hardly any difference.

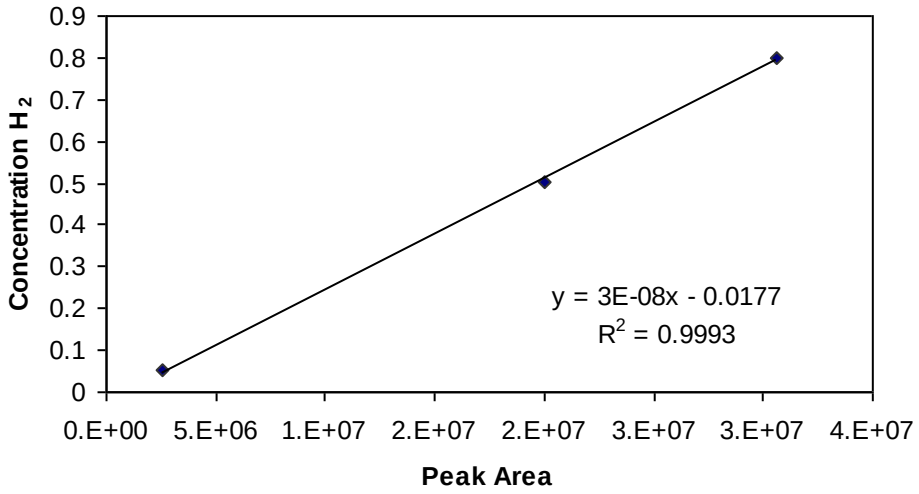

Figure A3: Gas Chromatograph Calibration for Hydrogen Gas

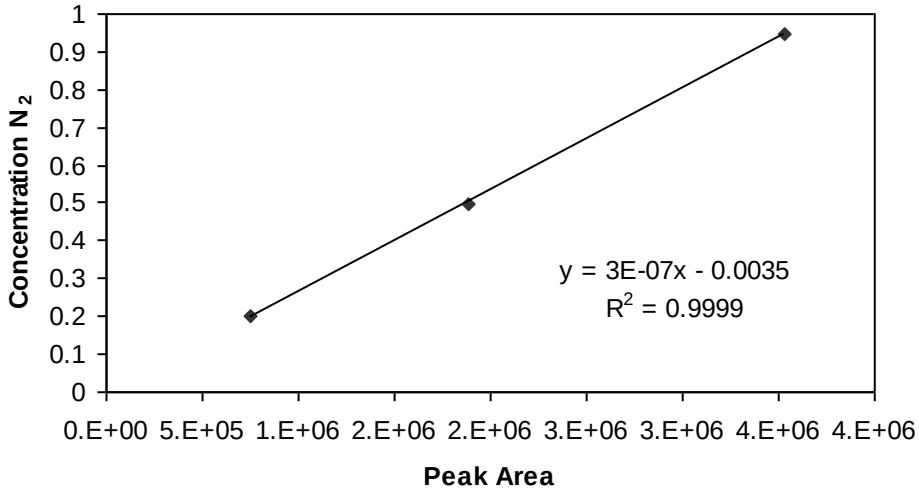

Figure A4: Gas Chromatograph Calibration for Nitrogen Gas

Calibration of Mass Flow Controllers

The mass flow controllers used in this study were of the type Brooks 5850 E series with a maximum nitrogen flowrate of 30l/min.

Calibrations were carried out in-house. If another gas other than nitrogen was used, a conversion factor is given in the mass flow controller manuals. For example, when doing pure gas experiments, a conversion factor for NH3 was used.

Table A1: Gas Conversion tables

Gas	**Formula**	**Sensor Conversion Factor**	**Density (kg/m3)**
Air	Mixture	0.998	1.2983
Ammonia	NH3	0.786	0.771
Hydrogen	H2	1.008	0.0090
Nitrogen	N2	1	1.251

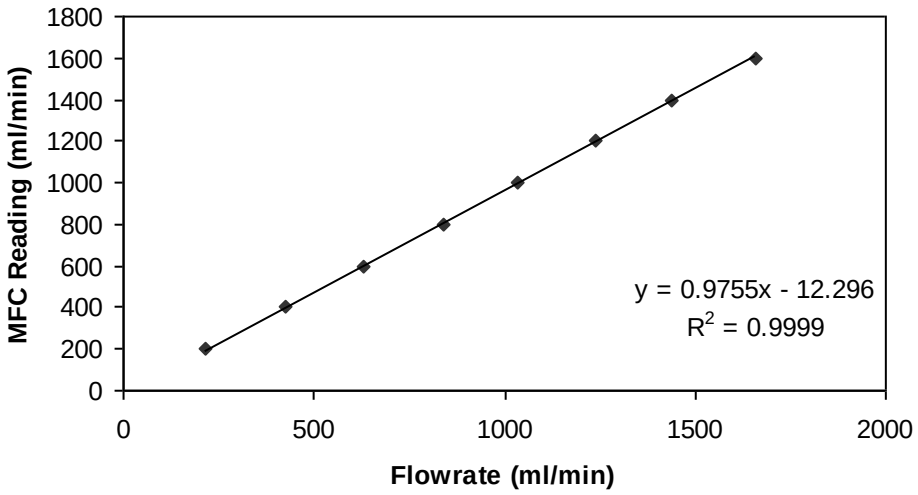

Figure A5: Calibration of mass flow controller

APPENDIX II

Calculations of Permeances in the Mixture

1. Well-mixed method

$$J = \Pi.A.\Delta P \qquad \textbf{A 43}$$

where $\prod$ is the permeance and ΔP is the pressure difference between the high pressure and low pressure side of the membrane.

Re-arranging the equation gives

$$\Pi = \frac{J}{A\Delta P} \qquad \textbf{A 44}$$

Using H_2 as an example

mol

$$\Pi_{H2} = \frac{J_{H2}}{A\Delta P_{H2}}$$

$$J_{H2} = F_{H2}{}^{perm} - F_{H2}{}^{sweep}$$

$$\Delta P_{H2} = P_{H2}{}^{reten} - P_{H2}{}^{perm}$$

where:

$$F_{H2}{}^{perm} = x_{H2}{}^{perm} * F^{perm}$$
$$F_{H2}{}^{sweep} = x_{H2}{}^{sweep} * F^{sweep}$$

$$P_{H2}{}^{reten} = x_{H2}{}^{reten} * P^{reten}$$
$$P_{H2}{}^{perm} = x_{H2}{}^{perm} * P^{perm}$$

The molar fractions are calculated from GC calibrations:

	xH_2	xN_2	xNH_3
Feed	0.68	0.23	0.09
Sweep	0.75	0.25	0.00
Permeate	0.71	0.23	0.06
Retentate	0.68	0.24	0.08

Total Flowrates. Feed and Sweep measured from MFC's and Permeate and Retentate measured from bubblemeters

Flow rates	**ml/min**
Feed	172.87
Sweep	15.59
Permeate	17.09
Retentate	163.62

Total Pressures from pressure transducers

Pressures	**Pa**
Feed	602000
Sweep	100000
Permeate	100000
Retentate	598000

Flowrates of Individual Components

Flowrates	**H_2**	**N_2**	**NH_3**	**Total**
Feed	117.78	41.26	13.82	172.87
Sweep	11.76	2.83	0	15.59
Permeate	12.14	3.87	1.08	17.09
Retentate	110.95	39.00	13.67	163.62

Partial Pressures of Individual Components

	H_2	N_2	NH_3	**Total**
Feed	410158.9	143705.2	48135.9	602000
Sweep	75419.22	24586.46	0	100000
Permeate	70991.55	22669.24	6339.212	100000
Retentate	405482.7	142551.54	49965.8	598000

Membrane area

A = 0.0173 m^2

Change from volumetric flow rate to molar flow rate using the ideal gas law:

$$PV = nRT \qquad \textbf{A 45}$$

where:

	Value	Units
P	101.325	Pa
V	Volumetric flowrate of Individual component	ml.s-1
R	8.314	kPa.dm3.mol-1.K-1
T	298	K
n	molar flowrate of individual component	mol.s-1

Sample Calculation

$$J_{H2} = \frac{(12.13 - 11.76) ml \min^{-1}}{1000 * 60} = 6.29x10^{-6} dm^3 s^{-1}$$

to convert the flux into a molar flow rate

$$n_{H2} = \frac{101.325 kPa * 6.29x10^{-6} dm^3 s^{-1}}{8.314 kPa.dm^3 mol^{-1} K^{-1} * 298 K} = 2.59x10^{-7} mols^{-1}$$

$$Permeance_{H2} = \frac{2.59x10^{-7}\, mols^{-1}}{0.0173m^2 * (40548.7 - 70991.55)Pa} = 4.47x10^{-11}\, mol.m^{-2}.s^{-1}.Pa^{-1}$$

Calculation of Permeances:

	H_2	N_2	NH_3
J (dm^3s^{-1})	6.29E-06	7.01E-07	1.81E-05
n (mol/s)	2.59E-07	2.89E-08	7.44E-07
$\prod$ ($mol.m^{-2}.s^{-1}.Pa^{-1}$)	4.47E-11	1.39E-11	9.83E-10

For the LMPD calculations ΔP is :

$$\Delta P = \frac{\left(P_i^{\,feed} - P_i^{\,perm}\right) - \left(P_i^{\,reten} - P_i^{\,sweep}\right)}{\ln\left(\frac{P_i^{\,feed} - P_i^{\,perm}}{P_i^{\,reten} - P_i^{\,sweep}}\right)} \qquad \textbf{A 46}$$

Using H_2 as an example again

$$\Delta P_{H2} = \frac{\left(P_{H2}^{\,feed} - P_{H2}^{\,perm}\right) - \left(P_{H2}^{\,reten} - P_{H2}^{\,sweep}\right)}{\ln\left(\frac{P_{H2}^{\,feed} - P_{H2}^{\,perm}}{P_{H2}^{\,reten} - P_{H2}^{\,sweep}}\right)} = \frac{(410158.9 - 70991.55) - (405482.7 - 75419.22)}{\ln\left(\frac{410158.9 - 7099.55}{40582.7 - 75419.22}\right)}$$

$$\Delta P_{H2} = 334594.7$$

$$Permeance_{H2} = \frac{2.59x10^{-7}\, mols^{-1}}{0.0173m^2 * (33459.7)Pa} = 4.46x10^{-11}\, mol.m^{-2}.s^{-1}.Pa^{-1}$$

2. **Calculation of Permeances using LMPD**

	H_2	N_2	NH_3
LMPD (Pa)	334594.7	119493.9	45759.78
$\prod$ (mol.m^{-2}.s^{-1}.Pa^{-1})	4.46E-11	1.39E-11	9.37E-10

3. Calculation of Permeances using the segmental method:

The membrane is divided into 50 chambers and the flowrates and fluxes in each component are calculated. This is solved using a Fortran Solver to iteratively predict permeances. For an initial guess, the permeances calculated from the well-mixed method or the LMPD method can be used.

Feed

172.87 ml/min

0.000128624 mol/s

	1	2	3	4	5	47	48	49	50
	x^{Feed}	xF1	xF2	xF3	xF4	xF5	xFeed	xFeed	xFeed	xFeed
xH_2	0.681327075	0.681389129	0.681451201	0.681513292	0.681575402	0.681637530	0.684263992	0.684326936	0.684389899	0.684452881
xN_2	0.238712954	0.238744456	0.238775967	0.238807488	0.238839018	0.238870558	0.240203889	0.240235843	0.240267806	0.240299779
xNH_3	0.079959971	0.079866416	0.079772832	0.079679220	0.079585580	0.079491912	0.075532119	0.075437221	0.075342295	0.075247340

Permeate

17.094 ml/min

1.27188E-05 mol/s

	xPerm	1	2	3	4	5	47	48	49	50
xH_2	0.709915526	0.710587650	0.711262588	0.711940361	0.712620991	0.713304500	0.743904247	0.744684431	0.745467191	0.746252538
xN_2	0.226692349	0.226992980	0.227294764	0.227597712	0.227901830	0.228207129	0.241893812	0.242242774	0.242592887	0.242944158
xNH_3	0.063392125	0.062419370	0.061442648	0.060461928	0.059477179	0.058488371	0.014201941	0.013072795	0.011939922	0.010803303

	$F^{Perm}=F_0^i$	F_1^i	F_2^i	F_3^i	F_4^i	F_5^i	F_{47}^i	F_{48}^i	F_{49}^i	F_{50}^i

F_{H2}^{Perm}	9.0292E-06	9.024E-06	9.0187E-06	9.0135E-06	9.0082E-06	9.003E-06	8.7824E-06	8.7772E-06	8.7719E-06	8.7667E-06
F_{N2}^{Perm}	2.8832E-06	2.8827E-06	2.8821E-06	2.8815E-06	2.8809E-06	2.8803E-06	2.8558E-06	2.8552E-06	2.8546E-06	2.854E-06
F_{NH3}^{Perm}	8.0627E-07	7.9268E-07	7.7909E-07	7.6548E-07	7.5185E-07	7.3821E-07	1.6767E-07	1.5408E-07	1.405E-07	1.2691E-07
Sum		1.2699E-05	1.268E-05	1.266E-05	1.2641E-05	1.2622E-05	1.1806E-05	1.1786E-05	1.1767E-05	1.1748E-05

Pressures	bar	Pa
Feed	5.02	602000
Permeate	0	100000

Assuming Pressure is constant throughout

		1	2	3	4	5	47	48	49	50
H_2	339167.347	339137.49	339107.364	339076.966	339046.293	339015.343	337536.498	337496.372	337456	337415.38
N_2	121035.963	121024.864	121013.656	121002.336	120990.906	120979.363	120413.36	120397.7	120381.931	120366.051
NH_3	41796.6899	41837.6451	41878.9801	41920.6979	41962.8014	42005.294	44050.1414	44105.9277	44162.0694	44218.5683

J		J_1	J_2	J_3	J_4	J_5	J_{47}	J_{48}	J_{49}	J_{50}
H_2		5.2512E-09	5.2507E-09	5.2503E-09	5.2498E-09	5.2493E-09	5.2266E-09	5.226E-09	5.2253E-09	5.2247E-09
N_2		5.8462E-10	5.8457E-10	5.8452E-10	5.8446E-10	5.8441E-10	5.8169E-10	5.8162E-10	5.8154E-10	5.8146E-10

NH_3		1.3584E-08	1.3598E-08	1.3611E-08	1.3625E-08	1.3638E-08		1.4299E-08	1.4317E-08	1.4335E-08	1.4353E-08

Using LMPD results as a first approximation:

	H_2	**N_2**	**NH_3**
$\prod$ ($mol.m^{-2}.s^{-1}.Pa^{-1}$)	4.83E-11	1.51E-11	1.09E-09

Calculation of Selectivities

Selectivities were calculated as a ratio of the permeances as given by this equation:

$$\alpha_{i/j} = \frac{\Pi_i}{\Pi_j} \qquad \textbf{A 47}$$

Example Calculation using permeances calculated with the segmental model

$$\alpha_{NH3/H2} = \frac{1.09x10^{-9}\, molm^{-2}s^{-1}Pa^{-1}}{4.83x10^{-11}\, molm^{-2}s^{-1}Pa^{-1}} = 22.507$$

Selectivities

	Well-mixed	**LMPD**	**Segmental**
$\alpha NH_3/N_2$	70.81	67.29	72.11
$\alpha NH_3/H_2$	22.01	20.99	22.51

APPENDIX III

Error Analysis

To ensure the reliability of the experimental results, it is very important to be aware of the repeatability and accuracy of the experimental rig.

Due to the complexity of the investigated system, the occurrence of experimental errors was likely. Two main areas can be identified by which these errors could have been introduced:

- The experimental apparatus employed to carry out the experiments
- The determination of gas composition using the GC

Experimental Apparatus

A possible source of errors in a gas phase experimental apparatus is the occurrence of leaks through compression fittings and other pipe work connections. The pressurised apparatus was regularly checked for the occurrence of leaks using a soap solution. Any faulty connections found were replaced or retightened. It is however possible that an unquantifiable amount of leaked gas could lead to a falsification of experimental results. The thermocouples used throughout the apparatus were found to be correct within $1^{o}C$ of the measured value. The readings of the pressure transducers were assumed to be accurate within 1.5% of the measured values (1.5% is value of performance accuracy given in the operating manual). The readings did not influence the measured flow rates or compositions.

The feed and sweep flow rates were controlled by two mass flow controllers of type Brooks 5850 E series. These were calibrated in-house. The maximum error for these controllers was assumed to be 1 % of their full range as this is the performance accuracy given in the operating manual.

The flow rates of the gas exiting the membrane (Permeate and Retentate) were measured with soap bubble flow meters. The time the soap bubble required to travel between two marks on the glass tube was stopped by hand using a stopwatch. Therefore human error was introduced at this point. It is difficult to quantify this error introduced into the flow rate measurements, however, in this case, it was assumed that the mass balances calculated for each component accounted for this.

GC Errors

The composition of the gases going in and out of the experimental apparatus was analyzed using a molecular sieve 5A column for the determination of N_2 and H_2. The NH_3 did not elute (it is likely that it just took a very long time to elute, rather than not being detected). The molecular sieve was regenerated regularly and the column was calibrated each day. During each experiment, the molecular sieve 5A was calibrated twice. Two known gas compositions were used. The compositions of H_2 and N_2 measured by the GC were assumed to be fairly accurate. (See calibration curves Figure A1-A4 in Appendix I). The error for NH_3 composition was difficult to quantify.

Calculation of Errors

The uncertainty Principle was used to estimate the experimental error in the calculated permeances. The concept of calculating the uncertainty in the final value of the

calculated parameter from the uncertainties of each measured variable. The effects of each measured variables on the final calculated variable value is derived from the concept of propagation of errors.

The concept is better illustrated with the following example:

For the evaluation of the uncertainty in the value of parameter z, where z is a function of independent variables xi, i.e.

$$z = z(x_1, x_2, x_3 \ldots\ldots\ldots\ldots x_n)$$

and if Δ denotes the uncertainty in the result z and Δx_i is the uncertainty in each variable x_i, then the uncertainty Δz is given by:

$$\Delta z = \sqrt{\left[\left(\frac{\partial z}{\partial x_1}\Delta x_1\right)^2 + \left(\frac{\partial z}{\partial x_2}\Delta x_2\right)^2 + \left(\frac{\partial z}{\partial x_3}\Delta x_3\right)^2 + \ldots\ldots\ldots\ldots\ldots\left(\frac{\partial z}{\partial x_n}\Delta x_n\right)^2\right]} \qquad \textbf{A 48}$$

Applying this to our case staring with the permeability equation:

$$J_i = \Pi..A.\left(P_i^{\,p} - P_i^{\,r}\right) \qquad \left(\Pi = \frac{P_{M_i}}{l_M}\right) \qquad \textbf{A 49}$$

where Π is the permeance

$$J_i = \left(F_i^{\,perm} - F_i^{\,sweep}\right) \qquad \textbf{A 50}$$

$$\Pi = \frac{\left(F_i^{\,p} - F_i^{\,s}\right)}{A\left(P_i^{\,p} - P_i^{\,r}\right)} \qquad \textbf{A 51}$$

The measured errors are in the mass flow rates (mass flow rates were converted to volumetric flow rates using the ideal gas law $PV = nRT$) and the pressure readings. For hydrogen and nitrogen, the errors from the GC (and therefore the concentrations) were negligible.

A summary table using hydrogen gas as an example is given:

Table A2: Error calculation example

	Measured	**Error %**	**Error**
F_{perm}	17.0940	+/- 1%	+/- 0.1709
F_{sweep}	15.5900	+/-1%	+/- 0.1559
$xH_{2\ sweep}$	0.7542	0%	0.0000
$xH_{2\ perm}$	0.7099	0%	0.0000
$xH_{2\ ret}$	0.6781	0%	0.0000
P_{perm}	100000.0000	+/-1.50%	+/- 1500.0000
P_{ret}	598000.0000	+/-1.50%	+/- 8970.0000
$FH_{2\ sweep}$	11.7579	+/-1.00%	+/- 0.1176
$FH_{2\ perm}$	12.1353	+/-1.00%	+/- 0.1214
PH_2 perm	70991.6000	+/-1.50%	+/- 1064.8740
$PH_{2\ ret}$	405482.8700	+/-1.50%	+/- 6082.2431
J	6.2911E-06	+/-1.00%	+/- 3.7747E-03
n	2.5902E-07	+/-1.00%	+/- 0.0000E+00
A	1.7342E-02	-	-
$\prod H_2$	4.4654E-11	+/-1.80%	+/- 8.0500E-13

The error presented above is a systematic error from the measuring instruments such as the Mass Flow controllers (MFC) and the Pressure transducers. However, there are other errors that are difficult to quantify such as the measurement of the outlet flows, the permeate and the retentate (measured with bubble meters). The reading of the scale on the bubble meter, as well as the timing using a stop watch could introduce some errors. Other sources of errors could include the laboratory conditions such as ambient temperature which could affect the GC. Small leakages in the system could also influence the results. Although they can be estimated, it was decided that the mass balance differences accounted for these errors. The errors from the mass balance for each individual component were therefore included in the overall error calculation.

The errors for N_2 and H_2 are quite small in comparison to NH_3.

Errors for H_2

	Measured	**Error %**	**Error**
F_{perm}	17.0940	+/- 1%	+/- 0.1709
F_{sweep}	15.5900	+/-1%	+/- 0.1559
$xH_{2\ sweep}$	0.7542	0%	0.0000
$xH_{2\ perm}$	0.7099	0%	0.0000
$xH_{2\ ret}$	0.6781	0%	0.0000
P_{perm}	100000.0000	+/-1.50%	+/- 1500.0000
P_{ret}	598000.0000	+/-1.50%	+/- 8970.0000
$FH_{2\ sweep}$	11.7579	+/-5.09%	+/- 0.1176
$FH_{2\ perm}$	12.1353	+/-5.09%	+/- 0.1214
Mass balance H_2		4.99%	
PH_2 perm	70991.6000	+/-1.50%	+/- 1064.8740
$PH_{2\ ret}$	405482.8700	+/-1.50%	+/- 6082.2431
J	6.2911E-06	+/-5.09%	+/- 3.7747E-03
n	2.5902E-07	+/-1.00%	+/- 0.0000E+00
A	1.7342E-02	-	-
$\prod H_2$	4.4654E-11	+/- 5.31%	2.3692E-12

Errors for N_2

	Measured	**Error %**	**Error**
F_{perm}	17.09402	+/- 1%	+/- 0.1709
F_{sweep}	15.59	+/-1%	+/- 0.1559
$xN_{2\ sweep}$	0.245865	0%	0.0000
$xN_{2\ perm}$	0.226692	0%	0.0000
$xN_{2\ ret}$	0.238381	0%	0.0000
P_{perm}	100000	+/-1.50%	+/- 1500.0000
P_{ret}	598000	+/-1.50%	+/- 8970.0000
$FN_{2\ sweep}$	3.83303535	+/-5.02%	+/- 0.1176
$FN_{2\ perm}$	3.875077582	+/-5.02%	+/- 0.1214
Mass balance N_2		4.92%	
PN_2 perm	22669.2	+/-1.50%	+/- 0.19244128
$PN_{2\ ret}$	142551.838	+/-1.50%	+/- 0.194552051
J	7.00704E-07	+/-5.02%	
n	2.88502E-08	+/-1.00%	+/- 340.038

A	0.017342	-	+/-2138.27757
∏ N_2	4.843860436	+/- 5.24%	+/- 1798.23957

Errors for NH_3

	Measured	**Error %**	**Error**
F_{perm}	17.0940	+/- 1%	+/- 0.1709
F_{sweep}	15.5900	+/-1%	+/- 0.1559
$xNH_{3\ sweep}$	0.0000	0%	0.0000
$xNH_{3\ perm}$	0.0634	0%	0.0000
$xNH_{3\ ret}$	0.0836	0%	0.0000
P_{perm}	100000.0000	+/-1.50%	+/- 1500.0000
P_{ret}	598000.0000	+/-1.50%	+/- 8970.0000
$FNH_{3\ sweep}$	0.0000	+/-6.85%	+/- 0.1176
$FNH_{3\ perm}$	1.0836	+/-6.85%	+/- 0.1214
Mass balance NH_3		-6.78%	
PNH_3 perm	6339.2125	+/-1.50%	+/- 1064.8740
$PNH_{3\ ret}$	49965.7995	+/-1.50%	+/- 6082.2431
J	1.8060E-05	+/-6.85%	+/- 3.7747E-03
n	7.4361E-07	+/-1.00%	+/- 0.0000E+00
A	1.7342E-02	-	-
Permeance NH_3	9.8289E-10	7.02%	2.3692E-12

Repeatability

An example is given of a set of experiments (Pure gas N_2 permeances) that were performed and the exact same experiments were repeated 1 month later. This was to ensure repeatability of the experiments. Not all experiments conducted throughout the research could be repeated due to time constraints, however, some experiments such as mixture experiments were repeated and also produced similar results.

The results show very similar results, within 10% apart from the values at 1300Pa differential pressure. This could be attributed to experimental errors.

Differential pressure Pa	$\prod N_2$ 1	$\prod N_2$ 2
300	1.13E-10	1.12E-10
500	1.10E-10	1.17E-10
700	1.24E-10	1.28E-10
1000	1.39E-10	1.44E-10
1300	1.37E-10	1.58E-10
1500	1.67E-10	1.72E-10